How does the brain extract acoustic patterns?
A behavioural and neural study

Katarina Charlene Poole

University College London

Supervisors: Professor Jennifer Bizley and Professor Maria Chait

Submitted for the degree of Doctor of Philosophy

March 2023

Declaration

I, Katarina Charlene Poole, confirm that the work presented in my thesis is my own. Where information has been derived from other sources, I confirm that this has been indicated in the thesis.

Signed:

Date: 26/03/23

Abstract

In complex auditory scenes the brain exploits statistical regularities to group sound elements into streams. Previous studies using tones that transition from being randomly drawn to regularly repeating, have highlighted a network of brain regions involved during this process of regularity detection, including auditory cortex (AC) and hippocampus (HPC; Barascud et al., 2016). In this thesis, I seek to understand how the neurons within AC and HPC detect and maintain a representation of deterministic acoustic regularity.

I trained ferrets (n = 6) on a GO/NO-GO task to detect the transition from a random sequence of tones to a repeating pattern of tones, with increasing pattern lengths (3, 5 and 7). All animals performed significantly above chance, with longer reaction times and declining performance as the pattern length increased. During performance of the behavioural task, or passive listening, I recorded from primary and secondary fields of AC with multi-electrode arrays (behaving: n = 3), or AC and HPC using Neuropixels probes (behaving: n = 1; passive: n = 1).

In the local field potential, I identified no differences in the evoked response between presentations of random or regular sequences. Instead, I observed significant increases in oscillatory power at the rate of the repeating pattern, and decreases at the tone presentation rate, during regularity. Neurons in AC, across the population, showed higher firing with more repetitions of the pattern and for shorter pattern lengths. Single-units within AC showed higher precision in their firing when responding to their best frequency during regularity. Neurons in AC and HPC both entrained to the pattern rate during presentation of the regular sequence when compared to the random sequence. Lastly, development of an optogenetic approach to inactivate AC in the ferret paves the way for future work to probe the causal involvement of these brain regions.

Impact Statement

Separating and extracting meaningful information from a complex auditory scene, known as auditory scene analysis, presents numerous challenges to a listener. To accomplish this, the nervous system must decode the incoming acoustic signals and extract useful cues, from low level features such as frequency content to high-level features such as the predictability of the acoustic stimulus. How the brain is able to extract these high-level cues and use them to better perform auditory scene analysis is still unknown, with numerous studies trying to understand how the auditory system detects this regularity.

Previous experiments trying to explore the circuit and cellular-level basis of auditory scene analysis have used very simple stimuli. In this thesis, I employed a more complex stimulus that is commonly used in human cognitive studies, pure tone sequences that transition from randomly selected frequencies to a regularly repeating pattern. In this work, I demonstrated for the first time that a non-primate model, the ferret, can accurately detect these changes in regularity within the stimuli. My findings confirmed that non-human animals are capable of true regularity detection and publication of these findings will add to the comparative neuroethology database and serve as a foundation for future studies exploring how the auditory system detects regularity.

With this paradigm and model I performed a comprehensive study using microelectrode arrays spanning primary and secondary fields of auditory cortex that identified neural correlates of regularity detection in the local field potential bridging the gap in knowledge between meso-scale electrophysiology in animals and macro-scale imaging in humans. In conjunction with analysis of the LFP, I analysed single and multi-unit activity in response to these random to regular sequences and how they are modulated by the behavioural response of the ferret. This measurement and understanding of central auditory processing that moves beyond pure tone assessment and into more high-level processing is rarely performed within animal models due to the complexity of the perceptual task. The knowledge of how the brain extracts regularities and processes these more complex stimuli is critical for the development of cortical prosthesis used to restore hearing and advances our

understanding into why certain listeners may struggle to perform effective auditory scene analysis.

In this project I have developed numerous novel techniques. Firstly, I devised a method for robustly and chronically recording neural responses in auditory cortex and hippocampus simultaneously using high-density linear probes (Neuropixels 2.0). The specialized tools developed for this technique have already been shared with other research groups. Secondly, I published the validated method for inactivating cortex using optogenetics with an mDlx promoter that targets the opsin Channelrhodopsin-2 to GABAergic neurons. This method has proven to be much more effective for cortical silencing, as it leverages the brains existing inhibitory network. This has opened up new possibilities for studying more complex auditory processing and behavioural tasks in non-rodent models, providing a novel avenue for causal research.

Acknowledgements

I am amazingly fortunate to have two incredibly talented and supportive supervisors, Professor Jennifer Bizley and Professor Maria Chait. They have both been wonderful inspirations both academically and personally. Jenny, thank you so much for taking me under your wing all the way back from when I did my Masters project with you, and introducing me to the wonderful world of auditory neuroscience and teaching me so much. Maria, thank you so much for your support, passion and invaluable wealth of knowledge. You have been so welcoming and it's been an absolute pleasure working with you.

Thank you to the Bizley lab and the ferreteer team with a special thanks to Stephen and Soraya. Stephen, you trained me in so much from ferret husbandry to neural data analysis and were such a pleasure to work with, providing endless entertainment during long days in the lab with countless stories from your PhD. Soraya, thank you so much for allowing me to pick your brain about ferret local field potentials, and also all the help in getting the Neuropixels system up and running, I hope we get to hustle some more people at table football one day. Thank you to my colleagues at the Ear Institute, who I've pestered with questions about immunofluorescence, and whether they want to go for pints at The Harrison. Thank you to the RVC staff, who take such great care of the ferrets, with special thanks to Tony and Ruth (my skating buddy).

I'd like to thank my family (Mum, Dad, Misha, Gandalf, Nessa and my Grandma), feeding and supporting me every step of the way, with a special thanks to my Grandad (Professor Eduard Gorkunov), an academic inspiration. I would also like to thank all my friends, my buddies and my pals (special thanks to Laura and George, putting up with me during lockdown and throughout my thesis) and finally Alistair for all of his support that kept me sane.

All of this would not be possible without the European Research Commission for funding my PhD. Last but not least a very special thanks to all the ferrets that contributed in all the big and small ways: Mr Muscle, Daz, Squinty, Windowlene, Ariel, Pendleton, Grainger, Carter, Mia, Cheeseburger, Skittles, Ursula, Jasmine, Sponge, Fusili, Nala, Rajah, Crumble, Éclair, Crème Brulee, Gnocchi, Orecchiette, Linguine, Spirali, Fettucini, Orecchiette. The loveliest cat snakes.

UCL Research Paper Declaration Form
referencing the doctoral candidate's own published work(s)

Please use this form to declare if parts of your thesis are already available in another format, e.g. if data, text, or figures:

- *have been uploaded to a preprint server*
- *are in submission to a peer-reviewed publication*
- *have been published in a peer-reviewed publication, e.g. journal, textbook.*

This form should be completed as many times as necessary. For instance, if you have seven thesis chapters, two of which containing material that has already been published, you would complete this form twice.

1. For a research manuscript that has already been published (if not yet published, please skip to section 2)

a) **What is the title of the manuscript?**

Reversible inactivation of ferret auditory cortex impairs spatial and non-spatial hearing

b) **Please include a link to or doi for the work**

https://doi.org/10.1523/JNEUROSCI.1426-22.2022

c) **Where was the work published?**

Journal of Neuroscience

d) **Who published the work?** (e.g. OUP)

The Society for Neuroscience

e) **When was the work published?**

1st February 2023

f) **List the manuscript's authors in the order they appear on the publication**

Stephen M. Town, Katarina C. Poole, Katherine C. Wood and Jennifer K. Bizley

g) **Was the work peer reviewed?**

Yes

h) **Have you retained the copyright?**

Yes

i) **Was an earlier form of the manuscript uploaded to a preprint server?** (e.g. medRxiv). If 'Yes', please give a link or doi)

Yes.
https://doi.org/10.1101/2021.11.16.468798

If 'No', please seek permission from the relevant publisher and check the box next to the below statement:

☐

*I acknowledge permission of the publisher named under **1d** to include in this thesis portions of the publication named as included in **1c**.*

2. **For multi-authored work, please give a statement of contribution covering all authors** (if single-author, please skip to section 4)

Stephen M. Town

Designed the behavioural task, collected the behavioural data, analysed the behavioural data, collected the data for the optogenetic validation experiment, and wrote the paper.

Katarina C. Poole

Designed the optogenetic validation experiment, collected the data for the optogenetic validation experiment, analysed the data from the optogenetic validation experiment and wrote the paper.

Katherine C. Wood

Designed the cooling system and collected the behavioural data.

Jennifer K. Bizley

Designing the cooling system, designed the behavioural task, collected the behavioural data, collected the data for the optogenetic validation experiment and wrote the paper.

3. **In which chapter(s) of your thesis can this material be found?**

Chapter six

4. **e-Signatures confirming that the information above is accurate** (this form should be co-signed by the supervisor/ senior author unless this is not appropriate, e.g. if the paper was a single-author work)

Candidate

Click or tap here to enter text.

Date:

25/03/23

Supervisor/ Senior Author (where appropriate)

Click or tap here to enter text.

Date

25.03.23

CONTENTS

LIST OF FIGURES

LIST OF TABLES

LIST OF ABBREVIATIONS

Abbreviation	Full description
AAV	adeno-associated virus
AC	auditory cortex
AEG	anterior ectosylvian gyrus
AFC	alternative forced choice
ASA	auditory scene analysis
BF	best frequency
BOLD	blood oxygenation level dependent
CA	cornu Ammonis
CF	characteristic frequency
ChR2	Channelrhodopsin-2
CNIC	central nucleus of the inferior colliculus
CSD	current source density
dB	decibel
dBSPL	decibel sound pressure level
DCIC	dorsal cortex of the inferior colliculus
ECG	electrocardiogram
ECoG	electrocorticography
EEG	electroencephalography
EX	excitatory neurons
fMRI	functional magnetic resonance imaging
FOI	frequencies of interest
FR	firing rate
FRA	frequency response area
GFP	green fluorescent protein
GLM	generalized linear model
GLMM	generalized linear mixed model
H1	human experiment 1
H2	human experiment 2
HPC	hippocampus
Hz	Hertz

IC	inferior colliculus
IDyOM	Information Dynamics of Music model
iEEG	intracranial electroencephalography
IFG	inferior frontal gyrus
ISI	inter-stimulus interval
ISI	inter-spike interval
KDE	kernel density estimate
kHz	kilohertz
LCIC	lateral cortex of the inferior colliculus
LFP	local field potential
LGN	lateral geniculate nucleus
MagEG	magnetoencephalography
MEG	medial ectosylvian gyrus
MGB	medial geniculate body
MGD	dorsal division of the medial geniculate body
MGM	medial division of the medial geniculate body
MGV	ventral division of the medial geniculate body
MMN	mismatch negativity
MU	multi-unit
PCA	principal component analysis
PEG	posterior ectosylvian gyrus
PFC	prefrontal cortex
PPM	Prediction by Partial Matching
PSTH	peristimulus time histogram
PV+	parvalbumin positive interneurons
RAN	random
RCIC	rostral cortex of the inferior colliculus
REG	regular
RMS	root mean square
RT	reaction time
SC	spike count
SNR	signal-to-noise ratio
SOMs	somatostatin-positive interneurons
SSA	stimulus specific adaptation
STG	superior temporal gyrus

SU	single-unit
VIP	vasoactive intestinal polypeptide

1 CHAPTER ONE: AN INTRODUCTION AND LITERATURE REVIEW

1.1 INTRODUCTION

The human brain continuously analyses the features of sounds within our acoustic environment to detect the emergence of new sources, extracting their meaning, and adjusting behaviour accordingly. Such features could involve loudness or pitch changes and emerging sources could be that of new speakers or even footsteps. This process is challenging as at first all auditory sources heard are condensed into one time-varying waveform that reaches the listener's eardrum. This acoustic signal is separated into various frequency components via the cochlea, yet this alone is typically unable to perceptually separate different auditory sources. Instead the auditory system must use various cues within the stimulus and recruit several auditory regions in the nervous system to successfully analyse the acoustic scene (Bizley and Cohen, 2013). Despite the challenging nature of this process, it is necessary as the auditory system continuously monitors, in all directions, our environment and therefore acts as our best sensory early warning system. Uncovering the principles that govern a listeners' ability to continuously analyse the acoustic scene has therefore been at the forefront of hearing research.

One feature that humans and animals must be sensitive to is the regularity or predictability of sounds, as many sounds in nature contain repeating elements to create a statistically regular structure or pattern. Regularity can take form as a deterministic repeating predictable pattern, where for example the pattern of the frequency of tones or inter-tone onset intervals, are repeated (see **Figure 1.1A**). The repeated patterns can be repeatedly periodically, recurring at regular intervals as shown in **Figure 1.1A**. On the other hand, the pattern may be deterministic but aperiodic, such that identical patterns are presented with either the intervals between patterns occurring at irregular intervals (see **Figure 1.1B**), or the individual elements themselves may occur at irregular intervals, such as described in Asokan et al. (2021; see **Figure 1.1C**). Alternatively, regularity can have a more probabilistic form which rather than relying on direct repetition will contain some randomness where similar patterns will emerge based on the probability of one sound following another (see **Figure 1.1D**). These probabilities can be learnt and can take the form of simple rules

such as the mean and variance of the frequencies present in a tone cloud (Skerritt-Davis and Elhilali, 2018) to more complex rules such as the statistical rules that govern language.

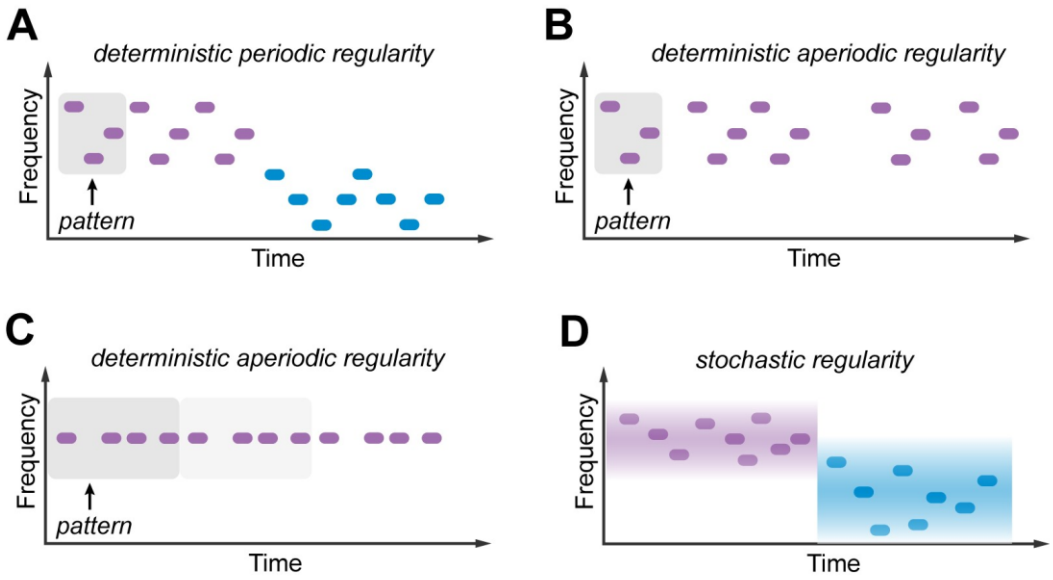

Figure 1.1: Regularity as a function of frequency over time. A) An example of a deterministic regularity (purple) with a repeating pattern of frequencies (highlighted in grey) which then changes to a different pattern (blue). The regularity here is periodic, occurring over regular intervals. B) An example of an aperiodic pattern where the pattern repeats exactly but at non-regular intervals. C) An example of a pattern where the intervals between the elements are aperiodic. D) An example of a stochastic or probabilistic regularity where the probability is linked to the mean and variance of the frequency range which is higher and narrower in purple and then moves to a lower and wider range in blue.

Regularity, both aperiodic deterministic and probabilistic, are features common to both human speech and animal vocalisations. During statistical learning of language, listeners become exposed to probability distributions that govern the transition between syllables, rather than encountering deterministic repeating patterns (e.g. in English, “pat” is not always followed by “tern” but sometimes by “io”) (Santolin and Saffran, 2018; Wilson et al., 2017). This is also true for vocalisations within animals, where in one example zebra finches have been shown to learn and generalize dependencies between song elements (Chen and ten Cate, 2017; Petkov and Cate, 2020). Regularity is heavily exploited within music both within the periodic tonal structure (Tillmann et al., 2001), and rhythmic structure (Large and Palmer, 2002), both deterministically and probabilistically. Deterministic periodic repetition of a spoken phrase can cause the perception of it being ‘sung’ (Deutsch et al., 2008), and the composition of music ubiquitously relies on the manipulation of predictability

throughout the piece (Temperley, 2014). Periodic and aperiodic deterministic regularities have both been shown to provide equal perceptual improvement in deviant tone discrimination when dissociated from behavioural motor responses, where periodic regularity accelerated motor responses which the authors suggest is due to sensorimotor synchronisation from the entrainment of the periodic regularity (Morillon et al., 2016; see for a review: Rimmele et al., 2018). Other naturalistic regularities may be imprecise, such as in a train of footsteps, each of which differs slightly in intensity and timing. Nevertheless, the auditory system can identify the considerable acoustic overlap across elements, generalising to predict the approximate continuation of the pattern despite this variability.

In this review I highlight the importance of regularity in auditory perception during auditory scene analysis and change detection. I then give an overview of the various paradigms that have been used to study various aspects of regularity detection, from simple deterministic patterns to more complex probabilistic rules and finally paradigms that directly test regularity detection. With these paradigms in mind, I then review previous literature that has explored the cellular and circuits mechanisms that are likely involved during regularity detection. I review the overarching brain areas and networks that are implicated in this process, such as auditory cortex and hippocampus. Lastly, I outline how my thesis aims to elucidate the neural mechanisms underlying auditory regularity detection.

1.2 REGULARITY AND NAVIGATING THE ACOUSTIC ENVIRONMENT

1.2.1 Regularity facilitates organisation of the acoustic scene

The acoustic environment is transparent to our auditory system where different sound sources are continuously presented simultaneously to our ears and arrive as an overlapping mixture. Despite this we can effortlessly segregate these sounds into their constituent sources. To answer how the auditory system solved this ‘cocktail party problem’ (Cherry, 1953), Albert Bregman provided a model called auditory scene analysis (ASA). In this model he proposes that the auditory system extracts cues to integrate or segregate sound sources within an acoustic scene (Bregman, 1994). A segregated sound source is one that can be identified as a distinct auditory ‘object’ or ‘stream’. This perceptual entity is formed through the separation, analysis and abstraction of acoustic information to allow for generalisation across sensory

domains and experiences (Griffiths and Warren, 2004). Individual auditory objects that are grouped perceptually together in a temporal sequence, such as the grouping of individual footsteps, can be thought of as an auditory stream (Winkler et al., 2009).

Accumulating evidence suggests that the auditory system relies on regularities to parse acoustic scenes into these discrete objects (Denham and Winkler, 2006; Winkler et al., 2012, 2009). Winkler et al (2009) proposed that sound segregation is aided by mechanisms which are continually assessing sounds for structured patterns or regularities to form models, or rules, about how auditory objects in the environment are expected to behave. These internal models can then be exploited to facilitate source segregation and perceptual selection by 'drawing out' components from the aggregate input that behave according to the predicted pattern (Winkler et al, 2012; see **Figure 1.2**). This proposal, which is changing the way we think about, and study hearing (Nelken, 2012), is motivated by demonstrations that listeners are sensitive to patterns in sound sequences and that regularity extraction often occurs independently of conscious involvement.

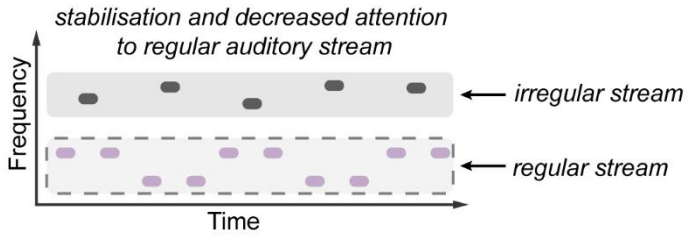

Figure 1.2: Schematic of organisation of an auditory scene via regularity. The regular stream (a deterministic repeating pattern in purple) is stabilised into a separate stream (dashed outline) to that of the irregular stimulus. It is easier to ignore than the irregular stream, illustrated by the reduced opacity of the regular stream.

In support of these accounts, Bendixen et al. (2010) provided the first evidence for an effect of regularity on auditory stream segregation. They employed a bi-stable ABA streaming stimulus (a sequence of two tones of two different frequencies, A and B, organized into repeating ABA triplets; Noorden, 1975) in which a variation in frequency and intensity was introduced to the A and B tones (see **Figure 1.3A**). In separate conditions, these modulations introduced a regular pattern (over frequency and/or intensity) to the A stream, B stream, or to both. Listeners were instructed to continuously indicate whether they perceived the sequence as integrated (one stream) or segregated (two streams). Measuring the duration of intervals during which the

participant perceived integration or segregation, Bendixen et al. (2010) demonstrated that within-stream regularity stabilised the segregated perceptual phases, increasing their duration.

A further demonstration of the role of regularity in scene analysis, this time temporally, was reported by Devergie et al. (2010) who used a set of familiar melodies ('targets'), temporally interleaved with random distracter sequences that shared the same pitch and timbre ranges spanned by the targets. Listeners were instructed to identify the target melodies from amidst the distractors. The authors compared conditions where both the target and distractor were temporally irregular to conditions where the distractor melodies were regular. Target detection performance was enhanced when the distractor sequences were regular, suggesting that listeners were able to use predictable temporal structure to suppress the distractor stream, thus facilitating the identification of the melody. This finding was extended to arbitrary sound sequences by Andreou et al. (2011; see also Rimmele et al., 2012) who used independent, concurrent sequences of A and B tones which were either temporally regular or random (see **Figure 1.3B**). To evaluate segregation, they quantified listeners' ability to selectively attend to one of the streams in the presence of the other and demonstrated that performance was affected by the regularity of the concurrent unattended sequence. This effect was explained by suggesting that, as hypothesized by Winkler et al (2009), the auditory system was able to discover the patterning within the to-be-ignored sequence and use this 'predictive rule' to pull the elements adhering to the regularity away from the aggregate mixture, thus facilitating the focusing of attention on the attended stream.

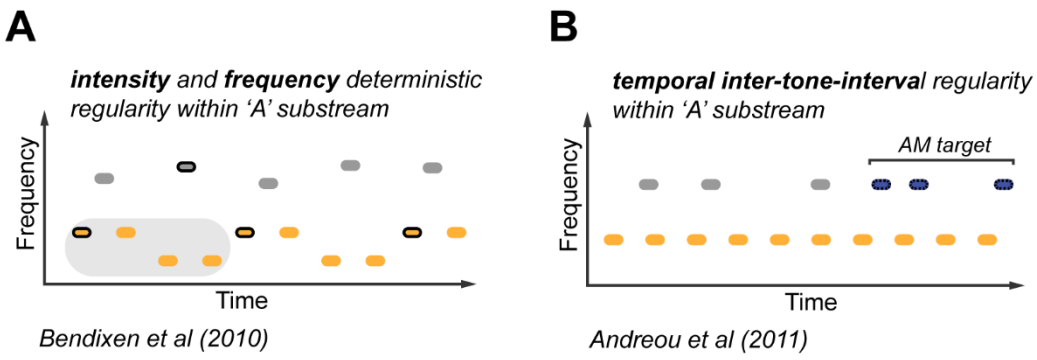

Figure 1.3: Schematic of ABA paradigms that vary the regularity between auditory streams. A) ABA streaming paradigm where the A stream (orange) contains a frequency pattern (one cycle highlighted in grey) and irregularity in the B stream (grey). The A stream also contains a regularity in the form of tone level (black outline = louder tones; Bendixen et

al., 2010). B) ABA streaming paradigm where the A stream (orange) has the same inter-tone interval to create temporal regularity and the B stream has various inter-tone intervals and also contains the detection target (amplitude modulated tones, purple; Andreou et al., 2011).

That regular sequences are easier to ignore was further confirmed in a study that quantified the extent to which task-irrelevant regular or random frequency patterns interfere with listening tasks (Southwell et al., 2017). Stimuli were rapid sequences of tone pips, arranged in regular (REG; repeating sequences of 10 frequencies) or a random (RAN) order. They were delivered to one ear, while participants performed a demanding detection task on sounds presented to the other ear. The results revealed that RAN sequences were more detrimental to performance than matched REG sequences. Notably, these effects were observed despite new REG (and RAN) patterns being presented on each trial, suggesting that listeners rapidly acquired the regularity within the trial and used it to facilitate the suppression of the predictable patterns. Therefore, in addition to the large body of work which demonstrates that it is easier to perceptually follow regular than random sequences (Drake et al., 2000; Jones et al., 2006, 2002, 1982; Large and Jones, 1999), accumulating research also reveals that regularity (across a range of acoustic features) plays an important role in supporting our ability to parse auditory scenes (see **Figure 1.2**).

1.2.2 Regularity facilitates change detection in complex acoustic scenes

As well as aiding scene segregation, the ability to exploit statistical structures in the sensory input allows listeners to rapidly detect new, unexpected (and thus potentially critical) events in their surroundings. To understand how change detection is shaped by the statistics of the unfolding sound context, Southwell and Chait (2018) used tone-pip sequences that varied in the predictability of frequency patterns. Sequences were either regular cyclical patterns (REG) or contained the same frequencies but arranged randomly (RAN). Therefore first-order statistics, such as the distribution of tone frequencies, were matched between REG and RAN sequences but the predictability of successive frequencies differed. The authors asked whether this predictability affects listeners' sensitivity to brief 'deviant' sounds. Deviants were designed to be equally outlying in frequency space and equally probable, as compared to the preceding tones, whether in the REG or RAN contexts (see **Figure 1.4**). The results demonstrated that even though patterns were unique on each trial, sequence regularity aided the detection of deviant events, expressed as increased sensitivity (d') and shortened reaction times. A different, but not mutually exclusive account relates

to perceptual organization mechanisms: the tones in REG sequences are bound together through the underlying predictive rule (Winkler et al., 2012, 2009) such that events which do not conform to the rule are perceptually segregated as separate 'objects' and are therefore easier to detect. These findings are also consistent with the notion that the brain continually maintains a detailed representation of ongoing sensory input and that this representation shapes the processing of incoming information: deviants within a highly predictable context evoke higher prediction errors than identical events in sequences characterized by low predictability.

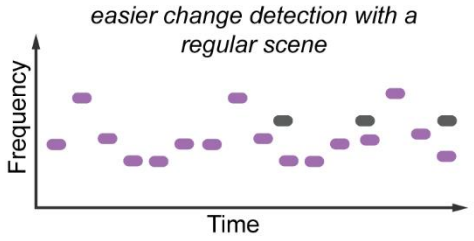

Figure 1.4: Schematic of change detection in a regular scene. Regularity within the acoustic scene, in the form of deterministic frequency patterns in purple, increase the saliency of new auditory objects (grey) in the scene.

Aman et al. (2021; see also Sohoglu and Chait, 2016) extended the investigation to stimuli which contain multiple simultaneous sources. Sensitivity to regularity was examined in the context of a change detection task. Stimuli were 'scenes' populated by up to 14 concurrent tone-pip sequences, each with a distinct frequency and temporal pattern that was either regular or random. The listeners' task was to detect occasional changes (appearance or disappearance of a source) within these 'soundscapes'. Performance was facilitated when scene components were characterized by a regular fluctuation pattern. The regularity of the changing stream as well as that of the background (non-changing) streams contributed independently to this effect. Notably, listeners benefited from regularity even when not consciously aware of it. These results are consistent with Southwell and Chait's (2018) explanation on deviance detection that: if the auditory system can discover the predictable temporal structure within each stream, it can rapidly detect the non-arrival of an expected tone, easier and faster in REG scenes relative to RAN scenes. Likewise, the ability to acquire the patterns of ongoing objects in REG scenes allows listeners to discount transients that obey this pattern, facilitating the detection of those that are associated with the onset of a new object.

Overall, these findings reveal that sensitivity to regularity plays a fundamental role in shaping our perception of crowded auditory scenes, even when listeners are not actively attending to that signal but tracking the scene as a whole. The auditory brain appears to extract and keep track of the patterning of *each* scene component and exploits this information while detecting new auditory events. However, the processing stages that are affected by predictability remain elusive. Does regularity affect the initial segregation stages of ASA or in the later stages where auditory streams compete or stabilise? Andreou et al (2011) reported that the effect of regularity was observed when the frequency separation between A and B streams was very small, hinting at an early (bottom-up) effect of regularity on segregation. In contrast, in Bendixen et al (2010) regularity appeared to stabilize, but not affect the initial formation of streams. Further research is required to elaborate on these processes, identify the computations which underpin sensitivity to regularity and uncover the processing stages on which they operate.

1.3 PARADIGMS TO INVESTIGATE REGULARITY DETECTION

To understand the neural machinery which underpins how the brain uses and discovers regularity within the acoustic environment we need to be able to manipulate the predictability of the stimulus parametrically and perform appropriate controls. The predictability of the stimulus can be probabilistic or deterministic, and the predictability may lie within different dimensions such as spectral or temporal. Each of these dimensions imposes different constraints on the interpretation of the impact of regularity on the measured signal, whether behavioural to neural imaging to electrophysiology. For example, for single-unit recordings in auditory cortex, neural responses are largely dictated by their frequency tuning and thereby the frequency of the stimulus. What we have seen from the studies in the previous section is that there are many types of regularity and paradigms in which to test its effects. In this next section I will consider the paradigms that have allowed us to begin to understand how the brain extracts and processes regularities from simple repeated tones to complex vocalisations.

1.3.1 Regularity detection: detecting deviations from regularity

Oddball paradigms have been deployed to indirectly study regularity detection where a repeating pattern of sounds contains rarely occurring deviants (see **Figure 1.5A**). In its simplest form it is a sequence of tones of two frequencies, one occurring

commonly and the second only rarely, and can vary in their probability of occurrence (i.e. 10% deviant / 90% standard; 30% deviant / 70% standard), though the oddball paradigm has also been extended to noise bursts (Nelken et al., 2013). Responses can be measured either to the standard or deviant, where commonly in humans mismatch negativity's (MMNs) are elicited to the deviant. The MMN is the difference in the evoked potential in response to the standard compared to that of the deviant. The magnitude of the MMN can then be used as a proxy to measure deviance detection within the brain (see for a review: Näätänen et al., 2001).

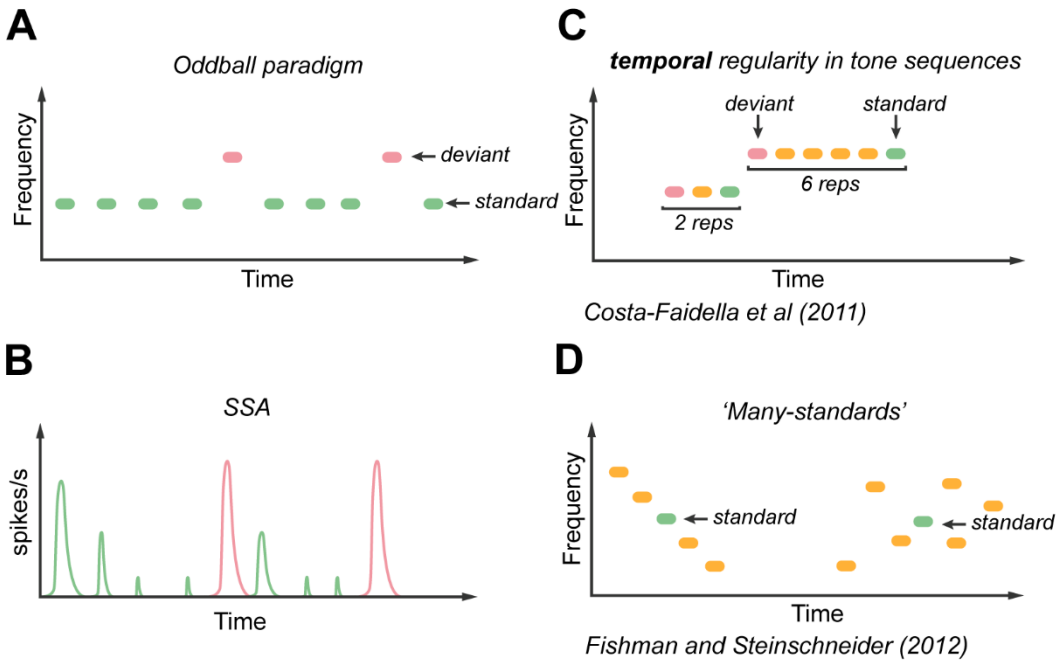

Figure 1.5: Schematic of oddball paradigms and SSA. A) Oddball paradigm, the standard (green) is repeated more often than the deviant (pink) which is presented at a different frequency. B) Schematic of neurons firing rate to the stimuli in panel A. Responses to the standard are in green and responses to the deviant are in pink. C) Paradigm where tones are repeated either 2 or 6 times before changing in frequency so that the first tone in a repetition is the deviant (pink) and the last is the standard (green) (Costa-Faidella et al., 2011). D) Many-standards control with a descending sequence (left) and a random sequence (right) to control for effects of predictability and repetition suppression (Fishman and Steinschneider, 2012).

In animal models, the firing rate of individual neurons are directly measured in response to the standard or deviant (see **Figure 1.5B**). Firing to a repetitive stimulus causes the neuron to adapt and thereby decreasing its firing rate (Dudai, 2002; Nelken et al., 2014). The decrease in firing in this paradigm only occurs to the standard tone frequency, and therefore is classed as stimulus-specific adaptation (SSA), as this reduction does not generalize to other, rare stimuli (Nelken et al., 2014). This adaptation has also been shown to occur over varying time courses (milliseconds to

tens of seconds), adapting to both short (within trial) and long (within block) stimulus statistics (Ulanovsky et al., 2004). Though similar, MMN and SSA differ in the latencies and neural structures involved, with MMN responsive to complex regularities, which have been rarely tested with SSA (see Ayala and Malmierca, 2013). It is still unclear the role of SSA within regularity detection or within MMN generation.

Other than the frequency of the standard and deviant in relation to each other, increasingly complex parameters can be manipulated within the oddball paradigm. Global local paradigms have been used in which deviants could be local (e.g. the B's in a sequence AAAAB AAAAB) or global (e.g. the AAAAA in a pattern AAAAB AAAAB AAAAB AAAAA; Bekinschtein et al., 2009; El Karoui et al., 2015; Nourski et al., 2018). The occurrence of standards and deviants can be manipulated such that they occur either randomly within a sequence (i.e., AABABAAAAB) or equiprobably but at a regularly repeating interval (i.e., AAABAAABAAAB; Yaron et al., 2012); or the inter-deviant-interval can be adjusted to identify the contribution of repetition of the standard (i.e., AABAAAAAABAAAAAAAAAAAB; Costa-Faidella et al., 2011; see **Figure 1.5C**). The inter-tone-interval of the repeating standard can also be jittered to increase the irregularity of the standard (Costa-Faidella et al., 2011).

As well as this reduction in firing to the standard, an enhanced response to the deviant can occur during SSA, which has been suggested as a correlate of prediction error (Polterovich et al., 2018; Taaseh et al., 2011). Studies have used controls, within the oddball paradigm, to disentangle the effects of repetition and predictability by manipulating the context in which the standard and/or deviant lies. A 'many standards' control has been used where the standard is presented in an ascending, descending or random tone sequence such that the frequency of the standard remains the same however its context, predictable or unpredictable, differs (Fishman and Steinschneider, 2012; Parras et al., 2017; Pérez-González et al., 2020; see **Figure 1.5D**). The neural response to the standard within these different control conditions can be compared to the standard in the repeated oddball to identify the contribution of repetition suppression (the difference in response between the predictable control and repeating standard) and prediction error (the difference in response between the predictable control and deviant).

More complex sequences have recently been employed to understand regularity generated from concurrent sources and that of regularity generated from patterns over a larger range of frequencies (Sohoglu and Chait, 2016; Southwell and Chait, 2018). Using tone sequences provides the advantage of using wide-band and spectrally diverse signals to reduce the contribution of neural refractoriness and adaptation, enabling the investigation of more abstract aspects of regularity detection. Presenting concurrent tone sequences at various sequences such that the inter-tone-interval remains the same within each tone sequence provides a statistically regular acoustic scene, where jitter within each sequence increases irregularity (Sohoglu and Chait, 2016). In this paradigm neural responses and behavioural performance are measured to the appearance and disappearance of tone sequences within these regular and irregular scenes (Aman et al., 2021; Sohoglu and Chait, 2016; see **Figure 1.6A**). Consecutive tone sequences can also be presented where a frequency outlier is presented outside of the 'standard' frequency span in either a regular context (select frequencies are repeated to form a pattern) or a random context in which frequencies are randomly chosen (Southwell and Chait, 2018; see **Figure 1.6B**). These paradigms have remained deterministic but have become more rapid (i.e., 20 tones per second) compared to that of the oddball (5 tones a second), to tap more into automatic deviance detection.

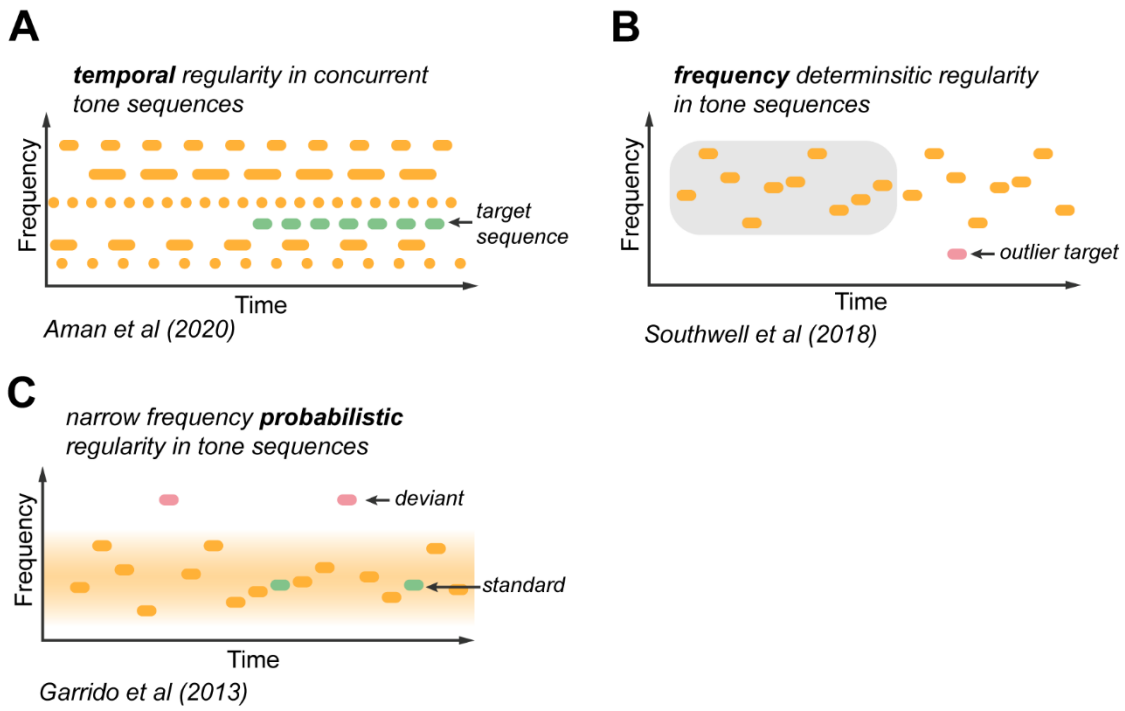

Figure 1.6: Schematic of complex paradigms to study the effects of regularity. A) Temporally regular concurrent tone sequences at various frequencies with a regular tone sequence that appears at a different frequency during the scene (green; Aman et al., 2021). B) Regular frequency pattern of 10 tones with an outlier target outside the frequency span of the pattern (Southwell and Chait, 2018). C) Sequence where the majority of tones were drawn from a distribution (shaded yellow area) and contained either a standard probe tone (green) in which the frequency was equal to the distribution centre or a deviant probe tone (pink) in which the frequency was 2 octaves above the centre of the distribution (Garrido et al., 2013).

Garrido et al. (2016, 2013) revealed the flexibility of the auditory system in detecting probabilistic regularities, as well as deterministic, by varying the mean and variance of consecutive tone sequences in frequency with a smaller variance in frequency giving rise to higher predictability and narrower frequency context. Deviants would be presented at the same frequency in both narrow and broad contexts and the MMN and behavioural performance in deviant detection measured (Garrido et al., 2013; see **Figure 1.6C**). Another complementary approach, jittered the standards (and therefore its regularity) around 1000Hz (e.g. 980 to 1020Hz in 5Hz steps; Daikhin and Ahissar, 2012). Deviants were embedded in either the sequence of fixed standard or jittered standards and an MMN measured to investigate the effects of the regularity of the standard on deviance detection.

1.3.2 Regularity detection: discovering regularity

Though deviant detection, and the neural responses that correspond with it, gives us a looking glass into what the brain tracks in terms of predictability, exactly how the brain discovers regularity is still unknown. To focus on the process of pattern extraction, Barascud et al. (2016), developed a paradigm in which stimuli were constructed as sequences of random tone-pips that switched to a regularly repeating pattern comprised of the same frequencies (RAN-REG), or regularly repeating tones that switched to a randomly drawn pattern (REG-RAN; see **Figure 1.7A**). In behavioural experiments, participants were asked to detect the change (and catch trials were included which were entirely random or regular). This paradigm departs from previous investigations that mostly used simple regularities or were based on prolonged exposure to a single pattern (often hundreds of consecutive repetitions). The stimulus preserves a balance between pattern complexity, as required for the study of rich sensory phenomena, and simplicity, which is critical for detailed modelling. The ability to model the information content of unfolding sequences is instrumental as a benchmark against which to compare human performance and for concretising hypotheses about computational underpinnings (Bianco et al, 2020; Harrison et al, 2020; Barascud et al, 2016).

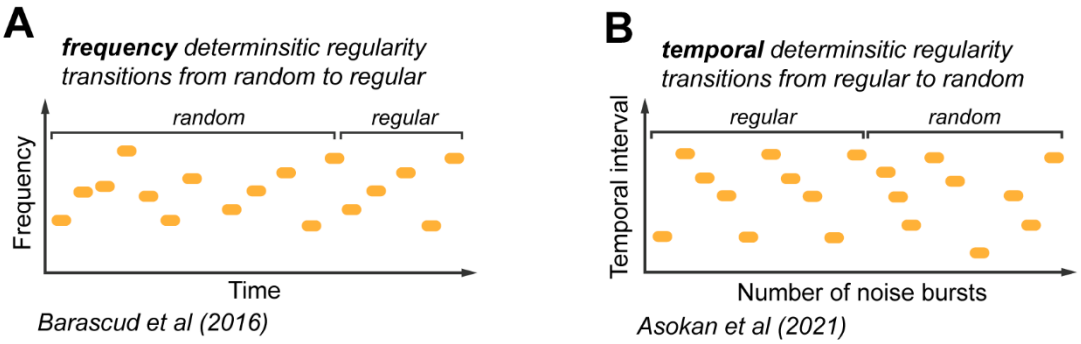

Figure 1.7: Schematic of complex paradigms to study the discovery of regularity. A) Tone sequences with randomly selected frequencies that transition to a repeated selection of frequencies (Barascud et al., 2016). B) Noise bursts that are either contain a repeating pattern of inter-noise burst intervals, or a random selection of inter-noise burst intervals (Asokan et al., 2021).

Asokan et al. (2021) on the other hand, took the time between auditory events to encode regularity and irregularity. Taking advantage of broadband noise and its ability to evoke auditory responses across larger areas of the auditory pathway, they presented frozen 20ms noise bursts with variable silent intervals that where either repeated in their duration, or random to provide either a rhythmic sequence of noise

bursts or a random sequence (see **Figure 1.7B**; note the change from spectral to temporal domain in the y-axis). In their paradigm, the sequence switched from a baseline random sequence to the rhythmic sequence and then the random sequence to which the head-fixed mouse passively listened whilst neural recordings were taken of inferior colliculus (IC), medial geniculate body (MGB) and auditory cortex (AC). Though in this study the transition between random to regular was examined, the reverse is possible within this paradigm.

Overall, the role of regularity sensitivity in sensory perception has commonly been investigated using very simple stimuli, consisting of just one or two concurrent sequences - far from the complex multi-object scenes we face in the environment. Relatively little is understood about the role of sensitivity to predictable structure in complex scenes which contain multiple concurrent objects as only in recent years have these stimuli been used in human studies, and even less have used these within animal studies. In animals studies it is often unknown whether the animal can even perceive the changes in stimulus statistics that invoke regularity.

1.4 Cellular and Circuit mechanisms: lessons from animal studies

Previously, the majority of animal work has employed simple oddball paradigms and repetitive stimuli with a focus on understanding the mechanisms behind stimulus specific adaptation (SSA) and the areas that contribute (see for a review: Nelken, 2014). Understanding how neurons respond to standard tones (predictable stimuli) and to deviant tones (a departure from predictable stimuli), allows us to learn invaluable information on how the auditory system processes regularity and predictability within acoustic input. Furthermore, parametrically changing the predictability of the stimulus affects the neural responses to the acoustic deviants, and provides insight into what features of regularity modulate neural responses. The stimuli typically used allows for tight control of acoustic input that is needed when recording from single-units with individual response properties. This single-unit resolution provides a great amount of insight into response dynamics in both a spatially and temporally defined manner.

By targeting individual areas such as MGB in the thalamus or subfields of AC, we garner a clearer understanding of how information is encoded, where it is encoded, and how it changes across the auditory processing hierarchy. In recent years there

has been a move away from simple repetitive oddball stimuli or noise bursts to tone sequences (Asokan et al., 2021; Barczak et al., 2018) and vocalisations (Perrodin et al., 2020). Coupled with recent advances in acquiring data from larger samples of single-units and more complex behavioural tasks they provide exciting new insight in to how neurons encode increasingly complex acoustic regularities.

1.4.1 Cellular mechanisms

A common observation in extracellular recordings in animals, is that responses to the standard sound within oddball paradigms change with repeated presentations. Since many of the investigated sequences have been very simple, often a repeated tone, neural adaptation or SSA, is likely a major contributor to this process (Grill-Spector et al. 2006; Briley & Krumbholz 2013; Nelken 2014). During SSA, the neural adaptation from the repeating stimulus does not generalize to other rare stimuli, even if the rare stimulus yields the strongest response within that neuron (Nelken, 2014). SSA within a neuron can be quantified using a SSA adaptation index calculated as the difference in neuronal firing rates to the standard and deviant, normalised over the sum of responses to both standard and deviants (Ulanovsky et al., 2003). The magnitude of this effect scales with the probability mismatch between standards and deviants, such that the lower the deviant presentation probability, the greater the observed SSA (Ulanovsky et al., 2003). Therefore, SSA has been proposed to be a correlate of ‘deviance detection’, an important computational task of sensory systems and is ubiquitous in the auditory system: It is found both in cortex and in subcortical stations, and it has been demonstrated in many mammalian species (Anderson et al., 2009; Antunes et al., 2010; Fishman and Steinschneider, 2012; Malmierca et al., 2009; Nelken, 2014; Taaseh et al., 2011; Ulanovsky et al., 2003).

Neural adaptation itself can be considered from the view of a single neuron where, as described in the fatigue model, there is an internal ‘gain’ mechanism where the amplitude of firing of stimulus-responsive neurons decreases (Grill-Spector et al., 2006). One mechanism that could induce this is an intrinsically generated hyperpolarisation of the membrane potential resulting in a reduced sensitivity to synaptic inputs (Sanchez-Vives et al., 2000a). In a complementary paper, Sanchez-Vives et al. (2000b), identified that this long term hyperpolarisation is due to the increased intracellular concentration of sodium and calcium ions that occur during firing leading to the activation of calcium- and sodium-dependent potassium currents

causing potassium ions to move outside the cell initiating hyperpolarisation of the neuron. This tends to be short lived, decaying over hundreds of milliseconds but can potentially last tens of seconds (Schwindt et al., 1989).

Yet, neurons do not operate in isolation, and the described intrinsic mechanism cannot account for all forms of adaptation, particularly SSA (Sanchez-Vives et al., 2000a). Synaptic depression, typically of pre-synaptic inputs, has been implicated in SSA (Nelken, 2014) and can be caused by a decrease in the presynaptic calcium influx and the depletion of vesicles containing neurotransmitters, lasting tens of seconds (Grill-Spector et al., 2006; Schneggenburger et al., 2002). Furthermore, studies have suggested that adaptation can occur through a tonic mechanism, by a decrease in the excitation received by a cell through an activity-dependent decrease in synaptic efficacy (Carandini, 2000; Carandini and Ferster, 1997). Overall, we see that both intrinsic, such as membrane conductance, and external factors, such as pre-synaptic inputs, can modulate a neurons response to a repeating stimulus.

1.4.2 Circuit mechanisms

Neurons can form various circuits with one another, creating feedforward or feedback inhibition or excitation, with many different configurations of inputs to each neuron. Animal studies provide a unique opportunity to understand the mechanisms underlying regularity detection and multiple studies have revealed a differential effect of different inhibitory neurons underlying regularity detection. Animal models allow targeting of precise neuronal subtypes, and spikes recorded by electrophysiology can be divided into putative excitatory broad-spiking or inhibitory narrow-spiking neurons by measuring spike width.

A study using this technique identified that putative inhibitory A1 neurons, rather than excitatory neurons, showed a larger index of neuronal mismatch (the difference in neural response between standard and deviant tones; Pérez-González et al., 2020). They suggested that these inhibitory neurons mostly contribute to deviance detection correlates in the lemniscal pathway, whereas both putative excitatory and inhibitory contribute to deviance detection in non-lemniscal areas (Pérez-González et al., 2020; see **Figure 1.8** for a diagram of the lemniscal and non-lemniscal auditory pathways). Emerging evidence suggest that it is these somatostatin-positive interneurons (SOMs) that contribute to the selective reduction

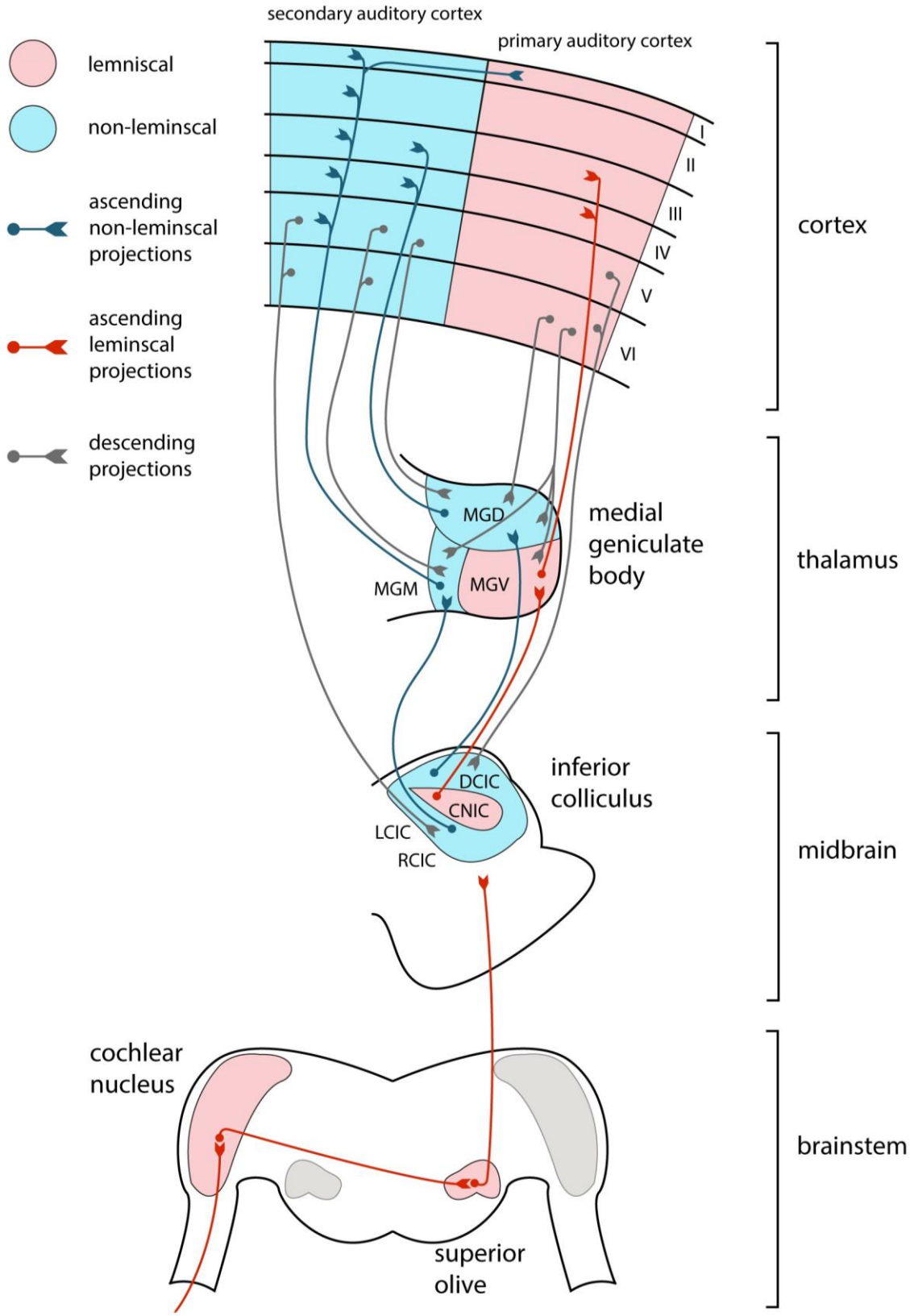

Figure 1.8: Simplified schematic of the lemniscal and non-lemniscal pathway of the auditory system. A diagram of the auditory pathway coloured by lemniscal (red) and non-lemniscal (blue) regions. The cochlear nucleus projects via the lemniscal pathway to the CNIC of the midbrain, then to the MGV of the thalamus and then finally to layers III and IV of auditory

cortex. Projections descend (grey) from layers V and VI of auditory cortex to all regions of the medial geniculate body and non-lemniscal inferior colliculus. Non-lemniscal projections ascend up the pathway from the inferior colliculus to the medial geniculate body and to layers I to V of auditory cortex. MGD: dorsal division of the medial geniculate body; MGM: medial division of the medial geniculate body; MGV: ventral division of the medial geniculate body; DCIC: dorsal cortex of the inferior colliculus; CNIC: central nucleus of the inferior colliculus; LCIC: lateral cortex of the inferior colliculus; RCIC: rostral cortex of the inferior colliculus. Adapted from Carbajal and Malmierca, 2018.

of excitatory responses to frequent tones in oddball paradigms, leading to more efficient processing of deviants (Natan et al, 2015; Wood et al, 2017). Whereas parvalbumin positive interneurons (PV+) are insensitive to tone repetition but contribute a reduction to excitatory responses to both standard and deviant tones (Natan et al., 2015; see for a model: Park and Geffen, 2020).

Recent work by Yarden et al. (2022), performed two-photon targeted cell-attached recordings to characterise and target PV+, SOM and vasoactive intestinal polypeptide (VIP) interneurons in layer 2/3 and serotonin receptor 5HT3a-expressing interneurons of layer 1 of auditory cortex. They identified an early SSA response in all cell subtypes but interestingly identified a late response, typically stronger for the standard, in only the layer 2/3 interneuron subtypes, with PV+ interneurons contributing the majority of spikes for both standards and deviants. Through circuit dissection, by targeted optogenetic silencing of each subtype, they identified that the reduction of pyramidal neuron responses to the standard is driven mostly by the reduction in excitatory input they receive rather than through inhibition. Supressing PV+ neuron responses facilitated pyramidal responses to the deviant rather than the standard. Therefore, it is the relative sizes of responses to standards, deviants that are modulated by the inhibitory network, therefore shaping SSA rather than creating it.

Mehra et al. (2022) introduced periodicity to the oddball paradigm in which the deviant was periodic or random, to understand the role of long-term adaptation time scales, adaptation to entire stimulus structures, and the role of PV+ and SOM interneurons on this process. Extracellular single-unit and two-photon Ca2+ imaging recordings in layer 2/3 neurons of the mouse showed a preference for the random stimulus, yet a subset also showed preference for the periodic. When they examined the functional connectivity between excitatory neurons (EX) and the PV+ and SOM neurons, PV+ and SOM neurons showed differential control. EX-PV showed denser

functional connectivity for periodic stimuli and EX-PV and EX-SOM showed a strong role in long-term time scale context specific modulation.

Circuit models have been created to attempt to model the phenomena of SSA. One simple model that has been used to explain SSA is the adaptation of narrowly tuned modules (ANTM; see for a review: Nelken, 2014). For example, a widely tuned neuron may integrate multiple narrowly tuned inputs, which if repeatedly stimulated adapts whilst other inputs remain unadapted, generating SSA. However, this does not explain deviance detection as regularity of the standard does not play a role in this model in shaping the responses to the deviant, with real neural responses larger than predicted by the model for deviants (Nelken, 2014; Taaseh et al., 2011).

Now the decreased spike rate observed during SSA is thought to be due to a dual effect of an increased failure to spike to the standard tone, and an overall decreased firing rate due to synaptic depression and/or depression through recurrent networks (Yarden and Nelken, 2017). In the proposed recurrent network auditory cortex is split into 'cortical' columns (each column tuned to a specific frequency) where all neurons within the column are connected to all others, allowing spikes to propagate between columns (Loebel et al., 2007; Yarden and Nelken, 2017). This widens the tuning of cortical neurons due to cortico-cortical connections rather than through the receipt of multiple thalamic inputs. During activation of the 'standard' column, the column whose best frequencies was the standard frequency, responses of neurons in the column to the standard tones rarely propagated past the standard column due to resource depletion and thereby lay within a depressed state. Presentation of a deviant, however, can evoke a population spike in the deviant column, which can propagate to other parts of auditory cortex (Nelken, 2014). This model however cannot explain sensitivity to predictability or periodicity, where if a deviant or standard is presented in a regular context, neural responses to both standard and deviant are less than that if presented in a random context (Yaron et al., 2012).

Generally, it seems that the effects of repetition suppression within excitatory neurons seem to be inherited from subcortical connection rather than through the inhibitory cortico-cortico network. The differential control of the various inhibitory subtypes such as PV+, SOM and VIP interneurons, through their circuit interactions, then modulate the response to the standard and deviant. Whether this modulatory

control is generated *de novo* in auditory cortex or is in itself modulated lower within the hierarchy is still unclear. Yet we can look to how SSA and prediction error is encoded and is changed along the auditory hierarchy, to give us insight into this process.

1.4.3 Inferior colliculus and auditory thalamus

SSA was first reported in neurons in A1 of the cat, where neuronal firing demonstrated stronger adaptation to the standard than the deviant, such that deviant responses were enhanced relative to the standard. However, targeting specific regions within the auditory pathway, studies have shown that neurons in subcortical stations exhibit SSA, both in IC (Malmierca et al., 2009; Pérez-González et al., 2005; Valdés-Baizabal et al., 2021; Zhao et al., 2011) and thalamus (Anderson et al., 2009; Antunes et al., 2010). While weakly present in the ventral division of MGB, it is much stronger in medial and dorsal divisions raising the possibility that it is inherited via descending connections from auditory cortex. Evidence from cortical deactivation studies have suggested that rather than SSA being propagated from AC to subcortical stations that AC has more of a modulatory role on neurons exhibiting SSA (Anderson and Malmierca, 2013; Antunes and Malmierca, 2011). For example, reversibly silencing by cooling auditory cortex whilst recording in MGB revealed that mean SSA levels were not significantly changed but instead showed changes in scaling its sensitivity suggesting that auditory cortex performs gain modulation on SSA within MGB neurons instead of inheriting SSA directly from AC (Antunes and Malmierca, 2011). In addition, recording from IC during inactivation of AC revealed half of the neurons showed changes in SSA sensitivity in either direction with only a small number showing complete abolishment of SSA (Anderson and Malmierca, 2013). These studies suggest that SSA does arise *de novo* subcortically and, though may be weaker than in AC, it does suggests that local circuits in subcortical stations may generate SSA (Ayala and Malmierca, 2013).

1.4.4 Auditory cortex

SSA itself was first described in primary auditory cortex (Ulanovsky et al., 2003) and has been robustly reported across labs and species (Behrens et al., 2009; Szymanski et al., 2009; Taaseh et al., 2011; Ulanovsky et al., 2003). The magnitude of SSA in A1 scaled with the probability mismatch between standards and deviants, such that the lower the deviant presentation probability, the greater the observed SSA index (Ulanovsky et al., 2003). It has also been argued that SSA is generated *de novo*

within A1 as SSA subcortically is mostly confined to the non-leminscal pathway and A1 receives most of its thalamic input from lemniscal MGB (Yarden and Nelken, 2017). Furthermore current source density (CSD) analysis of laminar AC identified rapid SSA in all cortical layers which became more pronounced in infragranular layers, suggesting multiple sites for SSA in AC with intracortical mechanisms mostly contributing to the phenomenon rather than thalamic input (Szymanski et al., 2009).

While adaptation is a key component of SSA, increased firing to the deviant can be observed, encoding a correlate of 'surprise' in the form of a prediction error signal (Parras et al., 2017; Taaseh et al., 2011; Yaron et al., 2012). Within primary auditory cortex studies have used a variety of approaches to attempt to tease apart the contribution of adaptation (i.e. repetition suppression) and enhancement of firing to rare stimuli (i.e. prediction error) to the difference in firing rate to the standard and deviant (Carbajal and Malmierca, 2018). For example, Fishman and Steinschneider (2012) recorded from A1 in monkeys and found that responses to rare deviant tones presented within a series of the same standard tones evoked similar responses as when embedded in a 'many standards' control condition, wherein the same tones evaluated in the oddball context were presented rarely but were not perceptually distinguishable as deviants. They concluded that the deviant response in A1 reflects adaptation rather than a prediction error signal. Contrastingly more recent work using laminar probe recordings, again in macaques, observed deviant-related activity in sites in A1 that were unresponsive to standards in the first place, ruling out adaptation as an explanation of the observed effects and suggesting that primary auditory cortex may be able track regularities and their violation (Lakatos et al., 2020).

To further tease apart the contribution of repetition suppression vs. prediction error signalling, cascade' sequences (a predictable increase or decreasing in frequency tone sequences; see **Figure 1.5D**) have been employed which enables the recording of the neural response to rare but predictable sounds to be compared to rare and unexpected sounds. A genuine prediction error signal can be identified by considering the difference in response to the same tone in a deviant context versus a cascade sequence, while repetition suppression (i.e. adaptation) can be identified by examining the difference in response to the same tone in a standard versus cascade context (Parras et al., 2017). Parras et al. (2017) identified repetition suppression in all recorded sites (IC, MGB and AC) but only prediction error signalling in the non-

lemniscal (non-primary) AC. This prediction error signalling may change how we investigate the puzzle of SSA and how the auditory system encodes regularity but looking to how these change across the auditory hierarchy can give us more insight into its underlying process.

Moving beyond SSA, recent studies have looked at the neural mechanisms supporting the detection of regularity. Barczak et al (2018) utilized pure tone sequences embedded in noise bursts which transitioned from randomly occurring tones to regular patterns. Recording in A1 of passively listening macaques identified oscillatory entrainments within A1 at the pattern repetition rate and a decrease in local field potential (LFP) and multi-unit activity. In addition, oscillatory entrainments to the pattern presentation rate were reported in A1, but not in MGB. Recordings in the medial pulvinar, a higher-order thalamic nucleus, demonstrated that neurons here also locked to the temporal structure of pattern repetition. This pattern-induced modulation of multi-unit activity occurred earlier in the pulvinar than in A1. Such a pattern would be consistent with a top down cortico-subcortico-cortical route, suggesting a top-down directionality of regularity detection via neuronal oscillations (Barczak et al., 2018). Within the pulvinar these oscillations also occurred at a similar timing to the correlates identified in previous human studies (Barascud et al., 2016) showing entrainment after the first repeat. However, it remains to be determined whether the pulvinar itself detects regularity or whether it is relaying a signal from one of the many higher cortical areas that project to the pulvinar such as parietal or prefrontal cortex (Cappe et al., 2009; Romanski et al., 1997) and whether large changes in multi-unit activity or oscillations would be observed with shorter repeated sequences.

Asokan et al., (2021) employed an elegant stimulus design where they presented noise tokens at either randomly drawn intervals or in a temporal pattern of repeating temporal intervals (see **Figure 1.7B**). Neurons in mouse A1 showed more rapid spike latencies and dampening to noise bursts presented in the regular context than in the random one. These effects were only observed for patterns of up to 8 elements, in which they suggested the spiking dynamics in A1 in response to the regular stimuli are likely products of other circuits that respond directly to regularity such as cortical GABAergic neurons, as cortical spiking timescales are short at approximately 20ms whereas the timescale of repetition here is 800ms (Asokan et al., 2021). These changes were not observed within IC but only marginally in MGB which

could suggest the involvement of an additional corticothalamic circuit (Asokan et al., 2021).

A handful of studies have investigated the neural correlates of regularity detection beyond auditory cortex. Just as the influence of regularity increases through the lemniscal auditory pathway, non-primary auditory cortex shows a yet stronger influence (Parras et al., 2017). Recordings in the auditory cortex, frontal gyrus and amygdala in macaques have indicated that oddball responses are present in all three areas but that the magnitude, latency and stimulus specificity varied. Auditory cortex responses were largest and earliest, but specific for the frequency of the stimulus, while those in prefrontal cortex (PFC) and basolateral amygdala were weaker and longer in latency, but stimulus independent (Camalier et al., 2019). In contrast, another study (Casado-Román et al., 2019) identified stronger prediction error signalling to oddball sequences in medial prefrontal cortex neurons compared to that of neurons in the auditory pathway (IC, MGB and AC; Parras et al., 2017). Additionally, the prediction error signalling in medial PFC neurons appears after approximately 100ms whereas in AC the response emerges just after a few milliseconds suggesting that the processing within these two regions occur in a sequential manner where spectral deviances are detected within AC and then PFC identifies more abstract deviations (Casado-Román et al., 2019).

Across these studies there seems to be a consensus that as you ascend the lemniscal pathway to auditory cortex and then enter non-lemniscal regions and frontal areas that there is an increase in the amount of prediction error signalling, predominantly after non-primary regions of auditory cortex. However, it is hard to disentangle how the regions are involved due to the interconnectivity of non-primary regions with various auditory and non-auditory regions. Therefore it is unclear where this signal may initially be generated, or what networks are primarily responsible.

1.5 Brain networks that contribute to regularity detection: lessons from human studies

While brain imaging lacks the spatial resolution of invasive neurophysiology and cannot resolve the mechanistic details of the circuits responsible for detecting and representing acoustic regularities, they do provide an unmatched ability to determine the brain networks responsible. Looking across animal studies it seems apparent that

while simple phenomena such as deviant detection with oddballs might emerge within AC, there is considerable evidence for top-down involvement from other areas beyond the classic auditory cortex. Human imaging provides candidate regions for further study in animals, such as inferior frontal gyrus (IFG), parietal cortex and hippocampus (HPC). In this review, however, I will mainly be focusing on auditory cortex and hippocampus.

1.5.1 Auditory cortex and frontal areas

Research using simple oddball paradigms has consistently reported the involvement of temporo-frontal areas in the detection of any discriminable change in auditory stimulation (see for a review: Garrido et al., 2009; Heilbron and Chait, 2018; Näätänen et al., 2007). Several magnetoencephalography (MagEG) and electroencephalography (EEG) studies, localised primary and secondary auditory areas and right IFG as major sources of MMN (Dietz et al., 2014; Garrido et al., 2008, 2007; Kiebel et al., 2007). Functional magnetic resonance imaging (fMRI) (Molholm et al., 2005; Opitz et al., 2002; Schönwiesner et al., 2007; see also evidence from lesion studies: Alain et al., 1998) and intracranial EEG studies (Dürschmid et al., 2016; Nourski et al., 2018), which offer higher spatial resolution than EEG/ MagEG, have supported these findings, although the contribution of IFG is not always present (see fMRI: Lumaca et al., 2020.; MagEG: Quiroga-Martinez et al., 2020).

Moving on from simple oddball paradigms (see **Figure 1.5A**), Bekinschtein et al. (2009) introduced a 'global/local' paradigm, to distinguish between deviant effects occurring over a short time scale with a single stimulus change from those unfolding over many seconds. Deviants could be local (e.g. the B's in a sequence AAAAB AAAAB) or global (e.g. the AAAAA in a pattern AAAAB AAAAB AAAAB AAAAA; see 1.3.1 for discussion on these paradigms). Using EEG, intracranial recordings, and fMRI they found automatic local deviant effects in primary and non-primary auditory cortex, with global deviant effects occurring in frontal cortex. Within auditory cortex, some distinction between primary and non-primary auditory cortical processing of regularity was made by Nourski et al. (2018) when considering high gamma activity (70-150 Hz; thought to reflect local neuronal activity). Global deviant effects in the high gamma range were largely absent in primary auditory cortex, in posteromedial Heschl's gyrus, but present in higher auditory areas such as the lateral superior temporal gyrus (STG).

Accordingly, another study using an oddball task indicated that responses to deviant sounds in the oddball context were mainly driven by tone-frequency differences between standard and deviant in primary cortex, but were dependent on inter-stimulus interval in non-primary auditory cortex (Kropotov et al., 2000). A recent study that used intracranial electroencephalography (iEEG), combined surface and depth electrodes, and recorded high gamma activity to functionally map the temporal integration window across auditory cortex (Norman-Haignere et al., 2022). They showed acoustic temporal integration widths increased from primary to non-primary regions (median: 74 to 274ms). These functional differences could aid in detecting predictability across many different time scales from to short oddball pattern to longer more complex repeating patterns across a range of frequencies.

With the use of tone clouds that transition from a random to regular sequence (see **Figure 1.7A**), Barascud et al. (2016) identified increases in power in the fMRI signal over AC during the regular sequence compared to the random sequence. This was supported by their further MagEG experiments that revealed increases in the root mean square (RMS) amplitude in the MagEG signal (see **Figure 1.9A**), again localised to AC (bilaterally) but also HPC (bilaterally), and IFG (right hemisphere). This increase in power varied with the complexity of the pattern, with the smallest patterns of 5 tones eliciting the largest increase and the largest patterns tested of 15 tones creating the smallest increases power. The time point at which the signal to the regular sequence increases and diverges from the response to the random sequence, occurred approximately one cycle and three tones from onset of the pattern. This power increase, modulated by the length of the pattern, and the timing of onset was further confirmed with EEG experiments performed by Southwell et al. (2017, 2018, and 2019).

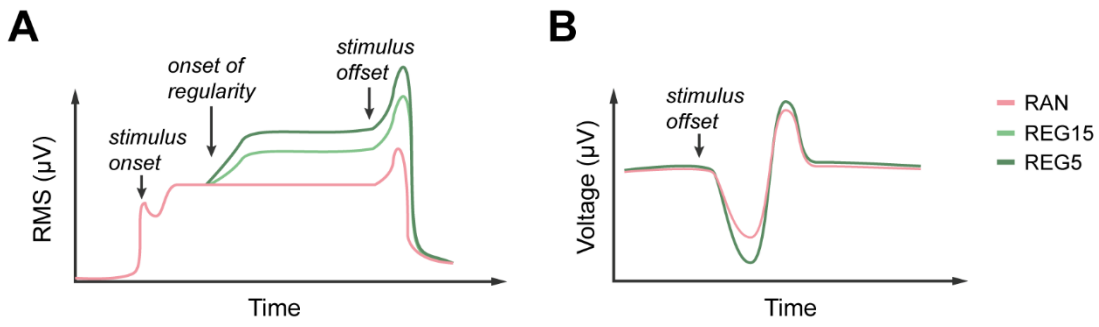

Figure 1.9: Simplified schematic of neural responses to random tone sequences and random tone sequences that transition to regular tone sequences. A) Schematic of an MagEG signal to a random sequence (pink), a random to regular sequence, with a short pattern of five tones (dark green) and a long pattern of 15 tones (light green). Stimulus onset evoked an increase in power and then plateaus during the random sequence. At the transition from random to regular (onset of regularity), the MagEG signal increases power, larger for shorter patterns (Barascud et al., 2016). B) Schematic of the normalised EEG response to the offset of either the random (pink) or regular sequence (dark green). The offset is larger for the regular sequence (Southwell, 2019).

Southwell et al. (2018) investigated the nature of this signal further, with similar random and regular sequences, and identified differences in the offset response to the regular and random sequences. REG sequences produced larger offset-responses in the EEG signal than RAN sequences, with the authors proposing that this is due to the offset of the sound being more 'surprising', as it violates the expected next tone, in a regular context compared to that of the more volatile random context (see **Figure 1.9B**). Analysis of the oscillatory power in these EEG responses to RAN and REG sequences showed both larger oscillations in the pattern repetition rate in the REG sequences reflecting the periodicity of the REG sequences when compared to matched RAN sequences (Southwell, 2019). This oscillatory entrainment to the REG patterns could explain behavioural detection (Barascud et al., 2016; Southwell, 2019).

As we move from auditory areas in the temporal lobe that are sensitive to changes in acoustic features, (Hofmann-Shen et al., 2020; Molholm et al., 2005) to more frontal areas, there is an increased sensitivity to statistics within the environment with some distinction of labour between temporal and frontal areas (Bekinschtein et al., 2009; El Karoui et al., 2015; Nourski et al., 2018; Wacongne et al., 2011). Dürschmid et al. (2016) showed clear deviant-related responses over both the temporal and frontal cortex, with temporal sites responding to any change in the immediate history, and IFG being exclusively sensitive to globally unpredictable changes. Using a similar paradigm, other electrocorticography (ECoG) work (El Karoui

et al., 2015; Nourski et al., 2018) found that local deviant effects were focused mainly on auditory primary and non-primary areas, while global deviant effects were more concentrated on higher-level regions (e.g., in Nourski et al 2018: insular cortex, superior temporal sulcus, middle temporal gyrus, supramarginal and angular gyrus) and frontal recording sites.

The temporo-parietal network has also been implicated in analysis of temporal structure of sounds. Molholm et al. (2005) found that parietal cortices contributed to the generation of duration MMN response, as well as pitch MMN (see also Southwell and Chait, 2018). Sohoglu and Chait (2016) showed that, during (passive or active) listening, auditory and parietal areas showed greater activity when stimuli were characterised by regular than irregular rapid temporal structures. Similarly, parietal cortex has also been associated with bottom-up figure-ground processing when the figure is defined by temporally repeatable and fast evolving spectral components in an otherwise randomly structured background (Teki et al., 2016, 2011) Thus, the parietal cortex may play an automatic role in the representation of information integrated over frequency-time features, thus contributing to the perceptual organization of auditory streams (Sohoglu et al., 2020).

Largely these studies suggest that auditory cortex is not solely involved in regularity detection, but rather a large network of brain regions that recruit more frontal areas such as IFG, parietal cortex, that may work in a hierarchical system to learn higher order statistical rules. One brain region in this network that has been implicated in regularity detection (Barascud et al., 2016), and recently in auditory processing is the hippocampus.

1.5.2 Hippocampus

The hippocampus' role in spatial navigation and episodic memory has already been established, but it also has an important role in auditory processing (see for a review: Billig et al., 2022). In a second study, Barascud et al. (2016) used MagEG recordings during the same sequences of regular and random tones. Due to higher temporal resolution, compared to fMRI, they were able to show the additional contribution of bilateral hippocampus during the early phase of regularity detection, consistent with recent suggestions of the role of the hippocampus in temporal integration of acoustic patterns (Geiser et al., 2014). While its most well-established roles relate to long-term memory and spatial navigation, the hippocampus has been

shown to be responsive to sounds in rodents and humans (Aronov et al., 2017; Başar-Eroglu and Başar, 1991; Eidelberg et al., 1959; Green and Arduini, 1954; Halgren et al., 1980; Martorell et al., 2019; Vinogradova, 1975; Xiao et al., 2018) especially when they are to be associated with other stimuli (Berger et al., 1976; Logan and Grafton, 1995; Olds and Hirano, 1969) or retained in working memory over several seconds (Ahmed et al., 2020; Kumar et al., 2021, 2016). This is the case despite somewhat indirect connections from auditory cortex, at least in primates (Munoz-Lopez et al., 2010; Rocchi et al., 2021).

In the visual domain, the hippocampus responds to novel stimulus configurations (Kumaran and Maguire, 2007) and indexes the uncertainty of stimulus streams (Harrison et al., 2006; Strange et al., 2005). Recent neuroimaging work has extended some of these findings to the audition, identifying that the hippocampal Blood oxygenation level dependent (BOLD) signal tracks the interaction between uncertainty and surprise associated with unfolding musical chord sequences (Cheung et al., 2019). A role for the hippocampus in learning auditory associations is supported by neuropsychological studies in which patients with hippocampal lesions were impaired in learning statistical relationships between tones or syllables (Covington et al., 2018; Schapiro et al., 2014). There is also evidence that the hippocampus represents the content of auditory sequences, rather than simply learning the associations or computing statistics over them. Over long timescales, hippocampal representations of speech sounds develop such that items that routinely occur in temporal proximity are encoded by increasingly similar activity patterns (Henin et al., 2020; Kalm et al., 2013). Predicted visual content can also be decoded from hippocampal activity patterns (Kok et al., 2019; Kok and Turk-Browne, 2018), although this has not yet been demonstrated for sound, nor for stimuli presented at the fast rate of the Barascud et al. (2016) study.

Nevertheless, there is reason to think that the hippocampus can also support predictive representations of such rapidly unfolding sound sequences. Hippocampal place cells (O'Keefe and Dostrovsky, 1971) and grid cells in adjoining entorhinal cortex (Hafting et al., 2005) fire selectively when an animal is in a particular physical location. These populations can also represent non-spatial dimensions of experience when behaviourally relevant (Bao et al., 2019; Constantinescu et al., 2016; MacDonald et al., 2011; Solomon et al., 2019; Umbach et al., 2020), including tone frequency

(Aronov et al., 2017). Importantly, the phenomenon of theta phase precession (O'Keefe and Recce, 1993; Qasim et al., 2020) allows temporally compressed sequences to be represented in hippocampus, with past, present, and future experience being encoded at successive phases of a theta cycle. This indicates that hippocampus has the capacity to learn and store representations of rapidly unfolding stimuli, which could form the basis for predictive activity during exposure to regular patterns of sound.

A recent study, by Tzovara et al (2022), directly tested the responses of neurons within hippocampus to patterns within acoustic stimuli. They presented sequences of pure tones with predictable and unpredictable frequencies to epileptic patients with macro-contacts and micro-wires to record local field potentials and spiking activity in hippocampus. With these macro-contacts they identified larger responses in the 1-8Hz band to predictable sequences within hippocampus. Micro-wire recordings showed the majority of hippocampal neurons responding selectivity to deviant sounds, with parahippocampal/entorhinal neurons responding to standard sounds (Tzovara et al., 2022). Tract-tracing studies in primates also suggest that auditory cortex projects directly to parahippocampal cortex (Munoz-Lopez et al., 2010).

How each of these areas, auditory cortex (primary and non-primary subfields), IFG, parietal cortex and HPC differ in their contribution to auditory regularity processing is not yet clear. However, there is increased evidence that hierarchical processing through the recruitment of these different brain regions is involved. Models such as dynamic causal modelling (DCM) studies (Garrido et al., 2009, 2008, 2007; Phillips et al., 2016, 2015) have found that simple regularities that produce an MMN response is best explained by the model updating at different hierarchical – intraregional and interregional – levels.

1.6 MODELLING REGULARITY DETECTION

Experimental studies provide us with invaluable data to understand how real behaviour and neurons behave when exposed to these acoustic patterns. However, models can provide a broader understanding of the cognitive and biological processes underlying this process and generate testable predictions for neural signals of regularity.

Models based on prediction by partial matching (Information Dynamics of Music (IDyOM), Prediction by Partial Matching (PPM); (Pearce, 2018, 2005) – a Markov modelling method (Cleary and Witten, 1984) that represents the statistical structure of input sequence by segmenting them into sub-sequences (n-grams) of increasing order have been readily applied to understanding how the auditory system deals with processing regularity, particularly with music. In the case of deterministic frequency patterns, the model assumes that the auditory input can be represented as a sequence of symbols drawn from a discrete 'alphabet'. IDyOM then statistically learns variable-length sequential dependencies and while processing the sequence event by event (or symbol by symbol), generates expectations for the next event. The expectations are presented in the form of a probability distribution such that an event that followed a repeating pattern and was present in the previous repetition would have a high probability of occurring. This probability distribution can be represented as 'information content' which reflects how unexpected the model finds a given event in a particular context, such that event with a high probability of occurring will have low information content. The authors were successful in reproducing human behaviour in a variety of paradigms and therefore they suggested that listeners monitor the predictability of each incoming stimulus against the n-gram statistics stored in memory as a generative probabilistic model. The neural underpinnings for these various representations, and whether they engage overlapping machinery are critical questions for future work. Deterministic structure may draw on the formation of sensory memory traces whilst more stochastic patterns will involve more abstract representations and different computational architecture.

Further considerations relate to the timescale over which evidence regarding the patterns is gathered. Some patterns occur over the course of milliseconds while others unfold over seconds, minutes or longer. This places different demands on evidence accumulation and memory mechanisms and may recruit different perceptual or neural processes (Cowan, 1984; Santolin and Saffran, 2018). An updated PPM model (PPM-Decay) was developed that introduced memory decay as a parameter, so that more weight is allocated to the most recent observations (Harrison et al., 2020). This decay parameter helps to explain why behaviourally, human subjects struggled detecting patterns of 15 to 20 tones in length, their reaction times longer than those predicted of the original PPM model (Barascud et al., 2016). The PPM-Decay model

identified that a 15-tone buffer, short and high-fidelity memory, seemed to describe this behavioural 'lag' for longer pattern lengths, suggesting that the human auditory system begins to fail at patterns of longer than 15 tones. The model is a powerful tool that can be used to model behavioural detection of patterns in human and animal models.

One major disadvantage to the PPM model is that it can only consider a small set of discrete unordered events and therefore cannot generalise to continuous acoustic features such as pitch or sound level (Skerritt-Davis and Elhilali, 2018). Skerrit-David and Elhilali (2018) developed a Bayesian sequential prediction model to tackle this limitation and identify change points, or transitions from low to high entropy within the tone sequence (Adams and MacKay, 2007). At each time point the model builds a predictive distribution of what the next tone could be which weights different hypothesises of when the transition has occurred, if it has occurred (Skerritt-Davis and Elhilali, 2018). This model, whilst building predictive distributions from higher-order statistics, such as the covariance between successive tone pitches, was able to capture all human behaviours tested in the detection of the transition from low to high entropy sequences and vice versa.

Whether the process underlying regularity detection in the brain uses a Bayesian framework that holds onto multiple hypotheses, or a Markov model with memory decay parameters is unknown. However, what is known is that the brain can follow and form predictions based on the statistical rules it has learnt about the incoming acoustic stimulus.

1.7 UNDERSTANDING THE NEURAL MECHANISMS UNDERLYING AUTOMATIC DETECTION OF DETERMINISTIC REGULARITIES

Currently studies have focused on either computational models or human studies utilising psychophysics, EEG, MagEG or fMRI on the role of regularity within ASA and how regularity is detected and encoded within the brain. Due to the limitations of these techniques, it is still unclear how single neurons themselves encode regularity within the auditory pathway and especially within auditory cortex. The published studies discussed above have implicated areas within and beyond auditory cortex, such as hippocampus, in regularity detection but their functional role remains unknown. Thereby recording neural responses that target various subfields of AC and non-

auditory areas such as hippocampus, will give a deeper insight into the neural networks underlying regularity detection. The effect of behaviour must also be considered to understand the perceptual limits of the model used and how they relate to human behaviour, and to distinguish whether regularity detection is completely pre-attentive or if neural correlates are modulated by behavioural responses to regularity.

In this thesis I aim to understand how the brain detects and maintains a representation of deterministic acoustic regularity. To do this I need to present stimuli that allows me to study automatic unconscious sequence processing and to probe how the predictability of the sequence modulates behaviour and neural correlates. The rapid random to regular tone clouds, used by Chait and colleagues (Barascud et al., 2016; Southwell et al., 2017; Southwell and Chait, 2018), permits me to parametrically control the frequency content and length of the repeating patterns. With these stimuli in mind, I can examine the perceptual capabilities of the auditory system in detecting transitions from random to regular sequences with a behavioural task. Using an animal model, I can execute high density neural recordings from multiple subfields of auditory cortex, to understand the roles of primary and secondary areas in representing these acoustic patterns. Lastly, with high-density linear probes I can record from both auditory cortex and hippocampus simultaneously to understand the role of hippocampus in the statistical learning of these acoustic patterns.

Ferrets are an ideal model to achieve these aims as they can be trained on complex auditory tasks and it has been shown that ferrets are behaviourally sensitive to repetitions of broadband noise samples, making them a good candidate for behavioural regularity detection tasks (Saderi et al., 2019). Unlike mice, a ferrets hearing range overlaps that of humans (ferret range: approximately 20Hz to 44kHz; human range: approximately 20hz to 20kHz; Heffner and Heffner, 2007; Kavanagh and Kelly, 1988), and with larger cortical anatomy allows multiple large-scale implants that can perform electrophysiological recordings across multiple regions. Substantial literature on the ferret regarding the anatomy of neural structures in the form of an atlas (Radtke-Schuller, 2018) and the functional organisation of sensory areas such as the tonotopy of auditory cortex are also available (Bizley et al., 2005).

1.7.1 Thesis outline

To bridge the gap of regularity detection at a neuronal level, developing a behavioural paradigm using an animal model, in this case the ferret, is a first crucial

step. This will allow me to record the activity of single-units and the local field potential in multiple brain regions. Whilst neural signatures have been found in passively listening humans of regularity detection, currently it is unknown whether animals can detect regularity or their limits on detecting increasingly complex patterns. I hypothesise that ferrets, given their sensitivity to repetition as described previously, will be able to detect the transition from random tone sequences to regular tone sequences. Furthermore, performance will likely be perturbed with increasing complexity of the pattern. Regarding neural correlates, I hypothesise that there will be changes in spike timing and firing rate, predicting greater synchronous spike timing in the presence of regularity, and increased oscillatory power at the pattern rate in the local field potential. Previous human and animal studies investigating regularity detection provide conflicting predictions as to whether the firing rate will show adaptation or facilitation in the context of regularity. The aim of this thesis is to determine the relationship between regularity and neural firing.

In chapter 2, I establish the ferret as a suitable animal model by assessing its ability to detect acoustic patterns through a behavioural task. I trained a total of six ferrets on a GO/NO-GO task to detect a transition from a random tone sequence to a regular tone sequence. I show that ferrets can consistently perform this task above chance, validating their use as an animal model for the behavioural and neural study of acoustic regularity detection. Having determined ferrets can detect regularity, I assessed how modulating the complexity of the pattern, by increasing the pattern length, affected their ability to perform this task. Ferrets showed perturbed performance and reaction time as the pattern length increased from 3, through to 7 tones. To investigate the cues that the ferret uses to detect this transition from random to regular, I present control stimuli that evoke similar changes in frequency content but do not provide deterministic regularity as a cue, showing that ferrets are in fact using the deterministic patterns to perform the task. I also explore how the number of unique frequencies can also modulate behaviour, with less unique frequencies enhancing performance. I then describe their behaviour in the context of the PPM-Decay model, and why their behaviour may differ to that of human subjects due to memory constraints. Lastly I perform control experiments in human subjects, to test the effects of an expanded frequency range (compared to that of previous human work) on

regularity detection showing no differences in performance but instead perhaps increases saliency due to reduced cross-frequency adaptation.

In chapters 3, 4 and 5, I consider the neural responses recorded in these trained animals. Animals were either implanted with multi-electrode arrays (n = 3, WARP-32 Neuralynx) to record from multiple subfields of auditory cortex, or high-density linear probes (n = 2, Neuropixels probes, 2.0) to record from multiple depths of auditory cortex and hippocampus itself. In chapter 3, I consider the local field potential, as this provides the best bridge to human imaging studies. I show that in comparison to the human studies that there is no change in the evoked LFP between random and regular sequences. However, oscillations at tone presentation rate are present and lower during regularity, whereas oscillations at the pattern rate are higher during regularity and are also modulated by the behavioural response of the animal. Analysis of the time course of these pattern rate oscillations show they occur almost immediately after the transition from random regular and continue on after the offset of the stimulus.

In chapter 4, I ask whether single-units can differentiate between tones in a random vs. regular context using the animals' behavioural performance to generate hypotheses about how responses to regularity should vary with pattern complexity. Analysis of the spike count across the population of units in the epoch after the transition to stimulus offset showed higher spike counts for shorter pattern lengths that then decreased with more complex patterns. Neurons also showed increased entrainment to the pattern rate but not the tone presentation rate. Analysis of neural responses to their best frequency (BF) revealed increased precision in firing to BF tones in regular contexts compared to random but also decreased firing. Lastly through modelling I show that across the population, neurons increase their firing with increasing repetitions of the pattern, and that units in auditory cortex show a multiplexed response to a variety factors rather than neurons encoding regularity singularly. In chapter 5, I leverage the high-density linear probes of the Neuropixels to assess how the identified neural correlates change which depth, and show that neural firing in hippocampus is modulated by the pattern length and its entrainment to the pattern and tone presentation rate is enhanced during the presentation of regular sequences. Lastly, in chapter 6, I develop a optogenetic method to reversibly silence regions of auditory cortex which I validate by showing decreases in the firing of neurons during photostimulation, and that this inactivation occurs to broad-spiking,

putative excitatory neurons. I then show behavioural impairment, during auditory cortical silencing, in a vowel discrimination in noise task. The development of the optogenetic method lays the ground work for future studies performing causal manipulation of auditory cortex to test its role in regularity detection.

2 CHAPTER TWO: REGULARITY DETECTION IN THE BEHAVING FERRET

2.1 STATEMENT OF CONTRIBUTION

The online human psychophysics work in this chapter was undertaken with an MSc student (Afua Andam) under my supervision. I designed the experiment and wrote the code to present the experiment online. AA collected the data. I analysed and interpreted the data for inclusion in this chapter.

2.2 INTRODUCTION

As highlighted in chapter 1, the brain's ability to detect repeating patterns and statistical regularities within the acoustic environment is important in analysing the auditory scene and making sense of incoming sensory information. Deterministic patterns and more complex stochastic regularities have been well studied in the field of cognitive neuroscience, and human imaging techniques such as EEG, MagEG and fMRI have highlighted multiple brain regions involved during regularity detection (auditory cortex, hippocampus, and frontal areas). Cognitive models have been developed to infer how the auditory system is able to detect these regularities rapidly and automatically. Despite this, few studies use complex predictable stimuli within an animal model. A handful of studies have presented stimuli to passively listening animals with the goal of exploring the neural correlates of regularity detection. Some examples are random and rhythmic sequences of noise bursts presented to the rat (Asokan et al., 2021), whereas another used pure tones and band passed noise bursts to create repeating patterns to study in the macaque (Barczak et al., 2018). Yet all of these were presented to passively listening animals and did not test their behavioural detection of these complex stimuli.

Paradigms that have used behaviour are even fewer: using modified vocalisations as stimuli, showed mice demonstrate a preference for regularity within vocalisations (Perrodin et al., 2020). Figure-ground segregation behaviour (i.e. detecting a repeating pure tone chord 'figure' in a random chord mixture) has also been demonstrated in the macaque (Schneider et al., 2021, 2018). A few studies have demonstrated that ferrets have some capacity to detect statistical regularities. One study showed they can detect the onset of regularly repeating single frequency pure tones embedded in an otherwise random tone cloud (Ma et al., 2010) and another showed they could detect a repeated

frozen noise burst within a random noise mixture (Saderi et al., 2019). Together, these studies suggest that animals are sensitive to repetition and statistical regularities within acoustic stimuli. Nonetheless, a ferret's, or any non-primate animal model's, capabilities in detecting transitions from random to regular tone sequences has not yet been assessed through the parametric variation in the predictability of the stimulus. In this chapter, I aim to show that ferrets can detect these transitions, show enhanced performance for more predictable patterns, and have a similar detection strategy to humans, cementing their role as a suitable animal model for studying the neural basis of regularity detection.

In this chapter, I present deterministic acoustic patterns, used in previous studies (Barascud et al., 2016; Southwell et al., 2017; Southwell and Chait, 2018), that are rapidly presented after a variable period of randomly presented (i.e. irregular) tones to study how the brain extracts acoustic patterns, using an animal model - the ferret. By presenting the acoustic patterns in the form of pure tone sequences rather than repeated noise samples or more ethological and naturalistic stimuli, I can maintain strict control over and parametrically vary the frequencies presented, stimulus statistics and complexity of the pattern. Previous work has also implemented models to cognitively explain the detection of this stimuli (IDyOM, PPM-Decay; Barascud et al., 2016; Harrison et al., 2020) which I can compare against animal performance.

Though this behavioural task is based on the paradigm used by Barascud et al. (2016), some small changes were implemented to best take advantage of the ferret model. Firstly, to give the animals the best chance of performing the task, I chose shorter patterns, lengths of 3, 5 and 7 rather than 5, 10, 15 and 20, thus reducing the complexity of the regularity that was being presented. In human studies, the tones were spaced at 1/6th octaves. Given that cochlear filters are estimated to be roughly twice as wide in the ferret compared to that in humans (Alves-Pinto et al., 2016a; Sumner et al., 2018; Sumner and Palmer, 2012), I had tones spaced twice that width at 1/3rd octaves which consequently meant the frequency range doubled from 222Hz - 2kHz to 120Hz – 9.7kHz. This reduces the possibility of frequency-adjacent tones falling within the same cochlear filter. However, increasing the frequency range could increase the possibility of streaming out different tones changing the underlying detection strategy (Micheyl and Oxenham, 2010a; Noorden, 1975). To test if changes in frequency range could alter regularity detection by enabling listeners to use

alternative strategies, I performed parallel online psychophysics experiments in humans to identify if a wider frequency range could affect performance and reaction time in regularity detection. If there were to be a difference, I hypothesised that this could be due to enhanced stream segregation from the wider frequency range, which would be detected by a 2-alternative forced choice (AFC) temporal order detection task.

In this chapter, I introduce a behavioural animal paradigm and demonstrate that ferrets can detect acoustic regularities and show key features of behaviour already described in humans; namely that as pattern length increases, performance decreases and their reaction time increases. I take a further look at the cognitive strategies underlying regularity detection in the ferret, and present control stimuli that has the same change in frequency content in the transition from random to regular sequences, but do not contain repeating patterns. This removes deterministic regularity as a cue, showing the ferrets are performing true regularity detection. Furthermore, I present evidence that ferrets have a shorter memory buffer compared to that in humans. Lastly, I perform control experiments in human subjects, to test the effects of an expanded frequency range (compared to that of previous human work) on regularity detection and I show no differences in performance but perhaps instead that increasing the frequency range increases saliency of the pattern due to reduced cross-frequency adaptation.

2.3 METHODS

2.3.1 Animals

Six adult female-pigmented ferrets *(mustela putorius furo)* were trained in the behavioural task (F1805, F1812, F1813, F2001, F2003, and F2103). Ferrets were supplied from Highgate Farm at eight weeks of age and behavioural training began when ferrets were at least 16 weeks old and weighed a minimum of 600g. Animals were housed in groups of two to eight and given free access to water and food pellets. Animals that were undergoing training/testing were housed in separate groups to be water restricted where at the beginning of each testing run (typically lasting five days), water was removed from animals to be on study on a Sunday afternoon and replaced the following Friday evening. Animals were tested twice a day, once in the morning

and once in the late afternoon so that none went longer than 12 hours without access to water. Animals were housed in a light-dark cycle of 14:10 hours in the summer and 10:14 hours in the winter and all went under regular otoscopic examinations to make sure ear canals were healthy and clear of any wax.

Animals were water restricted less than 50% of the time from two weeks before the start date of when they went on study and were weighed daily to ensure that their body weight did not drop below 88% of the initial weight measured at the beginning of each testing run (typically a Monday morning). A minimum of 6% of their body weight in water was provided to the animal daily either through water rewards during the task, water manually supplemented by the experimenter, and mash (crushed food pellets mixed with water) provided to each water restricted ferret at the end of the day. All experimental procedures performed were first approved by a local ethical review committee. Procedures were carried out under license from the UK Home Office in accordance with the Animals (Scientific Procedures) Act (1986) and PPL: PP1253968.

2.3.2 Stimuli

Acoustic stimuli consisted of 50ms tone pips in either a random tone sequence (RAN) or random sequence which then transitioned to a regular tone sequence (RAN-REG) 1.5 to 2.5s after stimulus onset (see **Figure 2.1**).These tones ranged from 120Hz to 9.7kHz with third octave spacing, to give a frequency pool or random alphabet of 20 different frequencies (RAN20). Tones were played immediately one after another with 5ms raised cosine onset and offset ramps. The short tone duration and zero gap between the tones presented provided rapid tone sequences to tap in automatic sensory processing. The regular sequence was then generated by selecting *n* tones from the transition time to then be repeated, where *n* is the number of tones in the pattern (i.e. 3, 5 or 7), with the regular sequence lasting 2s. I presented three different pattern lengths of 3, 5 and 7 tones (see **Figure 2.1B-D**) and the time at which the random sequence transitioned to a regular sequence was randomised between each trial between 1.5 to 2.5 s (in 50ms steps) after stimulus onset. These entire sequences were randomly attenuated between the ranges of 54 to 60dBSPL at 1.5dB steps.

To probe whether the animal uses the deterministic pattern during detection to perform the task, rather than other cues such as changes in spectral content, I tested two further conditions. Firstly, a condition where the random tone sequence only

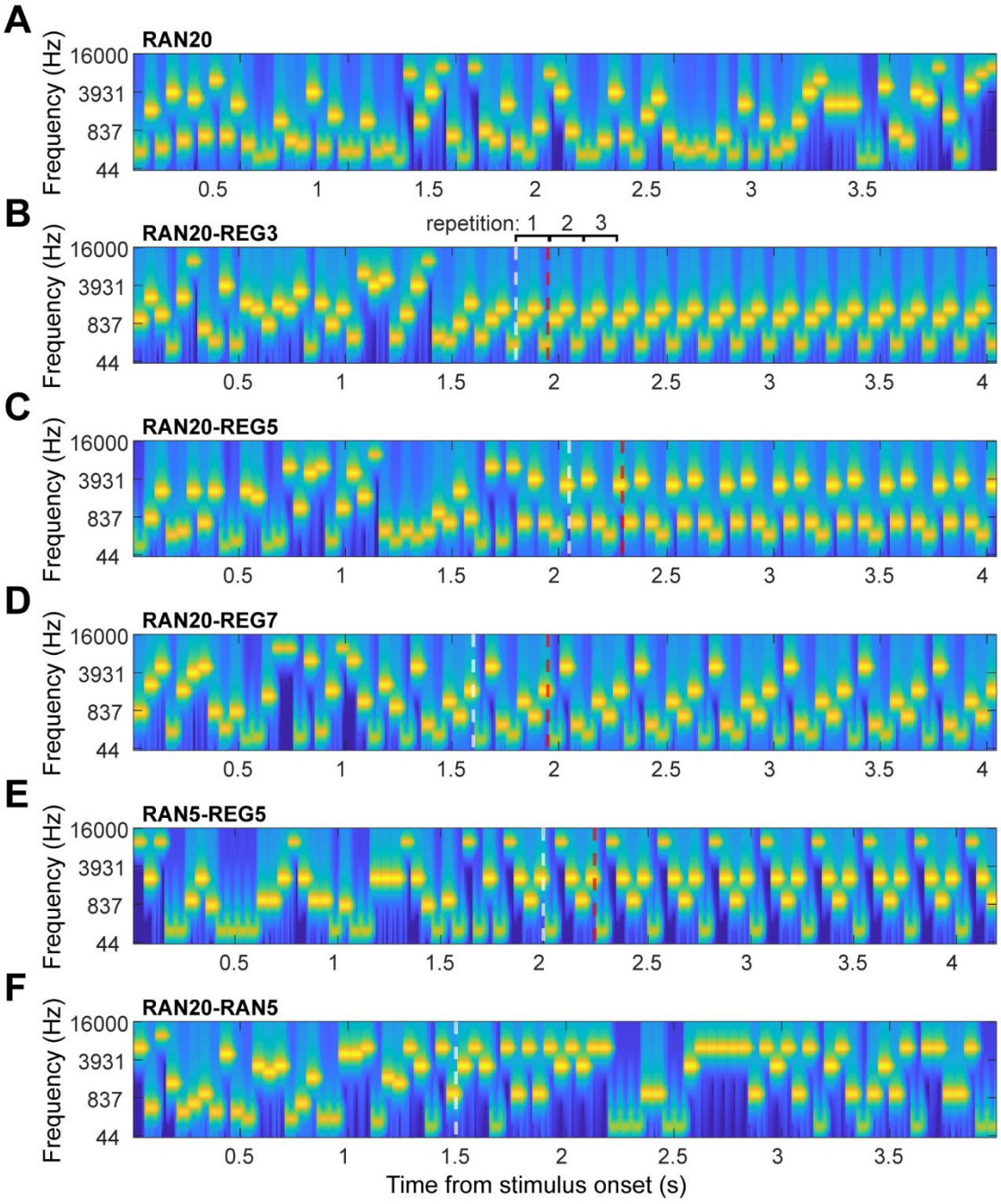

Figure 2.1: Spectrograms of tone sequences. Sequences consisted of 50ms tone pips and ranged in length from 3.5 to 4.5s. A) Random tone sequence with an alphabet of 20 tones that does not transition to a regular sequence and in the behavioural task is used as a catch trial. B-D) Random sequence that then transitions to a regularly repeating pattern of 3 with the first three repetitions indicated. Other random sequences transitioning to a repeating pattern of (B), 5 (C) and 7 (D) tones. The transition time is shown with the white dashed line. The red dashed line shows the end of the next cycle of the repeating pattern. E) Sequences where the random alphabet consisted of 5 different frequencies and then transitioned to a repeating pattern of 5 tones generated from the previous same frequencies. F) Probe trials were presented where a random sequence was generated from 20 different frequencies but then transitioned to a random sequence generated from 5 frequencies at the transition time (white dashed line).

consisted of five randomly chosen frequencies (RAN5) that were followed by a pattern of 5 tones (REG5) using the same preceding frequencies (see **Figure 2.1E**). Accordingly preventing animals from using any information about the probability of occurrence of any one tone as a cue for detection. The second was a probe condition, tested only on 10% of trials within a testing session and randomly rewarded to avoid biasing trained behaviour. The probe stimuli contained a random sequence (RAN20) that transitioned to a random sequence of 3, 5 or 7 tones (RAN20-RAN3, RAN20-RAN5 and RAN20-RAN7 respectively) (see **Figure 2.1F**). Thus, capturing the change in spectral statistics that occurred in the RAN20-REGN conditions, without introducing a regular pattern.

Each sequence was generated a new for each trial apart from a subset of sessions where stimuli were repeated approximately 10 times within a session to provide reliable spiking responses for electrophysiological recordings in later experiments. In the repeated presentations the transition time was fixed at 2s and the level at 60dBSPL. Stimuli were generated in MATLAB and presented at a sampling frequency of 24414.0625Hz. All frequencies were individually level calibrated at the position of the animal's head using a microphone (Brüel & Kjær ½" Microphone 4134), measuring amplifier (Brüel & Kjær 2610) and tone generator (Brüel & Kjær 4231), between a noise-floor of 30 to 40dBSPL to maximum presentation of 70dBSPL to minimise non-linearities in frequency presentation within the speaker.

2.3.3 Apparatus

Animals were trained in a double-walled sound attenuated booth in a semi-circular arena encased in acoustically transparent plastic mesh (IAC Acoustics; see **Figure 2.2A**). The stimulus was presented from a free field central loudspeaker (Visaton SC 5.9) approximately 20cm from the subject's head position. A central spout on a post in the centre of the arena held an infrared (IR) sensor (Optek / TT Electronics OPB710) and IR beam breaker consisting of an emitter (Optek / TT Electronics OP165A) and phototransistor (Optek / TT Electronics OP506A) contained in a custom 3D printed structure to detect when the animal was at the central spout to initiate trials or to hold (see **Figure 2.2B**). When the IR sensor in the centre of the spout was activated through a nose poke the trial was initiated. The IR beam breaker, located on the wings of the central spout, was then used to detect whether the animal had left the central spout after a given length of time (e.g. 150ms) as the beam breaker was less

sensitive to small head movements that could otherwise log an unintended release from centre, compared to the centre IR sensor.

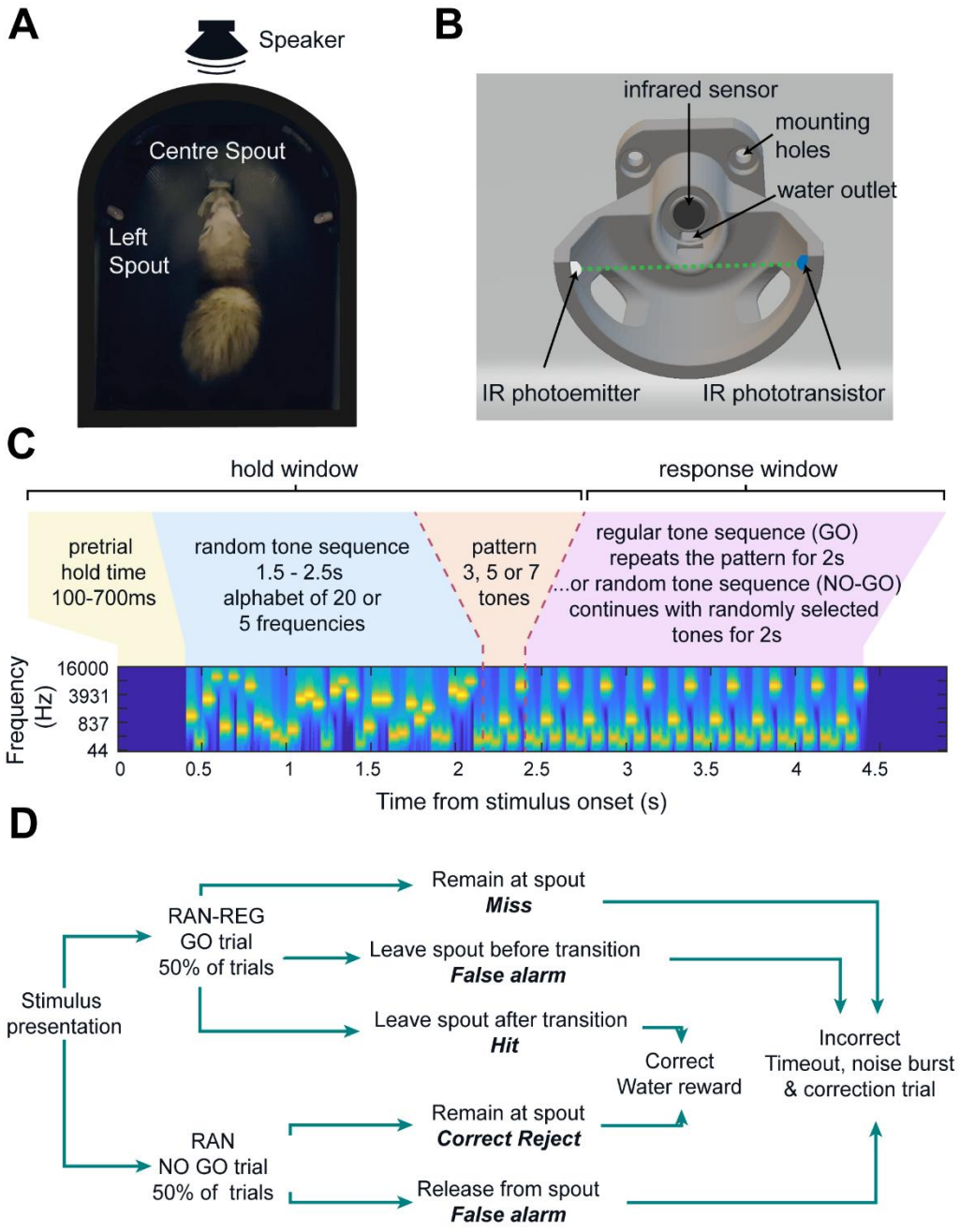

Figure 2.2: Schematics of the behavioural apparatus and trial structure. A) The animal was housed in a double-walled sound attenuated booth and was required to initial the trial at the central spout. Once initiated the sound was then presented from a central speaker ~20cm from the animals head. If the animal heard a transition from random to regular they were required to leave the centre spout and nose poke at the left spout. B) A custom 3D printed structure was used to house the electronics and sensors to detect when the animal had initiated and was holding during a trial. An IR beam break (green dashed line) and IR reflecting sensor (black circle) were two of the sensors used during behaviour. A water outlet was also built into the structure to provide a water reward. This structure was then mounted on a post in the centre of the arena. C-D) The structure of a trial consisted of a pre-trial hold time where

the animal was required to hold their head at the spout to initiate the trial. The stimulus would then be presented and could either be a random sequence, a random to regular sequence or a probe trial. In a GO trial (random to regular sequence) the animal would be required to respond within 2s of the transition time at the left spout in order to receive a water reward. The animal had to remain at the central spout during a NOGO trial (random sequence) in order to receive a water reward from the central spout.

The central spout also housed a channel that when a solenoid (Valeader B2B112.BVO 12VDC) was activated it allowed water from a reservoir to flow into the channel providing a water reward (approximately 0.25ml per reward). A secondary spout to the left-hand side of the central post (approximately 15cm away) was used as the response location for when the animal was required to respond after the transition from the random to regular sequence. This spout contained just an IR sensor and a channel for the water reward. The experiment was run on custom scripts written in MATLAB (The Mathworks) which communicated to the TDT signal processor (RX8) to control stimulus presentation and receive sensor information. One camera (Intel Realsense D435) was installed to observe the animal during the experiment.

2.3.4 Training and testing

At the beginning of training, ferrets were positively reinforced to associate the left and central spouts with reward by providing a water reward anytime the ferret approached the spout. Once they reliably minimised exploration in the arena and focused their attention on two spouts (approximately 3-4 sessions), they were then trained to respond in a pattern of going to the central spout then to the left spout. Once this pattern was adopted by the animal (2-4 sessions) the auditory stimulus was introduced with GO and NO-GO trials. These GO trials consisted of a random to regular tone sequence (RAN20-REG3), however the transition from random to regular was short (0.5s) whilst the regular sequence was long (10s). NO-GO trials consisted just of the random tone sequence (see **Figure 2.1A**) but only lasted a short time (0.5s). With this short duration until the transition, the animal was likely to already be moving to the left spout after initiation of the trial, and thereby associating the left spout with regularity. If the animal let go too early from the central spout or didn't respond at the left spout before the end of the response window, then they would be met with a noise burst, timeout and no water reward (see **Figure 2.2C-D**).

As the subject's performance increased after multiple training sessions the time between the transition and stimulus onset was gradually increased up until the testing conditions of the range 1.5 to 2.5s; thereby the response time was gradually

decreased from 10s to 2s. Once the animal was able to successfully detect the change from random to regular in the RAN20-REG3 condition with the testing parameters, increasingly longer pattern lengths, 5 and 7, were then introduced to the animal. These were initially presented separately in each session but then all pattern lengths were randomly interleaved within a session. This provided trials that varied in difficulty in a single session and the animals were tested on a variety of stimuli (see **Table 2.1**). The RAN5-REG5 condition was presented separately and only after the animal became competent detecting the other conditions. This stimulus was presented in its own training/testing sessions.

Once the animal reached a consistent performance and stopped improving their performance across conditions during training, sessions before this point were excluded from analysis (see **Figure 2.3**). Once the animal was trained on all conditions, they were then implanted with microelectrode arrays at the next available opportunity for electrophysiological recordings (see chapter three). During testing animals were presented interleaved pattern lengths and on other sessions were presented the RAN5-REG5 condition. Probe trials (RAN20-RANX, where X = 3, 5 or 7; see **Figure 2.1F**) were presented on selected sessions randomly on 10% of trials. To avoid inducing bias each probe trial was randomly assigned whether it was a GO trial or NO-GO trial. Implanted animals were presented repeating stimuli that was generated anew every 4 weeks to coincide with electrode movements of the animals' implants.

	Novel regularities				Repeated regularities				Novel
RA	20			5	20			5	20
Ferret/PL	3	5	7	5	3	5	7	5	X
F1805	5292	1509	584	2499	-	-	-	-	-
F1812	5277	4400	3214	5458	2021	1980	1034	1113	108
F1813	4549	3670	1887	1940	988	794	341	411	100
F2001	5280	4603	3035	6303	2344	2610	1206	1726	158
F2003	4955	4941	2699	3601	1459	1132	300	403	181
F2103	1933	2380	1787	2200	720	640	146	214	138

Table 2.1: Table of the total number of trials each subject completed that contained regularity for each condition included in behavioural analysis.

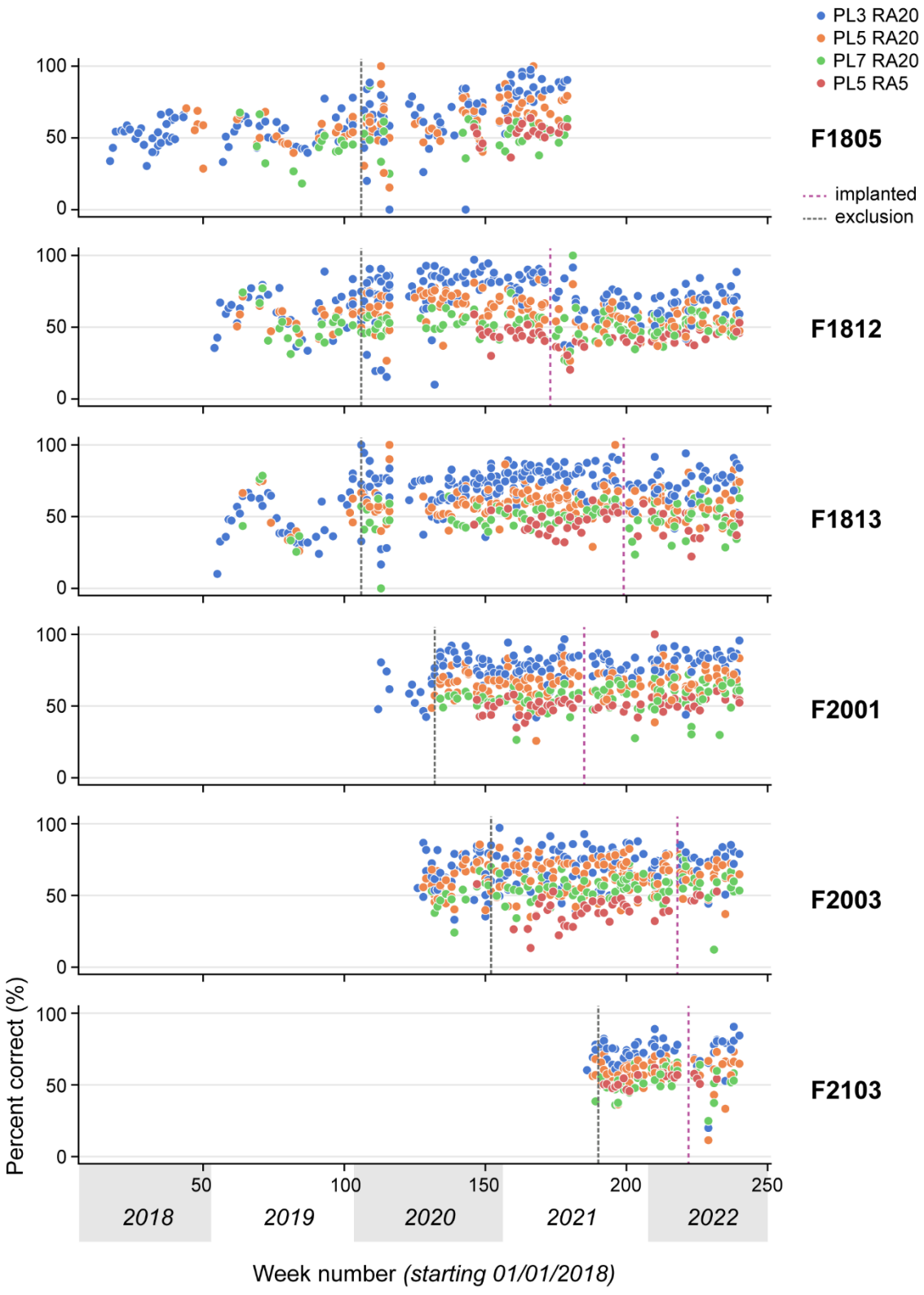

Figure 2.3: Performance of each ferret in each condition in each week from the start of behavioural training. Each dot is the ferret's performance each week and is coloured by the condition. The dashed grey line shows the date at which data is excluded from that ferret due to training/piloting. The purple dashed line shows the date of implantation.

2.3.5 Task development

During piloting, random sequences (NO-GO trials) initially occurred 25% of the time and regular sequences (GO trials) contained transition times which varied from 0.5 to 4.5 seconds. A binomial mixed effects regression on all trials (see **Table 2.2** and **Figure 2.4A-B**), with ferret as the random effect, show a main effect of transition time where an increase in transition time gave poorer performance. A binomial mixed effects regression also revealed a significant increase in the false alarm rate as the precursor increased (see **Table 2.3**) suggesting that the animals are less able to hold at the central spout as the transition time is increased in this task. To mitigate this effect I increased the percentage of NO-GO trials to 50% and reduce the range of transition times to 1.5 – 2.5s to balance a short enough hold period with a long enough presentation of the random sequence.

					CI 95%	
Fixed effects	Estimate	Standard error	T	p value	Lower	Upper
Intercept	1.075	0.270	3.982	**< 0.001**	0.543	1.608
Precursor length	-0.567	0.0114	-49.638	**< 0.001**	-0.589	-0.544

Table 2.2: Estimates of each fixed effect in the binomial mixed effects regression model on performance to various precursor lengths. R^2 = 0.834; Df = 216; random effect std. = 0.457

					CI 95%	
Fixed effects	Estimate	Standard error	T	p value	Lower	Upper
Intercept	-2.089	0.309	-6.768	**< 0.001**	-2.697	-1.481
Precursor length	0.860	0.0130	66.21	**< 0.001**	0.834	0.885

Table 2.3: Estimates of each fixed effect in the binomial mixed effects regression model on false alarm rate to various precursor lengths. R^2 = 0.963; Df = 216; random effect std. = 0.524

Adding a dual sensor system, one reflective IR sensor in the middle of the spout to be responsible for initiating the trial and a crossbeam that registered the presence of the ferret's head, aided in reducing false alarms and thereby increased performance (mixed effects binomial regression, see **Table 2.4** and **Table 2.5** and **Figure 2.4C-D**).

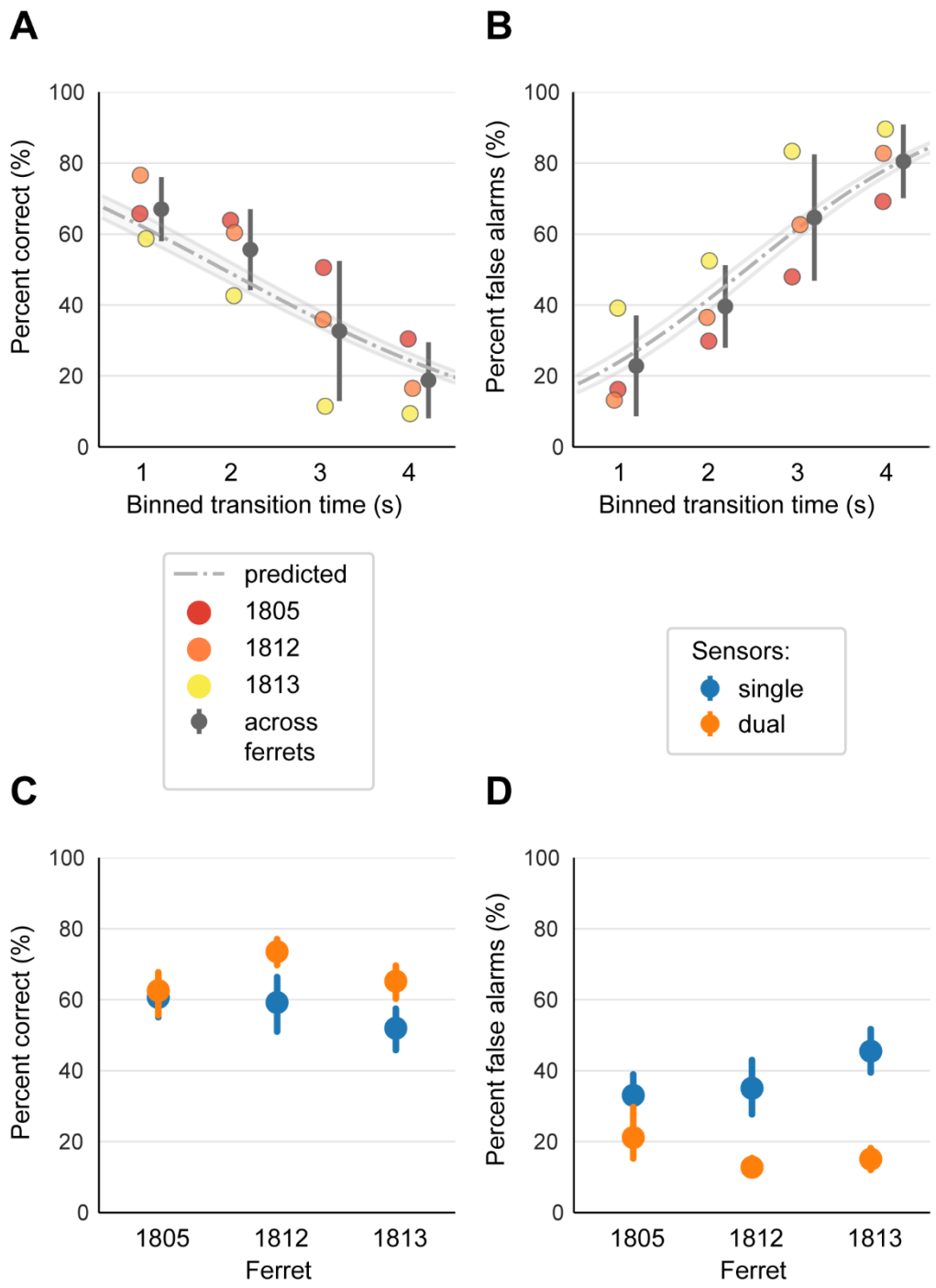

Figure 2.4: Performance at various transition times and with the improved sensor system. A) Performance (percent correct of trials) of each ferret to each transition time binned in 1s bins (0.5s around each second) with the mixed effects binomial model (dashed line, shaded area = CI) on the unbinned transition time. B) Percentage of false alarms on trials for each ferret and mixed effects binomial model on the unbinned transition time. C-D) Performance and percentage of false alarms with the single and dual sensor systems for each ferret (error bar = s.e.).

Fixed effects	Estimate	Standard error	T	p value	CI 95% Lower	CI 95% Upper
Intercept	0.191	0.101	1.884	0.0616	-0.00938	0.391
Sensor type *(single = 0, dual = 1)*	0.286	0.0335	8.539	**< 0.001**	0.220	0.352

Table 2.4: Estimates of each fixed effect in the binomial mixed effects regression model on performance to single and dual sensors. R^2 = 0.126; Df = 146; random effect std. = 0.154

Fixed effects	Estimate	Standard error	T	p value	CI 95% Lower	CI 95% Upper
Intercept	0.308	0.118	2.607	**0.0100**	0.0745	0.542
Sensor type *(single = 0, dual = 1)*	-1.025	0.0409	-26.057	**< 0.001**	-1.106	-0.944

Table 2.5: Estimates of each fixed effect in the binomial mixed effects regression model on false alarm rate to single and dual sensors. R^2 = 0.433; Df = 146; random effect std. = 0.182

2.3.6 Behavioural analysis

Each session's behavioural data was logged during the experiment and then later extracted using custom Python scripts. A response was a hit if the trial was a GO trial and the animal responded at the left spout after the transition time and before the end of the response window (2s). A correct reject was logged if the animal held at the centre spout during a NO-GO trial but was logged as a missed if they responded this way during a GO trial. False alarms were logged when the animal either responded at the left before the transition time on a GO trial or at any time during a NOGO trial. Percent correct was calculated for each session as follows:

$$percent\ correct = \left(\frac{number\ of\ hits + number\ of\ correct\ rejects}{total\ number\ of\ trials}\right) * 100 \quad (1)$$

As equipment can and would fail, this would cause drops in performance, or cause the ferret to fail to trigger trials or the equipment may fail to record the animal at the central spout, sessions were excluded from further analysis if the animal had a score of less than 40% correct (on average 25.8% of sessions per ferret) or a false alarm rate of greater than 65% (on average 4.54% of sessions per ferret).

$$false\ alarm\ rate = \frac{number\ of\ false\ alarms}{total\ number\ of\ trials}$$

(2)

Trials in which the animal responded within 500ms from stimulus onset were also excluded as this was typical of the animal triggering the trial by accident and failing to hold at the central spout. The first four trials from every session were also excluded as ferrets would initially explore the box and take a few trials to focus on the task. To assess reaction time, sessions where the ferret performed at greater than 60% correct only were included to avoid analysis on chance responses.

To detect whether each animal was successfully able to perform above chance in each condition, I performed a permutation test to create a chance distribution for each individual ferret at each condition. To do this I grouped each ferret's responses by condition and then shuffled their reaction time for each trial (including trials with no available reaction time due to the ferret remaining at the central spout). Performance was then calculated on the shuffled data, for example if there was a reaction time but the trial was a NO-GO trial, the trial would now be labelled as a false alarm, whereas if the trial was a GO trial and the shuffled reaction time was after the transition time then the trial would be labelled a hit. This process was iterated 1000 times for each condition and ferret to produce a chance distribution and a 97.5^{th} percentile calculated for each ferret and condition (for violin plots of these chance distributions, see Appendix 9.2.1).

Statistical analysis of effects of pattern length and effects of matched/unmatched alphabets and other conditions used general linear models and generalized linear mixed models fitted using fitglme in MATLAB (version 2022a). These models were also applied to the online psychophysics. The details of each model are outlined alongside the relevant results; however, in general, analysis of behavioural performance (correct vs. incorrect responses) was based on logistic regression in which the generalised linear model used binomial distribution and logit link function settings and analysis of reaction times was based on a general linear model. For each model, I used ferret as a random factor and reported the magnitude of coefficients (estimate) of fixed effects of interest, the t-statistic for a hypothesis test that the coefficient is equal to 0 (T) and its respective p-value (p). The 95% confidence intervals are also reported for each fixed-effect coefficient and the adjusted R^2 value

of the model to assess model fit. All behavioural data extraction and analysis was performed offline using Python packages and MATLAB.

2.3.7 Online human psychophysics

Two online human psychophysics experiments were performed using the platform Gorilla (gorilla.sc) to present the experiment with the platform Prolific (prolific.co) to recruit and test participants online due to the COVID-19 pandemic where in person testing could no longer take place. Twenty participants aged 18-34 years old participated in human experiment 1 (H1; mean age: 24.3 years) and in human experiment 2 (H2; mean age: 23.4). All participants were devoid of any history of auditory and/or neurological disorders and were fluent in English. Participants were excluded if they did not meet the screening criteria of the headphone check test (Milne et al., 2020) and pure tone assessment (see below). All stimuli were presented at a comfortable level to the listener and at a sample rate of 44.1kHz.

Due to the lack of control of headphone frequency responses and any means of calibration through online testing, a pure tone assessment was performed. The pure tone assessment was a 3AFC task where three intervals were presented with the tone only played in one of the intervals. The participant had to press the numbered key (1, 2 or 3) that corresponded to the interval with the tone present. Four frequencies (0.1, 1, 4, 10 kHz) were tested with five repeats. The intervals with the tones were played at the same level as that in the experimental stimuli to check if participants could perceive the range of tones necessary for H1 and H2. If the participant performed 3 or more trials incorrect for any frequency tested, they were excluded from the study.

In order to identify whether participants listened to the experiment over headphones I used an assessment that we developed that utilised the Huggins Pitch phenomenon (Milne et al., 2020). It is based on the perception of a dichotic percept, the Huggins pitch, that is audible over headphones but not free field loudspeakers. By presenting white noise stimulus to one ear and the same white noise to another but with a phase shift of 180° over a narrow frequency band (centred around 600Hz ±6%) to the other ear, an illusory pitch phenomenon is generated, but only when the left and right channels are fed individually to each ear (see Milne et al., 2020 for more details). The Huggins pitch was presented within a 3AFC task design where only one interval,

the target, contained the phenomenon and the other two contained diotic white noise. The subject was asked via a graphic user interface to select the interval in which they heard the tone and if they got less than five out of six trials correct, they were excluded from the study.

For participants that passed the screening, they read and signed an online information sheet and informed consent was obtained from each participant (see Appendix 9.1). In H1 participants were also awarded a bonus payment based on the percentage of trials in which they responded in less than one second to motivate quick reaction times. In H2 participants were awarded a bonus payment based on their percentage of correct trials in order to motivate correct answers. Participants were additionally paid £10 per hour in both experiments with each experiment typically lasting 45 minutes. Experimental procedures were approved by the research ethics committee of University College London, project ID number: 3866/003.

2.3.7.1 Human experiment 1

To test the effects of changes in frequency range in regularity detection, I performed an online GO/NO-GO experiment where I tested two different frequency ranges (wide: 0.12kHz to 9.7kHz in 1/3 octave steps; narrow: 0.22kHz to 2kHz in 1/6 octave steps) of the frequency 'alphabet' and three different pattern lengths (3, 5 and 10) and a condition with just a frequency change (STEP) to measure a basic reaction time without regularity detection (8 conditions in total; see **Figure 2.5**). To mimic the response measure of the animal experiment, participants were asked to hold down the 'spacebar' on their keyboard to initiate the trial and release as quickly as possible within 2s, when they heard regularity, or a change in frequency in the STEP change trials.

Ten repetitions were presented for each of the eight conditions, with each condition containing a corresponding NO-GO condition (catch trial) in which the regularity or STEP change was absent. These 160 trials in total were split equally into two eight-minute blocks, with an inter-stimulus interval (ISI) ranging from 250ms to 750ms between trials, with a one minute break included after the first block of 80 trials to maintain attention during the online task. Prior to the experiment, just after screening, the participants completed a practice session of 12 trials which provided feedback based on their reaction time to the GO trials, asking them to react quicker if

their reaction time was slower than one second and/or telling them if they had missed the regularity or responded before the regularity had occurred. The practice session

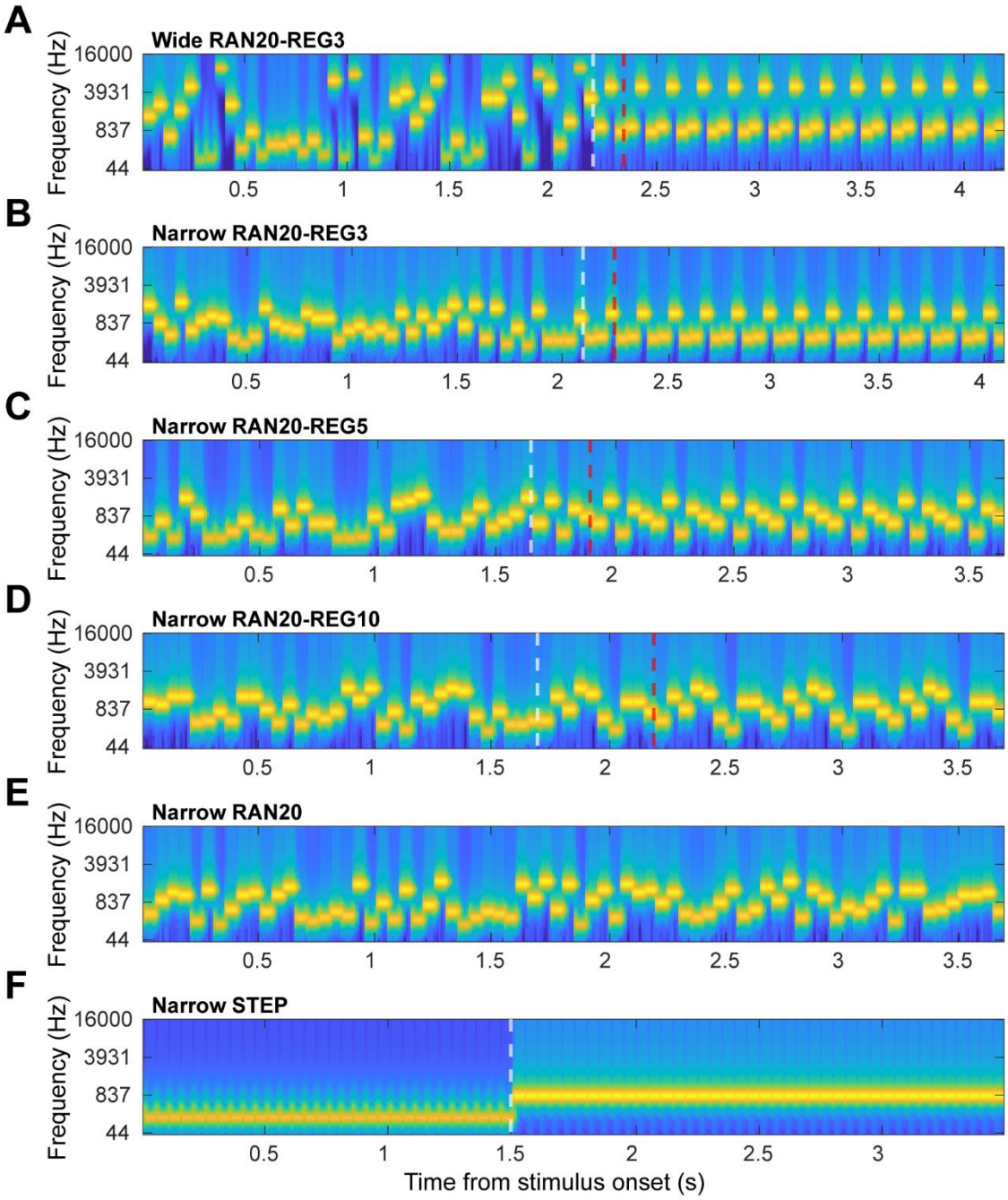

Figure 2.5: Spectrograms of the stimuli used in experiment 1 (H1) of the online psychophysics. A) Wide frequency range of 0.12 to 9.7kHz with 1/3 octave steps between frequencies, that transitions to a pattern length of 3. B) Narrow frequency range of 0.22 to 2kHz with 1/6 octave steps between frequencies, that transition to a pattern length of 3. Pattern lengths of 5 (C), and 10 (D), where also tested. Half of trials were catch trials in which there was no transition to regularity (E). A step function which contains one frequency that either continues throughout the trial or transitions to another frequency (F). Transitions are shown with a white dashed line and one complete pattern cycle is illustrated with the red dashed line.

contained one repeat of each condition and only tested the STEP change, and pattern lengths 3 and 10 in each frequency range. 21 participants were tested with one excluded for using a Macintosh (20 participants analysed in total).

2.3.7.2 Human experiment 2

With a wider frequency range, streaming is more likely to occur (van Noorden, 1975; Micheyl & Oxenham, 2010) where one tone or group of tones becomes perceptually segregated from the other tones in the sequence. This could therefore change the underlying process in detecting the transition from random to regular, perhaps focusing on one frequency than the whole pattern. To identify whether enhanced stream segregation would occur in the regular period due to the wider frequency range, I designed a paradigm to investigate the subjects ability detect the temporal order of sounds, on the basis of the known effect that during stream segregation participants will struggle to accurately report the order of tones that are segregated into two separate perceptual streams (van Noorden, 1975; Micheyl & Oxenham, 2010).

The stimulus began with a regular sequence of five cycles long (either a pattern length of 7 or 10) in either the narrow (0.22 to 2kHz) or wide (0.12kHz to 9.7kHz) range (see **Figure 2.6**). A 2s interval of silence followed and then the probe was presented, which was either one cycle of the regular sequence or one cycle of the regular sequence but two of the frequencies were swapped in order (see **Figure 2.6C-D**; white arrows identify swapped tones). It was presented in a 2AFC task in which the subject was asked whether the probe was the same as the presented regularity or different.

Fifteen repetitions were presented for each of the eight conditions (two frequency ranges, two pattern lengths and whether they were the same or different). There were 120 trials in total with an ISI range of 750 to 1250ms and the trials were split into two blocks with a minute break in between. There was an information screen that provided examples of a trial with the same order in the probe and a different order in the probe as well as a practice session of 12 trials (that they could repeat) where they could listen to and respond to all variations with feedback. 22 participants were tested with two excluded for using a Macintosh, leaving 20 to be analysed.

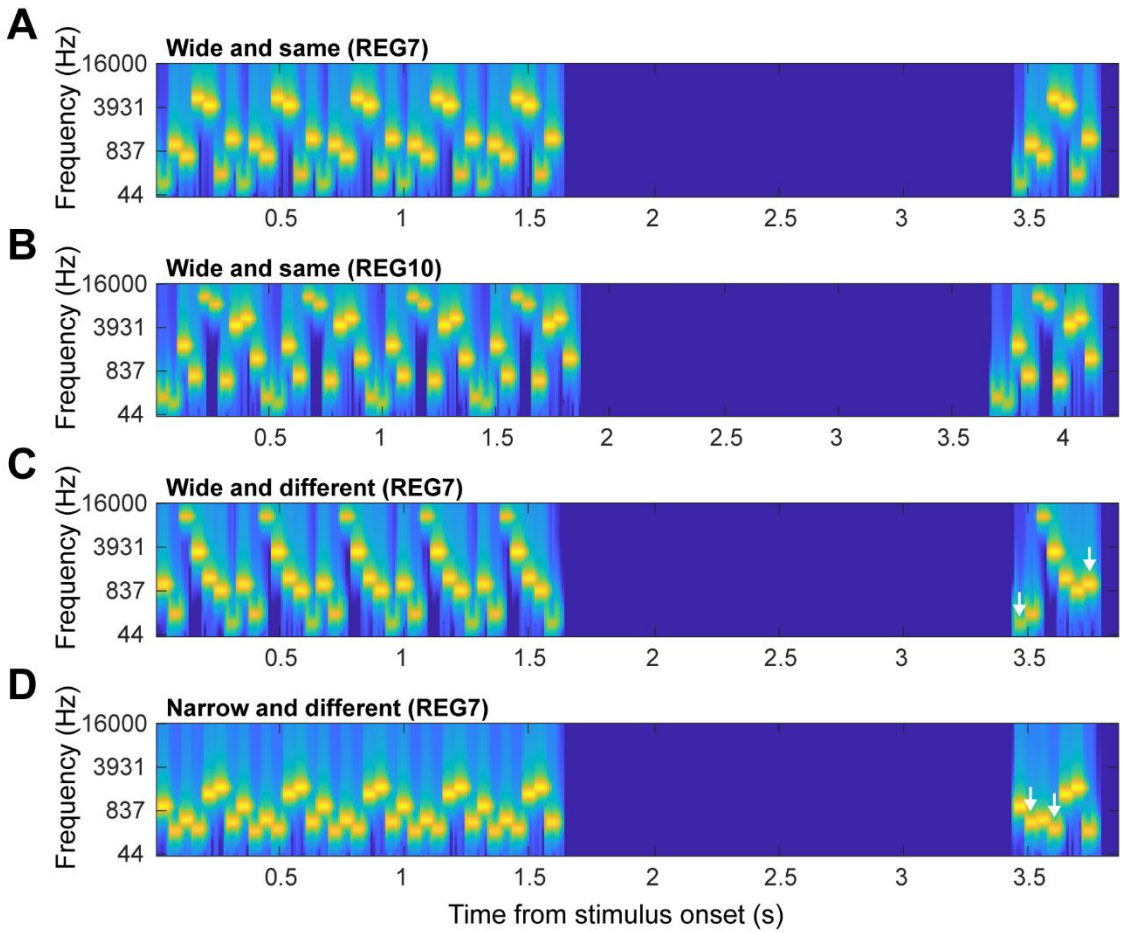

Figure 2.6: Spectrograms of the stimuli used in experiment 2 (H2) of the online psychophysics. A pattern of 7 or 10 was selected from a wide or narrow frequency range that repeated 4 or 5 times respectively. A 2s interval of silence followed and then a cycle of the same pattern was presented either in the same order (A-B) or with two tones swapped (C-D) in order. The tones swapped are illustrated in the examples with white arrows.

2.3.7.3 Analysis

Each participant's behavioural data was logged through Gorilla during the experiment and extracted offline with custom MATLAB scripts. To analyse performance in H1 and H2, the percent correct over total trials was taken for each subject. For H1 the reaction time was baselined to each subject's individual reaction time to the STEP condition. For H2 a d', with the Stanislaw and Todorov (1999) correction on hit rate and false alarm rate, was calculated as a measure of performance, due to the 2AFC design, as follows:

$$d' = Z(Hit\ Rate) - Z(False\ Alarm\ Rate) \quad (3)$$

Responses were labelled as follows for the 2AFC task based on whether the probe was the same or different to the preceding pattern and how the subject responded within the task:

	Stimulus: Same	**Stimulus: Different**
Response: Same	Hit	False alarm
Response: Different	Miss	Correct reject

All behavioural data extraction and analysis was performed offline using Python packages and MATLAB.

2.4 RESULTS

2.4.1 Ferrets can detect transitions from random to regular sequences

Ferrets (n = 6) were trained on a GO/NO-GO-task where they were required to respond at a peripheral spout when they heard a transition from a random sequence to a regular sequence. The NO-GO trials were random sequences of frequencies either selected from a pool of 20 (RAN20) or a pool of 5 (RAN5). GO trials were random to regular sequences that either went from a pool of 20 frequencies down to a repeating pattern of 3, 5 or 7 tones (RAN20-REG3, RAN20-REG5 and RAN20-REG7 respectively); or a pool of 5 frequencies down to a repeating pattern of 5 tones (RAN5-REG5). All ferrets successfully performed the task for all tested conditions (defined as performing greater than the 97.5th percentile of the randomly permuted chance distribution; range of 97.5th criterion across ferrets = 47.475 to 55.312). Mean performance (% correct) for each ferret in each condition can be seen in **Table 2.6**).

Ferret	RAN20-REG3	RAN20-REG5	RAN20-REG7	RAN5-REG5
F1805	83.14	74.02	63.51	65.08
F1812	85.18	72.91	62.09	58.54
F1813	83.33	70.35	62.99	61.39
F2001	86.59	74.06	63.98	61.83
F2003	81.46	74.77	66.03	61.44
F2103	77.53	63.71	59.24	59.24

Table 2.6: Mean performance (percent correct) of each ferret in each condition

Having established that all ferrets are able to perform the behavioural task above chance levels for all conditions tested, I wanted to ask how the length of the pattern in the regular sequence affects behavioural performance. As can be seen in

Figure 2.7 performance for detecting regularity within the RAN20 condition appears best for the shortest pattern lengths. It is also apparent that the RAN5 condition elicited worse performance than trials with the same pattern length but drawn from an alphabet of 20 (RAN20-REG5). This was confirmed with a binomial mixed effects regression model (see **Table 2.7**) that shows a main effect of pattern length, decreasing performance as the pattern length increases ($\beta = -0.270$, $p < 0.001$) and a main effect of the random alphabet, increasing performance with increasing alphabet size ($\beta = 0.0406$, $p < 0.001$). This evidence reveals that ferrets benefit from simpler repeating patterns in detecting the transition from random to regular but also benefit from a random sequence that selects from a larger pool of frequencies.

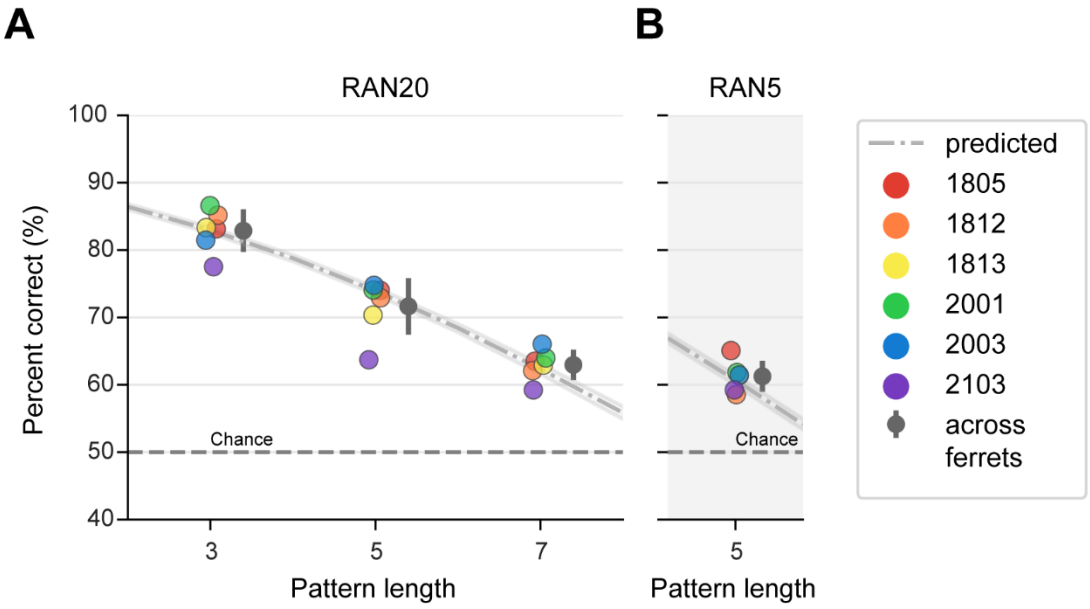

Figure 2.7: Performance of ferrets to various pattern lengths and random alphabet sizes. A-B) Performance (all above chance) is calculated by computing the average percent correct from each session for each ferret (coloured circles) with the mean performance across all ferrets shown in grey (error = std.) for each pattern length and each random alphabet (A) RAN20 and (B) RAN5. Approximate chance is depicted as the dashed line. The binomial mixed effect model prediction is plotted in the dotted-dashed line with the 95% confidence intervals.

					CI 95%	
Fixed effects	Estimate	Standard error	T	p value	Lower	Upper
Intercept	1.585	0.0554	28.622	**< 0.001**	1.476	1.693
Pattern length	-0.271	0.00423	-63.911	**< 0.001**	-0.278	-0.262
Random alphabet	0.0406	0.000765	53.114	**< 0.001**	0.0391	0.0421

Table 2.7: Estimates of each fixed effect in the binomial mixed effects regression model on performance. $R^2 = 0.529$; Df = 5849; random effect std. = 0.121

2.4.2 Reaction times are faster for shorter pattern lengths

Next, I aimed to assess how reaction times changed with each pattern length to understand if ferrets would take longer to detect longer patterns as can be seen with humans (Barascud et al., 2016). In **Figure 2.8A-B**, I show the kernel density estimate (KDE) of the mean reaction time for each ferret and condition at each testing session. The reaction time is baselined to the transition time which, is the time the first tone is repeated within the pattern. In the data, the reaction time distributions are generally shifted rightwards for each increasing pattern length (see **Figure 2.8A**). Interestingly the reaction times for pattern length 5 with a random alphabet 5 are quicker than that of the RAN20-REG5 condition (see **Figure 2.8B**). I ran a mixed effects linear regression (see **Table 2.8**) that confirmed a main effect of the pattern length, increasing reaction times with increasing pattern lengths ($\beta = 0.0461$, $p < 0.001$), such that an increase in the pattern by one tone increases the reaction time by approximately 46ms. The model also indicated a main effect of the random alphabet, increasing reaction times with increasing alphabet size ($\beta = 0.00503$, $p < 0.001$). Overall, it is apparent that ferrets are quicker at responding to shorter patterns and are also quicker when the random sequence contains less frequencies.

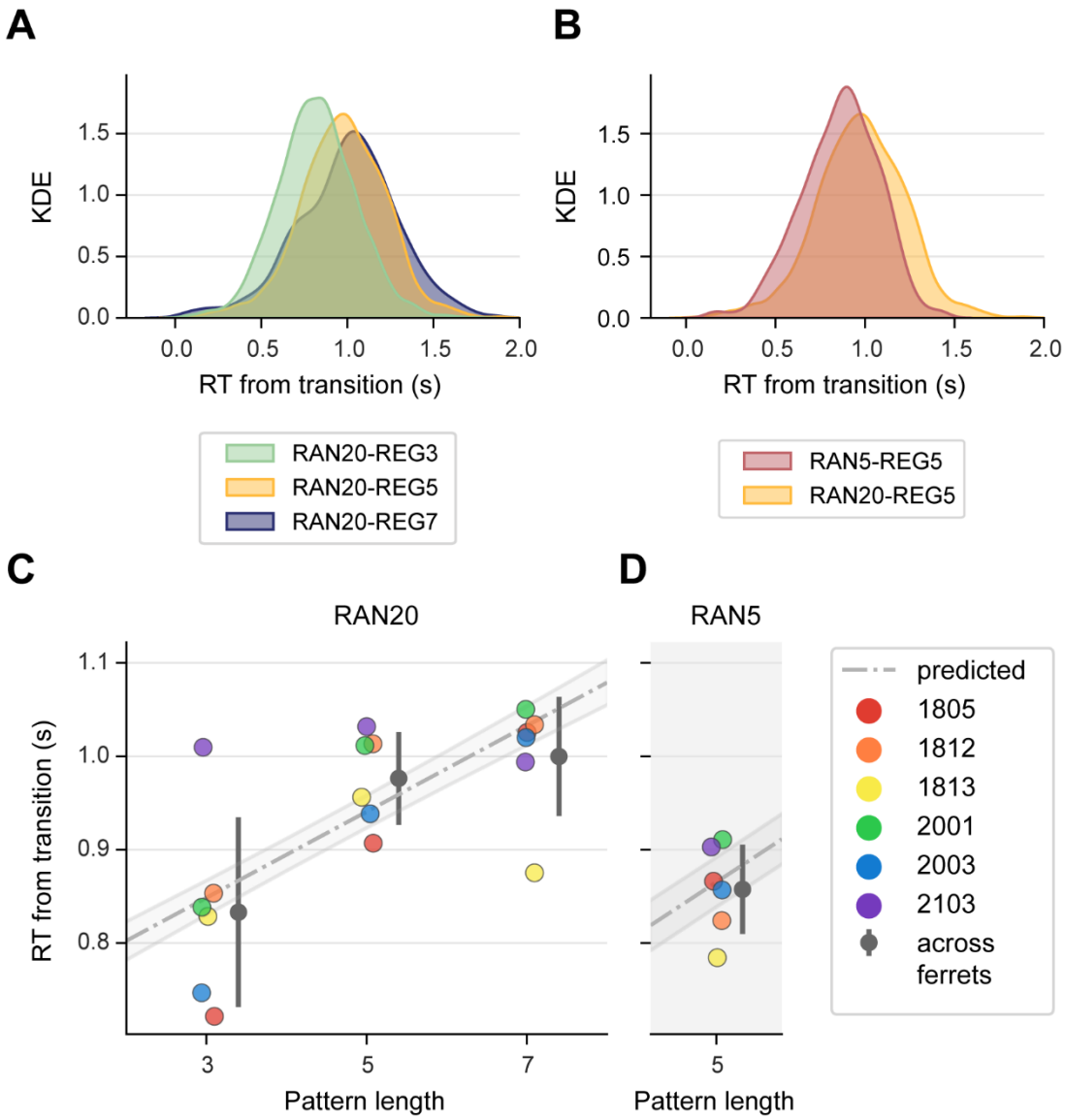

Figure 2.8: Reaction times of ferrets to various pattern lengths and random alphabet sizes. A-B) Kernel density estimates of reaction times, pooled across ferrets, to GO trials in sessions with > 60% correct separated by pattern length for RA20 condition (A) and separated by random alphabet for the PL5 condition (B). C-D) Average reaction time for each ferret and condition with the predicted values from the mixed effects linear regression shown (grey dashed line).

					CI 95%	
Fixed effects	Estimate	Standard error	T	p value	Lower	Upper
Intercept	0.626	0.0284	21.428	**< 0.001**	0.554	0.665
Pattern length	0.0461	0.00238	19.366	**< 0.001**	0.0414	0.0508
Random alphabet	0.00503	0.000678	6.554	**< 0.001**	0.00353	0.00654

Table 2.8: Estimates of each fixed effect in the linear mixed effects regression model on reaction time. R^2 = 0.0993; Df = 5107; random effect std. = 0.0514

2.4.3 Detection strategies: changes in stimulus statistics or pattern detection?

The analysis above provides evidence that ferrets are able to detect transitions from random to regular sequences. However this task could potentially be solved by detecting the change from 20 frequencies down to 3, 5 or 7, rather than detecting the pattern. The previous data does show that they can detect the change when the number of frequencies stays the same (RAN5-REG5) however they perform significantly worse compared to the unmatched counterpart (RAN20-REG5). This raises the possibility that they could be picking out the change in stimulus frequency statistics rather than detecting the repeating pattern, and thereby not performing true regularity detection. To test more directly whether this is occurring I presented a stimulus in which there was a change in the number of frequencies at the transition but no pattern. These were presented as probe trials on 10% of trials within a session and randomly rewarded to avoid behavioural bias. I analysed the proportion of trials in which the animal responded as if they perceived regularity, by responding at the left spout (GO), and subsampled conditions in which there was a repeating pattern accordingly.

As can be seen in **Figure 2.9A** the proportion of trials in which they responded GO was much lower than when they heard the repeating pattern (see **Figure 2.9B**). We see a slightly larger proportion of GO responses for pattern length 3 in the probe trials (RAN20-RAN3) but overall, these are much lower than the equivalent repeating pattern (RAN20-REG3). A mixed effects binomial regression (see **Table 2.9**) revealed main effects of probe vs. pattern (reference category: pattern), and pattern length as well as an interaction ($p = 0.00126$) between pattern length and whether a pattern was present. To determine the effect of pattern length on probe trial individually and to compare these to pattern trials, separate models were run on trials containing the probe and trials without. This revealed a smaller coefficient for pattern length in the probe condition ($\beta = -0.154$, $p = 0.00459$) compared to that of the pattern conditions ($\beta = -0.334$, $p < 0.001$). Therefore, if the stimulus just contained a drop in statistics and without a pattern the animal is significantly less likely to respond GO, suggesting that the ferrets are genuinely using the repeating pattern as marker to respond GO in the task.

To understand whether removing the cue of the repeating pattern would impact detection speed, I looked at the reaction time (see **Figure 2.9C-D**). We can see that the distributions between the different variations in drop in stimulus statistics (RAN-REG3, 5 and 7) are overlapping. This is confirmed with a mixed linear regression that showed no effect of pattern length ($p = 0.861$) but did show a main effect of whether there was a pattern or a probe, where if it was a probe trial the reaction time significantly increased compared to when a regular pattern was present ($\beta = 0.346$, $p < 0.001$, probe = 1, pattern = 0, see **Table 2.10**). Therefore, this suggests that the animals do detect the transition quicker when additionally having the repeating pattern in the tone sequence.

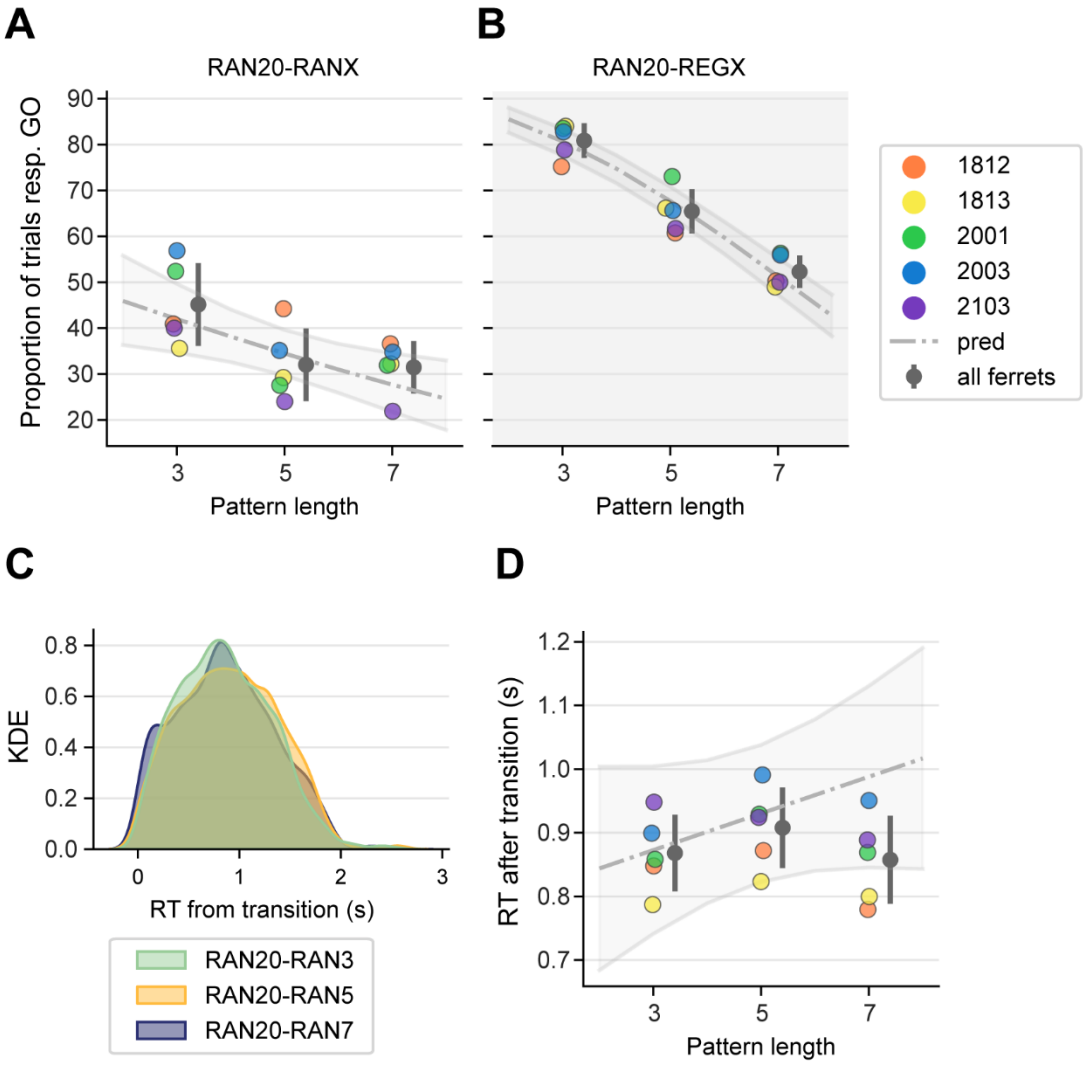

Figure 2.9: Performance and reaction time on trials with a change in stimulus statistics but no repeating pattern (probe trials). A) Proportion of probe trials in which the subject

responded to the left (GO). B) Proportion of trials containing a pattern in the same session in which the subject responded to the left. C) Kernel density estimate of all reaction times across ferrets split by alphabets. D) Reaction time from transition from random alphabet of 20 to 3, 5 and 7 for each ferret. Error bars = std. Model predictions in grey dashed line with 95% confidence intervals.

					CI 95%	
Fixed effects	Estimate	Standard error	T	p value	Lower	Upper
Intercept	2.412	0.111	21.818	**< 0.001**	2.184	2.639
Probe vs pattern (ref = pattern)	-2.200	0.257	-8.561	**< 0.001**	-2.727	-1.671
Pattern length	-0.331	0.0194	-17.112	**<0.001**	-0.371	-0.295
Pattern length × probe	0.177	0.049	3.616	**0.00126**	0.0765	0.278
Probe						
Intercept	0.212	0.235	0.900	0.385	-0.296	0.719
Pattern length	-0.154	0.045	-3.417	**0.00459**	-0.251	-0.0566
Pattern						
Intercept	2.397	0.126	18.977	**< 0.001**	2.125	2.670
Pattern length	-0.334	0.0194	-17.213	**< 0.001**	-0.376	-0.292

Table 2.9: Model output for mixed effects binomial regression on the p(go) after the transition on probe and pattern trials $R^2 = 0.932$; Df = 26; random effect std. = 6.203×10^{-10}. Separate model for probe ($R^2 = 0.384$; Df = 13; random effect std. = 0.0844) and pattern ($R^2 = 0.964$; Df = 13; random effect std. = 0.135) underneath.

					CI 95%	
Fixed effects	Estimate	Standard error	T	p value	Lower	Upper
Intercept	0.842	0.0339	234.818	**< 0.001**	0.775	0.908
Pattern length	-0.000618	0.00479	0.129	0.861	-0.00877	0.0100
Probe vs pattern (ref = pattern)	0.346	0.0831	4.167	**< 0.001**	0.183	0.509
Pattern length × probe	0.0181	0.0165	1.108	0.273	-0.0143	0.0504

Table 2.10: Model output for mixed effects linear regression on reaction time on probe and pattern trials. $R^2 = 0.0704$; Df = 3768; random effects std. = 0.0512

2.4.4 Detection strategies: unique elements within a pattern

One factor that could modulate performance in pattern detection is the number of elements within the pattern. For example, a pattern length of 5 could contain five or fewer unique frequencies, depending on whether any frequencies were repeated within the pattern. We might expect that patterns with all unique frequencies could be more taxing on the auditory memory and therefore may be harder to detect when

compared to patterns with only a few unique elements. If this is the case, we would then predict performance to be higher for patterns with fewer unique frequencies, potentially independent of the length of the pattern. For example, a pattern length of 3, comprised of three unique frequencies could generate similar performance to a pattern length of 5 with three unique frequencies. If the number of unique elements did not modulate performance, we would then observe similar performance across the number of unique frequencies, but only modulated by the pattern length.

In **Figure 2.10A** we can see that performance decreases as the number of unique frequencies within the pattern increases, even within the same pattern length. For example, at pattern length 7 (navy) the performance at four unique frequencies is similar to that of pattern length 5 for four unique frequencies, but drops below chance (50%) at unique frequencies of 6 and more. The matched alphabet case of RAN5-REG5 also shows a decrease in performance with increasing frequencies and overall, there is lower performance compared to that of the unmatched RAN20-REG5 condition (see **Figure 2.10B**). A mixed effects logistic regression on the number of correct trials reveals a significant effect of unique frequencies, with performance decreasing as the number of unique frequencies increases ($\beta = -0.366$, $p < 0.001$). We also still see main effects of pattern length and random alphabet. This suggests that the number of unique frequencies are a significant factor in helping the ferret judge if there was a transition from random to regular, and they struggle to perform above chance with approximately five or more unique frequencies.

As we see a modulation in performance with the number of unique frequencies, I wanted to see if the same is true for the ferret's reaction time and if we would also observe delayed reaction times for patterns with more unique frequencies. In **Figure 2.10C** we see that reaction time remains consistent, with perhaps a small delay, as the number of frequencies increases. In **Figure 2.10D** we see that there is almost no change in reaction time for patterns comprised of different numbers of unique frequencies within the RAN5-REG5 conditions. A mixed effect linear regression revealed a significant interaction between condition and unique frequency ($p < 0.001$; see **Table 2.12** and **Figure 2.10C**; coloured dashed lines). Separating by condition we can see that for shorter pattern lengths, the larger number of unique frequencies the larger the difference in reaction time however this difference starts to decrease as you increase the pattern length. This may suggest that there is some delay in reaction time

as you increase the number of unique frequencies, but this is dependent on the condition.

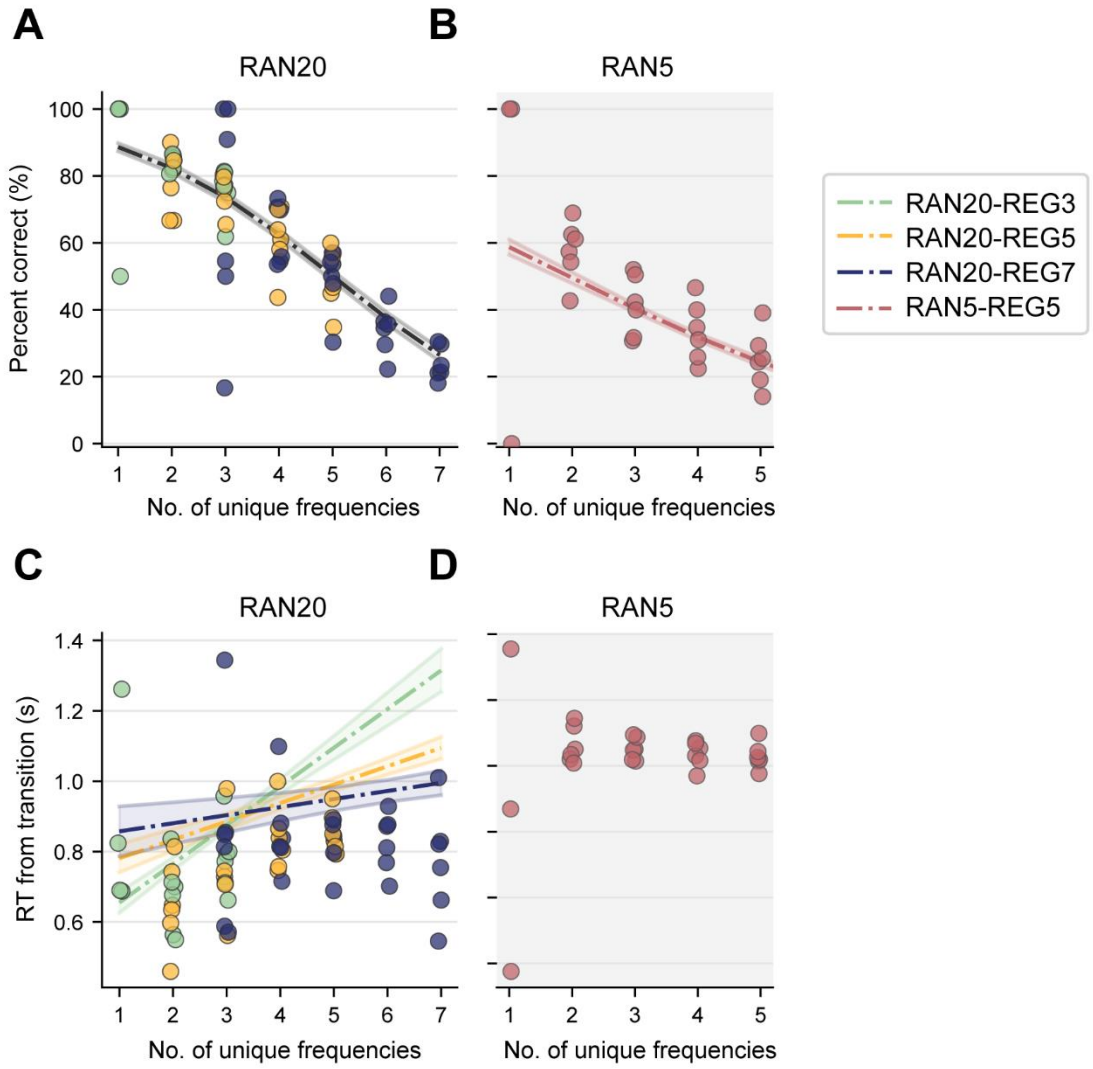

Figure 2.10: Performance and reaction time for patterns with various unique frequencies. A) Percentage of correct trials for each ferret for different unique frequencies in the pattern, coloured by pattern length (RAN20-REGX) for RAN20 sequences and B) RAN5 sequences. Predicted values from the mixed effects logistic regression is shown with the dashed line and 95% confident intervals. C) Reaction time on all sessions for RAN20 sequences for each ferret coloured by pattern length (RAN20-REGX) for RAN20 sequences and D) RAN5 sequences

Fixed effects	Estimate	Standard error	T	p value	CI 95% Lower	CI 95% Upper
Intercept	0.532	0.193	2.748	**0.00560**	0.152	0.911
Pattern length (PL)	-0.0843	0.0220	-3.834	**< 0.001**	-0.127	-0.412
Random alphabet (RA)	0.126	0.00583	21.59	**< 0.001**	0.114	0.137
Unique frequencies	-0.366	0.0319	-11.458	**< 0.001**	-0.428	-0.303
PL × Unique freqs	0.00695	0.00456	1.522	0.128	-0.00200	0.0158
RA × Unique freqs	-0.00967	0.00146	-6.634	**< 0.001**	-0.0125	-0.00681

Table 2.11: Model output for mixed effects logistic regression on performance with regards to unique frequencies within the pattern. R^2 = 0.186; Df = 104005; random effect std. = 0.311

Fixed effects	Estimate	Standard error	T	p value	CI 95% Lower	CI 95% Upper
Intercept	0.686	0.0456	15.038	**< 0.001**	0.597	0.775
Pattern length (PL)	0.0530	0.00604	8.770	**< 0.001**	0.0412	0.0649
Random alphabet (RA)	-0.0123	0.00169	-7.290	**< 0.001**	-0.0157	-0.00903
Unique frequencies	0.0527	0.00999	5.279	**< 0.001**	0.0332	0.0723
PL × Unique freqs	-0.0156	0.00130	-12.026	**< 0.001**	-0.0182	-0.0131
RA × Unique freqs	0.00418	0.000442	9.450	**< 0.001**	0.00331	0.00505
RAN20-REG3						
Intercept	0.545	0.0340	16.03	**< 0.001**	0.479	0.612
Unique frequencies	0.110	0.00731	15.044	**< 0.001**	0.0956	0.124
RAN20-REG5						
Intercept	0.729	0.0265	27.529	**< 0.001**	0.677	0.781
Unique frequencies	0.0523	0.00523	9.987	**< 0.001**	0.0420	0.0625
RAN20-REG7						
Intercept	0.835	0.0440	18.966	**< 0.001**	0.748	0.921
Unique frequencies	0.0229	0.00659	3.481	**< 0.001**	0.0100	0.0358
RAN5-REG5						
Intercept	0.881	0.0237	37.108	**< 0.001**	0.835	0.928
Unique frequencies	-0.00448	0.00597	-0.750	0.453	-0.0162	0.00722

Table 2.12: Model output for mixed effects linear regression on reaction time with regards to unique frequencies within the pattern. R^2 = 0.0252; Df = 56525; random effect std. = 0.0394. RAN20-REG3: R^2 = 0.0217; Df = 25462; random effect std. = 0.0655. RAN20-REG5: R^2 = 0.0217; Df = 15857; random effect std. = 0.0280. RAN20-REG7: R^2 = 0.0113; Df = 5618; random effect std. = 0.0485. RAN5-REG5: R^2 = 0.0034; Df = 9586; random effect std. = 0.0274.

2.4.5 Exploring ferret behaviour with a PPM-Decay model

Overall, the above findings show that ferrets can detect all conditions above chance, pattern lengths ranging from 3 to 7 tones and the matched RAN5-REG5 condition. Mirroring behavioural work in humans, decreases in performance as the pattern length increases and in the matched condition are observed. Additionally, the ferrets show longer reaction times for the longer pattern lengths. In humans we do not start to see a lag in reaction time (compared to the transition) until pattern lengths of 15 tones and greater (Barascud et al., 2016). According to the PPM model, an ideal observer with perfect short- and long-term memory should detect the transition from random to regular within 3 to 4 tones (see **Figure 2.11A**). However by using a modified version of the PPM model in which short- and long-term auditory memory capacities can be varied (the PPM-Decay model), the authors were able to replicate the latency seen for longer pattern lengths (Harrison et al., 2020).

Taking into account that ferrets, like humans (Harrison et al., 2020), may not act as ideal observers for all pattern lengths but instead contain memory constraints, and that these memory constraints are likely to be stricter than in humans, I explored whether I could recapitulate the reaction time differences in my ferret data using the PPM-Decay model. To manipulate memory constraints one can adjust the long-term memory phase half-life within the PPM-Decay model, thus limiting how long the previous events in the sequence are kept in memory. Calculating the information content with and without these constraints (see **Figure 2.11A,B**) and comparing the difference, we can see firstly that the variance of information content across the random sequences increases, but also the baseline information content after the transition also increases as the pattern length increases. This in turn reduces the separation in the distribution in information content between the random sequence (grey) and regular sequence (coloured) which could reduce detection and thereby limit performance with increasing pattern lengths.

To examine reaction times we can assume that the ferret might rely on a particular value of information content as their threshold for detecting regularity. Examining the data from the PPM-Decay model with the memory constraint (with an arbitrary threshold of 2) we can compare the time at which the regular sequence reaches this threshold increases with increasing pattern lengths. Like the ferret data, the model predicts an increasing reaction time with increasing pattern length.

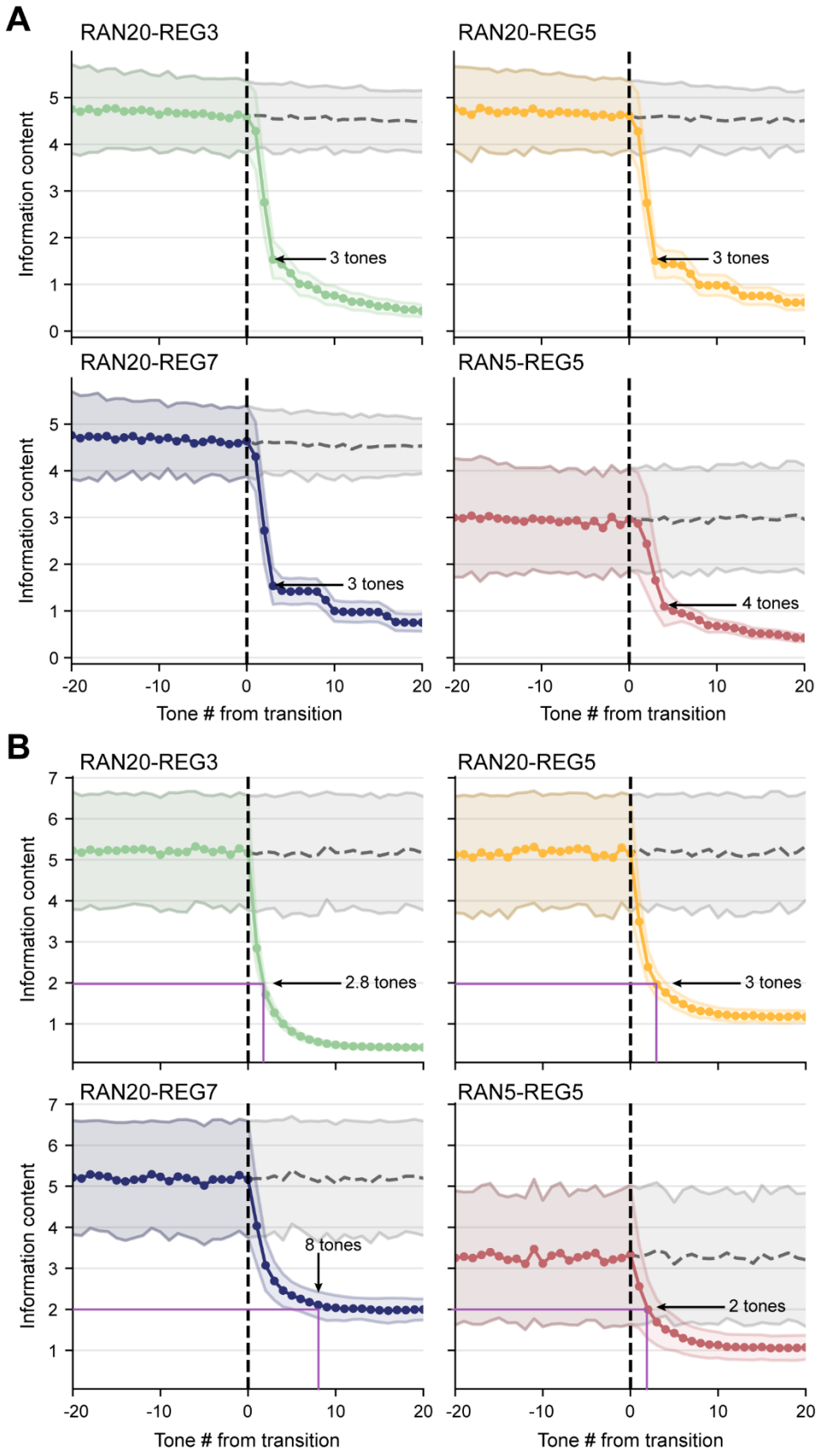

Figure 2.11: PPM-Decay model of random to regular tone sequences. A) Average information content (based on the PPM-Decay model without decay parameters) for each condition for the regular (coloured) and random (grey) sequence with the number of tones at

which the information content reaches baseline information content. B) Average information content (based on the PPM-Decay model with a long term memory half-life of 0.1) for each condition for the regular (coloured) and random (grey) sequence marked in purple when the information content of the regular sequence reaches an information content of 2, with the number of tones after the transition annotated. The transition (when the pattern first starts repeating) is marked with a black vertical dashed line.

Interestingly we see that in the matched alphabet case (RAN5-REG5) it reaches this threshold quicker than in the unmatched case (RAN20-REG5) due to the overall lower information content in the matched case. This would lead to a shorter reaction time in the matched over the unmatched, which is what we see in the behavioural data.

2.4.6 Human psychophysics: effects of frequency range on regularity detection

To accommodate the wider cochlear filter widths in the ferret compared to that of humans, I increased the frequency range of the frequency pool each tone could be selected from, from 222Hz - 2.2kHz to 120Hz – 9.7kHz (Alves-Pinto et al., 2016a; Sumner et al., 2018; Sumner and Palmer, 2012). However, it is widely known that increasing the frequency separation between elements within a sequence of repeating tones can induce auditory streaming, whereby the sequence splits in two distinct auditory streams (Micheyl and Oxenham, 2010a; Noorden, 1975). Regularity could affect whether the sequence is perceived as a whole or segregated into separate streams, thus providing the subject with an additional or alternative strategy for detection. Therefore, I firstly wanted to test whether there would be any general changes to reaction time or performance in regularity detection for human subjects, given sequences with a narrow (222Hz – 2.2kHz; 1/6th octave spacing) and wide (120Hz – 9.7kHz; 1/3rd octave spacing) frequency range.

To do this, we tested human participants online, in a similar GO/NO-GO task to that of the previous ferret experiments, such that the subject had to release a button when they heard the repeating pattern (H1). There were four different conditions: RAN20-REG3, RAN20-REG5, RAN20-REG10 and a STEP condition which contained just a frequency change from one to another to assess a baseline reaction time for each participant. Performance was calculated for each participant (n = 20) by taking the percentage of correct trials for each condition. As we can see in **Figure 2.12A**, performance for the STEP condition was near ceiling, with the detection of the patterns (REG3, 5 and 7) also near ceiling with an average performance of 95.78% ± SE

0.440%. However there does seem to be a small decrease in performance for the narrow frequency range compared to the wide frequency range. Taking the mean difference in performance between the wide and narrow condition for each participant reveals a small but insignificant difference in performance (see **Figure 2.12B**; mean = 1.167; W = 313, p = 0.166, *Wilcoxon*). A mixed effects logistic regression also confirms no main effects of pattern length, or frequency range, or any interactions (see **Table 2.13**). Therefore changing the frequency range from which tones are sampled from does not affect the ability for humans to detect regularity.

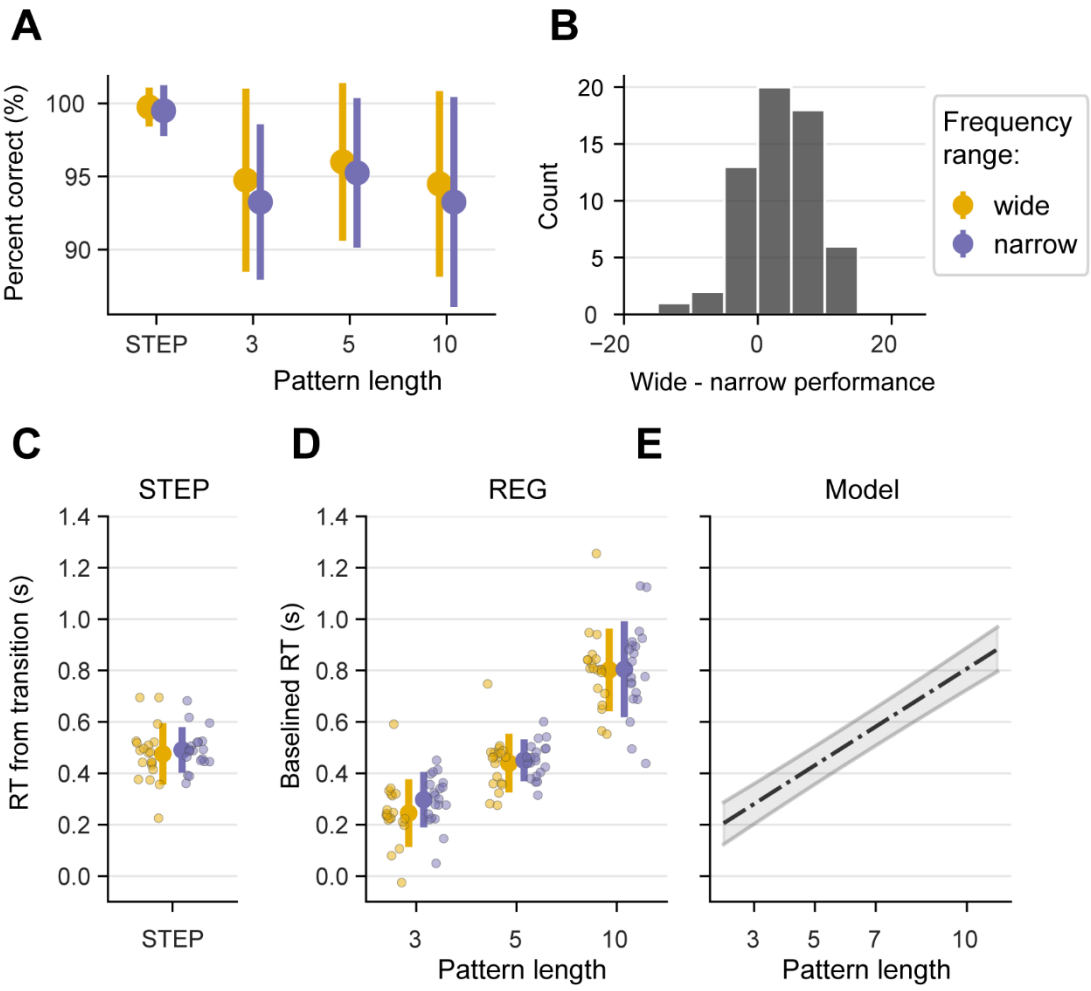

Figure 2.12: Performance and reaction times to regularity detection with wide and narrow frequency ranges of tone sequences in H1. A) Average percentage of correct trials across subjects for each condition, split by frequency range (wide = yellow, narrow = purple). B) Difference in performance of each subject to each condition (excluding the STEP condition) where positive indicates a higher performance for the wide frequency range. C) Reaction time after the transition to the STEP condition for each subject and averaged across all subjects. Error bars = standard deviation.

Now that I've shown that increasing the range of frequencies over which tones are presented doesn't change performance, I wanted to next investigate if reaction time would be affected due to any potential streaming from differences in the frequency range. The subjects mean reaction time was calculated for each condition and baselined against their mean reaction time to the change in frequency in the STEP condition. These data show that with on average participants had a reaction time of 0.5s to the basic change in frequency and this was mostly the same between the wide and narrow frequency ranges (see **Figure 2.12C**). Looking at their ability to detect RAN20-REG3, RAN20-REG5 and RAN20-REG10 patterns, we see that their reaction time does increase with pattern length, which we expect for the narrow, but also behaves the same for the wide, with little difference between the two conditions. A mixed effects linear regression confirmed this and showed a main effect of pattern length ($p < 0.001$) but no main effect of frequency range on reaction time ($p = 0.187$) or any interaction between the two ($p = 0.358$; see **Figure 2.12E** and **Table 2.14**). We can therefore conclude that changing the frequency range does not affect a participant's time to detect a transition from a random to regular sequence for the pattern lengths tested.

					CI 95%	
Fixed effects	Estimate	Standard error	T	p value	Lower	Upper
Intercept	3.513	0.670	5.019	**< 0.001**	2.126	4.899
Pattern length	-0.0237	0.0996	-0.238	0.813	-0.221	0.174
Frequency range	-0.261	0.417	-0.625	0.533	-1.086	0.565
Pattern length × Frequency range	0.00499	0.0613	0.0815	0.935	-0.116	0.126

Table 2.13: Model output for mixed effects logistic regression on performance for human experiment 1. N = 20; $R^2 = 0.341$; Df = 116; random effect std. = 0.732

					CI 95%	
Fixed effects	Estimate	Standard error	T	p value	Lower	Upper
Intercept	-32.855	71.251	-0.461	0.646	-173.98	108.27
Pattern length	84.385	10.475	8.056	**< 0.001**	63.637	105.13
Frequency range	58.755	44.279	1.327	0.187	-28.945	146.45
Pattern length × Frequency range	-6.117	6.625	-0.923	0.358	-19.239	7.006

Table 2.14: Model output for mixed effects logistic regression on reaction time (ms) for human experiment 1. N = 20; $R^2 = 0.831$; Df = 116; random effect std. = 0.0592

No differences in performance were observed, which is suggestive but not definitive as to whether humans use the same strategy in detecting the transition from random to regular with a wide or narrow frequency range. Moreover, there remains some concern that the online methods may not be sensitive enough to pull out small differences in reaction time that might occur between the narrow and wide condition. Therefore I wanted to rule out if any streaming of the pattern in the wide frequencies occurred compared to that of the random. Several studies have shown that listeners are worse at identifying the temporal order of sounds if they segregate into separate auditory streams, than compared to within stream (Micheyl and Oxenham, 2010a, 2010b; Noorden, 1975; Roberts et al., 2008). In this experiment (H2), I aimed to test this by testing the listener's ability to detect if the target pattern is the same as the reference pattern. In 50% of trials the target had the order of two tones swapped compared to the reference. I hypothesised that an increased tendency to group the pattern into two distinct streams in the wide condition would be reflected in the listener being worse at detecting such changes in temporal order relative to the narrow condition.

For H2 I calculated each subjects hit rate, false alarm rate and d' for each condition (see **Figure 2.13**). We can see that performance (both in the percent correct and d') is higher for the wide frequency range over the narrow, with a slight decrease in performance for the longer pattern length of 10. A two-factor (frequency range and pattern length) repeated measures ANOVA on performance (d') revealed a significant effect of frequency range ($F_{(1,19)} = 13.252$, $p = 0.0017$) but no effect of pattern length ($F_{(1,19)} = 3.815$, $p = 0.0657$) or interaction ($F_{(1,19)} = 0.022$, $p = 0.8832$). Analysis of the proportion of hits and false alarms show this decrease in performance for the narrower frequency range was due to a significant reduction of hits, where the subject correctly identified the probe as being the same as the preceding pattern, ($F_{(1,19)} = 27.335$, $p < 0.001$) rather than an increase in false alarms ($F_{(1,19)} = 0.809$, $p = 0.3797$). Post-hoc pairwise analysis on d', with Bonferroni correction, shows a significant decrease in performance between frequency ranges for pattern length 10 at the narrow frequency range ($T(19) = 3.193$, $p = 0.0096$), but no difference between frequency ranges for pattern length 7 ($T(19) = 2.109$, $p = 0.097$). So despite hypothesising that performance at the wider frequency range would be lower, I actually see the reverse at the longer pattern of 10. This may suggest that there may not be differences in streaming

between the frequency ranges but perhaps another mechanism such as increased saliency for tones that are more separated in frequency, but only for pattern length 10, when the task is more difficult.

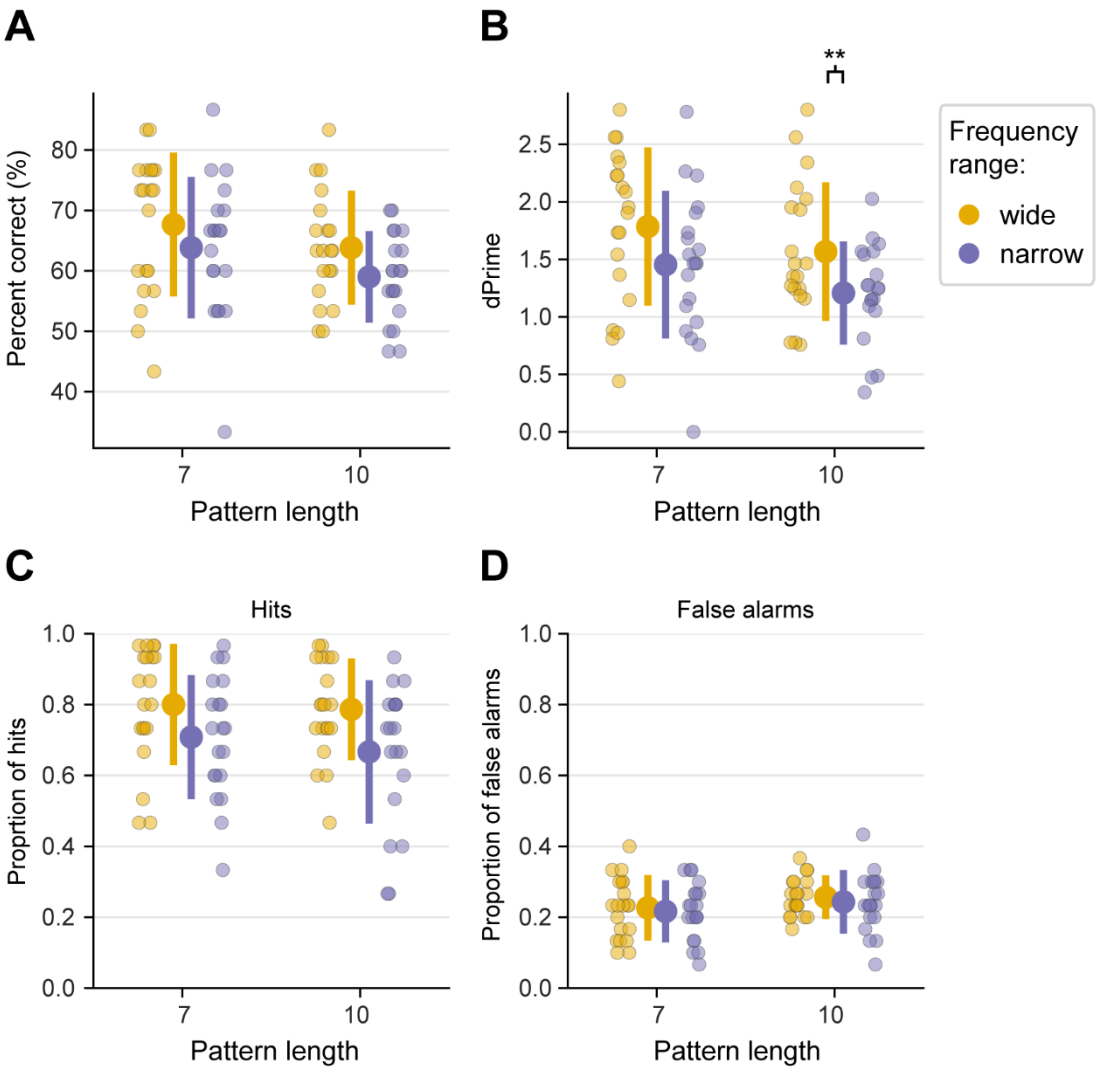

Figure 2.13: Performance of detection to the same/different patterns in experiment 2. A) Percent of correct trials (A), d' (B), hit rate (C) and false alarm rate (D) for each subject split across condition and frequency range (wide = yellow, narrow = purple). Error bars show the average across conditions. Error = standard deviation. * = $p < 0.05$, ** = $p < 0.01$, *** = $p < 0.001$.

2.5 Discussion

The aim of this Chapter was to create and validate a behavioural paradigm in an animal model that will allow us to uncover the neural basis underpinning regularity detection. A GO/NO-GO task was developed to test the detection of a change from

random to regular tone sequences for a range of pattern complexities. The rapid tone sequences, initially used in the study by Barascud et al. (2016), allow me to probe the automatic processing of regularity whilst retaining tight control over the frequency content of the stimuli.

The animal model used, the ferret *(mustela putorius furo),* is frequently used in auditory research as their hearing range, unlike other animal models such as the mouse (approximately 1kHz to 96kHz), overlap that of humans (ferret range: approximately 20Hz to 44kHz; human range: approximately 20hz to 20kHz; Heffner and Heffner, 2007; Kavanagh and Kelly, 1988). The access to low frequencies, typically absent in rodent models, allows study of vocalisation, sound localisation and pitch perception, and in this case stimuli with a frequency range that more closely resembles that used in previous human literature. Ferrets can be successfully trained on a wide variety of complex auditory cortex tasks (Bizley et al., 2013; Keating et al., 2013; Ma et al., 2010; Nodal et al., 2008; Walker et al., 2009; Yin et al., 2010) and have been shown to be sensitive to repetitions of broadband noise samples (Lu et al., 2018), and can separate acoustic repetitions into different auditory streams (Ma et al., 2010; Saderi et al., 2019) making them a prime candidate for research into regularity detection.

I chose a GO/NO-GO paradigm to assess the animal's ability to detect regularity in which they were required to hold at a central spout during random tone sequences and respond at a peripheral spout when they heard the regular sequence emerge. This paradigm allows me to assess both performance in the task and the animal's reaction time to identify any changes in the time they detect this change from random to regular. Overall, my results show that ferrets can successfully detect the change from random to regular in a tone sequence, previously only used in human behavioural and imaging studies (Barascud et al., 2016; Southwell, 2019; Southwell et al., 2017; Southwell and Chait, 2018). Analysis of performance within this paradigm consistently showed across every animal trained and tested that the ferret can detect changes from random to regular making them a good model for studying regularity detection.

Changing the length of the pattern offers the opportunity to understand how responses change with increasing complexity of the regularity. We see that performance decreases from about 85% at RAN20-REG3 to approximately 65% at

RAN20-REG7 showing a systematic decrease, as you increase the pattern length, in the ferret's ability to detect the regularity. In comparison to the human psychophysical experiment I implemented, humans performed at ceiling from pattern lengths of 3 to 10. I also observed an increase in reaction time as I increased the pattern length, ranging from 0.85s at RAN20-REG3 to 1s at RAN20-REG7. This suggests that the animals are waiting for more elements in the pattern to be presented in the longer pattern lengths before they make their decision to respond. However an ideal observer should be able to detect these transitions within 3 to 4 tones once the pattern has repeated, which humans do, but only at pattern lengths of less than 15 tones. After this we see the same latency in response when looking at human behavioural data for pattern lengths of 15 tones and more (Barascud et al., 2016), which has been explained by adding memory constraints to the PPM-Decay model (Harrison et al., 2020). This could suggest that the ferret auditory system behaves similarly to this model but has tighter or different memory constraints to that of humans. This would decrease their ability to differentiate the information content between the random and regular sequence in different conditions but also cause the point at which the information content drops below a detection threshold to be delayed in time, relative to the pattern length.

Another factor that could explain the ferret's ability to detect regularity is just detecting the change in stimulus statistics, i.e. the drop in frequencies present when moving from a random alphabet of 20 frequencies to a subset of 3, 5 or 7. Animals were trained and tested on a matched alphabet stimulus (RAN5-REG5) where the frequencies in the random and the regular sequence were the same and therefore the only way to detect the change is by detecting the repeating pattern. The animals were able to detect this change above chance and were also quicker in the matched condition (RAN5-REG5) compared to the equivalent unmatched condition (RAN20-REG5). In addition to the matched alphabet condition, we also presented probe trials which only contained a change in stimulus statistics (i.e. a drop in random frequencies from 20 to 3, 5 or 7) and we show that the animals are significantly less likely to respond at the periphery to the probe in comparison to the regular patterns.

Interestingly, we also observe that the number of unique frequencies in a pattern modulates the ferret's behaviour, where the higher number of unique elements, the poorer the ferret performs and the slower the reaction time (at conditions RAN20-

REG3 and RAN20-REG5). This could be indicative of perhaps the stricter memory constraints or may hint at the use of another detection strategy such as detection of a rhythm instead elicited by fewer unique frequencies (i.e. the rhythmic A in ABACA, over ABCDE). This has yet to be tested in humans and could be an interesting avenue for work as it is still not clear if the whole pattern is represented, or just a few salient frequencies that stream out in which the auditory system responds.

The spacing (1/3 octaves) using in this paradigm is double that of the spacing of that used in human literature (approximately 222Hz to 2 kHz at 1/6 octaves; Barascud et al. 2016) thereby spanning a larger range of frequencies. We chose to present a wider frequency to the ferrets as due to their wider auditory filters than humans (Alves-Pinto et al., 2016b; Sumner et al., 2018) as it avoided presenting two tones within the same auditory filter. It also maximises the likelihood of responsive neurons during extracellular electrophysiological recordings in later chapters as the microelectrodes span large areas of auditory cortex, giving a recording range of at least 120Hz to 19.2 kHz. The online psychophysics experiments demonstrated no difference between frequency ranges in performance or reaction time in an equivalent online GO/NOGO task for humans.

Interestingly in the 2AFC task designed to assess listeners' strategy we see the opposite effect of what we hypothesised. In the wider frequency range people performed significantly better in detecting changes in the temporal order of the pattern. This suggests that the wider frequency separation is not eliciting greater streaming than in the 'standard' frequency range and is therefore consistent with subjects perceiving the pattern as a whole. Furthermore, the performance advantage for the wider frequency range may be a result of leveraging the saliency and decrease of any cross-frequency adaptation that could be occurring in the narrow frequency range. Widening the spacing between frequencies does not appear to change the strategy for regularity detection in humans. While we cannot be certain what strategy the ferrets are using, these data suggest that a wider frequency range alone does not alter the strategy for detecting regularity and is consistent with similar detection strategies between the two species. Even if streaming was contributing to ferrets' ability to detect regularity, we cannot be sure that streaming does not occur in humans. Secondly, if streaming does occur and causes increased attention to a certain bandwidth of frequencies, it may not affect the detection of the pattern as regularity detection has

been shown to occur automatically during passive listening despite attention (Barascud et al., 2016; Southwell, 2019). However, to further probe this question, the same paradigm in which the frequency range is widened for ferrets and testing their ability to differentiate between the same and different order of tones could give insight into whether they are streaming.

Therefore overall, we can conclude that ferrets make an excellent model who likely are applying similar strategies to humans in regularity detection. The following chapters will now leverage this model with extracellular electrophysiology to uncover the neural processes underlying regularity detection both passively and during this behaviour.

3 CHAPTER THREE: CORRELATES OF REGULARITY IN THE LOCAL FIELD POTENTIAL OF AUDITORY CORTEX

3.1 INTRODUCTION

In chapter 2, I show that the ferret can detect transitions from random to regular tone sequences in a GO/NO-GO paradigm. Using this animal model and task, I aim to find whether neural correlates of regularity detection are present in auditory cortex in the recorded local field potential (LFP), where these correlates are localised, the time course of these oscillations, and how they change with the length of the pattern and behaviour. By analysing the LFP, I can bridge earlier MagEG, EEG and fMRI experiments in humans with microelectrode recordings in animals as the LFP, unlike single-unit recordings, is a measure of the dynamics of the local neural network.

Previous work in humans have revealed neural correlates of regularity detection when presented random to regular sequences, like that used in chapter 2 (Barascud et al., 2016; Southwell et al., 2017). MagEG recordings revealed an increase in power at the onset of the random sequence which continues to rise and then plateaus. When the sequence transitions to a regular sequence the power then increases further, before once again plateauing at this higher level (Barascud et al., 2016). The authors suggest that this increase in power is the upweighting of salient sensory evidence used to update the predictive model of the incoming stimulus. EEG recordings have identified that this increase in power varies with the pattern length of regular sequence; smaller patterns and therefore more predictable stimuli elicit larger increases in power in the neural signal (Southwell et al., 2017). This increase in power has been shown to occur at the time at which an ideal observer model, IDyOM, detects the change from random to regular based on the information content from the previous tones (Barascud et al., 2016).

In addition to DC modulation of the EEG signals, oscillations at the tone presentation rate and pattern rate were identified (Southwell, 2019). Analysis of the EEG signal revealed larger oscillations at the tone presentation rate for regular sequences compared to random sequences, with the difference decreasing with increasing length of the pattern (Southwell, 2019). These oscillations are seen as a proxy for the tone-onset response and show stronger or more synchronised responses in the regular condition despite any low-level adaptation that may occur through the

repetition of the patterns. An increase in oscillatory power at the pattern rate was also revealed for each pattern length with larger increases for shorter patterns (Southwell, 2019).

Source localisation revealed that these signals were found over auditory cortex, hippocampus and the inferior frontal gyrus (Southwell, 2019). This was supported by fMRI recordings that showed increased activation in Heschel's gyrus and the planum temporal (PT) for the regular sequences over random sequences (Barascud et al., 2016). However, EEG and MagEG are large-scale measures of neural activity and attempts to identify source locations of neural correlates are subject to unknown effects of volume conduction and are typically limited to superficial areas of the brain (Srinivasan, 2006). This can be aided with the addition of fMRI recordings however BOLD signals do not necessarily correlate with the neural signals captured via EEG (Nunez and Silberstein, 2000).

In this chapter I present similar deterministic acoustic patterns as those used in earlier human studies and aim to compare the neural correlates observed with meso-scale LFP recordings to those observed previously with macro-scale signals in humans. LFP signals were recorded from animals whilst they performed a GO/NO-GO task as described in chapter 2, from microelectrode arrays implanted over auditory cortex. Firstly, I assess the power in the evoked LFP during the presentation of random and regular sequences and how this varies with the length of the pattern. Secondly, I aim to identify any changes in oscillatory power at the tone presentation rate (20Hz) or pattern repetition rate for each pattern length: 3, 5 and 7 tones, at rates: 6.67, 4.0 and 2.86Hz respectively, and how these change over the course of regularity presentation. Furthermore, with the increased spatial resolution from the microelectrodes compared to that of EEG or MagEG recordings, I compare how these signals differ across the major subdivisions of AC in the ferret: primary (medial ectosylvian gyrus, MEG) and secondary (posterior ectosylvian gyrus, PEG; anterior ectosylvian gyrus, AEG) fields and approximate depth.

In contrast to work in humans, analysis of the LFP showed no significant differences in the average evoked power between random or regular sequences in any pattern length presented. Nonetheless, strong oscillations at the tone presentation rate (20Hz) were present which differed across conditions, although in contrast to

humans, the oscillatory power was weaker for regular sequences when compared to random sequences. As predicted from human work, oscillatory power at the pattern repetition rate (6.67, 4.0 and 2.86Hz for pattern lengths 3, 5 and 7 respectively) revealed significant increases in the SNR for all pattern lengths tested in the regular condition.

3.2 METHODS

3.2.1 Surgical procedure

Three trained adult female pigmented ferrets (F1812, F1813, F2001) were implanted with WARP microelectrode arrays once they reliably performed above chance on all conditions (see **Figure 3.1A**). Microdrives were surgically implanted under sterile conditions whilst the ferret was under anaesthesia. Local injections of Marcaine were injected subcutaneously around the temporal muscle. The temporal muscle was then exposed through an incision and removed. The underlying skull was cleaned with citric acid (1%) and covered with dental adhesive (Supra-Bond C&B, Sun Medical).

Two ground screws were embedded in the skull in each hemisphere approximately 5mm from the midline and either side of the craniotomy placement. To expose auditory cortex, I used the coordinates: 12mm from the midline and 11mm from the rear fissure, to target the top corner of auditory cortex in the ferret. Due to variation between animals, typically an initial craniotomy was performed and extended once the brain was exposed to reveal landmark sulci. Once the craniotomy exposed a large enough portion of brain tissue for microdrive implantation over target auditory areas (MEG, AEG, and/or PEG), the microelectrode array was positioned and then embedded within inert silicone elastomer in the craniotomy (Kwik-Sil, World Precision Instruments; see **Figure 3.1B-C**). The array was then affixed to the skull via dental cement (Palacos R+G, Heraeus) and the ground wires that were attached to the ground contact of the array were secured to the ground screws, electrically grounding the array to the subject.

Dental cement was then applied to encase the ground screws, to act as another anchor point, and custom 3D printed implant wells (see **Figure 3.1D**) that I designed and printed from durable resin (Formlabs, Form 3) were secured around the microelectrode array with dental cement to protect the array from physical damage.

The custom wells allowed attachment of custom barriers (see **Figure 3.1E**) to protect the headstages, when connected for recording, from physical contact caused by the animal, minimising motion artefacts. A head bolt was attached at the midline to aid head fixation during electrode moving and attachment of recording equipment such as recording cable supports. Excess skin was removed to secure the rest of the skin smoothly around the edges of the implant. Animals were then allowed to recover for a week post-surgery before the microelectrodes were advanced into auditory cortex. Pre-operative, peri-operative and post-operative analgesia and anti-inflammatory drugs were provided to animals under veterinary advice.

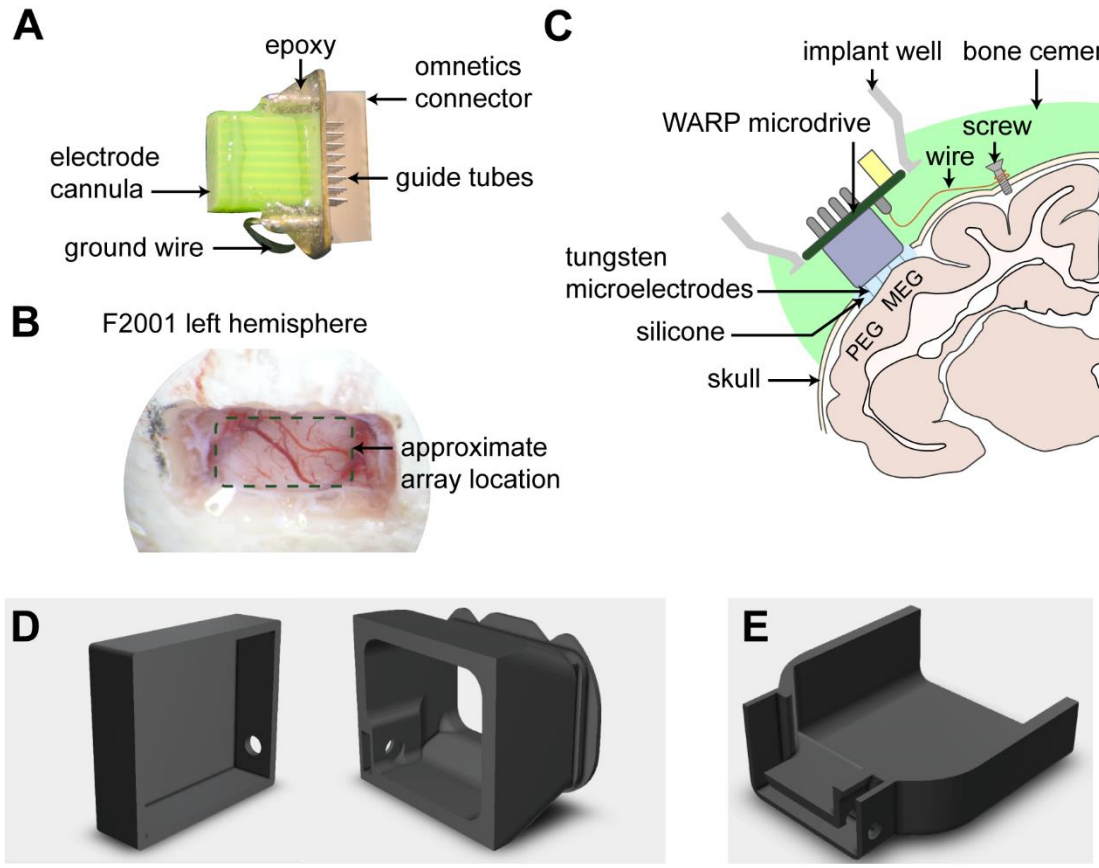

Figure 3.1: Diagrams of equipment and surgical implantation of arrays. A) Photo of the WARP 32 microdrive array that houses the tungsten microelectrodes. B) Microscope photo of a craniotomy exposing MEG and PEG in ferret auditory cortex with the footprint of the microdrive outlined (dashed line). C) Schematic of a coronal slice of the brain and implant. It illustrates the positioning of the microelectrode array, ground screws and implant well which is encase in dental cement. D) 3D models of the custom well to encase the microdrive (right) and lid (left) that screws on to protect the microdrive when not in use. E) Custom barrier than screws on the well to protect headstages plugged into the microdrive from outside physical contact.

3.2.2 Neural recordings

WARP microdrives were hand assembled with tungsten microelectrodes with the ends manually stripped of electrical insulation and bent to ensure good electrical contact to the cannula of the drive. The tips and surface of the guide tubes were covered in antibiotic gel and the surface of the implant was then coating in silicone and the join between the connector and PCB was strengthened with epoxy. WARP drives were placed over the cortical surface to target primary and secondary areas of auditory cortex (see **Figure 3.2** for anatomical locations). 7 to 11 days post-surgery the electrodes were advanced out of the drive, through the silicone and towards the surface of the cortex. The impendence of each electrode was measured during this initial advancement and once the impedance dropped to a lower value between 0 to 8 Ohms then this was measured as putative cortical surface as this drop in impedance signifies the electrode had passed through the silicone of the implant. The electrode was then advanced by approximately 0.3mm. Electrodes were further advanced every 3-4 weeks by 0.3 to 0.1mm to sample multiple units with recordings made over a period of approximately 12 to 18 months. On average 11 sites were recorded with each electrode (see **Table 3.1**). Electrodes that did not penetrate cortical tissue, did not have good electrical contact with the array, or were not localised to auditory cortex as confirmed by histology were removed from the dataset.

The neural signals from the WARP 32 drives were collected using headstages that digitized the signal (RHD 32-channel headstage C3314, Intan Technologies, which was passed to a preamplifier (PZ5, Tucker-Davis Technologies) that amplified and high passed the signal at 0.1Hz. Recordings were digitally acquired at a sample rate of 24414.0625Hz by a data acquisition system (RZ6, Tucker-Davis Technologies). Recordings were on average 20 minutes in length and occurred twice a day between Monday and Friday during behaviour.

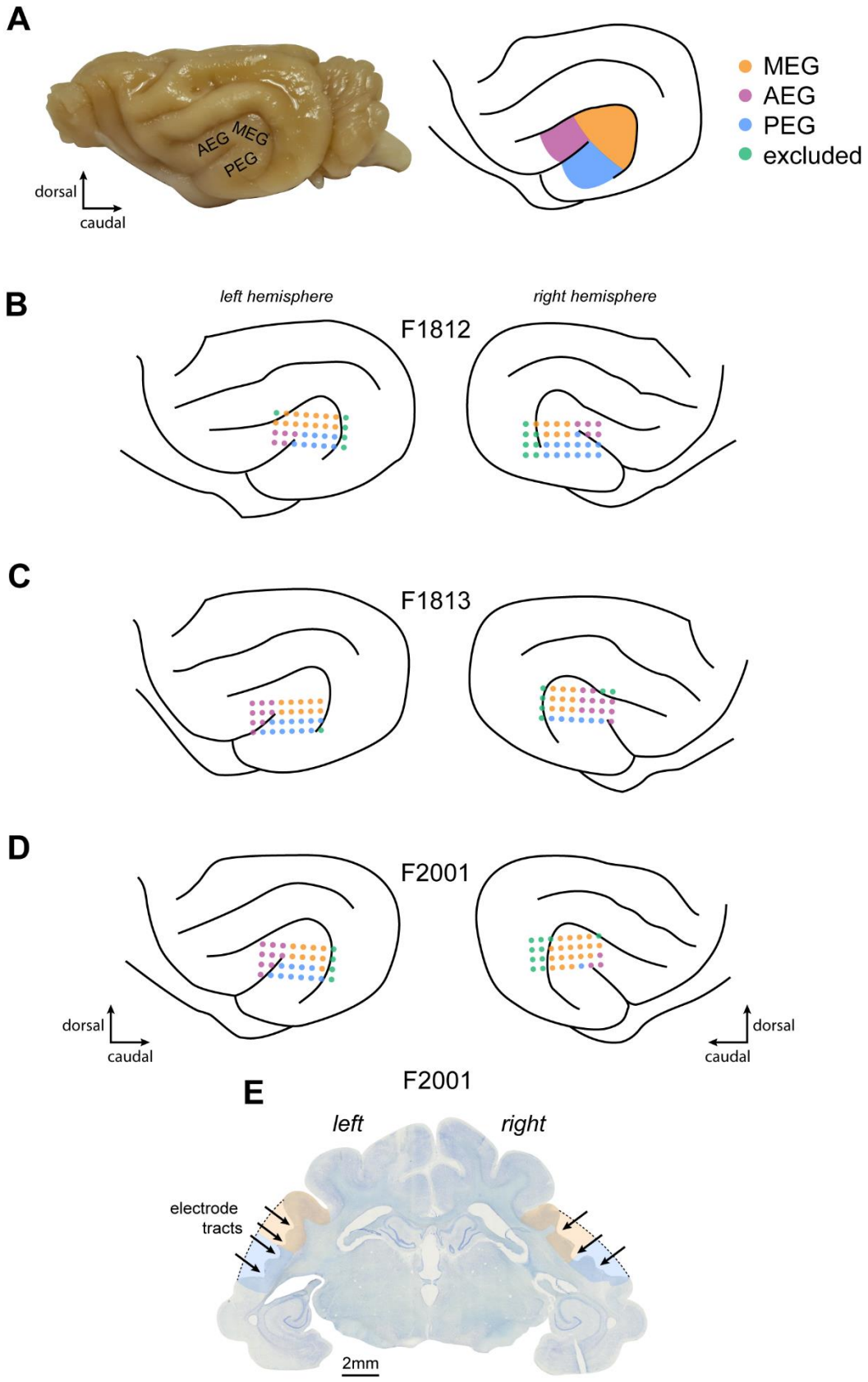

Figure 3.2: Schematic of the locations of electrodes over each hemisphere, for each subject covering primary and secondary fields of auditory cortex. A) Left - Picture of the left hemisphere of a ferret brain with labelled auditory subfields. Right - Schematic of ferret

auditory cortex (left hemisphere) with primary (MEG: orange) and secondary fields (AEG: purple; PEG: blue) highlighted. Electrodes outside of these areas were excluded. B-D) Schematics of electrode placement (filled circles) coloured by estimated location (MEG, AEG, PEG or outside of auditory cortex; excluded = green). Electrode placement is shown for F1812 (B), F1813 (C) and F2001 (D). E) Nissl-stained coronal section through auditory cortex of F2001 with the arrows indicating electrode tracts, dashed line indicated approximate edge of auditory cortex, and MEG (orange) and PEG (blue) highlighted.

Subject no.	Total no. recordings	Sites	Proportion of sites aud. evoked (%)	Mean no. of trials per site:				
				Across conditions	RAN20-REG3	RAN20-REG5	RAN20-REG7	RAN5-REG5
F1812	367	354	12.4	3,834	467	607	497	723
F1813	287	492	21.6	2,198	270	328	300	374
F2001	349	567	39.1	3,793	374	542	457	802
Total	1,003	1,413	-	9,825	1,111	1,477	1,254	1,899

Table 3.1: Number of recordings sites per animal and average number of trials of each condition at each site. Total number of recordings are the number of recording sessions completed per animal. Individual sites are defined as individual microelectrodes at individual recording depth, not including excluded sites (outside of auditory cortex).

3.2.3 Histology

To confirm electrode location and position, at the end of the experiment the animal was transcardially perfused with 0.9% saline and 4% paraformaldehyde (PFA) under anaesthesia. The brain was then removed for storage in PFA, before cryoprotecting in 30% sucrose for 4-5 days prior to cryosectioning. Coronal sections (50μm) were taken through the full extent of the ectosylvian gyrus. Slices were then mounted on slides in 0.5% gelatine and dried for at least 14 days. Slices were Nissl stained to identify electrode tracts and major structures within the brain to localise the position of these tracts. Sections were then stained with cresyl violet and washed with chloroform and acetic acid. The sections then went through a series of increasing concentrations of ethanol solutions to dehydrate the slides. Sections were then cleared with Histoclear, and cover slipped with a mounting agent (Omnimount). Slices were imaged using the Zeiss AxioScan Z1 at 10x magnification.

3.2.4 Neural analysis

All neural data analysis was performed offline in MATLAB (MathWorks) and Python through a custom data analysis pipeline. To extract the neural data from the

proprietary TDT file formats a TDT SDK was used. To remove large motion artefacts, a moving standard deviation was calculated along the trace with a window length of 10ms. Any points that were continuously larger than 80s.d. for ≥ 50ms or ≥ 5% of the trial, excluded the trial from further analysis. Any trials where a disconnection from the headstage lasting ≥ 50ms occurred were removed. Trials in which the animal false alarmed (left the central spout when no regularity was present) were also removed from further analysis as sound presentation was immediately terminated and followed by a noise burst. To extract out the LFP from the raw broadband neural signal, each trace was passed through a low-pass Butterworth filter (300Hz, filter order of 6). All filtering, unless stated otherwise, was zero-phase digitally filtered with the *filtfilt* function in MATLAB. The data was then down sampled to a sample rate of approximately 1kHz. After filtering and down sampling, any trials that had a signal > 350μV or a moving s.d. (window = 50 samples) of > 300 μV were also excluded from further analysis.

To eliminate poor quality sites and channels, or those outside of auditory cortex, each individual recording session site was assessed on whether it was 'auditory evoked'. Responsiveness was statistically determined via the use of the ZETA test for time series data, *zetatstest* (Montijn et al., 2021). For each site, this test compared the evoked activity of the trial-averaged LFP from the first 300ms after sound onset, across all trials within a session, to a null hypothesis distribution by running multiple bootstraps on 300ms epochs selected using jittered stimulus-onset times. A ZETA p-value of < 0.05 indicated significant auditory evoked onset activity for that recording session and site. A site was then classed as 'auditory evoked' if it had significant responsiveness in > 50% of recording sessions.

Sites were binned at approximate recording depths by assigning sites to one of three depth bins: upper, middle and lower (0.3 to 0.75, 0.75 to 1.5 and 1.5 to 2.25mm from putative cortical surface respectively). Any sites below 2.25mm were estimated to be below the cortex and excluded from analysis, based on histology (see **Figure 3.2**). To calculate the LFP power, I filtered the LFP with a low-pass Butterworth filter (30Hz, filter order of 6). Either the root-mean-square (RMS) was calculated across time points for each site and with the mean taken across all sites, or the filtered LFP was averaged across trials for each site and then averaged across sites.

To assess the oscillatory power within the LFP at specific frequencies of interest (FOIs), a power spectral density estimate (PSD) was performed and the power at these frequencies calculated for each individual site. Two second epochs of trials, starting from the onset of the transition from random to regular, across sessions from the same site were concatenated. Sites and conditions that contained < 9 epochs in the concatenation were excluded from analysis. A Welch's power spectral density estimate, *pwelch* (MATLAB), was then performed on these concatenated trials with a window length of approximately 6s (8192 samples) to achieve high frequency resolution at the lower frequencies needed to assess the pattern repetition rate. The RMS of the PSD at the FOI (± two frequency bins either side of the signal frequency bin) was then calculated and then divided by the RMS at neighbouring frequencies (± 5 frequency bins either side of the signal frequency bins) giving the signal-to-noise ratio (SNR) at the FOI (see **Figure 3.3**). This method mitigated any overall increases in power, such as an increase in 1/f neural noise, from interfering with the assessment of the change in power at the given FOI.

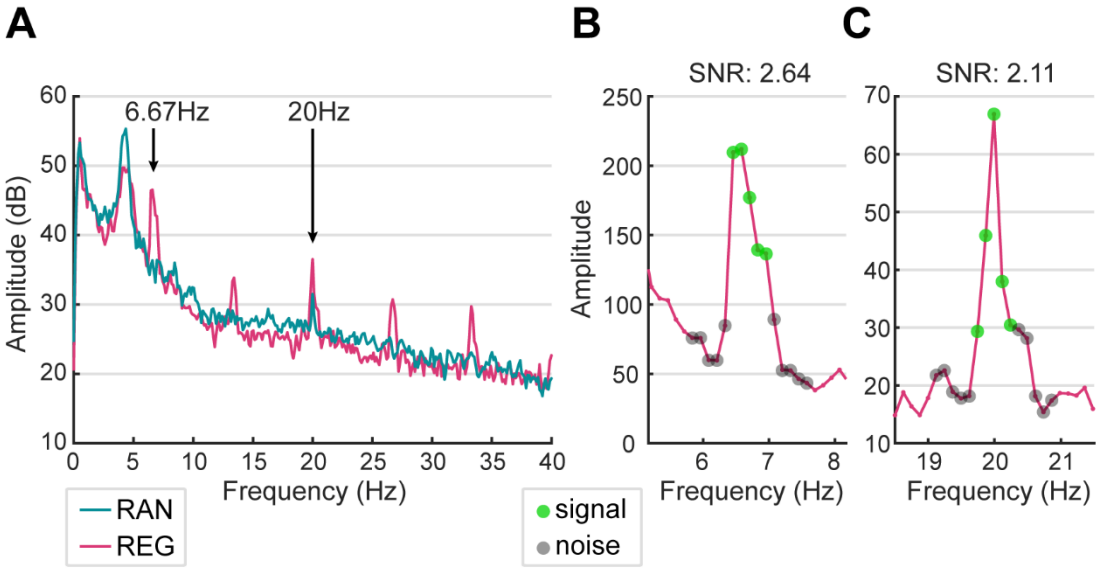

Figure 3.3: Power spectral density estimates of concatenated local field potential epochs post-transition. A) Power spectral density estimate calculated for an example recording site when presented random (blue) or regular (pink) sequence with a pattern length of three. There is a peak at the tone presentation rate (20Hz) for both random and regular sequences, but only a peak at the pattern rate (6.67Hz) in the random sequence. A peak at theta (~4Hz) is also present in both conditions. B-C) The SNR at frequencies of interest (FOIs) are calculated by taking the RMS of five points around the FOI (green) and diving it by the surrounding noise points (grey) to give a signal to noise ratio (SNR) at various FOIs such as the pattern rate (6.67Hz; A) and the tone presentation rate (20Hz; B).

To calculate the time course of the change in amplitude of these oscillations I decomposed the LFP using Morlet wavelets (width of 14 cycles) at various FOIs on epochs that were 1s before the transition from random to regular and 3s after the transition. The amplitude at each frequency for each condition was averaged across trials for each site. To identify significant differences in the amplitude of specific FOIs between random and regular conditions and the latency at which this change occurred, I performed nonparametric cluster statistical analysis that calculates a test-statistic from clusters of adjacent time samples (Maris and Oostenveld, 2007).

A modulation index was calculated for the SNR to identify differences between the random and regular conditions such that:

$$SNR\ Modulation\ index = (SNR_{REG} - SNR_{RAN})/(SNR_{REG} + SNR_{RAN}) \quad (4)$$

Statistical analysis of effects of pattern length and effects of the tone repetition number and other predictors used general linear models and generalized linear mixed models fitted using fitglm or fitglme in MATLAB (version 2022a). Only two-way interactions or less were modelled. The details of each model are outlined alongside the relevant results; however, in general, analysis of the SNR modulation index was based on a normal distribution. For each model, I report the magnitude of coefficients (estimate) of fixed and random effects, the t-statistic for a hypothesis test that the coefficient is equal to 0 (T) and its respective p-value (p) in full in the tables in the appendix. The 95% confidence intervals are also reported for each fixed-effect coefficient and the adjusted R^2 value of the model to assess model fit. Post-hoc analysis was performed in Python with the *scipy.stats* and *scikit_posthocs* modules with the appropriate pairwise comparisons stated in text.

3.3 RESULTS

3.3.1 Sequence-evoked response in the local field potential

Studies in humans showed that regular sequences elicited a higher sustained response compared to that of random sequences. In MagEG and EEG recordings, this manifested as a slow DC shift in amplitude from the transition from random to regular, ending in a plateau localised to auditory cortex (Barascud et al., 2016; Southwell, 2019; Southwell et al., 2017). Here I aimed to identify whether the local field potential

(LFP) recorded from microelectrodes in the ferrets over auditory cortex would also display this increase in power and DC shift.

To do this I recorded neural signals from microelectrode arrays placed over ferret auditory cortex whilst the animals took part in the GO/NO-GO task described in chapter 2. Ferrets were presented with tone sequences which, for 'regular trials' where random sequences transitioned to regular patterns, patterns could either be novel, or were repeated across trials. The evoked LFP was taken from the repeated regular trials to be able to average across all trials with the same transition time (2s). The LFP was low-pass filtered at 30Hz (Butterworth, filter order 6) and then windowed at -0.4 to 4.5s from stimulus onset and each trial was baselined to the median LFP in 0.4s preceding stimulus onset. I averaged the evoked LFP response over auditory evoked sites and across ferrets for the random and regular sequences of each condition (RAN20-REG3, RAN20-REG5, RAN20-REG7 and RAN5-REG5; see **Figure 3.4**).

The mean LFP shows a clear onset response to sound, as well as responses at the tone presentation rate for the duration of the stimulus. However, cluster-based permutation testing revealed no significant differences at any time point between the mean LFP in the random or regular conditions for any of the pattern lengths or random alphabet size. I calculated the RMS across time points for each site and averaged across auditory evoked sites and ferrets to measure the absolute power in the LFP and to equate to earlier human work (see **Figure 3.5**). Nonetheless, cluster-based permutation testing also revealed no significant differences between the random and regular sequences for any of the conditions evaluated.

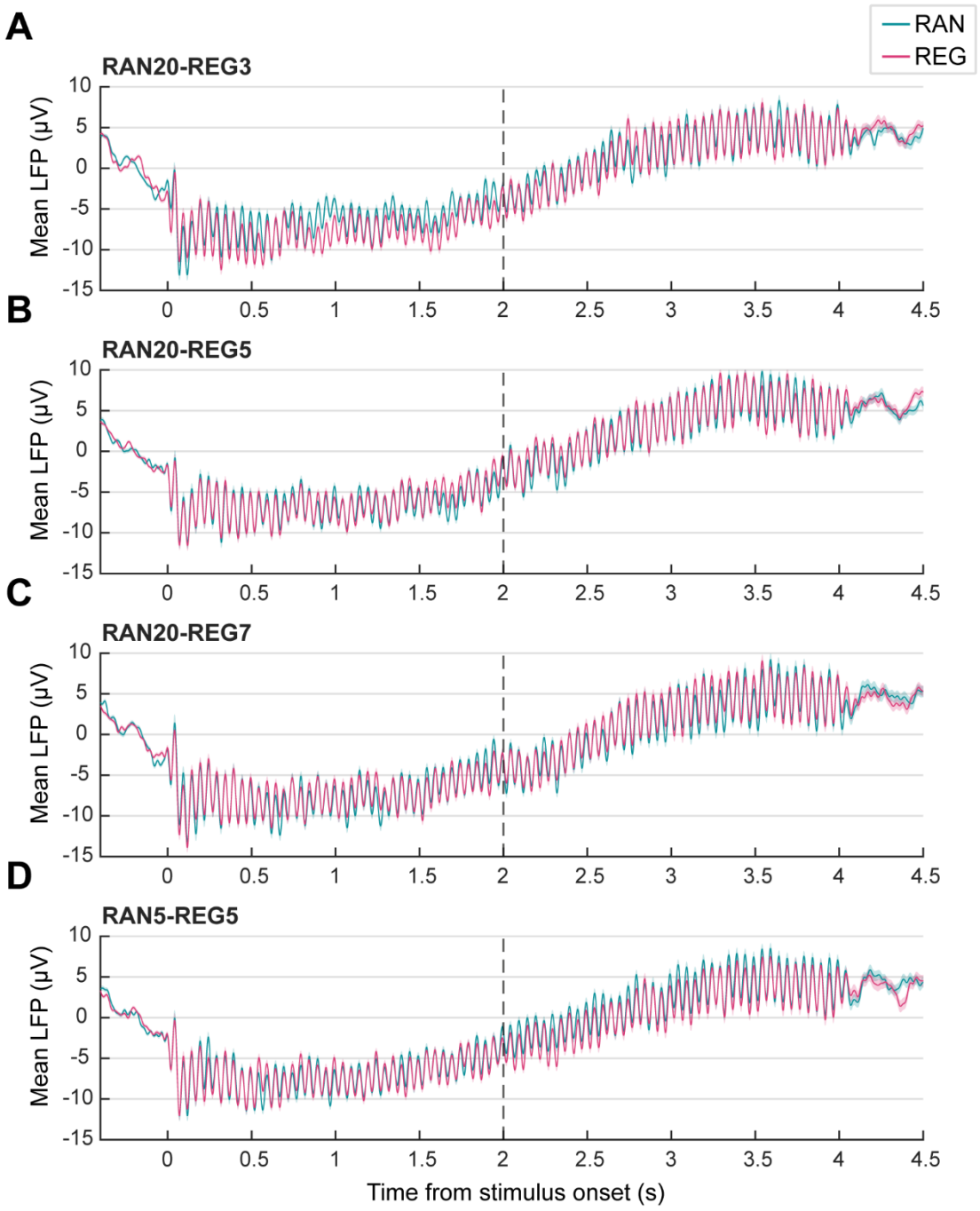

Figure 3.4: Regularity elicits no difference in the mean evoked local field potential. The mean evoked local field potential across all auditory evoked sites for entire duration of repeated regular (pink) and random (blue) sequences for A) pattern length 3 and random alphabet 20 (RAN20-REG3; n = 317 sites), B) RAN20-REG5 (n = 317 sites), C) RAN20-REG7 (n = 280 sites) and D) RAN5-REG5 (n = 266 sites). Shaded area = standard error. The dashed line indicates the transition from random to regular during the regular sequence.

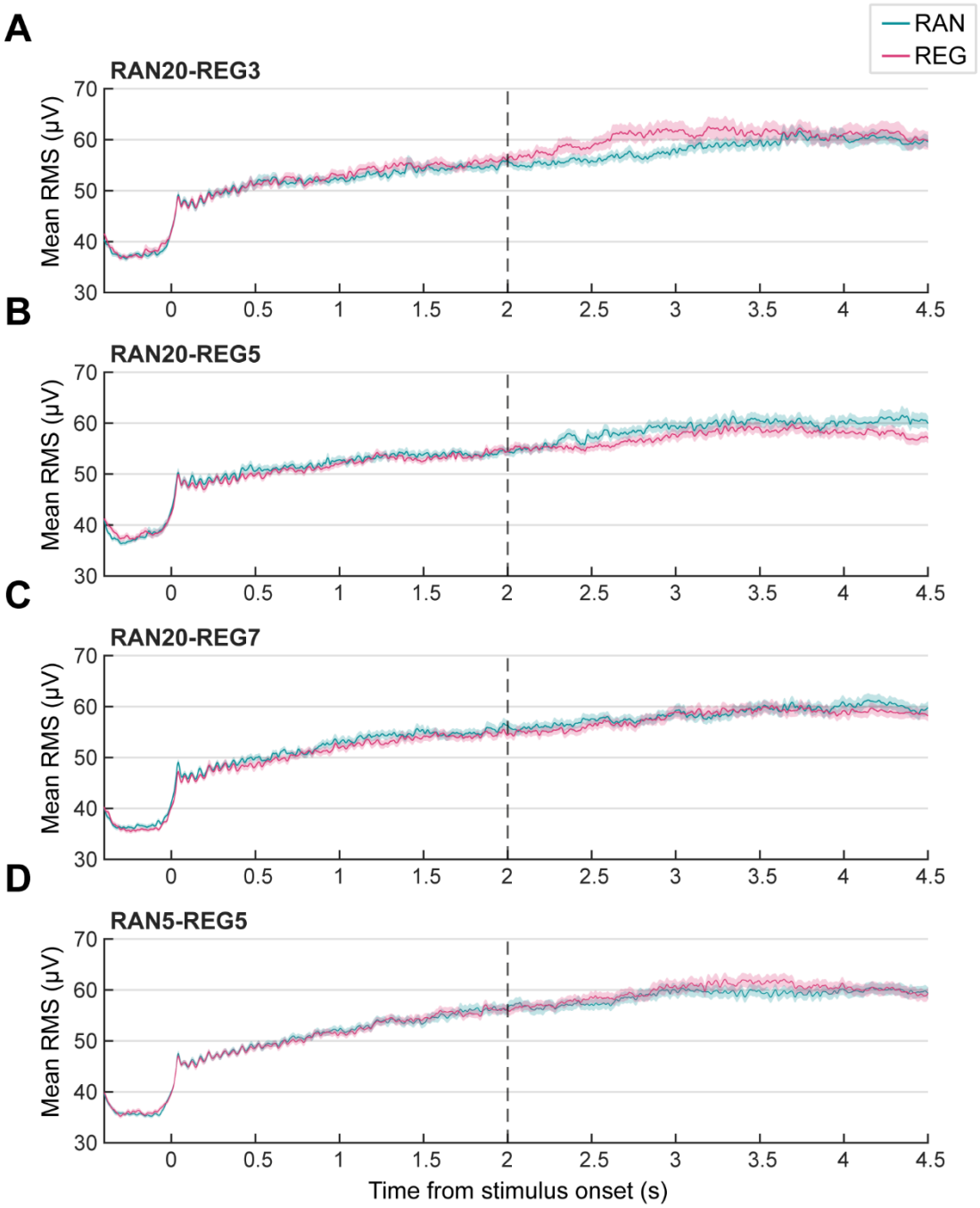

Figure 3.5: Regularity elicits no difference in the RMS of the evoked local field potential. The mean RMS of the local field potential for entire duration of repeated regular (pink) and random (blue) sequences for A) pattern length 3 and random alphabet 20 (RAN20-REG3; n = 317 sites), B) RAN20-REG5 (n = 317 sites), C) RAN20-REG7 (n = 280 sites) and D) RAN5-REG5 (n = 266 sites). Shaded area = standard error. The dashed line indicates the transition from random to regular during the regular sequence.

3.3.2 Regularity decreases oscillations at the tone presentation rate

The mean evoked and RMS of the LFP revealed no differences in power between the random and regular sequences, however evoked responses at the tone

presentation rate are easily observable. Previous work identified a small increase in power at the tone presentation rate for regular over random sequences, with the largest increase with a pattern length of 1 (a repeating tone), and the difference decreasing with increasing pattern lengths (3 and 5; Southwell, 2019). The oscillatory power at the tone presentation rate is an indicator of how responsive the local neural network is to individual tones within the stimulus, where a decrease in the oscillatory power at the tone presentation rate may indicate a drop in responsiveness due to adaptation or repetition suppression. It could also likely indicate an increase in synchrony of responses to the individual tones. To identify any differences in the oscillatory power at the tone presentation rate the spectral component of the LFP from auditory evoked sites was analysed by performing a Welch's power spectral density estimate (PSD) on concatenated 2s epochs of the trial post-transition at each recording site. The signal-to-noise ratio (SNR) was calculated at 20Hz where an SNR of > 1 indicates increased power at 20Hz compared to the side frequency bands between 19 and 21Hz.

The mean SNR across all sites and conditions showed strong tone locked responses with an SNR of 3.07 for the random (n = 296 sites) and 2.76 (n = 291 sites) for the regular condition. A Mann-Whitney U test revealed no significant difference between the conditions (U = 46995, p = 0.0560*,* see **Figure 3.6A**). Analysis by pattern length and random alphabet showed that the tone locked response remained consistent between all pattern lengths at a random alphabet 20 during the random sequence (see **Figure 3.6B**). However, the tone locked response was significantly decreased in the RAN20-REG5 condition in the random (U = 43632, p < 0.001*; Mann-Whitney U, Bonferroni*) but not the regular condition (U = 39253, p = 0.116; *Mann-Whitney U, Bonferroni)*. We see also observe a significant decrease in the tone locked response in the regular condition for RAN20-REG3 compared to that of the random condition (U = 49690, p = 0.00285; *Mann-Whitney U, Bonferroni).* This shows that in RAN20-REG3 we see a significant decrease in the power at the tone presentation rate in the regular condition which is likely due to the reduction in frequencies present, which is highest in the RAN20-REG3 condition, as this difference disappears in the matched alphabet condition (RAN5-REG5).

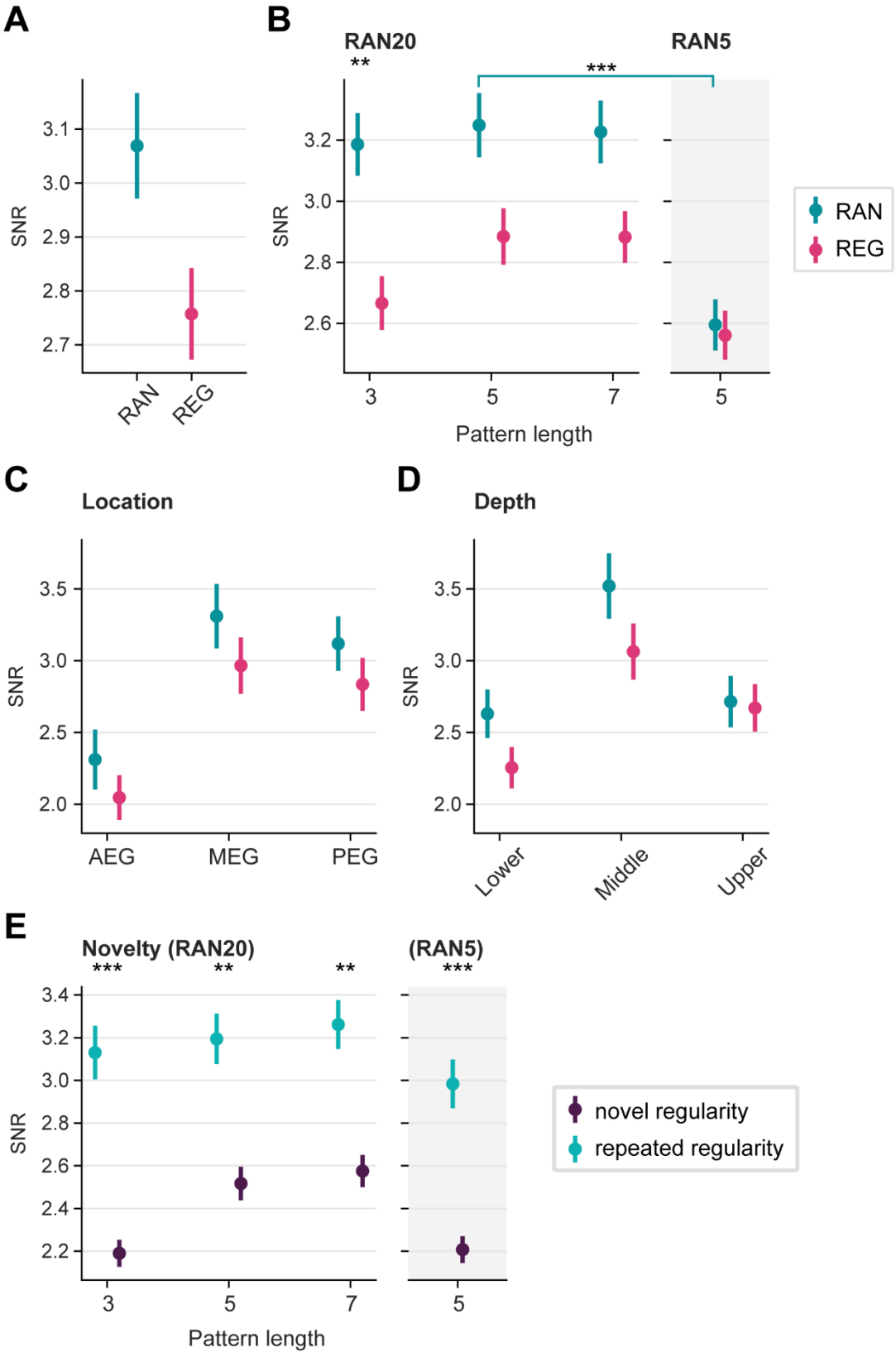

Figure 3.6: Differences in power at the tone presentation rate between random and regular sequences. A) The signal to noise ratio at 20Hz across sites for random and regular

conditions. The SNR split by condition (B), location (C) and depth (D). E) The SNR of only regular conditions that were either novel for each trial (purple) or repeated within and across sessions (cyan). Error = standard error. * = $p < 0.05$, ** = $p < 0.01$, *** = $p < 0.001$; *Mann-Whitney U, Bonferroni*.

To understand whether this difference may be stronger in primary (MEG) or non-primary (AEG and PEG) subfields, or in upper layers compared to lower layers, I split the data by location and depth. No differences between random and regular conditions at different auditory subfields (see **Figure 3.6C**) or depths (see **Figure 3.6D**) were observed, but overall stronger tone locked responses can be seen in MEG and PEG compared to that of AEG and in the "middle" depth bin of auditory cortex. Though there are differences in the absolute values of the tone presentation rate, there is no subdivision of differences between random and regular conditions between subfields or layers.

I presented regularities that were novel to each trial, and regularities that were repeated multiple times within a session and across session. To see how this would affect the tone presentation rate for repeated regularities, I took the SNR at 20Hz for trials that contained a repeating pattern and split them by novel and repeated (see **Figure 3.6D**). This revealed significant increases in the tone presentation rate in the LFP for all conditions for the repeated regularities over the novel (RAN20-REG3: $U = 40815$, $p < 0.001$; RAN20-REG5: $U = 39524$, $p = 0.00128$; RAN20-REG7: $U = 34109$, $p = 0.00101$; RAN5-REG5: $U = 33932$, $p < 0.001$; *Mann-Whitney U, Bonferroni*). This shows that repeated regularities give a higher SNR at the tone presentation rate, which is likely due to the higher signal to noise ratio by repeating neural responses to the same stimuli, compared to that of the novel regularities.

As the absolute values of oscillatory power at the tone presentation rate can vary, likely due to the frequency tuning of neurons in different subfield and layers, I took a more sensitive approach to understanding how the difference in oscillatory power between random and regular sequences at this oscillatory rate changes with various factors. I calculated a modulation index (REG-RAN/REG+RAN), such that a negative index indicates a stronger response at the tone presentation rate for the random sequence over the regular, and entered it into a mixed effect linear regression to identify any significant contributing factors (see **Figure 3.7A** and **Table 9.1** in the Appendix). Subfields (AEG, MEG and PEG) are referenced to the primary subfield (MEG), and layers (lower, middle and upper) are referenced to the upper layer, with

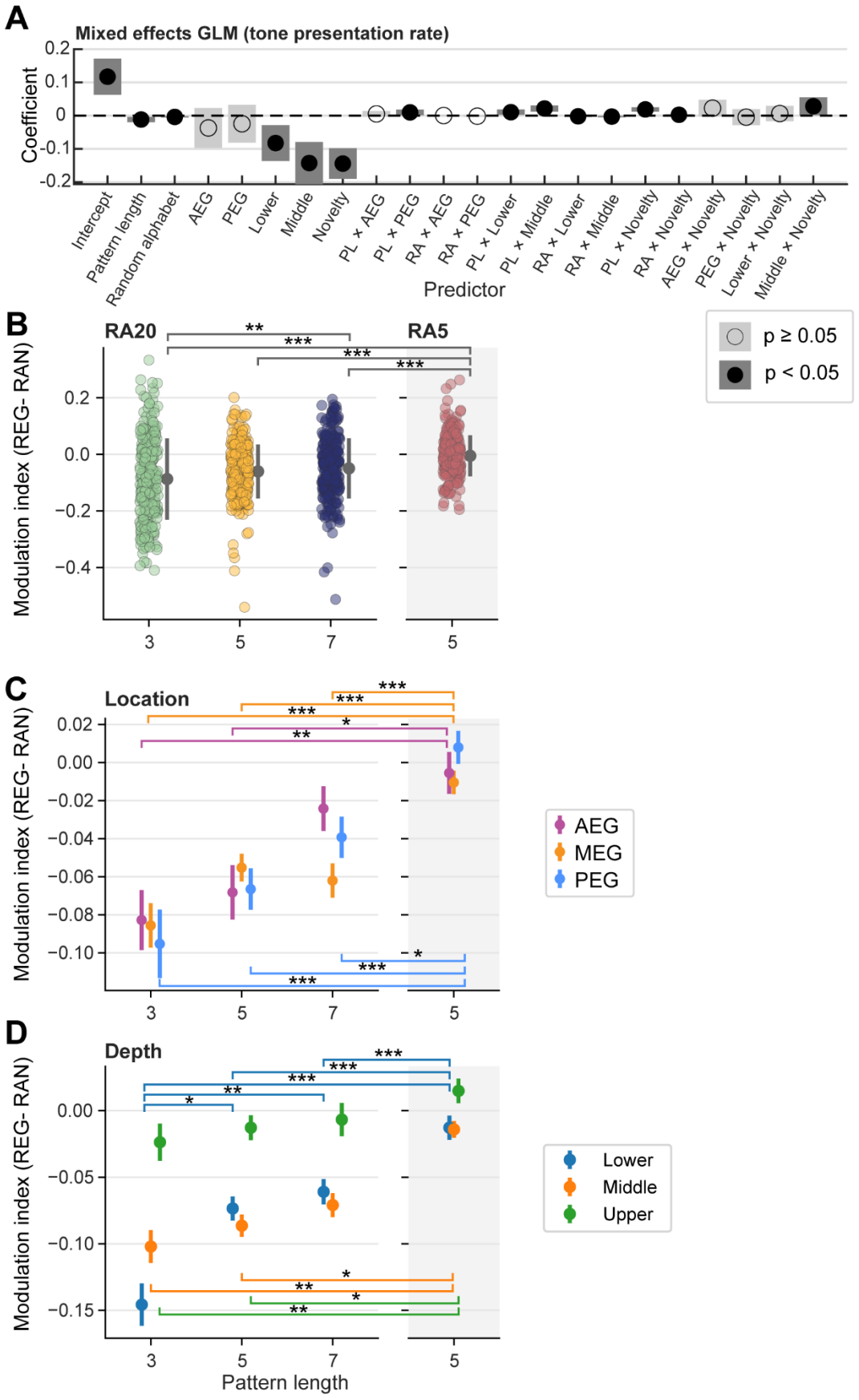

Figure 3.7: Difference in the SNR at the tone locked response between random and regular sequences across conditions and location. Mixed effects linear model on the

modulation index of the tone presentation rate. Each predictor (and two way interactions) and its coefficient, upper and lower confidence intervals are displayed with significance displayed with a filled black circle. B) Modulation index split by condition (each circle is a recording site) with the average and standard error shown across sites in grey. C) Modulation index split by location and D) split by layer. * = $p < 0.05$, **, $p < 0.01$ and *** $p < 0.001$. Errors bars = standard error.

the novelty of the regularity represented as 1 for novel, and 0 for repeated.

The model revealed a main effect of pattern length on the difference in oscillatory power at the tone presentation rate between random and regular sequences, with the difference decreasing with increasing pattern length ($\beta = -0.012$, $p = 0.005$; see **Figure 3.7B**). Pairwise comparisons between conditions show that RAN5-REG5 has significantly smaller differences in the power at the tone presentation rate compared to that of the unmatched alphabet conditions (RAN20-REG3, 5 and 7), as well as RAN20-REG3 showing a significantly larger difference in power at the tone presentation rate in comparison to RAN20-REG7. Together, this demonstrates that shorter pattern lengths result in a stronger suppression of power at the tone presentation rate than longer pattern lengths during regularity. I also observe that the matched alphabet (RAN5-REG5), elicits even smaller differences compared to the unmatched alphabet (RAN20-REG5) despite the same pattern length.

No difference between subfields is present in the modulation index (see **Figure 3.7C**) with all subfields still showing smaller differences between the random and regular sequences as you increase the pattern length and match the alphabet. However, I do observe a significant main effect of depth that reveals the upper layer behaving differently to that of the lower and middle layers (see **Figure 3.7D**). I observe less change in the tone presentation rate as the pattern length is increased in upper layers compared to that of middle and lower layers, with pairwise comparisons revealing that the lower layers show the largest difference between conditions. This shows that there are larger differences in the tone presentation rate between random and regular sequence in the middle and lower layers.

3.3.3 Pattern rate locked responses are present during regularity

Now that I've identified that oscillations at the tone presentation rate are smaller for regular sequences with shorter pattern lengths, I wanted to understand if the rate of the whole pattern can be observed within the LFP. For example, a pattern length of 3 would repeat 6.67 times a second and would potentially elicit a peak at 6.67Hz in the PSD; with pattern lengths 5 and 7 predicted to elicit peaks at their pattern rates of 4.0 and 2.86Hz respectively. I therefore followed the same analysis performed for the tone presentation rate, this time taking the SNR at each pattern rate in the 2s epoch after the transition in auditory evoked sites. Only trials where the animal was stationary at the central spout (either a miss for the regular trials or a correct reject for the random trials were included), as some of the pattern rates and their harmonics lie close to the range of theta (4-7Hz) in the ferret, which is strongly modulated by movement (Dunn et al., 2022).

I calculated the SNR at a range of frequencies of interest (FOI) including the pattern rate of each pattern length and its first harmonic (see **Figure 3.8**). For RAN20-REG3 I see significant increases in power at 2.86Hz ($U = 24312$, $p < 0.001$, *Mann Whitney U, Bonferroni*) and at the pattern rate (6.67Hz: $U = 18917$, $p < 0.001$) and the first harmonic (13.33Hz: $U = 9028$, $p < 0.001$) during regularity compared to the random sequence (see **Figure 3.8A**). For RAN20-REG5 I only see increases in power at the pattern rate and its first harmonic (4.0Hz: $U = 24204$, $p < 0.001$; 8Hz: $U = 13696$, $p < 0.001$; see **Figure 3.8B**). For RAN20-REG7 I see increases at the pattern rate and its first harmonic (2.86Hz: $U = 17895$, $p < 0.001$; 5.71Hz: $U = 27647$, $p < 0.001$; see **Figure 3.8C**). Significant decreases are also present at 8Hz ($U = 44729$, $p < 0.001$) and 13.33Hz ($U = 46170$, $p < 0.001$). For our matched alphabet condition, RAN5-REG5, I see significant increases at the pattern rate (4.0Hz: $U = 20587$, $p < 0.001$) and first harmonic (8Hz: $U = 8455$, $p < 0.001$) and a significant decrease at 13.33Hz ($U = 37346$, $p = 0.00186$; see **Figure 3.8D**). Overall, I observe increases in power at the pattern rate and first harmonic for every pattern length and condition during regularity. Typically, the SNR in the random condition sits at 1 at the various FOIs, apart from 4 and 5.71Hz, which sits within the range of ferret theta oscillations.

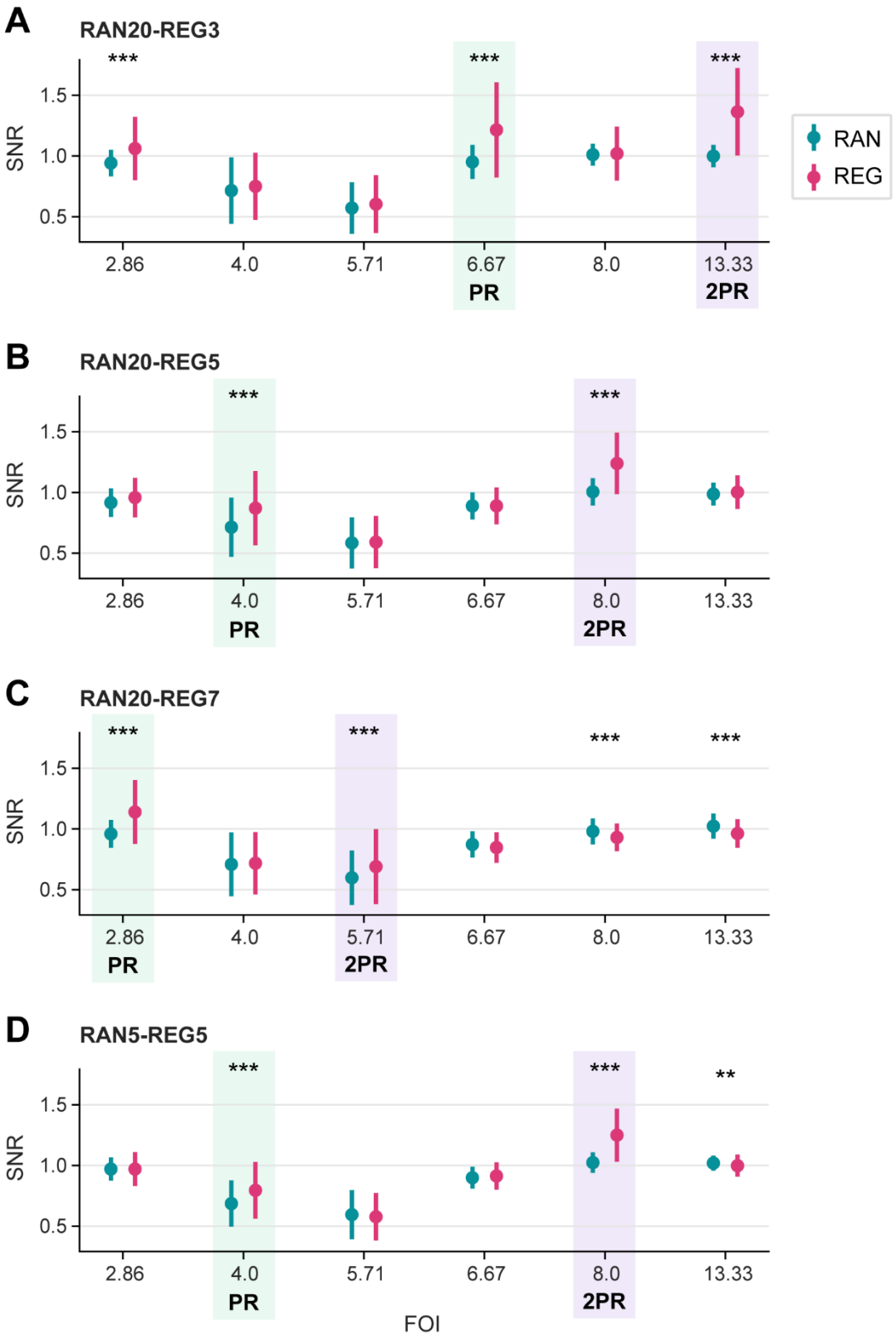

Figure 3.8: Increases in the signal to noise ratio during regularity at the pattern rate and its next harmonic for all conditions. The SNR shows largest increases during regularity at the pattern rate (PR, highlighted in green) and the pattern rates next harmonic (2PR, highlighted in purple) compared to during a random sequence for each condition: (A) RAN20-REG3 (B), RAN20-REG5, (C) RAN20-REG7, (D) and RAN5-REG5. A Wilcoxon test was

performed between the random and regular condition for each FOI to identify significant differences in the SNR (Bonferroni corrected: * = $p < 0.05$, **, $p < 0.01$ and *** $p < 0.001$). Errors bars = standard deviation.

To understand how the oscillations at the pattern rate are modulated by pattern length, random alphabet, novelty, location, and depth, I calculated a modulation index on the SNR at random and regular conditions (REG-RAN/REG+RAN) where a value of greater than 0 indicates a stronger oscillation at the pattern rate in the regular condition compared to that of the random. A mixed effects linear model revealed main effects of pattern length, the random alphabet and novelty and significant interactions between novelty and pattern length and random alphabet as well as the lower bin depth on pattern length on differences in the pattern rate between random and regular conditions (see **Figure 3.9A** and **Table 9.2** in the appendix).

Overall, I demonstrate that for all pattern lengths the modulation index remains above 0, showing that the oscillations at the pattern rate are stronger in the regular condition over the random for all conditions as expected. We also see that the as you increase the pattern length the oscillations at the pattern rate decrease significantly between RAN20-REG7 and the shorter pattern lengths of RAN20-REG3 and RAN20-REG5 and only a small difference between conditions with matched and unmatched alphabets (RAN20-REG5 and RAN5-REG5; see **Figure 3.9B**). When I split this by whether the pattern has repeated or not I observe that novel patterns elicit smaller differences in the pattern rate compared to that of repeated patterns in the shorter pattern lengths. Additionally the pattern length only seems to modulate the pattern rate oscillation in the patterns that are repeated (see **Figure 3.9C**). Analysis by depth reveals that only the deeper layers seem to show a modulation by pattern length with the RAN20-REG3 condition eliciting larger increases in the pattern rate over RAN20-REG7 (see **Figure 3.9D,** and a significant deeper layer and pattern length interaction in **A**). However, I see the largest modulation index in upper layers. In summary, the data show that firstly: an oscillation at the pattern rate for each condition is observed, with shorter patterns eliciting stronger pattern rate oscillations. Secondly, for shorter pattern lengths pattern-rate oscillations are stronger for patterns that are repeated as compared to novel ones. Finally, the modulation of oscillatory activity at the pattern rate, by pattern length, may be occurring most strongly in the lower layers, but does not vary by cortical subfield (MEG, AEG or PEG).

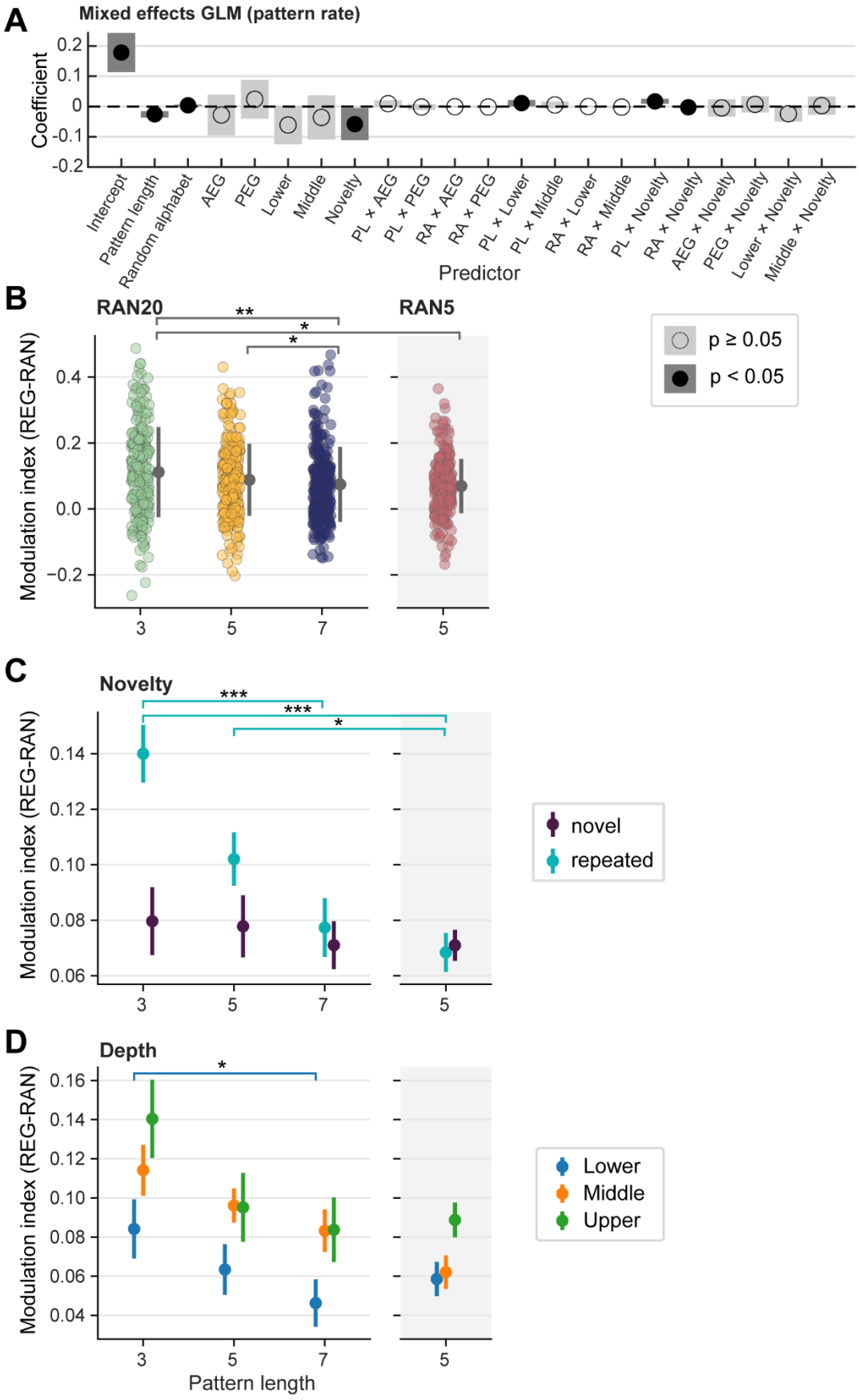

Figure 3.9: Modulation of the pattern rate oscillations within the local field potential. A) Mixed effects linear model on the modulation index of the oscillatory rate at each pattern

lengths respective pattern rate. Each predictor (and two way interactions) and its coefficient, and upper and lower confidence intervals are displayed with significance displayed with a filled black circle. B) Modulation index split by condition (each circle is a recording site) with the average and standard error shown across sites in grey. C) Modulation index split by novel and repeated patterns and D) split by depth. * = $p < 0.05$, **, $p < 0.01$ and *** $p < 0.001$. Errors bars = standard error. *Dunn test, Bonferroni*.

3.3.4 Pattern rate oscillations are modulated by behaviour

Neural recordings were presented during a behavioural task, and now that I provided evidence for oscillations at the pattern rate, I wanted to investigate how these are modulated by the animal's behaviour. So far the analysis has been performed on hit, miss and correct reject trials (false alarms were excluded, as the stimulus was terminated as soon as the animal left the central spout). However, how do these correlates change dependent on whether the animal was able to detect the regularity or not? For example, do we see enhancement or suppression of the pattern rate oscillation when the animal successfully detected regularity and how does this change with the complexity of the regularity, as neurons in auditory cortex can be modulated by behaviour. To do this I took the trials with just the regular sequences presented and then split them by trials in which the animal successfully detected the pattern (hit) and trials in which the animal failed to detect the pattern by remaining at the central spout (miss). I then calculated a modulation index such that an index of greater than 0 would indicate larger pattern rate oscillations in trials where the animal had a correct response.

The modulation index across all conditions and sites is significantly positive (mean: 0.0237, $Z = 11956$, $p < 0.001$, *Wilcoxon*) revealing that there is an increase oscillation at the pattern rate for hit trials over missed trials (see **Figure 3.10A**). However, when investigating each pattern length (and thereby pattern rate) individually, we can see that pattern length 5 is the only condition to show a positive modulation index, with pattern lengths 3 and 7 showing significantly decreased modulation indices (see **Figure 3.10B**; RAN20-REG3: $Z = 7124$, $p < 0.001$; RAN20-REG5: $Z = 3937$, $p < 0.001$; RAN20-REG7: $Z = 6504$, $p < 0.001$; RAN5-REG5: $Z = 3937$, $p < 0.001$; *Wilcoxon, Bonferroni*). This is likely due to pattern length 5's pattern rate of 4.0Hz proximity to theta oscillations (4-7Hz), which in the ferret are closely linked to movement (Dunn et al., 2022). Pairwise comparisons (*Dunn test, Bonferroni*) revealed that the modulation index for pattern length 5 was significantly different to that of pattern length 3 and 7 ($p < 0.001$). Clearly, I observe that the behaviour of the

animal, whether the trial was a hit or a miss, modulates the power at the pattern rate within the local field potential, but that the direction of modulation is dependent on the pattern rate itself (e.g. 6.67Hz or 4.0Hz). Particularly, modulation at 4.0Hz is confounded by the change in theta power from movement within the ferret.

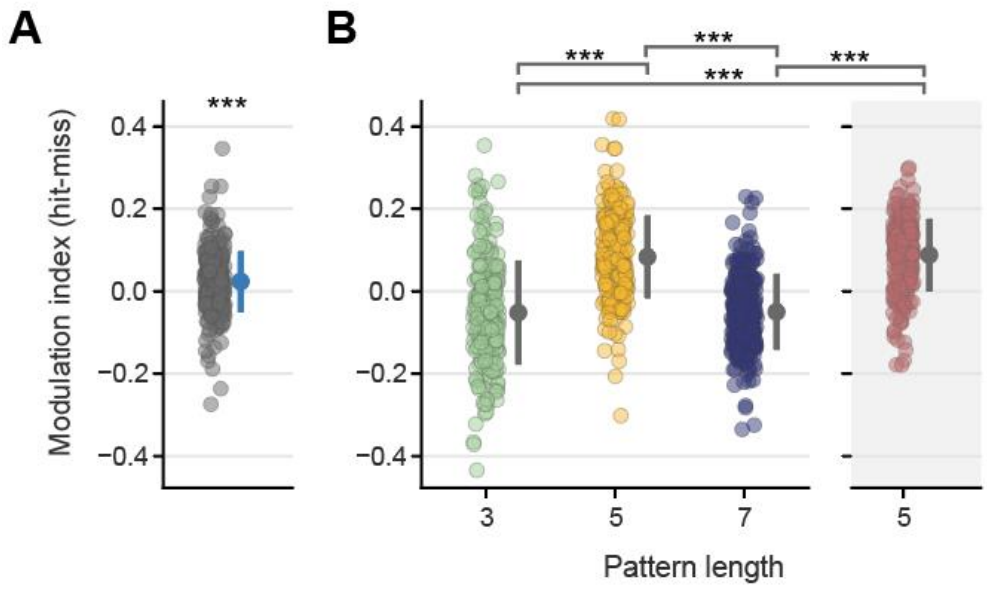

Figure 3.10: Behavioural modulation index (hit-miss) of the pattern rate oscillation SNR. A) The modulation index (where > 0 mean larger oscillations at the pattern rate in hit trials compared to miss trials) across sites and conditions where each dot is a recording site and the blue error bar is the mean and std. across all sites (*Wilcoxon test).* B) The modulation index split by condition with the grey error bars are the mean and std. across sites for each condition (*Dunn test, Bonferroni*). * = $p < 0.05$, **, $p < 0.01$ and *** $p < 0.001$. Errors bars = standard deviation

3.3.5 Emergence of pattern rate oscillations over time

As described above, oscillations at the pattern rate are present in the local field potential, though despite the previous method being sensitive to changes in power at specific frequencies, it does not give any information on how the pattern rate oscillation changes over time. It is unknown whether the representation of the pattern rate in the LFP could increase over repetitions due to increased entrainment, or whether the power at the pattern rate stays constant during presentation of the regular sequence. Likewise the timing of the emergence of the pattern rate representation could vary, emerging at different times as the signal moves through the auditory pathway. If the pattern rate increases earlier in primary subfields such as MEG, the increases in AEG and PEG may be inherited from MEG. To investigate this, I performed Morlet wavelet decomposition on the local field potential, with an example displayed in **Figure 3.11**.

In this example we can see in the spectrogram for the random condition the presence of strong theta related activity (approximately 4.5Hz) from onset (0s) to offset (4s). During presentation of the regular sequence, I observe a strong increase at the pattern rate (6.67Hz) and a strong harmonic structure (highlighted with dashed red lines) that occurs mostly 2s from stimulus onset (i.e. the time of the transition from random to regular) and abruptly ends at 4s (stimulus offset). There also appears to be modulation of oscillatory power in the theta band. In addition to examining the entire frequency range I can pull out individual frequencies of interest such as 6.67Hz (pattern rate for RAN20-REG3; see **Figure 3.11F**) and 20Hz (the tone presentation rate; **Figure 3.11G**) and perform cluster-based permutation testing to identify significant differences in power between the random and regular sequences. In this example, I observe significant increases in power at 2s from stimulus onset to just after 5s (1s from stimulus offset) at 6.67Hz, and a small but significant increase at 20Hz in the regular case, limited to between approximately 3.2 to 4.2s after stimulus onset.

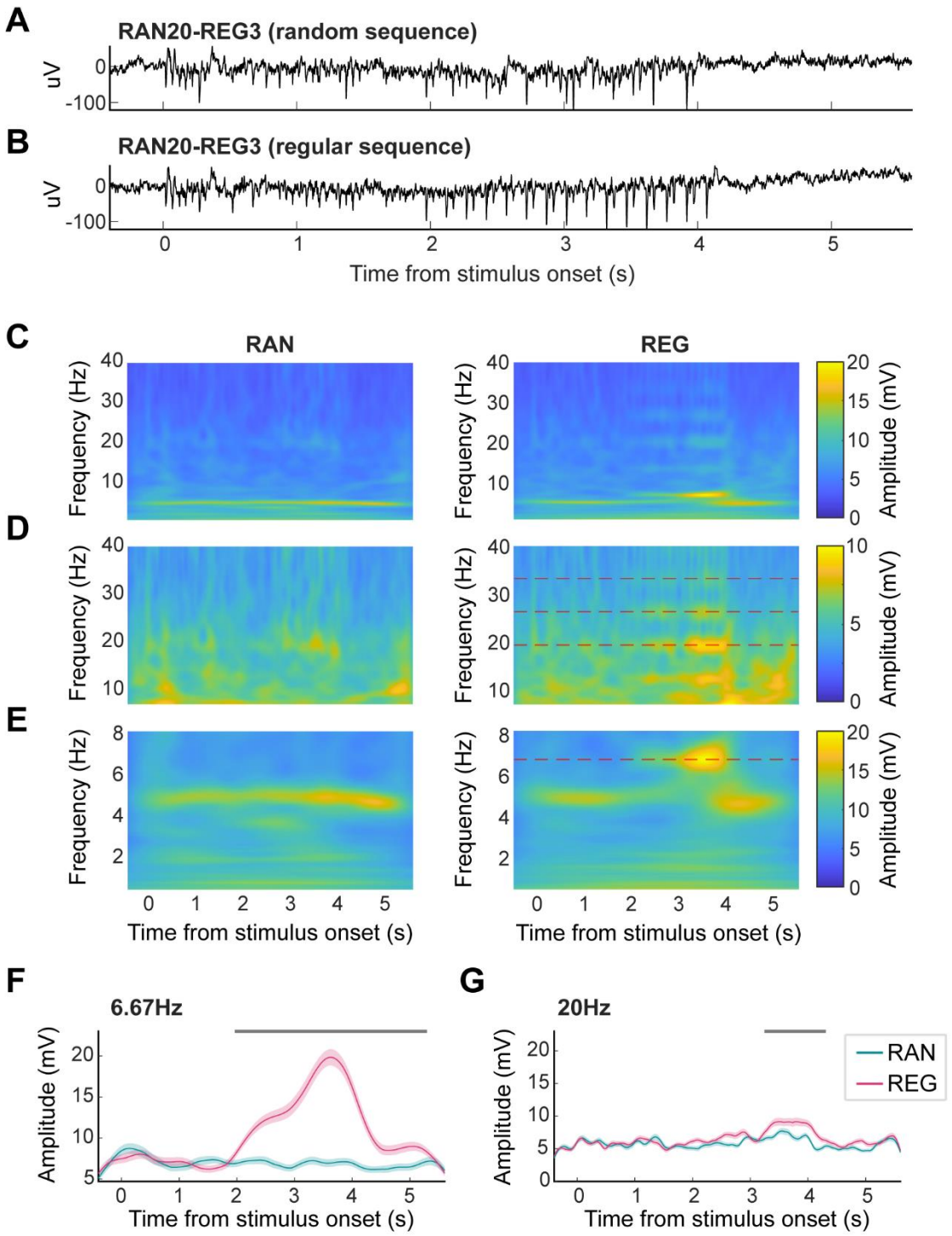

Figure 3.11: Example of Morlet wavelet decomposition of the local field potential for random and regular sequences. A) Trial averaged local field potential to a RAN20-REG3 random sequence. B) Trial averaged local field potential to a RAN20-REG3 regular sequence. C) Spectrogram using Morlet wavelet decomposition of LFP response to the random (left) and regular (right) sequence. D-E) Zoomed in spectrogram at frequencies 10 to 40Hz (D) and 0 to 8Hz (E). The dashed red lines highlight the pattern rate (6.67Hz) and its 2nd, 3rd and 4th harmonic. F-G) Power at 6.67Hz (F) and 20Hz (G) from Morlet wavelet decomposition of the LFP in response to a RAN20-REG3 sequence in the random (blue) and regular (pink) condition. The grey line detonates time points at which the power between the random and

regular sequences are significantly different from each other ($p < 0.05$, cluster permutation based statistics). Error = s.e.

Due to the trade-off between time and frequency resolution, I focused the analysis on RAN20-REG3 conditions to analyse the pattern rate of 6.67Hz and tone presentation rate of 20Hz with a fine enough time resolution to observe any changes as the regular sequence emerges. I also only examine, correct trials, due to noise bursts that are presented in incorrect trials at the end of stimulus presentation. At the pattern rate, I demonstrate that across all sites there is a large significant change in power by about 1mV at the peak starting 197ms from transition onset and ending at 3.07s, 1.07s after stimulus offset ($p = 0.0099$; see **Figure 3.12A**, left*).* When I separate sites by location, AEG (see **Figure 3.12B**, left) and MEG (see **Figure 3.12C**, left) show significant increases in the pattern rate in the regular sequence with oscillations in MEG starting earlier and lasting longer than that of AEG (AEG: 661ms to 2.72s, $p = 0.0495$; MEG: 211ms to 3.05s, $p = 0.099$). Surprisingly, we see that PEG is the only subfield to not show significant changes between random and regular sequences (see **Figure 3.12D**, left).

When I split the regular trials by hit and miss responses, I show that any divergence in the pattern rate oscillation occurs after the regular sequence has finished (see **Figure 3.12**, right). Across all sites I observe a significant increase in power at the pattern rate in the miss trials (2.13s to 3.11s, $p = 0.0297$; see **Figure 3.12A**, right) and that this significant difference is only significantly maintained within MEG (2.16s to 3.12s, $p = 0.0396$; see **Figure 3.12B-D**, right), however there does also seem to be an increase, albeit insignificant, within AEG. In conclusion, I demonstrate that the pattern rate oscillations, begin almost immediately after the transition in MEG, followed by AEG, up to a similar magnitude before starting to decrease at approximately 1.5s after the transition and continuing even after stimulus offset (2s after the transition). Interestingly I also see an increase in power in miss trials after stimulus offset at 6.67Hz, but this only reached statistical significance in MEG.

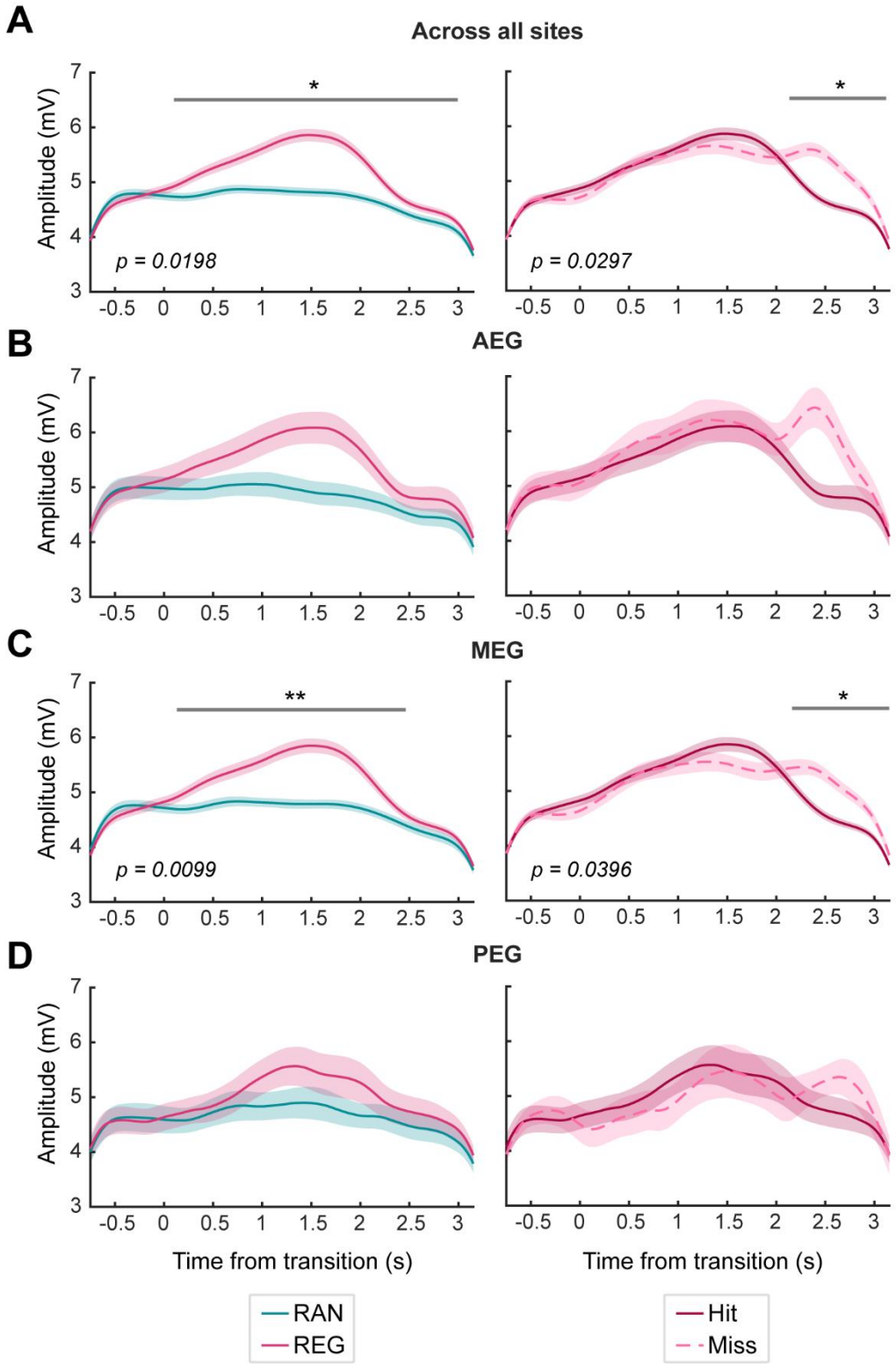

Figure 3.12: Oscillatory power over time at the pattern rate (6.67Hz) in the local field potential for the RAN20-REG3 condition. A) Left - Mean power at 6.67Hz across all sites for random sequences (blue) and regular sequences (pink), with the x axis denoting the start of the transition from random to regular, and 2s from the transition as the offset. Right – Mean power at 6.67Hz across all sites for regular sequences on hit trials (dark pink) and miss trials (dashed light pink). B-D) Mean power across sites at AEG (B), MEG (C) or PEG (D). Error = standard error. * = $p < 0.05$, ** = $p < 0.01$, *** = $p < 0.001$.

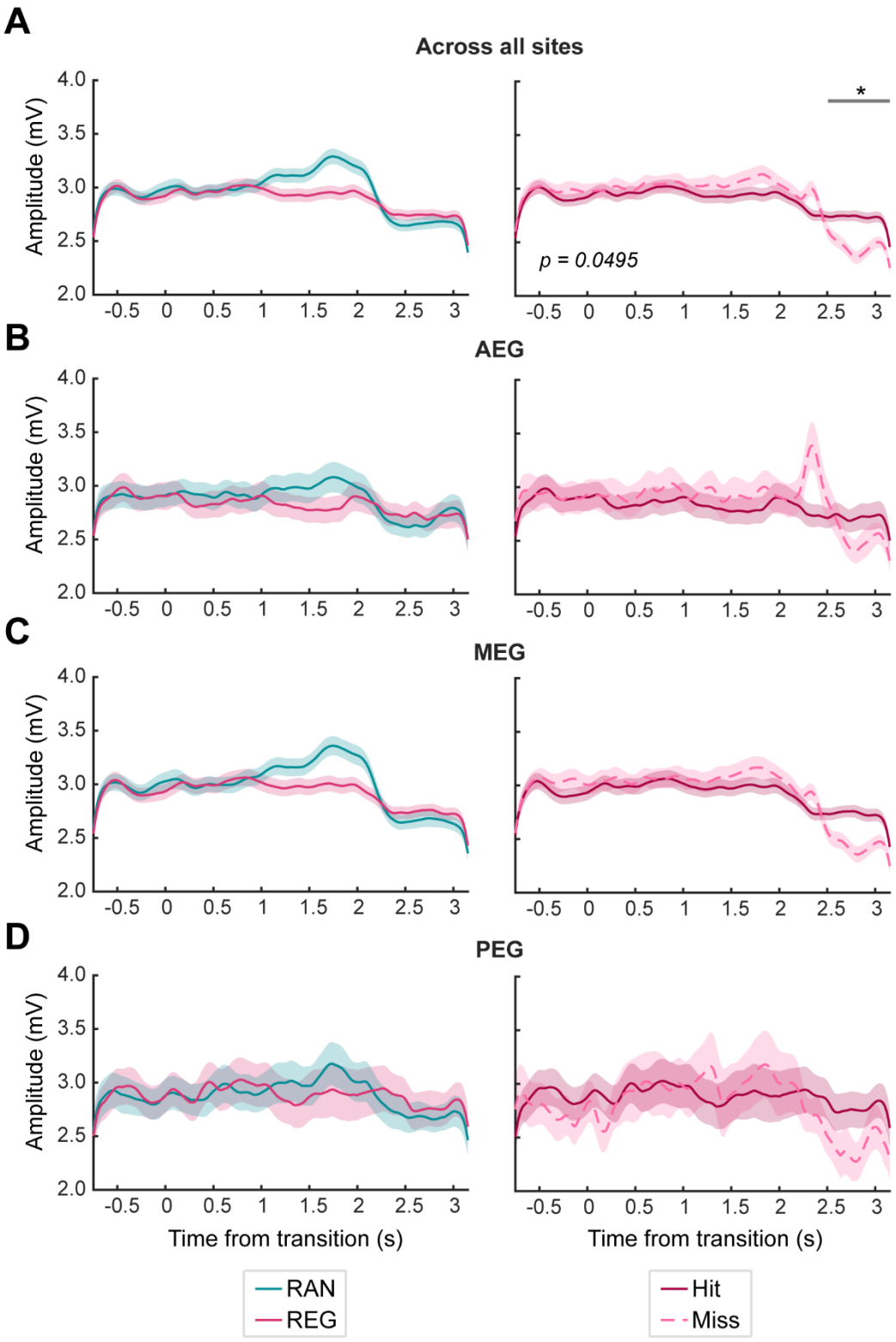

Figure 3.13: Oscillatory power over time at the tone presentation rate (20Hz) in the local field potential for the RAN20-REG3 condition. A) Left - Mean power at 20Hz across all sites for random sequences (blue) and regular sequences (pink), with the x axis denoting the start of the transition from random to regular, and 2s from the transition as the offset. Right – Mean power at 20Hz across all sites for regular sequences on hit trials (dark pink) and miss trials (dashed light pink). B-D) Mean power across sites at AEG (B), MEG (C) or PEG (D). Error = standard error. * = $p < 0.05$, ** = $p < 0.01$, *** = $p < 0.001$.

Switching our attention to the tone presentation rate (see **Figure 3.13A**, left), I observe that although I do see some increase in power in the random condition compared to that of the regular condition from approximately 1s after the transition, this is not significant. Looking at locations individually (see **Figure 3.13B-D**, left) also revealed no significant differences in oscillatory power. However, when I looked at the difference in tone presentation rate between hit and miss trials (see **Figure 3.13A**, right), across all sites we see a significant decrease in miss trials compared to that of hit trials after the trials has ended (2.51s to 3.12s; $p = 0.0496$). Overall, this method is not sensitive enough to pick up the significant times at which the tone presentation rate decreases in power during regularity compared to the random sequence (as I demonstrated in section 3.3.2). However, this method does show a continuation of the oscillations at the tone presentation in hit trials compared to miss trials, but this could be due to an interaction with the noise burst given at the end of miss trials.

3.4 DISCUSSION

The primary purpose of this chapter was to observe if the increases in power present during regular sequences, compared to that of the random sequences in MagEG and EEG recordings in humans are also present in the LFP from microelectrode recordings in ferret auditory cortex (Barascud et al., 2016; Southwell, 2019; Southwell and Chait, 2018). The recorded LFP from microelectrodes and signal from EEG and MagEG are similar but do have important differences which can make comparison between two non-trivial. The EEG signal is a spatiotemporally smoothed version of the LFP integrated over an area of $10cm^2$ or more, MagEG on the other hand has a spatiotemporal resolution of 2-3mm and ~1ms (Buzsáki et al., 2012; Hämäläinen et al., 1993). Where EEG and MagEG mainly sample electrical activity from superficial areas of cortex, microelectrodes can sample at any depth, and the increased spatial precision of microelectrodes, means that depth can affect the LFP drastically (Buzsáki et al., 2012). Furthermore, the contributors to each signal may vary, for example dendritic calcium spikes in superficial pyramidal neurons have been shown to provide a positive surface potential (Suzuki and Larkum, 2017). These dendritic calcium spikes are relatively slow acting compared to action potentials and can last up to several seconds which could contribute to sustained responses observed in the EEG signal.

In this chapter I performed microelectrode recordings in auditory cortex of the ferret and did not observe any differences, in either the RMS power or average evoked LFP, between random and regular sequences. One reason for this difference could be due to the different sampling ranges between EEG and microelectrode recordings, where EEG records the surface potential, whereas the microelectrodes used here sample various depths and have a more precise spatial resolution. This precise spatial resolution could reduce the influence from larger networks of neurons from higher order areas that may be encoding this sustained response, as lower frequency oscillations in MagEG and EEG signals tend to engage larger spatial domains compared to higher frequency oscillations (Lopes da Silva, 2013).

Despite the lack of difference in the evoked response in the LFP, I observed clear oscillations at the tone presentation rate (20Hz). The oscillatory power at the tone presentation rate could be indicative of the responsiveness of the local neural network to the individual tones in the sequence. In my results I observed significant decreases at the tone rate during regularity which could reflect adaptation or repetition suppression as the neurons responsiveness to the individual tones or tone-locked response is reduced. The largest decrease, between random and regular sequences, was observed at pattern length three, which repeats the most of all conditions tested during the 2s. Therefore, the increased repetition could be enhancing the effects of adaptation decreasing the neural responsiveness which is elicited in the LFP as decreased oscillatory power at the tone presentation rate of 20Hz.

Another possible explanation for this decreased tone-locked response is likely that the smaller number of frequencies in the regular pattern, due to the tonotopy of auditory cortex, do not evoke as many frequency-tuned neural populations. In fact, we see in the RAN5-REG5 condition that the absolute oscillatory power is reduced in both the random and regular case significantly compared to that of the unmatched counterpart (RAN20-REG5). Also supporting this argument is that I don’t observe significant differences in the tone presentation rate between random and regular sequences in the RAN5-REG condition. Interestingly the absolute power at the tone rate in the regular sequence is smaller in the RAN5-REG5 than the RAN20-REG5, which is not what we would expect if it was only the number of frequencies present that contributes to the power at the tone rate during sequence presentation, and therefore there may be some interaction from the predictability of the stimulus.

When I investigated this effect by location, the highest oscillatory power at the tone presentation rate was observed in MEG, then PEG and finally AEG which is what we might expect regarding the tuning properties of neurons within each region (neurons in MEG being highly frequency tuned compared to that of AEG; Bizley et al., 2005). The differences in the tone presentation rate response between random and regular sequences remained consistent between subfields which could suggest that this difference is likely inherited from lower or higher order areas rather than being generated within auditory cortex. Investigation of how this correlate changes across layers revealed that the biggest difference was present in the middle to lower cortical layers. Middle to deeper layers are more likely to contain lemniscal projections with upper regions containing more cortico-cortico and non-lemniscal projections (Malmierca et al., 2015). This pattern of modulation might be expected if the oscillatory power at the tone presentation rate is modulated by adaptation that is inherited from lemniscal lower-order areas in the thalamus and/or colliculus. Further work using high-density linear probes may be able to provide insight with more accuracy if there is a laminar effect of the change in tone locked response in the LFP.

Due to the repetitive nature of the deterministic patterns present during the regular sequences, I expected to see oscillations at the pattern rate of each pattern length, which has been observed in previous EEG work (Southwell, 2019). I show that this effect is present in microelectrode recordings in the ferret with the LFP eliciting pattern rate oscillations, and at its first harmonic, for each pattern length tested. The power at these oscillations does seem to be modulated by pattern length (smaller patterns eliciting larger oscillations) however this seems to be limited to patterns that were repeated within a session. This could be due to the reduction of noise by averaging across neural responses evoked by the same stimulus. Interestingly I observe that the largest difference between random and regular sequences in pattern rate oscillations is in the upper layers of auditory cortex. This could suggest that perhaps instead of completely being inherited from lower layers or areas, that entrainment to the pattern rate could occur, enhanced by neighbouring cortical regions.

If the oscillation at the pattern rate could be encoding the regularity in some form, we may expect during behaviour that increased oscillations may give rise to an increased likelihood of a correct response. Since the ferrets I am recording from are

performing a behavioural task simultaneously I was able to observe how the oscillations change if the ferret is able to correctly identify the regularity (a hit trial) or fails (a miss trial). Interestingly the data show that modulation of oscillatory power at the pattern rate is dependent on the pattern rate itself. For example, for pattern lengths 5, the pattern rate is 4.0Hz and we see in these conditions that if the ferret correctly identifies the regularity the oscillatory power in the LFP is increased. This is the opposite for pattern lengths 3 and 7 (pattern rates 6.67Hz and 2.86Hz respectively). This could be due to firstly the pattern rate of 4.0Hz being influenced by oscillations from hippocampus at the theta band (4 – 7Hz; Dunn et al., 2022), where movement to the peripheral spout causes an increase in theta band activity which is picking up by the electrodes in auditory cortex. Therefore I focused analysis just on conditions RAN20-REG3 and RAN20-REG7, in which hit trials showed weaker pattern rate modulation compared to miss trials. In both cases the behavioural modulation did not depend significantly on auditory subfield but do show stronger oscillations in the miss trials for lower and middle layers. This is surprising, as we might expect more oscillatory power for trials in which the animal was able to detect the target, but coupled with the lack of difference in power between pattern lengths, when we know the animal performed much worse for longer pattern lengths, it suggests that this oscillation may not be correlated with the ability to detect regularity. It also seems likely that there might be some suppression due to movement in rates outside of the theta band, which may limit our ability to correlate behavioural outcome. Further work in comparing the pattern rate oscillation in a two alternative forced choice task, may allow us to unpick this problem by decoupling movement and regularity detection.

Lastly, I wanted to investigate how these oscillations might emerge across time. Morlet wavelet decomposition of the RAN20-REG3 condition was not sensitive enough, due to the width of wavelets used, to reveal any significant differences between random and regular sequence at the tone rate. It, however, did reveal significant suppression at the tone rate in miss trials after stimulus offset. This is likely due to interaction of the noise burst presented during and incorrect trial after the stimulus had ended. Analysis at the pattern rate for RAN20-REG3 revealed a significant increase 197ms from transition onset and continuing after stimulus offset. This suggests that there may be entrainment that remains even after the end of the pattern, i.e. a genuine oscillation, rather than simply a consequence of frequency

tuned neurons responding to elements of the pattern. This entrainment could serve to sharpen neural responses or increase neural synchronisation to aid in the encoding of regularity.

In conclusion, in humans a sustained response has been associated with the predictability of the sequence: higher predictability (i.e. regular over random, or shorter vs. longer pattern lengths) producing larger responses, with changes in the sustained response thought to reflect the process of learning and representing the new statistics (Southwell, 2019). Therefore, future work is needed to understand what is contributing to the sustained response seen in the EEG and MagEG and whether changes in oscillatory power is various bands could contribute. ECoG studies could aid in bridging the gap as they record from a resolution between that of microelectrodes and EEG and can be applied to both human and animal models to potentially identify if this neural correlate is human-centric. However, perhaps the answer is within the action potentials of neural firing that reflects the outputs of auditory cortical neurons, rather than the LFP, that predominantly reflects synaptic inputs. In the next chapter I focus my analysis on the firing of single and multi-unit activity, and how the amount and timing of firing changes in regular and random contexts.

4 CHAPTER FOUR: SINGLE AND MULTI-UNIT RESPONSES OF AUDITORY CORTEX DURING REGULARITY

4.1 INTRODUCTION

In chapter two, I showed that ferrets can detect transitions from random to regular tone sequences in a GO/NO-GO task. Using this animal model and task, in chapter three I revealed neural correlates in the local field potential, in the form of oscillations in the tone presentation rate and the pattern rate. However, I saw no increase in sustained power within the evoked local field potential during regularity as seen in previous EEG and MagEG work (Barascud et al., 2016; Southwell, 2019; Southwell et al., 2017). In this chapter, I leverage the use of microelectrode recordings in auditory cortex in the ferret to extract single and multi-unit activity to understand whether the amount of firing or timing of individual spikes change during the presentation of regular sequences and whether this could be contributing to the sustained response observed within human EEG and MagEG studies and how regularity might be extracted and represented in auditory cortex.

So far, very little is understood of how neurons and their firing change in response to tones presented in regular sequences compared to tones in a random context. Specifically, the majority of studies using these complex random and regular sequences have been conducted in humans using techniques with broad spatial resolution such as EEG and MagEG. In contrast, animal studies have commonly used simple oddball paradigms with only recent work using complex predictable acoustic stimuli. Studies that have used more complex stimuli while recording neural firing have shown conflicting evidence. Focusing on studies that record from auditory cortex, Lu et al. (2018) identified habituation in secondary areas of auditory cortex, not A1, to familiar complex sounds (sounds that had previously been repeated). Barzack et al. (2018) recording responses from A1, to pure tone patterns within band passed noise bursts, showed an overall decrease in multi-unity activity in A1. These data have typically been viewed from the context of SSA, where repetition of the same stimulus induces lower firing. However, Saderi et al. (2019) showed global decrease in firing during repetition but an enhancement of the repeated stream that was more prominent in secondary areas of AC (PEG) than in A1.

On the other hand, spike rate is not the only manner in which neurons can encode acoustic features as spike timing plays an important role in encoding the fine temporal structure of the incoming sound. Barzack et al. (2018) identified entrainment to the repeating pure tone patterns, embedded in noise bursts, in AC, where this entrainment could aid in the parsing and grouping of repeating patterns into auditory streams. Asokan et al. (2021) most recently used noise bursts either in a random or regular rhythm and observed only within auditory cortex that the timing of spikes became more precise in the regular context, when compared to other subcortical auditory structures, with no changes in the amount of firing between contexts in AC. This was not observed in MGB or IC, leading them to suggest that the longer integration windows present in AC facilitate the encoding of slower contextual changes. In summary therefore it is likely that responses to sounds presented in a regular context may differ in their temporal precision as well as firing rate, in AC.

Therefore, AC is a prime target for understanding how the brain may encode the detection of auditory patterns. It has a longer integration window compared to that of subcortical structures, which is likely needed to encode the longer repeating patterns I present that range from 3 tones (150ms) up to 7 tones (350ms). Recording within AC, I can investigate how single-units (SUs) and multi-units (MUs) are encoding regularity through changes in firing or spike timing. Though there is some literature on the firing of neurons within complex predictable contexts, they are all performed within passively listening animals, and attention through a behavioural task may boost the sensory signal (Kok et al., 2012). In addition, there is a lack of consensus in whether I should observe facilitation or adaptation within the firing of SU and MU activity, as some studies show increases, decreases or no change at all with predictable stimuli. It is also uncertain what areas, whether primary and/or secondary areas of AC will be influenced by regularity in the context of these tone sequences. It is also unclear how spike timing may be influenced in the context of pure tone sequences and whether the regularity of frequency presentation will induce increasing precision of firing and/or entrainment to the tone presentation rate or pattern rate.

In this chapter, I present the same deterministic acoustic patterns as used in previous chapters, to ferrets performing a behavioural task to detect regularity as described in chapter two. I extract out MU and SU activity and analyse their responses to the regular sequences compared to random and investigate how the response

changes as the pattern repeats. To do this I firstly performed spike sorting and clustering to split and merge single-unit clusters and record pure tone response to collect the frequency response area of units and recordings sites. Then I presented repeated patterns of lengths 3, 5 and 7 (RAN20-REG3, RAN20-REG5, RAN20-REG7 and RAN5-REG5) to understand how the spiking changes after the transition to random to regular.

With these data I highlight the heterogeneity of responses in auditory cortex and assess the overall spiking activity to uncover whether there are overall changes in firing that could be contributing to the sustained response seen in humans, or if there are overall decreases in firing due to adaptation. Furthermore, I evaluated the entrainment of spikes, using vector strength as a metric, to show that firing synchrony to the pattern rate increases during regularity, but is unchanged at the tone presentation rate (20Hz). Focusing on the firing of the SUs to best frequency tones that occur within the sequences, I observed a significant decrease in firing across the population, and an increase in precision during regularity. Furthermore, using a Poisson GLM across the population of SUs, with the response to each tone as an observation, I could pull out an effect of behaviour and identified that overall, neurons increased their firing with more repetitions of the pattern. To understand which units are influenced by regularity, behaviour or just the frequency of the tone, I performed a GLM on each unit individually. This revealed the largest proportion of units responsive to the number of pattern repetitions lay within MEG and that units that were responsive to regularity were also influenced by other factors such as behaviour and frequency rather than regularity in isolation.

4.2 METHODS

4.2.1 Spike extraction, sorting and clustering

The same animals and microelectrode placements were used in this analysis from chapter three (F1812, F1813 and F2001). All neural data analysis was performed offline in MATLAB (MathWorks) and Python through a custom data analysis pipeline as described in chapter three up until extraction of the local field potential. Each trial was then subsequently split into epochs to remove noise that was correlated across channels with principle component analysis (PCA; *CleanData,* Musial et al., 2002). Neural data was spike sorted by filtering the data through a band passed Butterworth filter (filter order 10) between 300Hz and 5kHz using a zero-phase digital filter (*filtfilt*) to minimise any latency induced by filtering. Putative spikes where then extracted with a threshold at -4 s.d. of the signal.

The filtered waveforms were then collected, and then PCA was run to cluster these narrowband waveforms into putative SUs. Spike clusters were merged based on assessment of waveform similarity and classed as a SU using waveform size, consistency, and inter-spike interval distribution (all SUs had ≤2% of spikes within 2ms). Any clusters not classed as SUs were classed as MUs. Spike clusters without negative deflections in the waveform, which were primarily noise artefacts (identified as sharp peaks in the waveforms) were discarded from the analysis. Only a subsample of total neural recordings were spike sorted and only these spike sorted recordings were included in the following analysis to avoid introducing any noise from multi-unit activity through basic thresholding (see **Table 4.1** and **Table 4.2** for total number of MUs and SUs for each animal).

Subject no.	Total no. recordings	MU sites	Mean no. of trials per MU site:				
			Across conditions	RAN20 -REG3	RAN20-REG5	RAN20-REG7	RAN5-REG5
F1812	35	54	204	35	28	80	16
F1813	39	106	287	44	40	102	26
F2001	39	94	411	77	35	141	48
Total	113	-	**-**	-	-	-	-

Table 4.1: Number of multi-unit sites and average number of trials for each condition at each site. Average number of trials, across MU sites, across all conditions, and for each condition presented are shown.

Subject no.	Total no. recordings	SU sites	Mean no. of trials per SU site: Across conditions	RAN20-REG3	RAN20-REG5	RAN20-REG7	RAN5-REG5
F1812	25	149	44	14	67	5	25
F1813	102	157	26	20	52	17	102
F2001	91	331	57	33	118	36	91
Total	218	-	**-**	-	-	-	-

Table 4.2: Number of single-units and average number of trials for each condition for each unit. Average number of trials, across SUs, across all conditions, and for each condition presented are shown.

Spike times were used to extract the waveforms from the broadband neural trace of each spike and the average waveform within a recording session was taken of each SU assigned during spike sorting. As SUs could be held across multiple sessions (Town et al., 2017), or different units could contact the electrode due to drift or gliosis, I clustered SUs across sessions that were likely to be the same SU. To do this I performed PCA on the average broadband waveforms from single units from the same electrode site, only on sites that had single units for ≥ 4 recording sessions (see **Figure 4.1**). Sites with < 4 recording sessions with SUs were labelled as individual SUs as I needed more than three recording sessions to perform the PCA. K-means clustering was then performed on the first three principal components. I identified the appropriate number of clusters for each set of SU waveforms at each site by comparing the sum of point-to-centroid distances for k = 1 to 10 and finding the knee-point using vector bisection (Dmitry Kaplan 2022, Knee Point, MATLAB Central File Exchange; see **Figure 4.1A**). For MU activity, all spikes classed as MUs were collated across recording blocks that recorded at the same site to give MU activity for that site.

4.2.2 Frequency response measurements and analysis

Frequency response areas (FRAs) of units were collected by recording responses to a 100ms pure tone at various frequencies (120Hz to 19.3kHz with 1/3 octave spacing) and sound levels (20 to 70dBSPL in 10dBSPL spacing) after every electrode movement, approximately 100 micron movements down every 4 weeks (see **Figure 4.2, Figure 4.3** and **Figure 4.4**). To calculate the tuning curves, the spontaneous spike rate was calculated by taking the mean spike rate (bin width: 10ms) in the 100ms window preceding tone onset and the evoked spike rate in the 100ms window from tone onset. This was calculated for each frequency/level combination

(161 combinations in total). The FRA matrix was then smoothed with a nine-point running Hamming window (Bizley et al., 2005).

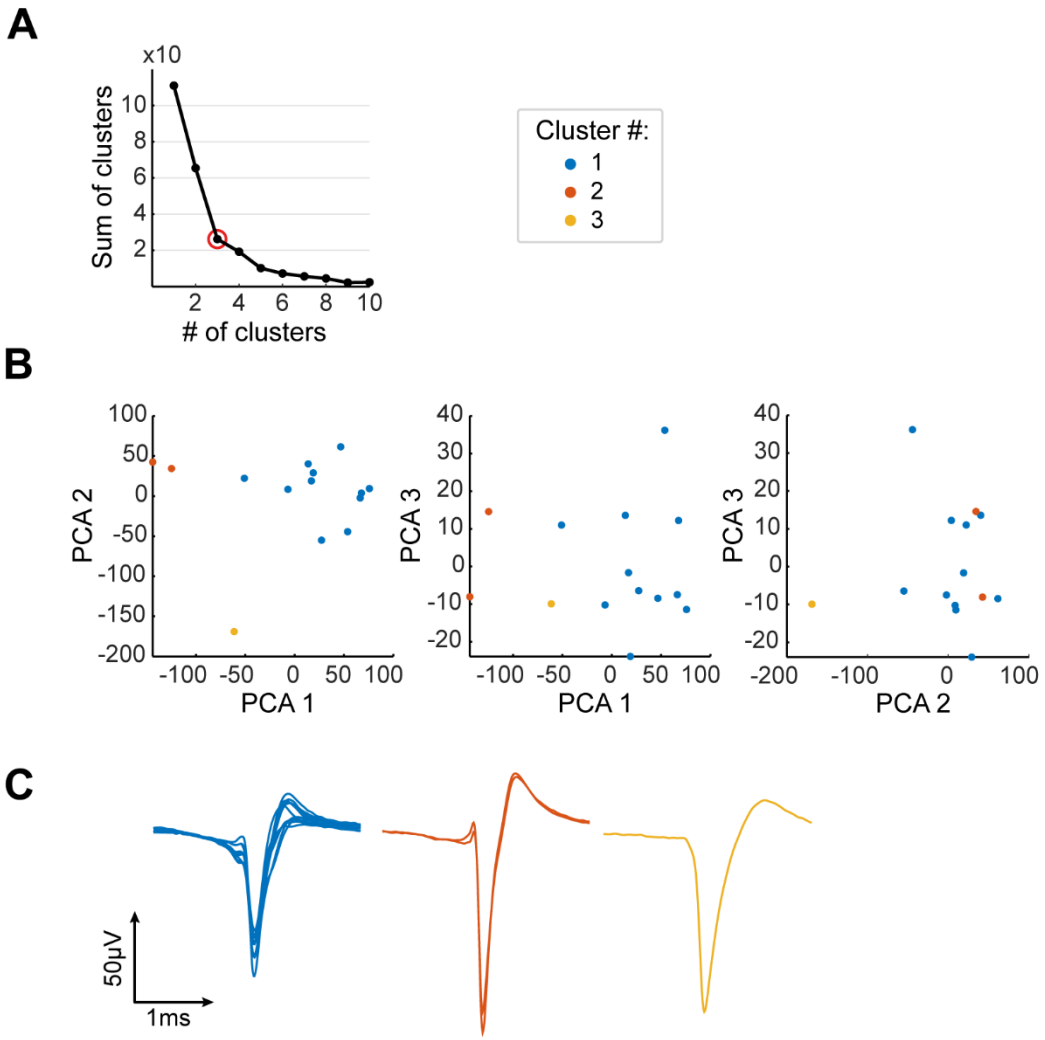

Figure 4.1: Clustering of single-units across recording sessions. A) The sum of point-to-centroid distances for K = 1 to 10, with the knee-point (via vector bisection), circled in red. B) First three principal components of the mean broadband waveform for SUs recorded from an example site. Dots are coloured by the cluster number calculated by k-means. C) Example waveforms overlapped and coloured by the separate clusters as identified by k-means clustering.

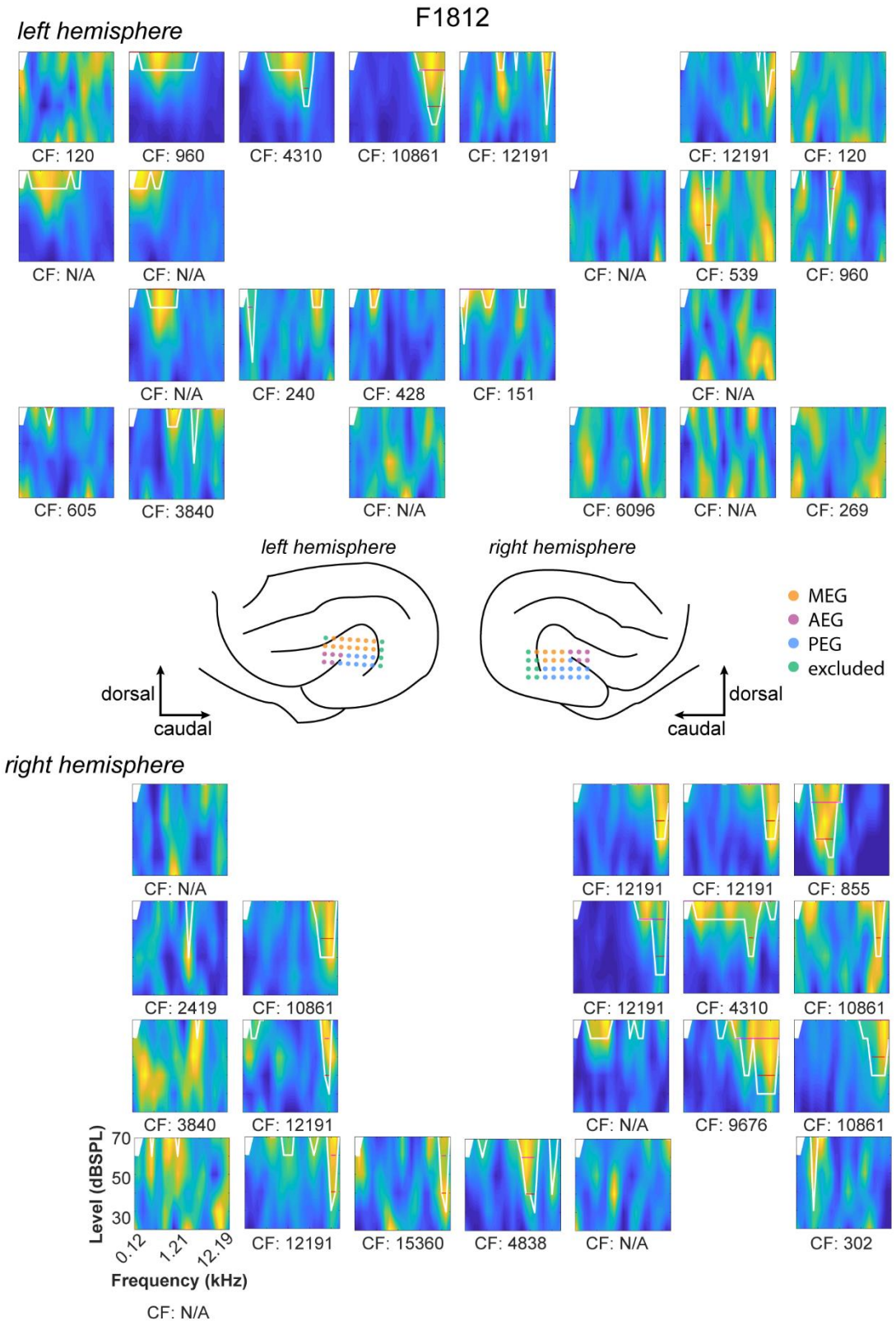

Figure 4.2: Frequency response area of each recorded channel that contained spiking activity in F1812 in the left (top) and right (bottom) hemispheres. Normalized heat maps are arranged in the WARP array configuration for each hemisphere (WARP array anatomy locations are shown in the middle), with yellow areas showing higher neural responses for the

frequency-level combination and lower in blue. Tuning curves are shown (white line) and the Q10 and Q30 (red lines). The characteristic frequency (CF) is shown below each heat map.

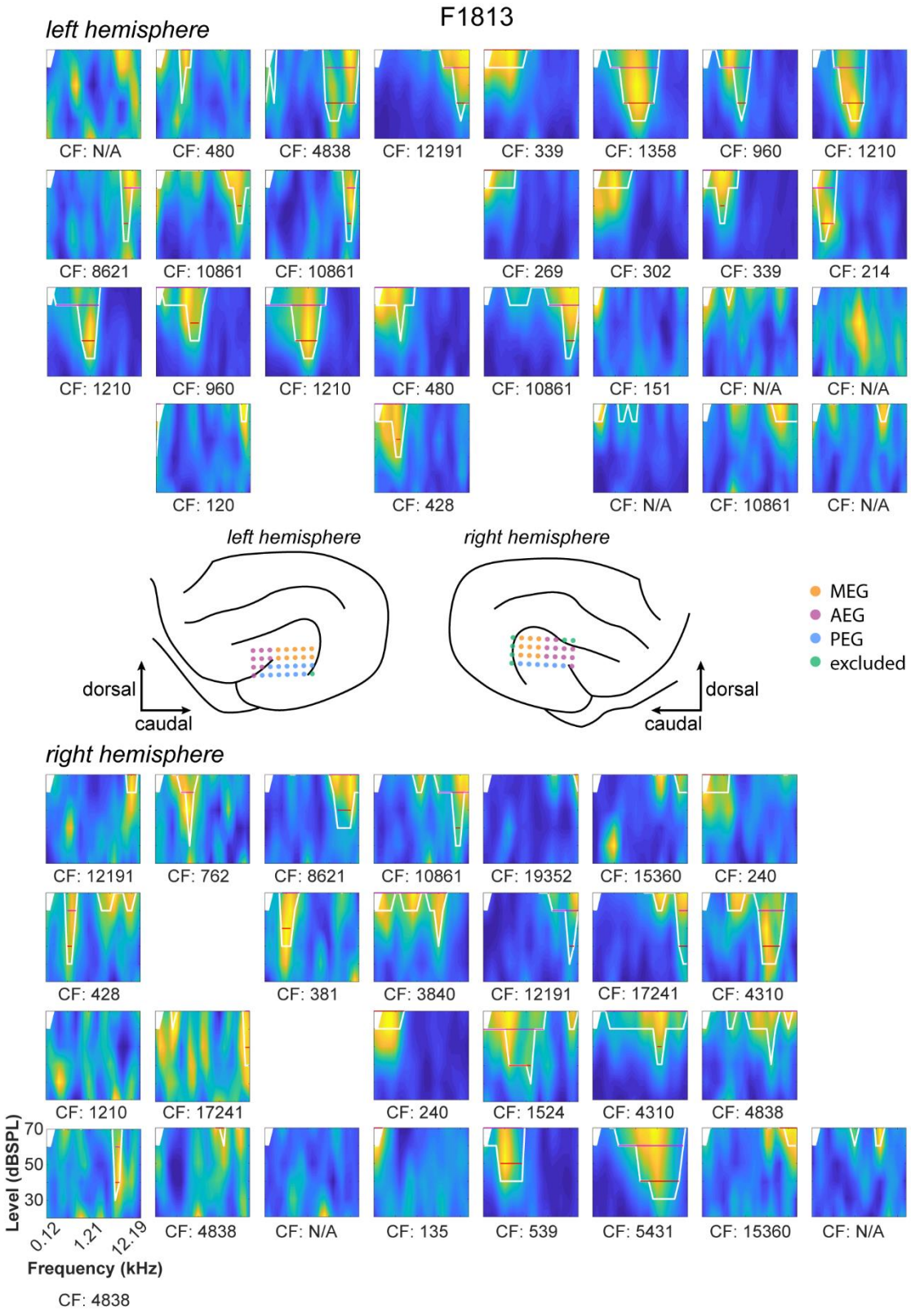

Figure 4.3: Frequency response area of each recorded channel that contained spiking activity in F1813 in the left (top) and right (bottom) hemispheres. Normalized heat maps are arranged in the WARP array configuration for each hemisphere (WARP array anatomy

locations are shown in the middle), with yellow areas showing higher neural responses for the frequency-level combination and lower in blue. Tuning curves are shown (white line) and the Q10 and Q30 (red lines). The characteristic frequency (CF) is shown below each heat map.

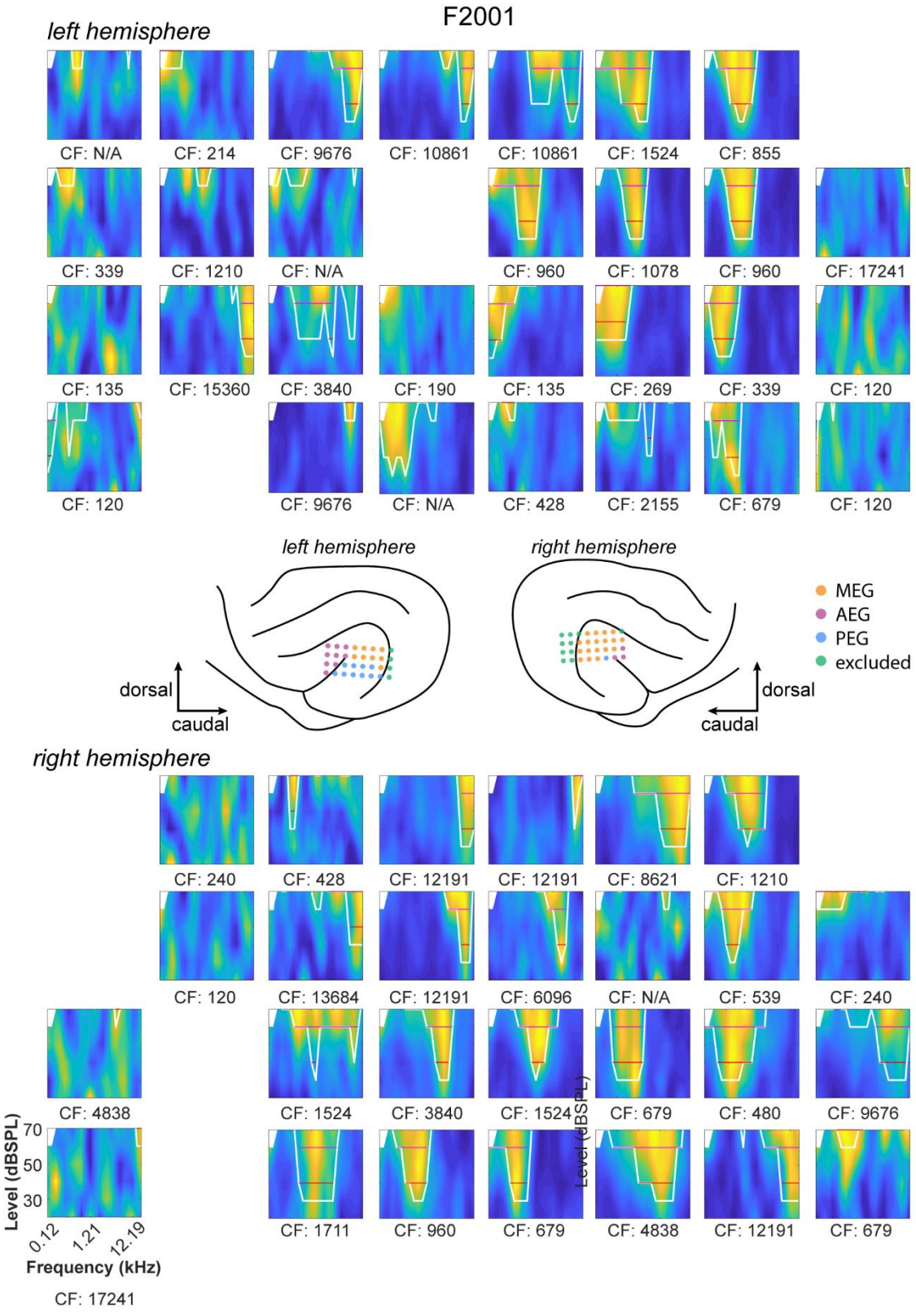

Figure 4.4: Frequency response area of each recorded channel that contained spiking activity in F2001 in the left (top) and right (bottom) hemispheres. Normalized heatmaps

are arranged in the WARP array configuration for each hemisphere (WARP array anatomy locations are shown in the middle), with yellow areas showing higher neural responses for the frequency-level combination and lower in blue. Tuning curves are shown (white line) and the Q10 and Q30 (red lines). The characteristic frequency (CF) is shown below each heatmap.

The frequency and level combinations of 120Hz, 151.19Hz at 70dBSPL were excluded due to clipping in the speaker system at these levels. Units that elicited an evoked rate that exceeded the spontaneous rate plus 20% of the peak spike rate were judged to be responsive to that frequency-level combination (Bizley et al., 2005; Sutter and Schreiner, 1991). This criterion was used to generate the tuning curve in which the characteristic frequency (CF), and tuning widths: Q10 and Q30 where extracted. The CF divided by the frequency range that evoked a significant response at 10 dBSPL and 30 dBSPL above threshold respectively (Bizley et al., 2005).

FRAs were usually gathered immediately following electrode movements (which were performed under sedation), with typically a total of 30 to 40 recording sessions in between (not all recording sessions were included for MU and SU analysis). Frequency tuning characteristics were combined with post-mortem histology in order to allocate electrodes to either MEG, AEG, PEG or outside of auditory cortex. Electrodes that showed broad tuning curves were most likely in PEG, sharp tuning curves in MEG and minimal frequency tuning where typically in AEG. Reversals in frequency tuning across electrodes indicated a boundary between auditory fields. Electrodes outside of AC, confirmed through histology and lack of auditory evoked responses, were excluded from further analysis.

Despite analysis of the FRAs, due to electrode drift, the CF derived from the FRAs may not represent the tuning of the unit in a particular recording session. Therefore, I calculated the best frequency (BF) for units within a recording session using the tone sequences that were presented during behaviour. The frequency that elicited the highest mean spike rate in the tone sequence, including only random trials and excluding the first 8 and last 2 tones to avoid onset/offset responses, was taken as the units BF within that session.

4.2.3 Neural analysis

4.2.3.1 Spike count analysis for random vs. regular sequences

To calculate the difference in overall spike count during regularity compared to the random sequence I calculated a modulation index. For each trial, the number of

spikes was summed from the transition to the end of the stimulus (2s). Trials that were a correction trial, contained a training reward at centre, contained a false alarm before the transition or were the first four trials of a recording session were excluded from analysis. To calculate the change in spike count between random and regular sequence modulation index, for each unit and condition the difference between the mean spike count (SC) of random and regular trials were taken and divided by the sum.

$$Spike\ count\ (SC)\ modulation\ index = (mean\ SC_{REG} - mean\ SC_{RAN})/(mean\ SC_{REG} + mean\ SC_{RAN}) \quad (5)$$

4.2.3.2 Firing rate and precision analysis of single tone responses

To calculate the modulation indices to asses firing and timing for each SU in regular and random contexts (Asokan et al., 2021), I calculated each SUs BF for each recording session. I then took each presentation of the SUs BF in the random and regular sequence in the 2s window after the transition and randomly subsampled to match the number of presentations in the random and regular context for each condition and SU. I used the number of spikes across presentations to calculate the post-stimulus time histogram (PSTH). To assess differences in the SUs firing during each tone, I took the average of the spike rate across the 50ms window of the tone presentation in the random and regular contexts and used these to calculate the mean firing modulation index:

$$Mean\ FR\ modulation\ index = (mean\ FR_{REG} - mean\ FR_{RAN})/(mean\ FR_{REG} + mean\ FR_{RAN}) \quad (6)$$

Additionally, I calculated a precision modulation index to assess the temporal precision of firing of SUs to individual tones (Asokan et al., 2021). For each unit and condition, I autocorrelated the PSTH for various time lags and fit a decaying exponential curve ($(t) = ae^{-bt}$, where a = 1) to the autocorrelation function. The decay time constant (τ) was calculated as $\tau = \frac{1}{b}$ as the time it takes to decrease by a factor of *e*. The decay time constant was calculated for random and regular contexts and used to calculate the precision modulation index:

$$Precision\ modulation\ index = (\tau_{REG} - \tau_{RAN})/(\tau_{REG} + \tau_{RAN})$$

(7)

4.2.3.3 Vector strength analysis for neural entrainment

Vector strength was calculated to measure the amount of entrainment of the spikes of SUs to the tone presentation rate and to the rate of the pattern. To calculate the vector strength of units I calculated the cosine and sine vector strength for each frequency of interest (FOI) for each SU at each trial:

$$VScos = sum(\cos(2\pi \times FOI \times spike\ times\ (s)))$$
$$VSsin = sum(\sin(2\pi \times FOI \times spike\ times\ (s)))$$

(8)

To calculate the vector strength of the unit at each FOI I took the sum of *VScos* and *VSsin* individually across trials and the total number of spikes across those trials and entered it into the equation below:

$$Vector\ strength\ (VS) = \frac{\sqrt{VScos^2 + VSsin^2}}{\#\ spikes}$$

(9)

4.2.3.4 Modelling sensory and non-sensory influences on neural spiking

To model spike count to consider behavioural factors such as movement and reward as well as regularity and stimulus content I used a generalized linear model (Poisson). Each trial was separate into 50ms bins to encompass one tone within the stimulus and the first four tones (200ms) was removed to mitigate any stimulus onset effects. At each bin I took the total number of spikes, whether regularity was present (0 or 1), whether the animal was given a reward (i.e. at the left spout after a correct trial), movement (i.e. whether the animal was not at either the central or left spout), how many times the pattern has repeated and the frequency of the tone in that 50ms bin expressed as a distance from the units best frequency (see **Figure 4.12** for a schematic). To calculate frequency distance, I calculated the SUs BF, then labelled the frequency of each tone as an index from the whole frequency pool (e.g. 120Hz would have an index of 1, 1210Hz an index of 11 and 9676 an index of 20) as well as the SUs BF. I then took the absolute difference in the indices between the tone frequency and the SUs BF that gave me the distance in frequency from the SUs BF as an index. For example, if the SU had a BF of 151Hz and the tone presented had a frequency of 120Hz the distance would 1.

Statistical analysis of effects of pattern length and effects of the tone repetition number and other predictors used general linear models and generalized linear mixed models fitted using fitglm or fitglme in MATLAB (version 2022a). The details of each model are outlined alongside the relevant results; however, in general, analysis of the spike count of each multi or single unit was based on Poisson regression and for other measures (such as modulation indices) was based on a normal distribution. For each model, we reported the magnitude of coefficients (estimate) of fixed and random effects, the t-statistic for a hypothesis test that the coefficient is equal to 0 (T) and its respective p-value (p) (see appendix for full tables). The 95% confidence intervals are also reported for each fixed-effect coefficient and the adjusted R^2 value of the model to assess model fit. Post-hoc analysis was performed in Python with the *scipy.stats* and *scikit_posthocs* modules.

4.3 RESULTS

4.3.1 Heterogeneity of firing to random and regular tone sequences

Whilst the ferrets performed the behavioural GO/NO-GO task to detect regular tone sequences as described in chapter two, I simultaneously recorded neural firing in auditory cortex. Neurons within auditory cortex are typically frequency tuned with tuning curves narrower in MEG, broader in PEG and with minimal tuning to pure tone frequencies in AEG. In comparison to the local field potential, which represents local presynaptic activity and the more distant activity of large numbers of neurons (Kajikawa and Schroeder, 2011), spiking activity reflects the outputs of one neuron (SU activity) or a small cluster of neurons in the immediate vicinity of the recording electrode (MU activity). Given the frequency tuning of individual neurons it is reasonable to assume that this frequency tuning has a much larger influence on the firing activity recorded for spiking data compared to that of the LFP which likely integrates over neurons encoding a range of sound frequencies. **Figure 4.5** describes the tuning for example units (top right of each panel) and metrics of the single unit activity (middle right: mean broadband waveform; bottom right: the proportion of different inter-spike intervals; ISI). On the left hand side of the figure, the stimulus spectrogram, peristimulus time histogram (PSTH) and raster plot show the actions potentials of each example unit and how they respond to that specific stimulus.

When examining the neural responses to the regular sequences I observed a variety of responses. Typically, neurons with narrow tuning showed quite precise locking to individual tones at the neuron's BF (see **Figure 4.5A**). The example unit shown in **Figure 4.5A** exhibits narrow tuning around its BF of 1210Hz and shows an evoked response to the 4^{th} tone in the pattern. On the other hand, the example unit shown in **Figure 4.5B** shows broader tuning around its BF of 240Hz and shows a reduced tone locked response but an overall increase in firing towards the end of the regular sequence. In **Figure 4.5C**, this unit doesn't exhibit tight tuning but does exhibit some tone locked responses which become less evident towards the end of the regular sequence. Therefore, aspects such as the firing rate, whether it is to the neurons best frequency or an overall increase as the sequence emerges, or spike timing, where firing may become less or more tone locked, are important factors when understanding how random and regular contexts in the sequence may influence a

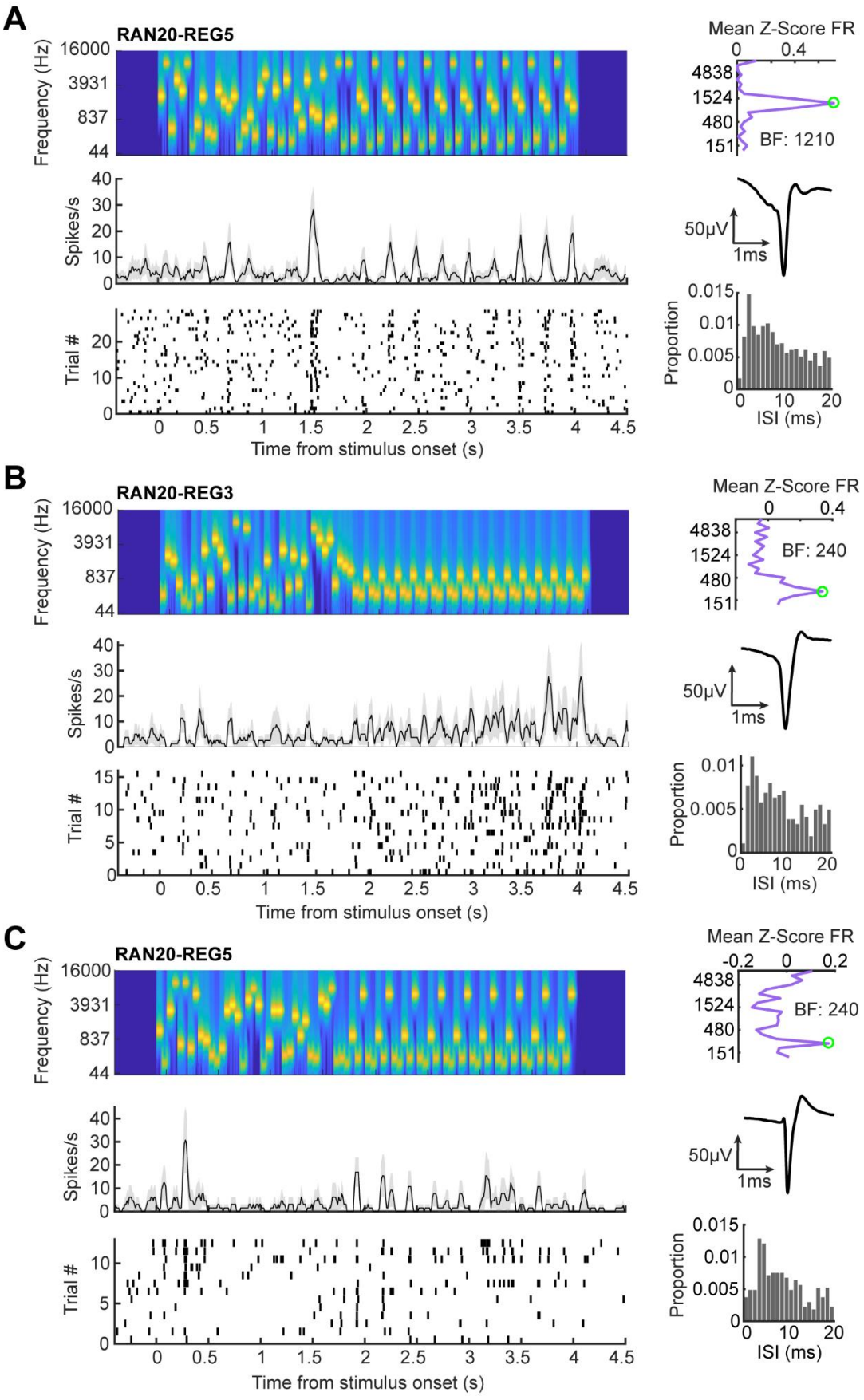

Figure 4.5: Heterogeneous spiking responses to regularity. A-C) Top – spectrogram of the auditory stimulus presented and (right) the mean Z-scored firing rate to each frequency

during all tone presented in the recording session before transition. The frequency which elicited the maximum firing (circled in green) was identified as the neurons best frequency (BF). Middle – Spike rate, binned at 25ms, of the single unit in response to the above spectrogram with the standard error shaded in grey and (right) the broadband waveform of the unit. Bottom – Raster plot of the spikes of the single unit to the above spectrogram and (right) inter-spike-interval histogram (ISI) of the unit. Spike count modulation indices: A = 0.0240, B = 0.0784, C = 0.195.

neurons response. Here I will consider both individual units as well as the population as a whole.

4.3.2 Spike count decreases during regularity with increasing pattern lengths

During the presentation of regular tone sequences to humans, a sustained increase in power within the MagEG and EEG signal is present compared to that during the presentation of random sequences (Barascud et al., 2016; Southwell, 2019). Such a power increase was not observed in the LFP but whether an enhancement in neural firing will be present is unknown. Broad analysis of the spike count during the presence of regularity in the microelectrode recordings from auditory cortex in the ferret might shed light on this phenomena. To do this, I assessed the change in MU and SU firing in ferret auditory cortex during presentation of random and regular sequences.

I looked at the activity for each trial/condition for each MU site (n = 240 MU sites) and SU (n = 172 single units) for trials in which the pattern was repeated multiple times within a session (unlike novel patterns that were generated anew each trial). I then calculated the average spike count per condition for each site for the 2s epoch following the transition from random to regular, contrasting this with the spike rate calculated over an equivalent time point from catch trials in which the sequence remained randomly generated. To mitigate differences in overall spiking between SUs and MUs, a modulation index was calculated for each MU site and SU where a positive index indicates higher firing during regularity.

Analysis was split between MU and SU activity and when all pattern lengths and alphabet sizes were considered I observed no significant difference in activity between regular or random sequences in MU (mean = -0.00410; p = 0.352, W = 7923. *Wilcoxon*) or SU activity (mean = -0.00936; p = 0.216, W = 6550. *Wilcoxon*). Nonetheless when I investigate the modulation index as a function of pattern length (see **Figure 4.6A-B**) the population mean reveals a positive index for pattern length 3

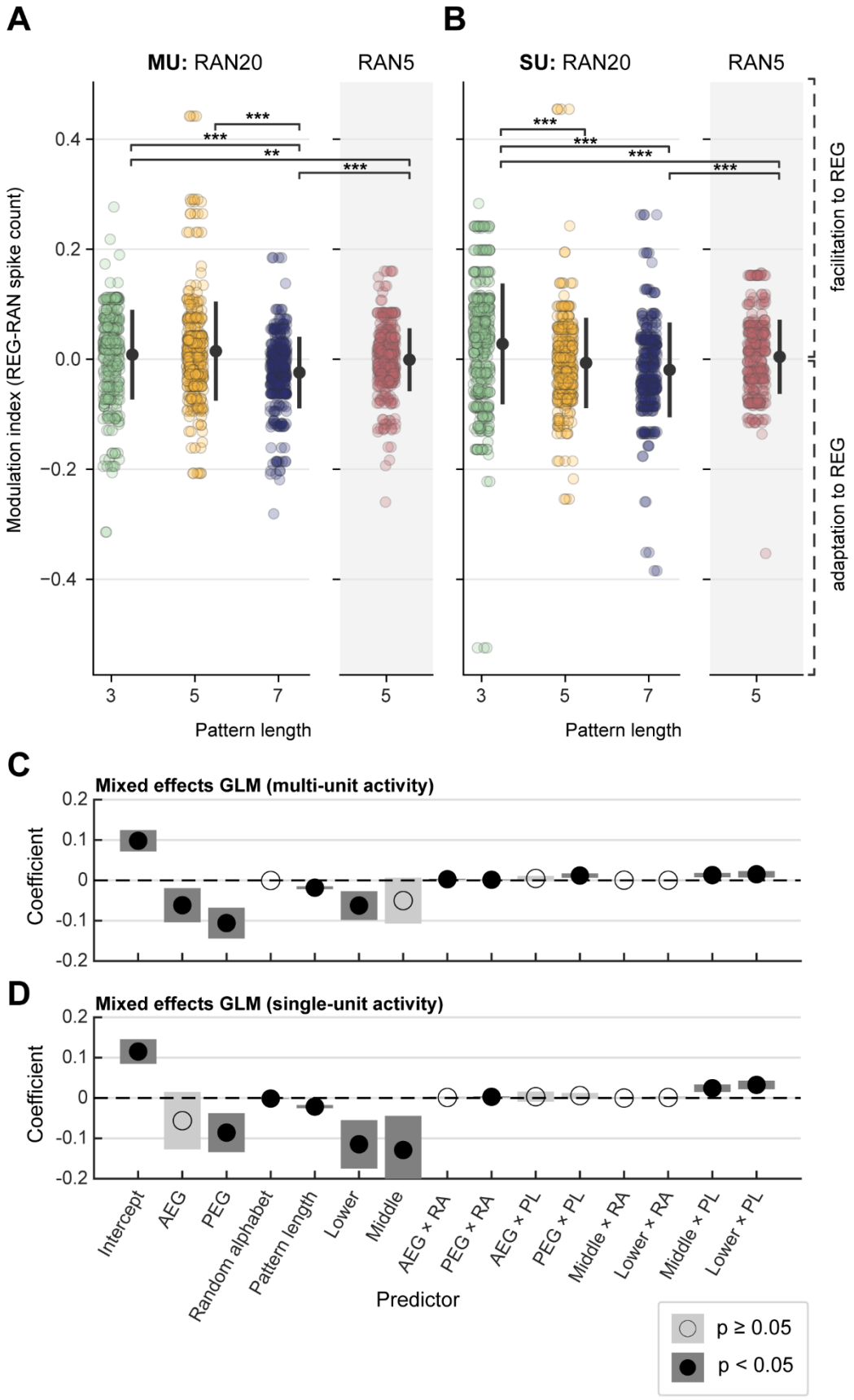

Figure 4.6: Changes in multi and single unit firing during the presence of regular sequences compared to random sequences. A-B) Modulation index for each MU (A) and

SU (B) for each condition (coloured circles). The grey error bars indicate the mean and standard deviation across units for that condition. Significance bars between conditions from a pairwise Dunn test are indicated. * = $p < 0.05$, ** = $p < 0.01$, *** = $p < 0.001$. Coefficients and limits for one and two-way factors in a mixed effects linear regression; (C) MU: $R^2 = 0.469$; Df = 1526; random effect std. = 0.0622. (D) SU: $R^2 = 0.448$; Df = 1482; random effect std. = 0.0705.

in both SU and MU activity. The modulation index decreases with increasing pattern length such that a negative modulation index is observed on average for pattern length 7. This is confirmed with a mixed effects general linear model for both SU and MU revealing a main effect of pattern length with negative coefficients (see **Figure 4.6C-D**). Pairwise comparisons on MU activity reveal significant differences between RAN20-REG3 and RAN20-REG7 ($p < 0.001$) and RAN20-REG5 with RAN20-REG7 ($p < 0.001$). In the SU activity I observe a greater difference between conditions with the modulation index for RAN20-REG3 significantly higher than RAN20-REG5 ($p < 0.001$) and RAN20-REG7 ($p < 0.001$). In both SU and MU activity no significant difference is present in the modulation index between RAN5-REG5 and RAN20-REG5 in the modulation index. This all suggests that pattern length seems to be a driver in the firing activity during regularity, with shorter pattern lengths, which the animals' easily detect, eliciting higher firing rates compared to that of longer pattern lengths, where behavioural performance is more modest.

The GLMMs revealed that location significantly influenced spike count during regularity. Focusing analysis on the SU activity, a Kruskal Wallis confirmed a significant difference between modulation indices ($\chi 2 = 8.067$, $p = 0.0177$), but pairwise comparisons identified no significant differences between locations though the mean modulation index is higher in MEG than the other subfields (see **Figure 4.7A**). Depth was also noted as an influence on spike count, with the GLMM suggesting units in lower and middle layers showing adaptation to regularity, with facilitation being concentrated in the upper layers (see **Figure 4.7B**). A Kruskal Wallis confirmed significant differences between layers ($\chi 2 = 10.177$, $p = 0.00617$), and pairwise comparisons revealing a significant difference between upper and lower layers ($p = 0.0363$; *Dunn test, Bonferroni*). This suggests that there is differentiation between layers in how neurons respond to regular and random sequences, with upper layers producing stronger firing to regular sequences compared to that of random.

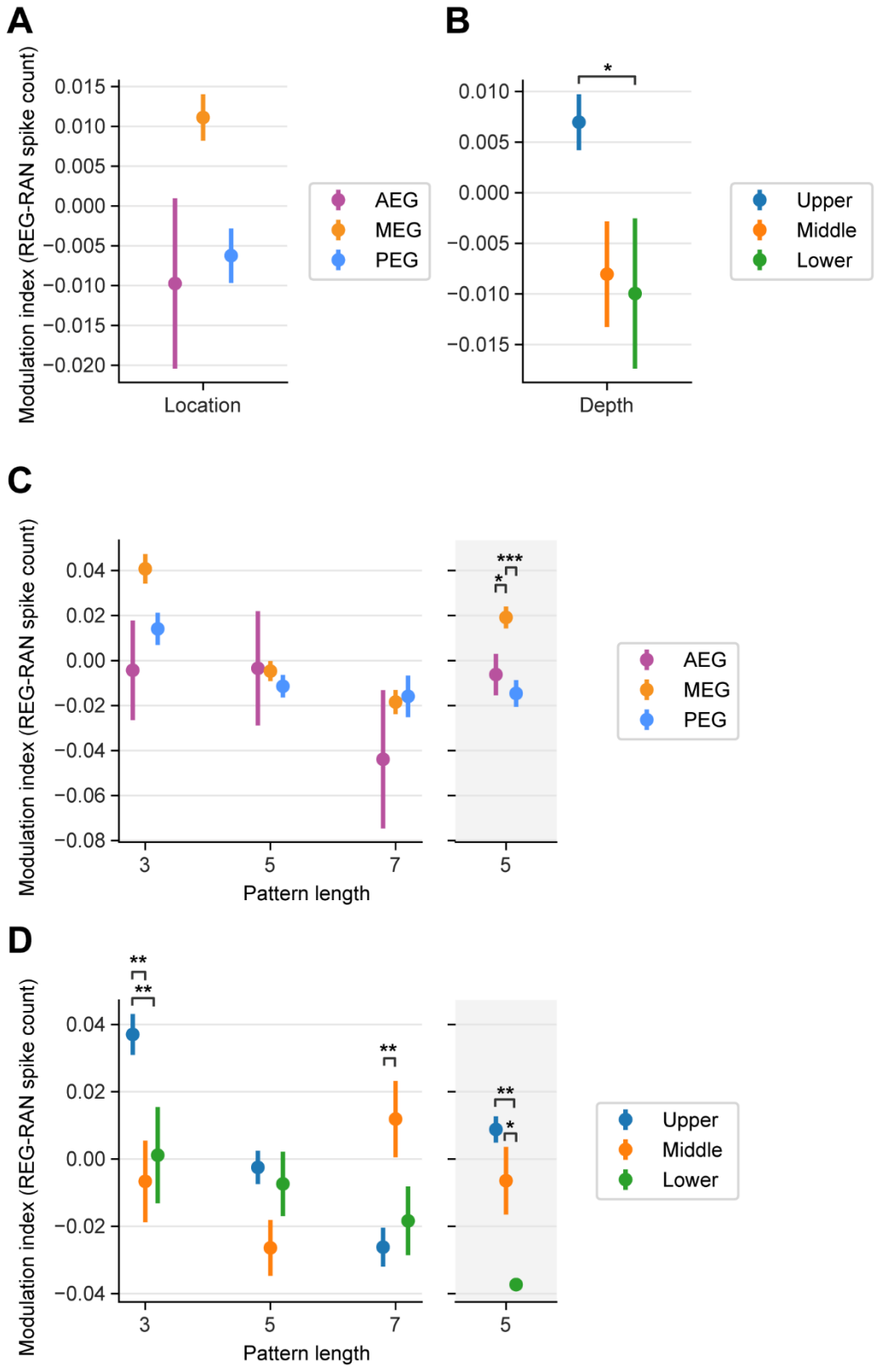

Figure 4.7: Changes in spike count during random and regular sequences by condition, cortical field and depth. A) Modulation index across conditions and single units separated by cortical field (AEG, MEG and PEG) and (B) approximate depth from cortical surface. C) Modulation index across single units separated by condition and location; and (D) condition

and depth. Pairwise comparisons using a Dunn test are indicated with significance bars. Error = standard error. * = $p < 0.05$, ** = $p < 0.01$, *** = $p < 0.001$

To investigate whether modulation index values were influenced by cortical field I considered modulation indices for each stimulus condition in turn, according to where the SUs were recorded. A Kruskal Wallis test on each condition was used to identify any differences in the modulation index between locations and depths at each condition. A significant difference in the modulation index was only found for RAN5-REG5 between cortical subfields (RAN20-REG3: $\chi2 = 4.050$, $p = 0.528$; RAN20-REG5: $\chi2 = 3.413$, $p = 0.728$; RAN20-REG7: $\chi2 = 0.954$, $p = 1$; RAN5-REG5: $\chi2 = 16.231$, $p = 0.00120$. *Bonferroni*). Pairwise comparisons at RAN5-REG5 revealed that MEG showed significantly larger modulation indices compared to that of AEG ($p = 0.0263$; *Dunn test, Bonferroni*) and PEG ($p < 0.001$; *Dunn test, Bonferroni*).

Significant differences in the modulation index across layers (upper, middle and lower at 0.3 to 0.75, 0.75 to 1.5 and 1.5 to 2.25mm from putative cortical surface respectively), were found for all conditions apart from RAN20-REG5 (RAN20-REG3: $\chi2 = 18.741$, $p < 0.001$; RAN20-REG5: $\chi2 = 3.215$, $p = 0.801$; RAN20-REG7: $\chi2 = 11.556$, $p = 0.0124$; RAN5-REG5: $\chi2 = 12.191$, $p = 0.00901$. *Bonferroni*). Pairwise comparisons revealed a higher modulation index in upper layers for RAN20-REG3 (upper & middle: $p = 0.00174$; upper & lower: $p = 0.00681$; *Dunn test, Bonferroni*); in middle layers compared to that of upper in RAN20-REG7 ($p = 0.00203$; *Dunn test, Bonferroni*); and higher in upper and middle layers compared to that of lower in RAN5-REG (upper & lower: $p = 0.00192$; upper & middle: $p = 0.0201$ *Dunn test, Bonferroni*). Overall, we see that location may play a differential role in encoding regularity for the matched condition RAN20-REG5. Depth, on the other hand, seems to vary in its influence depending on condition, with upper layers showing the strongest increase in spike count for regularity in RAN20-REG3 and RAN5-REG5; and middle layers in RAN20-REG7.

4.3.3 Neurons entrain to the pattern rate during regularity

In chapter three I show that oscillations in the local field potential at the tone presentation rate and pattern rate are present during the presentation of regular tone sequences. This oscillation may reflect local firing synchrony at the pattern rate and the spiking activity of neurons can entrain to these oscillations (Wilson et al., 2018).

Here I aim to investigate whether I see a reduced entrainment of spike times to the tone presentation rate (20Hz) in the regular conditions, as we see reduced oscillatory activity at this rate in the LFP during regularity, and/or whether there is increased entrainment at the pattern rate during regularity for pattern lengths 3, 5, and 7 (pattern rates: 6.67Hz, 4.0Hz and 2.86Hz respectively). To do this I calculated the vector strength at these frequencies of interest (FOIs) in the 2s window after the transition for each single unit where 1 indicates exact phase locking of spike times to the FOI and 0 indicates no phase locking.

Firstly, when focusing on the tone presentation rate (see **Figure 4.8**), I found no significant differences in the level of entrainment during the random or regular tone sequence for any condition (RAN20-REG3: W = 4687, p = 0.740; RAN20-REG5: W = 3753, p = 1; RAN20-REG7: W = 3188, p = 1; RAN5-REG5: W = 1767, p = 1. *Wilcoxon*, *Bonferroni*). A Kruskal Wallis test also revealed no significant differences between condition (W = 1.709, p = 0.635). Nonetheless, when I investigated entrainment at the pattern rate (see **Figure 4.9**), significant increases in vector strength at each conditions pattern rate during regularity was found across all conditions (RAN20-REG3: W = 2733, p < 0.001, RAN20-REG5: W = 2478, p = 0.00301; RAN20-REG7: W = 1983, p < 0.001; RAN5-REG5: W = 683, p < 0.001. *Kruskal Wallis, Bonferroni*). A Kruskal Wallis test revealed no significant difference in vector strength between condition either (W = 2.560, p = 0.464). Overall, this suggests that the timing of the spikes remains stable between random and regular conditions to individual tones, but at the pattern rate the timing becomes more entrained during regularity than during the random sequence.

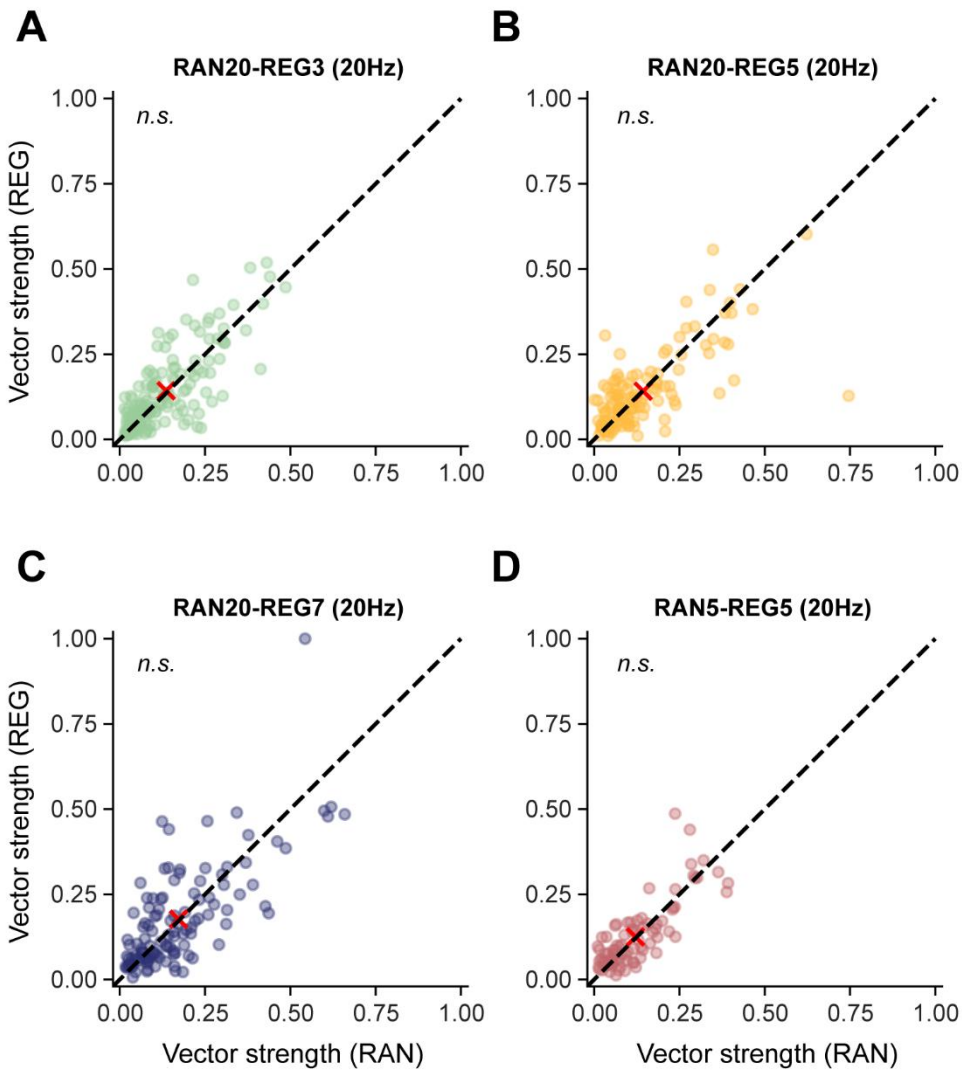

Figure 4.8: Vector strength of single unit firing to the tone presentation rate (20Hz) for each condition. Vector strength at 20Hz for each SU in the REG and RAN condition (coloured circle) for each condition (A = RAN20-REG3; B = RAN20-REG5; C = RAN20-REG7; D = RAN5-REG). A red cross denotes the centroid of the cluster. Equality line (dashed line).

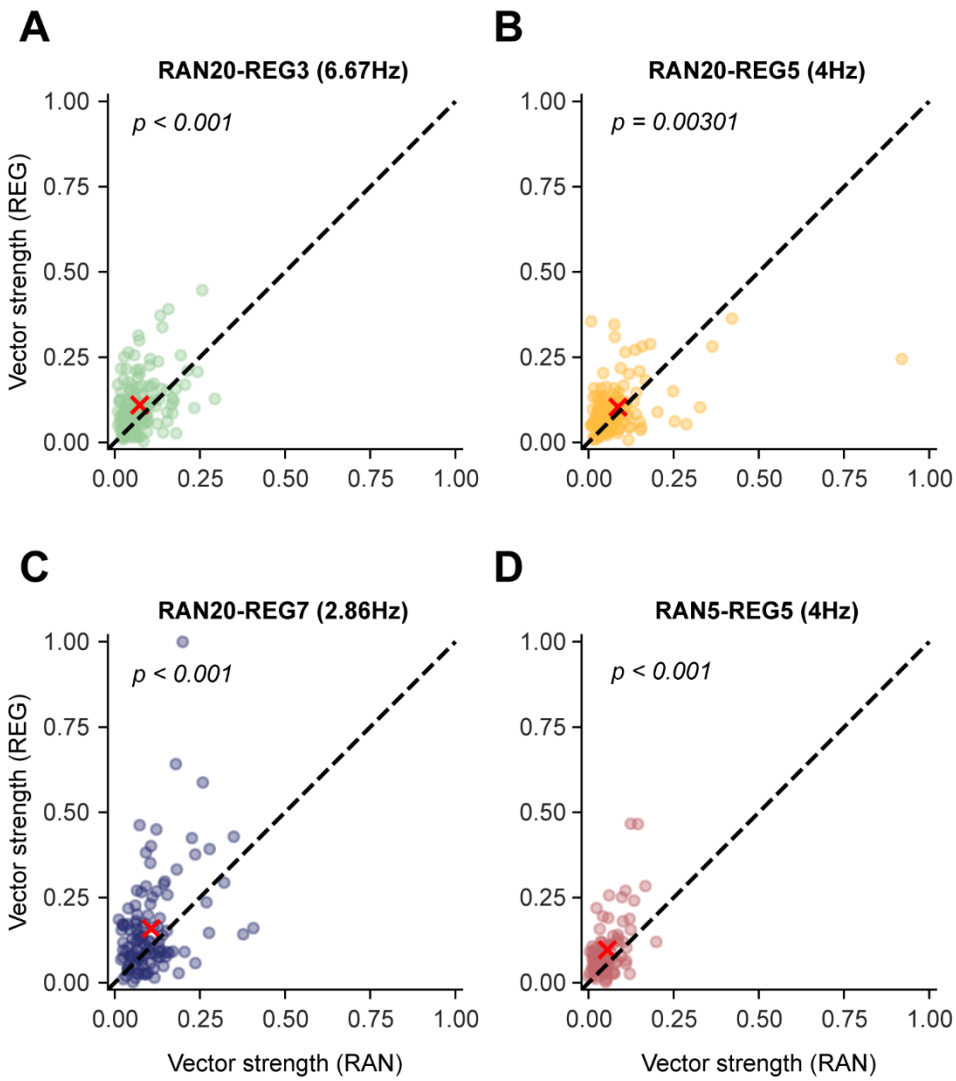

Figure 4.9: Vector strength of single unit firing to the pattern rate for each pattern length. Vector strength at the pattern rate for each SU in the REG and RAN condition (coloured circle) for each condition (A = RAN20-REG3 (6.67Hz); B = RAN20-REG5 (4.0Hz); C = RAN20-REG7 (2.86Hz); D = RAN5-REG (4.0Hz)). A red cross denotes the centroid of the cluster. Equality line (dashed line).

4.3.4 Single units show decreased mean firing and more precise temporal coding during regular contexts

The previous analysis has looked at the response of units to all tones within the sequence, however neurons in auditory cortex are typically frequency tuned and are more likely to respond to just a few tones within the sequence. The increased entrainment could therefore be a reflection of frequency tuned neurons responding at periodic intervals in the sequence. Therefore in this case I chose to investigate how the firing of units to their best frequency change whether it is in a random context (in

the random sequence) or in a regular context (during the regular sequence; see **Figure 4.10**).

In auditory cortex (but not MGB or IC) neuronal responses to identical noise bursts were influenced by whether the noise bursts were presented rhythmically or at randomly timed intervals (Asokan et al., 2021). SU spike rates were unmodulated but the temporal profile of the spiking responses differed such that in the rhythmic context responses were more temporally compact or precise. Here I take the analytic approach developed by Asokan et al. (2021) to determine whether the responses of each SU to BF tones differed between random and regular contexts and how both spike rate and timing might be impacted by regularity. To calculate the firing rate modulation index I took the average firing rate of the unit to its BF tone in the sequence, defined as the tone frequency in the random sequence preceding the transition that elicited the strongest response. I then measured a mean firing modulation index where a positive index indicated a higher mean firing for the regular context over random (see **Figure 4.10**, third row). I calculated a precision modulation index to indicate how precise or temporally compact the evoked spikes were. This was calculated from the decay time constant (t) of an exponential fit (solid line) to the temporal spike count autocorrelation (dashed line) such that a negative index indicated more precise temporal coding during the regular context over the random context (see **Figure 4.10,** last row).

Across the SUs I observed heterogeneous modulation in both the mean firing and the temporal precision of the firing. **Figure 4.10A** displays a SU that showed no difference in its mean or temporal firing, whereas **Figure 4.10B** shows a unit with similar mean firing across the window but much less precise temporal coding in the regular context. **Figure 4.10C** shows a larger increase in firing in the regular context and increased temporal precision. Across the population of SUs the mean firing rate modulation index was significantly below 0 (mean = -0.0205; W = 6573, p = 0.0328; *Wilcoxon*) and as was the precision modulation index (mean = -0.0348; W = 5945, p = 0.00237; *Wilcoxon*). These data suggest that neurons when responding to their BF decrease their firing in the regular context compared to the random and that their firing also becomes more precise, and time locked during regularity.

Asokan et al (2021) had also identified increased precision for spiking in a regular context for shorter pattern lengths. To test if and which conditions showed significant changes in the mean firing rate modulation index between random and regular contexts, the index was calculated for each condition separately and a Wilcoxon test was performed (*Bonferroni*; see **Figure 4.11**). Only RAN20-REG5 showed significant decrease in the mean firing rate index (RAN20-REG3: W = 1700, p = 0.0870; RAN20-REG5: W = 2173, p = 0.0237; RAN20-REG7: W = 2088, p = 0.209; RAN5-REG5: W = 900, p = 0.542. *Bonferroni*). The same tests were performed on the precision modulation index and again the only significant decrease was identified in the RAN20-REG5 condition (RAN20-REG3: W = 1748, p = 0.136; RAN20-REG5: W = 2281, p = 0.0415; RAN20-REG7: W = 2248, p = 0.629; RAN5-REG5: W = 769, p = 0.0833 *Bonferroni*). This suggests that the firing rate and precision of firing is modulation by condition, specifically RAN20-REG5.

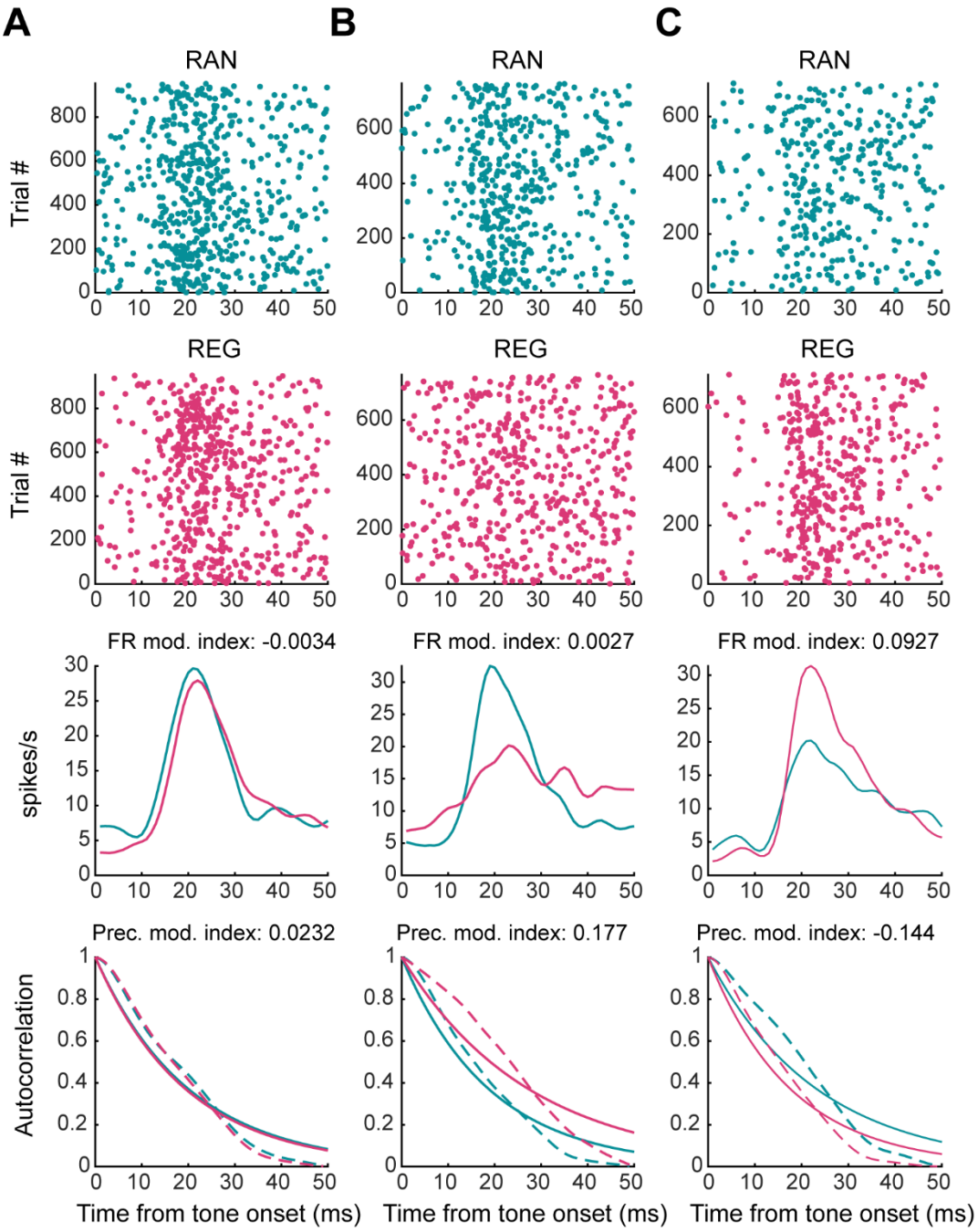

Figure 4.10: Mean firing rate and precision modulation indices for neural responses to their best frequency in random and regular contexts. Top – Raster plot of an example single unit responding to its best frequency tone presented in a random sequence (blue) or a regular sequence (pink). Middle – Smoothed mean spike rate of the single-units response to the tone in the random or regular contexts, with the individual units firing rate modulation index labelled above. Bottom – Autocorrelation function (dashed line) for the example units and fitted exponential decay function (solid line).

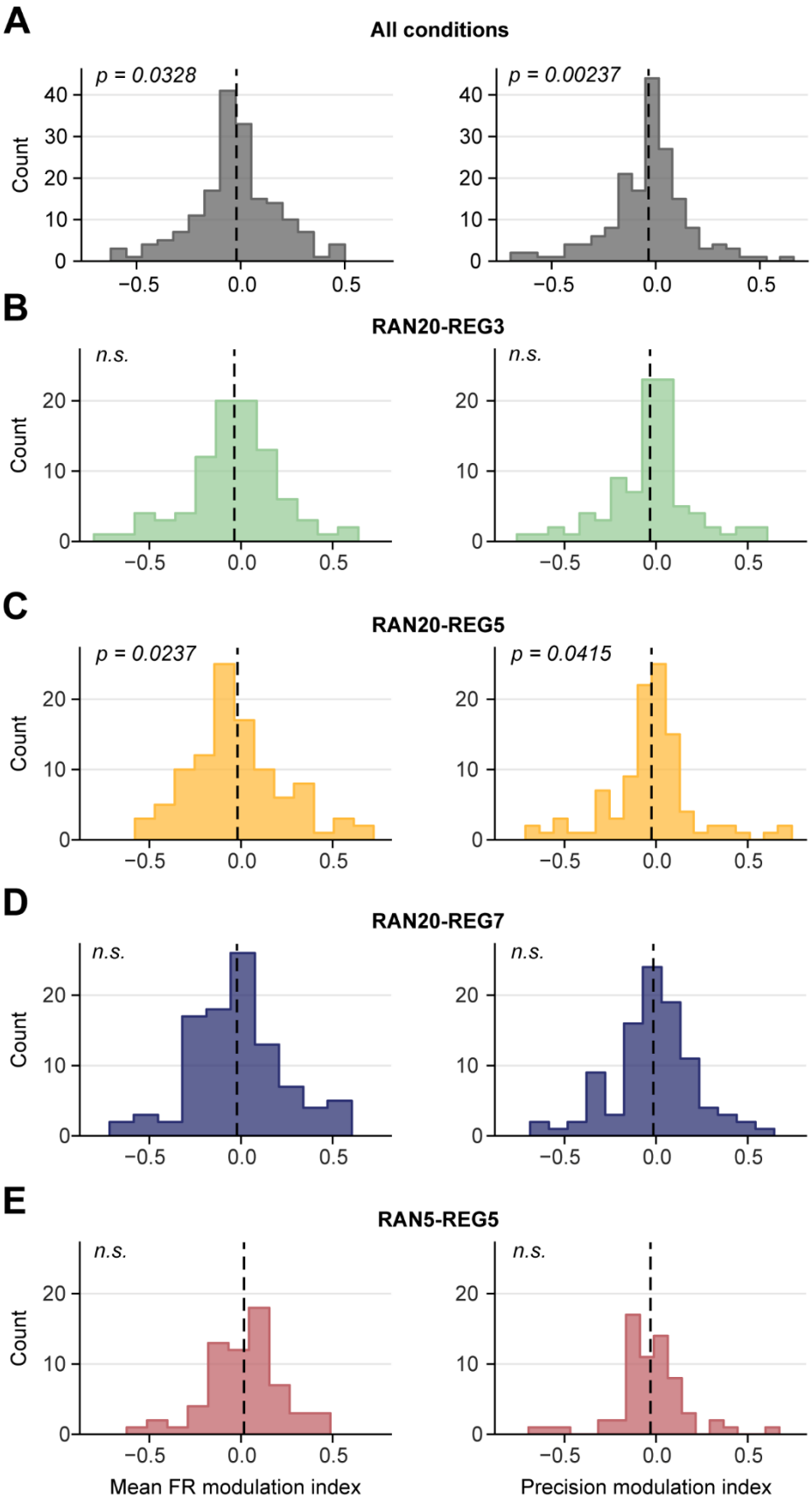

Figure 4.11: Modulation index of firing rate and firing precision over the population of single units and between conditions. A) Modulation index of firing rate (left) and precision (right) across the population of single units and conditions and separately for RAN20-REG3

(B), RAN20-REG5 (C), RAN20-REG7 (D) and RAN5-REG5 (E). Dashed line indicates the mean.

4.3.5 Unpicking sensory and non-sensory effects: population level analysis

As seen in the data above, multiple factors can affect the firing, from the frequency tuning of the neuron to whether the sequence is regular or random, and considering the whole 2s sequence post-transition from random to regular (see **Figure 4.6**) or just BF tones (see **Figure 4.11**) yields different conclusion about the impact of regularity on spike rates. Moreover, the animals are performing a GO/NO-GO task, and movement which is known to affect cortical firing (Schneider et al., 2021; Town et al., 2017), is highly correlated with the presence of regularity. To pull apart the influences of frequency tuning and regularity on neural firing throughout the entire sequence, and include additional non-sensory effects such as movement and reward, I used a generalized linear mixed effects model (Poisson) to model spike count in 50ms time bins (i.e. the length of a single tone pip). I recorded the frequency distance of the tone to the neurons BF, the number of times the pattern had repeated, whether there was regularity and the behavioural state of the animal (stationary or moving, receiving a reward or not receiving a reward; see **Figure 4.12** for a schematic) as fixed effects. In order to visualise the effects that were consistent across the population, while allowing the overall spike rate to vary across units, SU identity was considered as a random effect in a random intercept model. This analysis was performed across the population of SUs, for each condition separately as not all SUs were presented every condition.

The Poisson GLMM (see **Figure 4.13** and see **Table 9.5** for the full model), revealed that most of these factors produced significant effects in the spike counts of SUs. Firstly, and reassuringly, the frequency distance of a tone from the units' BF was a strong significant main effect in all conditions, with a larger frequency distance to the neurons best frequency inducing lower spiking. Secondly, the model identified a significant main effect of regularity in RAN20-REG3, RAN20-REG5 and RAN5-REG5, where regularity significantly decreased the spike count in these conditions. In RAN20-REG7 (estimated with different units) the trend was in the same direction, but the confidence intervals for the coefficient included zero. In contrast, the number of times a pattern repeated showed significantly positive effects in all conditions but RAN20-REG7, where the more the pattern repeated the higher the number of spikes. Non-sensory effects also influenced firing; movement showed significant effects in all

conditions, with positive coefficients in all but one condition (RAN20-REG5), and significant main effects of reward in RAN5-REG5 (with a large negative coefficient). This model suggests that multiple factors influence spiking in AC neurons, with regularity overall supressing spiking, but with facilitation increasing through the trial.

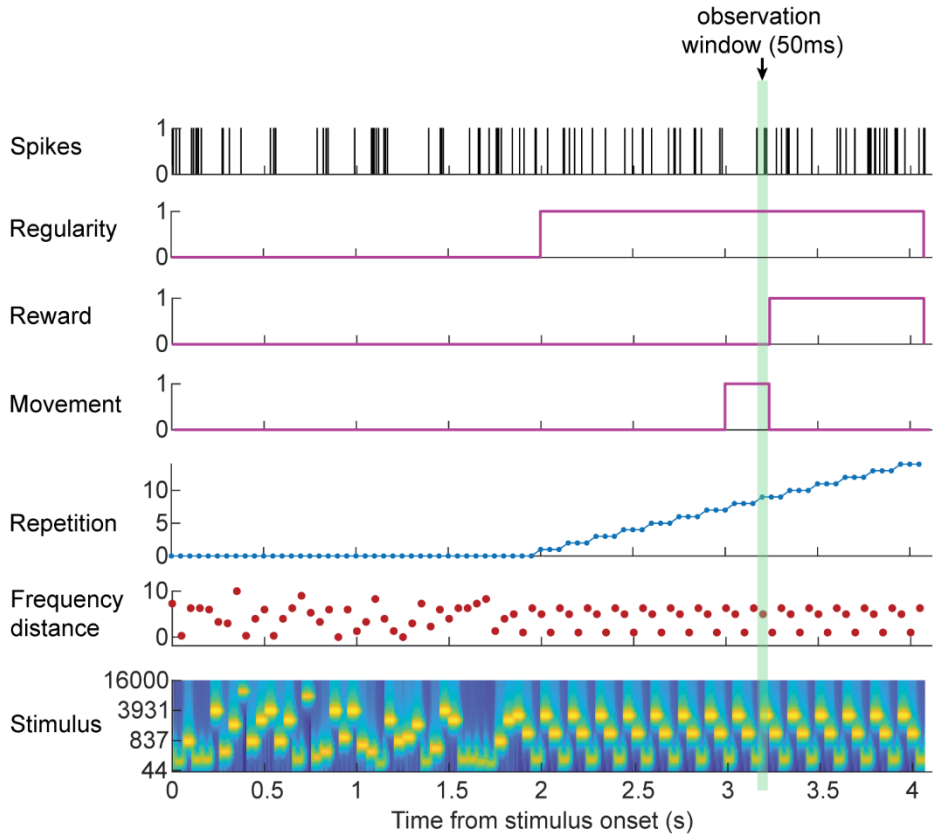

Figure 4.12: Modelling neural responses with stimulus and behavioural predictors. A schematic of example trial showing how each predictor is coded for the generalized linear model.

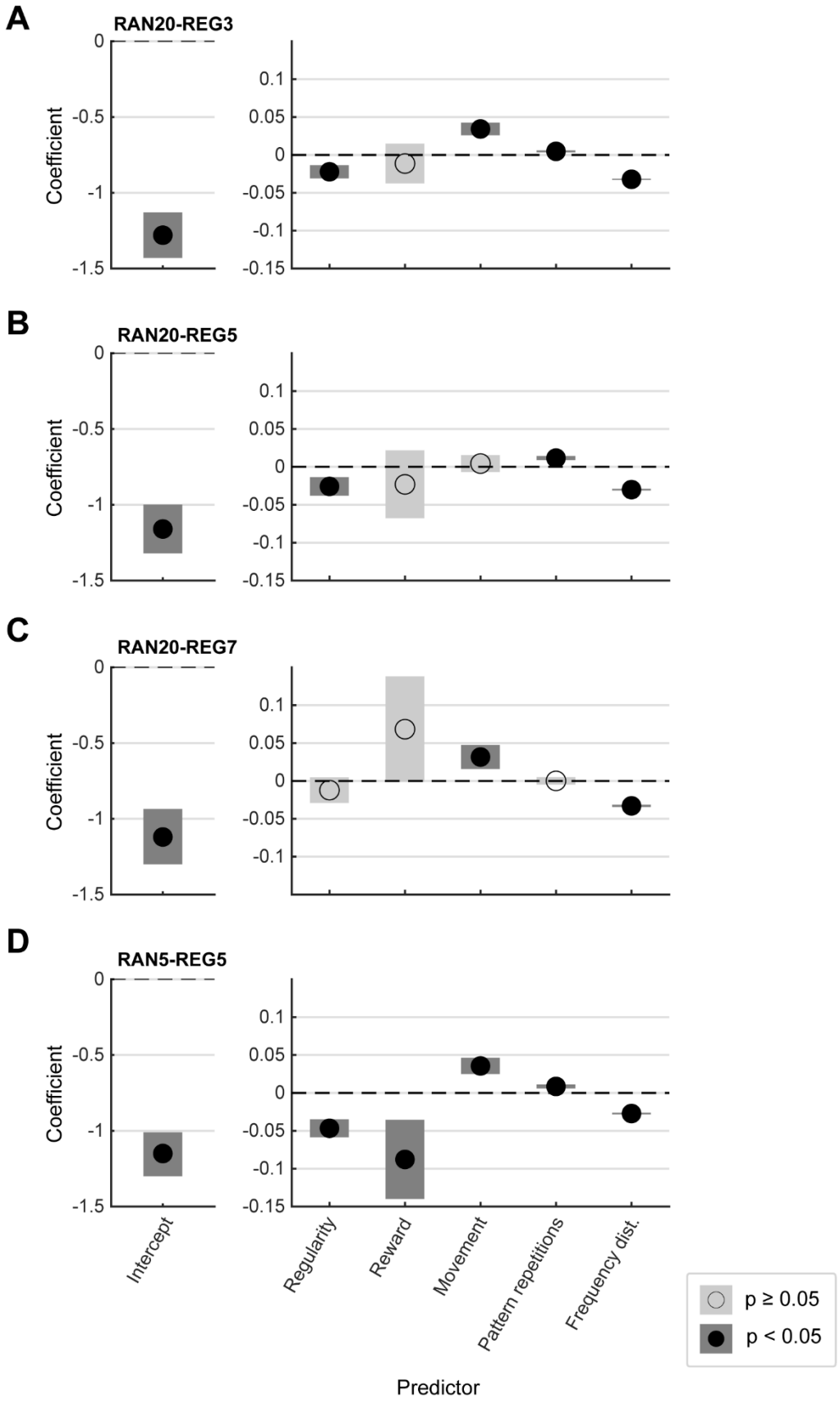

Figure 4.13: Mixed effect Poisson regression on the spike count across single-units for each condition. Coefficients and limits for one-way factors in a mixed effects Poisson

regression where a positive coefficient is indicative of increased spiking during the observed time bin. RAN20-REG3: R^2 = 0.111; Df = 964000; random effect std. = 0.789. RAN20-REG5: R^2 = 0.103; Df = 461000; random effect std. = 0.715. RAN20-REG7: R^2 = 0.0860; Df = 269000; random effect std. = 0.717. RAN5-REG5: R^2 = 0.0990; Df = 459000; random effect std. = 0.629

4.3.6 Unpicking sensory and non-sensory effects: single unit analysis

The previous analysis gives an overall picture of the neural population, but as seen before, the neural response is heterogeneous. Therefore it is necessary to understand whether the adaptation for regularity and the facilitation for the increasing repeats of the pattern are carried by separate neural populations or within the same neuron. Firstly, to understand what proportion of neurons are responsive to each of these factors and where they lie within the cortical subfields, I performed an equivalent GLM (Poisson) on each SU individually and looked at the proportion of SUs influenced by each factor in relation to location. Based on our understanding of auditory cortex, I predicted that the largest proportion of SUs to be influenced by frequency distance to be located within MEG (A1) and perhaps any SUs affected by behaviour to be present in secondary areas (AEG and PEG). Of great interest was whether effects of regularity differed across primary and secondary AC.

In **Figure 4.14A** we can observe the proportion of SUs that showed significant effects of each factor (regularity, reward, movement, pattern repetitions and frequency distance) separated by the cortical subfield each SU belongs to. The largest proportions of SUs are significantly affected by frequency distance, with the highest in MEG followed by that of PEG. Pattern repetitions influence a higher proportion of SUs compared to that of regularity; 56.5% in MEG, followed by AEG (48.7%) and PEG (43.2%). Movement is most strongly represented within AEG with 56% of SUs in AEG showed significant effect of movement. 26.4% of SUs in MEG and 32.8% of SUs in PEG were sensitive to reward and 35.1% in MEG and approximately 28% of SUs in AEG and MEG were sensitive to whether the sequence was regular.

To investigate whether the relationship between these predictors and the location of SUs varies, I assessed the coefficient for each factor per location (see **Figure 4.14**). MEG and PEG show negative coefficients for regularity whereas AEG has SUs that strong increases and decreases in spike count during regularity (see **Figure 4.14B**). Interestingly, SUs in MEG and AEG overall show close to 0 or negative coefficients for the number of pattern repetitions, however most SUs in PEG show positive coefficients, meaning that SUs in PEG increase their firing as the pattern

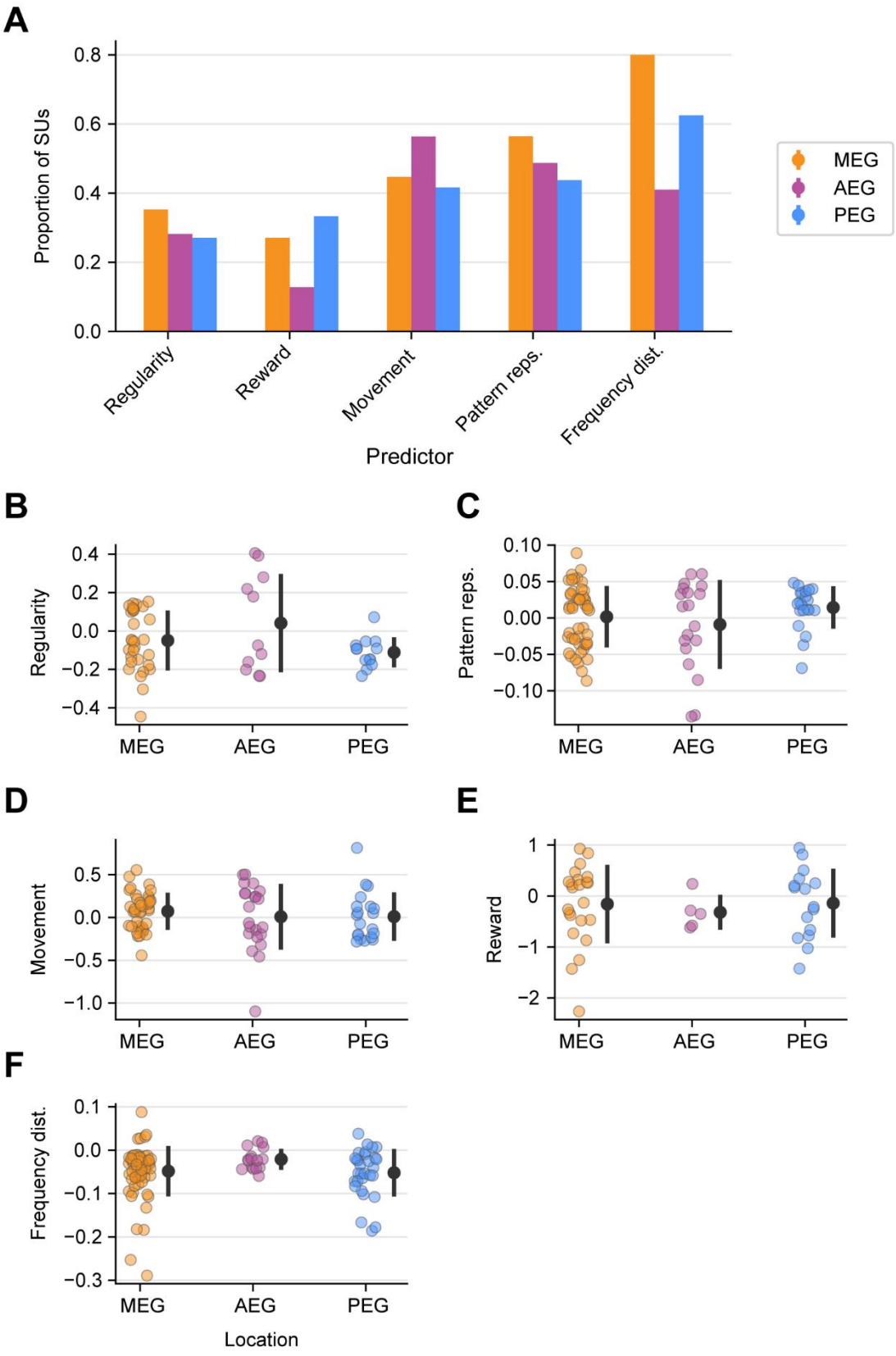

Figure 4.14: Proportion of single-units showing significant main effects of each predictor from the Poisson GLM. A) Bar chart showing the proportion of SUs per cortical subfield that show main effects for each predictor. B-F) Coefficients for each SU separated by

predictor and coloured by cortical subfield. Error bars show mean and standard deviation across SU coefficients for each subfield.

is repeated, unlike SUs in MEG and AEG (see **Figure 4.14C**). Movement is fairly equivalent across subfields with units in MEG showing a more positive trend (see **Figure 4.14D**) and reward showing mostly negative coefficients (see **Figure 4.14E**). Frequency distance showed the most negative coefficients in MEG and PEG (see **Figure 4.14F**). In conclusion, it suggests that MEG and PEG are most affected by the frequency of the tone, which is unsurprising. However, PEG shows mostly positive main effects of pattern repetitions, in comparison to MEG and AEG.

Neurons are not solely affected by only one factor, showing main effects of multiple predictors. To determine whether certain combinations occur more frequently than chance, I calculated the intersection size for each combination of predictors. For example, one set of units may show main effects for only the frequency distance whereas another set may show main effects of both movement and reward. Some combinations may occur by chance, so to identify significant intersections between predictors for single units, I performed a permutation test, independently shuffling the significance value for each effect and then I recalculated the intersection size for each intersection/combination. I then computed the 95^{th} percentile across 1000 iterations for each combination and remove intersection sizes smaller than this percentile for the corresponding combination (see **Figure 4.15** for the resulting intersections and **Figure 9.2** for the full categorisation plot). This analysis shows that the most significant common portfolio of main effects represented in individual SUs is frequency tuning in isolation, followed by movement. Next is a combination of pattern repetitions, regularity, movement, and frequency distance and lastly all the effects in conjunction. This suggests that in this population of SUs in AC that there is no cluster of neurons that solely encoding regularity or the number of times a pattern has been repeated. Instead we see these SUs are responsive either to just frequency, or movement, or to a large combination of factors.

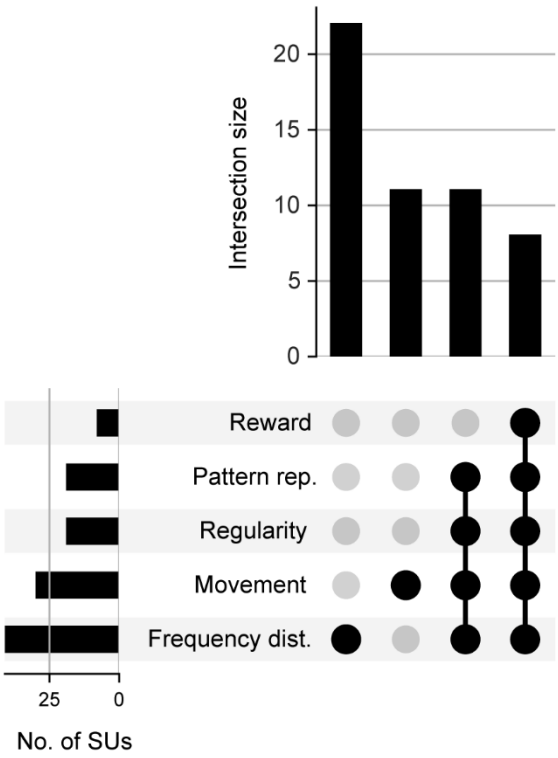

Figure 4.15: Categorisation plot of significant effects for each single-unit. Each factor is represented in each row, with a black circle indicating if that factor is present within that intersection, with lines joining factors in the same intersection/combination. The histogram above shows the number of SUs that belong to each intersection/combination, and the histogram on the left show the number of SUs that are significantly influenced by that factor. Only intersections that occurred above chance (95th percentile of shuffled data) were included.

4.4 DISCUSSION

The motivation behind this chapter was to advance the research towards understanding the neural mechanisms behind regularity detection. Previous work that has used these random to regular tone sequences have focused on conducting non-invasive recordings in the human brain (MagEG, EEG and fMRI), providing a macroscopic perspective on the neural computations underlying this process. However, it is unclear how the firing of neurons contributes to the effects seen at this larger scale. In contrast, studies using more invasive techniques such as extracellular electrophysiology in animal models have employed different paradigms that don't directly test the encoding of these deterministic frequency patterns. For example, simple oddball paradigms, repeating noise bursts, or tone patterns embedded within noise bursts, either lack the complexity, parametric control or direct comparison with the tone sequences used in the mentioned human studies. Therefore, with these data

I can begin to elucidate the neural mechanisms that underlie detection of these random to regular sequences.

In this chapter I analysed the SU and MU activity of neurons in auditory cortex, both in primary and secondary cortical subfields. One main theme that has ran through the chapter is the heterogeneity of responses to the stimuli, with some neurons showing strict tone locked responses to its BF or others showing less frequency tuning and a more overall decrease or increase in firing as the sequence emerges. This heterogeneity was present in the firing of units to their BF in random or regular contexts with some increasing or decreasing their firing or enhancing or reducing their firing precision. This is why a two-fold analysis was needed, examining across the population but also assessing individual units to how they respond and where they might be located. This can help us to infer whether their property is inherited from specific thalamic or cortical connections or whether it is inherent in primary or secondary areas of AC.

As a first pass, across the population of SU and MU activity I observed significant differences in the overall spike count between random and regular sequences, and these differences were modulated by the pattern length of the stimulus. Shorter patterns of 3 elicited larger responses in the regular sequences compared to the random, whereas longer patterns of 7 produced less spiking in the regular sequences compared to the random. This is unexpected given the view on SSA where a repeating stimulus should produce a reduced response due to adaptation; a pattern length of 3 provides repetition of tones at an increased rate compared to that of a pattern length 7. This suggests that repetition suppression does not seem to be driving the reduction of responses, at least not in the majority of neurons. From the context of human cognitive studies, they observed increased responses in the neural signals for sequences with increased predictability. Whether the increase in spike count I observe in pattern length 3 corresponds to what is observed in the increase in sustained power in EEG and MagEG data is unlikely, given that for longer pattern lengths, there are less spikes in the regular sequence compared to the random and that in MagEG and EEG the neural response always increases for regular sequences despite the pattern length.

Entrainment was observed in the spike timing at the pattern rate for all conditions, but not the tone presentation rate. Whether this is a property inherited from subcortical regions due to the induction of these oscillations by the inherent properties of repeating a frequency within a pattern is unknown. However studies indicate that this entrainment occurs earlier in A1 (and the medial pulvinar) than the thalamus, which supports the idea that this entrainment is from top-down connections rather than subcortical (Barczak et al., 2018). This entrainment of spikes was evident in the vector strength measures and when using a measure of how temporally precise or compact, spiking was in response to BF tones in regular over random sequences. This increase in precision potentially allows AC to become more primary-like, allowing bottom-up information to pass through the ascending auditory system more easily and increasing processing efficiency. This entrainment could be generated by frequency separated neuronal populations firing periodically inducing an oscillation that in turn causes further entrainment. One could predict that the more frequency tuned the SU, the greater the entrainment. On the other hand, in a predictive-coding framework this entrainment or increase in firing precision could be due to 'negative prediction-error neurons' that are excited by an enhancement of an internal model, or predictability of the incoming stimulus (Keller and Mrsic-Flogel, 2018). These 'negative prediction-error neurons' could modulate the precision of neurons in AC via local or long-range inhibitory network that decrease the latency of their output to excitatory neurons within AC, sharpening neural firing (Lee et al., 2020).

Using a Poisson GLMM on individual time bins allowed me to tease apart the effects on firing rate of the ferret's behaviour from those of regularity. Negative main effects of regularity were identified across RAN20-REG3, RAN20-REG5 and RAN5-REG5, with no effect in RAN20-REG7, the least predictable of the four conditions. This fits within the view of SSA and predictive coding, in which predictable stimulus should elicit smaller neural firing due to incoming stimulus already matching the internal model. In contrast, I did find that the number of repeats of a pattern showing significant positive effects, again in all these conditions apart from RAN20-REG7, suggesting that spiking increases with more repeats of the pattern. Furthermore, I identified movement as a significantly positive main effect in RAN20-REG3, RAN20-REG7 and RAN5-REG. This is consistent with primate work which showed elevated firing in AC during arm movements (Schneider et al., 2021) and a study in ferrets which identified

units in AC either increasing and decreasing their firing in relation to movement speed in a sound localisation task (Town et al., 2017). This is in contrast to studies in rodents that commonly identify a net decrease in stimulus-related firing by excitatory neurons in AC during movement (Bigelow et al., 2019; Schneider et al., 2014; Zhou et al., 2014).

As highlighted by Asokan et al. (2021), the temporal integration window of A1 is approximately 20ms which is much shorter than the duration of the patterns used in this study (ranging from 150 to 350ms), and their study (800ms). The authors suggest it is likely that this sensitivity to these pattern features are from other local or long range circuits that respond more directly to the acoustic patterns. In my work, I recorded from secondary areas of auditory cortex (AEG and PEG), that are likely to have longer integration windows (Norman-Haignere et al., 2022); though future work could directly test the integration windows of these areas in the ferret model. Consistent with a role for secondary areas in extracting acoustic regularities, SUs in PEG showed increase firing to increasing pattern repetitions compared to that of MEG and AEG. Saderi et al. (2019) had also found enhancement in firing to the repeated target stream (frozen noise bursts), in a ferret animal model. However, through analysis of the combination of factors that influence the firing of individual SUs, I did not find significant intersections that solely coded for regularity or the pattern repetitions, instead neurons were significantly more likely to encode multiple factors, including behaviour, if they did not encode frequency tuning in isolation.

In summary a variety of neural responses are observed. Analysis of spike timing revealed enhanced entrainment to the respective pattern rate of each pattern length during the regular tone sequence and when observing the neurons response to its best frequency, an enhanced precision of firing is evident in the regular context when compared to random. Investigating the overall spike count during the regular sequence, I show the majority of neurons demonstrate an increased number of spikes to the regular sequence for pattern length 3 which then decreases such that the random sequence elicits higher spikes than the regular sequence for pattern length 7. When mitigating against behavioural effects such movement and reward, I revealed that spiking decreases during regularity as a whole but increases with every subsequent repetition of the pattern. Neurons that are sensitive to regularity and the number of repetitions are not responsive to each factor in isolation but are rather

multiplexed and additionally sensitive to other factors such as frequency and behavioural factors. However, it is unclear the origin of neurons that are responding directly to the predictable stimulus, and whether it may be a region that is more adapt at learning statistical structure, unlike AC. One such structure is the hippocampus (HPC), which has also been implicated in previous human imaging studies (Barascud et al., 2016). In the following chapter I will use high-density linear probes to simultaneously record from multiple depths of AC and HPC to understand the potential role of HPC and laminar structure of AC on regularity detection.

5 CHAPTER FIVE: NEURAL RESPONSES IN HIPPOCAMPUS AND AUDITORY CORTEX

5.1 INTRODUCTION

In chapters 3 and 4 I examined the local field potential and SU/MU activity of auditory cortex in response to random and regular tone sequences. In the LFP, I observed decreases in oscillatory power at the tone presentation rate and increases in the pattern rate during the presence of regular sequences when compared to random sequences. Moreover, SU and MU responses showed increased spiking to regularity for shorter pattern lengths whilst also increasing with more repetitions of the pattern. Notably, SU firing entrained to the pattern rate and became more precise when the unit fired to its best frequency during the regular sequence.

Auditory cortex exhibits both tonotopic structure and columnar organisation, which results in neurons across AC having distinct response properties. AC has a well-defined laminar structure of six layers: layer IV contains strong thalamic input, layer V is populated by large excitatory pyramidal neurons, whereas upper layers such as II and III contain major cortico-cortical connections (Linden and Schreiner, 2003; Winer, 1992). Furthermore, acoustic features such spectral integration range, minimum latency, binaural interaction and intensity threshold vary in their representation as you move orthogonally from the cortical surface (see for a review: Linden and Schreiner, 2003). The predictive coding framework, in which the brain generates predictions based on previous input and encodes unexpected sensory inputs to update its internal model, has been modelled using a laminar basis of hierarchy (Bastos et al., 2020; Shipp, 2016). In this case units encoding prediction error are thought to be in the superficial layers of II and III with units encoding expectation in deep layers V and VI (Heilbron and Chait, 2018). However the literature supporting this theory is inconclusive; one study has shown attenuation to predicted sounds in deeper layers of auditory cortex (Rummell et al., 2016) whereas another study identified no clear difference between layers to expected stimuli (Szymanski et al., 2009). Largely it is unclear how units in different layers of auditory cortex may respond during regularity detection of random to regular sequences.

The neuronal mechanisms underlying the detection of changes in sound statistics that indicate a random to regular transition are not solely attributed to AC. In

recent years the hippocampus, though not usually described as auditory brain region, has continuously been associated with the wider networks that support auditory cognition and specifically auditory processing that requires statistical learning (see for a review: Billig et al., 2022). Patients with hippocampal lesions are impaired when learning probabilistic relationships between successive pure tones and syllables (Covington et al., 2018; Schapiro et al., 2014) and fMRI recordings in healthy subjects showed a positive correlation between bilateral hippocampal BOLD activity during exposure to tone sequence regularities in a sensorimotor task (Jablonowski et al., 2018). Hippocampus has also been implicated in the role of temporal integration of acoustic patterns (Geiser et al., 2014) and in sending auditory predictions to auditory cortex (Recasens et al., 2018, 2018). Furthermore, direct projections from secondary areas of auditory cortex to subdivision of hippocampus have been identified in the macaque and rodents (Amaral et al., 1983; Burwell and Amaral, 1998; Munoz-Lopez et al., 2010; Suzuki and Amaral, 1994; Yi et al., 2022) and subcortical auditory projections in rodents (Bordi and LeDoux, 1994; LeDoux et al., 1985; Wahlstrom et al., 2018; Xiao et al., 2018).

The hippocampus has been directly implicated in regularity detection as evidenced by MagEG and fMRI recordings of hippocampus during the presentation of these sequences (Barascud et al., 2016). In this study, the hippocampus showed increased activation during presentation of the regular sequence compared to that of the random sequence. A more recent study testing responses of neurons in hippocampus in epileptic patients to predictable and unpredictable pure tone sequences observed larger responses in the 1-8Hz band to predictable sequences (that had deviants presented at 0.29Hz and individual tones at 1.43Hz) with hippocampus neurons responding selectivity to deviant sounds, and parahippocampal/entorhinal neurons responding to standard sounds (Tzovara et al., 2022). However, few studies have examined the response of hippocampus to predictable pure tone sequences, as used in this in thesis, and therefore it remains to be determined how neurons, or oscillations within the LFP of hippocampus respond to these random to regular sequences in a behaving animal model.

In this chapter I use Neuropixels probes (2.0; Steinmetz et al., 2021) and leverage the linear high-density electrodes to record neural responses across all cortical layers of AC and HPC simultaneously. The aim is to investigate whether the

neural correlates identified in chapters 3 and 4 can be identified in HPC and if there is any variation by depth in AC. Neuropixels probes are a recent advancement in technology that allow the recording of a significantly greater number of electrodes, 384 recording sites, compared to the previous equipment used in this thesis (i.e. WARP microelectrode arrays contains 32 recording sites at a time). The acute and chronic recording of neural responses using Neuropixels (1.0) has now been well documented in rodent species (Durand et al., 2023; Juavinett et al., 2019; Luo et al., 2020), with acute recordings very recently performed in human cortex (Paulk et al., 2022). However, chronic recordings in awake and behaving ferrets have not yet been reported, with only acute recordings documented in the ferret in recent years (Gaucher et al., 2020; Town et al., 2023).

In this chapter I demonstrate the ability to target and chronically record from both AC and HPC simultaneously, with Neuropixels (2.0). I employ metrics such as the theta power (an indicator of HPC oscillations in the ferret; Dunn et al., 2022), the correlation in the LFP between channels, and assessing whether sites are auditory evoked to confirm the location of these brain regions. I present the same deterministic acoustic patterns in the form of random to regular sequences as used in the previous chapters, to two ferrets, one listening passively and one performing the GO/NO-GO task as described in chapter 2. I analyse the changes in spike count in response to random and regular sequences in both AC and HPC and with the increased spatial resolution down the cortical column, I then examine how the response of units change in accordance with depth. Additionally, I compare the entrainment of spikes between random and regular sequences in HPC, and whether I observe greater or reduced entrainment to either the tone presentation rate (20Hz) or pattern repetition rate for each pattern length: 3, 5 and 7 tones, at rates: 6.67, 4.0 and 2.86Hz respectively. Finally, I examine the oscillatory power at the tone presentation rate and pattern rate in sites in HPC to gain insight into whether regularity modulates oscillatory power in the LFP.

Supporting the evidence in chapter 4, analysis of spike count revealed higher spiking activity for regular sequences over random in AC, with this enhancement decreasing with increasing pattern length. Sites that showed the greatest difference in spike count between random and regular sequences tended to cluster around putative layers V and VI. In HPC, I observed modulation in the spike count to pattern length

and increased entrainment to both the tone presentation rate and pattern rate during the presentation of regular sequences when compared to random sequences. In the LFP of hippocampus, I revealed changes in power at the tone presentation rate dependent on both pattern length and regularity of the stimulus, and increases in the pattern rate during regularity for RAN20-REG5 and RAN5-REG5.

5.2 METHODS

5.2.1 Surgical procedure

One trained adult female-pigmented ferret (F2003), once they reliably performed above chance on all conditions (see **Figure 2.3**), and a naïve passively listening animal (F2101) were implanted unilaterally with a 4-shank (type 24) Neuropixels 2.0 probes (Steinmetz et al., 2021) in the left hemisphere. I pre-sharpened the probes using the Narishige EG-45 grinder at an angle of 30º, to aid insertion through the pia of the brain once the dura was removed. To assist the affixation of the probe to the dental cement during implantation, and to add a mounting point to attach a sliding rail, I designed and 3D printed an enclosure (see **Figure 5.1A**) which was affixed with epoxy to the circuit board of the probe. In addition, I designed and 3D printed custom implant wells from durable resin (Formlabs, Form 3), to encase the probe and ribbon cable and protect from physical damage during chronic implantation and after recovery from surgery in the animals' home cage (see **Figure 5.1B**). This minimised motion artefacts and safeguarded the probe, enabling recordings from the probe for > 1 year after implantation.

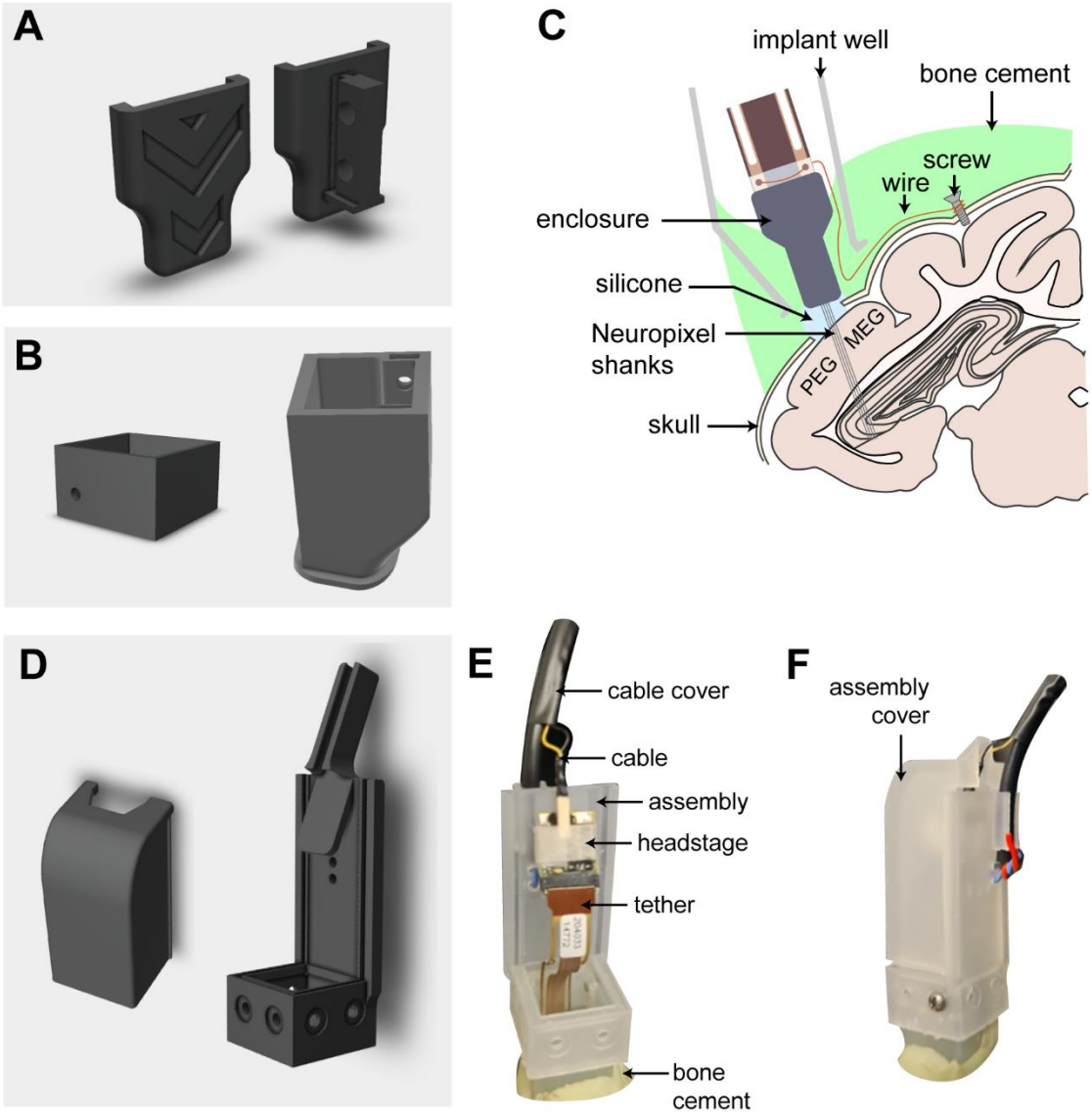

Figure 5.1: Chronic Neuropixels implantation and recording. A) 3D model both sides of the Neuropixels enclosure with the rail attachment on the right. B) 3D model of cap (left) and implant well (right) used to house the probe. C) Schematic of Neuropixels implantation, illustrating position of ground screws, probe, implant well and the location of the silicone and bone cement. D) 3D model of the recording assembly (right) and the cover (left). E) Picture of the recording assembly whilst the probe is plugged into the headstage. F) Picture of the recording assembly with the cover on.

Neuropixels probes were surgically implanted under sterile conditions whilst the ferret was under anaesthesia. Implantation protocol followed that as described in chapter three with some modifications for the Neuropixels probes (see **Figure 5.1C**). To implant the Neuropixels probes to target both AC and HPC, an atlas was used to approximate the location, angle and depth of implantation (Radtke-Schuller, 2018). As the hippocampal structure lies underneath but on the dorsal end of AC, to target both, I aimed for the posterior edge of AC, either in the top corner of MEG or a more

ventral position towards PEG (see **Figure 5.3** and **Figure 5.2** for anatomical positions). The depth of the probe was then measured with a micromanipulator during implantation to ensure the tips of the probe did not contact the skull. A small craniotomy was created and the dura, and in some cases the pia, was removed. The probe was then attached to a custom probe holder and then driven slowly into the brain tissue.

After implantation the probe was embedded within inert silicone elastomer in the craniotomy (Kwik-Sil, World Precision Instruments). The probe was then affixed to the skull via dental cement (Palacos R +G, Heraeus). After a small initial layer, the copper ground wires (attached to the external ground of the probe) were attached to the ground screws connected to the skull. The custom wells where then secured around the probe with additional dental cement. Once secured the chamber within the wells were backfilled with dental cement to provide additional stability to the probe. The ribbon cable of the probe could then be gently folded and stored within the well ready for recording. A head bolt was attached at the midline to aid head fixation during maintenance of the implant. Excess skin was removed to secure the rest of the skin smoothly around the edges of the implant. Animals were then allowed to recover for a week post-surgery before recordings commenced. Pre-operative, peri-operative and post-operative analgesia and anti-inflammatory drugs were provided to animals under veterinary advice.

5.2.2 Neural recordings

To record from the Neuropixels chronically, I designed, and 3D printed a removable assembly that attached to the custom implant wells via a small 3mm in diameter screw (see **Figure 5.1D**). The assembly housed the headstage (Neuropixels, IMEC, version 2.0) and the cable (Neuropixels, IMEC) which was protected with heat shrink and supported by a metal wire that attached to the assembly to minimise any tensile forces on the Neuropixels cable itself (see **Figure 5.1E**). A custom cover that slid onto the assembly protected the components during recording (see **Figure 5.1F**). From the headstage, the cable connected to a PXIe data acquisition card (IMEC), this in turn connected to a PXI chassis (PXIe-1071 and PXI-6132 I/O module, National Instruments) connected to the PC via a MXI cable and PCIe-8381 card (National Instrument). Recordings were digitally acquired at a sample rate of approximately

30kHz (with some small variation between headstages) via SpikeGLX (version 3.0., billkarsh. github.io/SpikeGLX). To sync the neural signals with the stimulus presentation, an I/O module (PXI-6132, National Instruments) was connected to the chassis and received a sync pulse from the Neuropixels via the PXIe data acquisition card at trial onset from the signal processor (RX8, Tucker-Davis Technologies). Recordings were on average 20 minutes in length and occurred twice a day between Monday and Friday. To perform passive recordings, a custom-built syringe pump delivered a constant flow of water at the central spout (see **Figure 9.3**), keeping the animals head in the centre of the arena during the presentation of the stimulus.

The Neuropixels probe itself can record from a possible 5120 electrode sites (1280 sites per shank). However only a subset of 384 sites can be recorded from at once and the location of these sites are limited by electronic mapping of digital channels across the shanks. Therefore, I generated custom maps to indicate which sites to record from, that initially contained broad coverage of the shanks to identify sites of interest (i.e. in AC and HPC) and then different maps to focus in on regions of interest. Typically, only one shank out of four on the Neuropixels 2.0 probes was recorded at a time during each recording session. This maximised the density of recording sites within a region of interest to increase spike yield, whilst maintaining simultaneous recording of both auditory cortex and hippocampus. During recording I used the external ground, attached to the screws embedded in the skull, as the electrical reference.

5.2.3 LFP and spike extraction, sorting and clustering

All neural data analysis was performed offline in MATLAB (MathWorks) and Python through a custom data analysis pipeline. To extract the local field potential, I used the CatGT tool (version 3.0., billkarsh. github.io/SpikeGLX) to filter the broadband signal with a band-passed Butterworth filter (0.1 to 300Hz, filter order of 6) and down sampled to a sample rate of 2.5kHz. To extract the spike times from the neural signal I used the CatGT tool (version 3.0., billkarsh. github.io/SpikeGLX) to filter the broadband signal with a band-passed Butterworth filter (300 to 5000Hz) and putative action potentials were then extracted and sorted in Kilosort (version 3.0., www.github.com/MouseLand/Kilosort), and manually curated to identify single (n = 38) or multi-unit (n = 182) activity. Spike clusters were merged based on assessment of waveform similarity and classed as a single unit using waveform size, consistency,

and inter-spike interval distribution (all single units had fewer than 2% of spikes within 2ms). Any clusters not classed as single units were classed as multi-units. Each recording session was spike sorted individually, and therefore for MU and SU activity, all units recorded from the same shank and depth at the Neuropixels probe across recording blocks were classed as the same MU or SU across recording sessions (see **Table 5.1** for total number of MUs and SUs for each animal in each region).

Subject no.	Total no. recordings	MU sites (AC)	MU sites (HPC)	SU sites (AC)	SU sites (HPC)
F2003	29	73	57	19	13
F2101	12	33	19	5	1
Total	41	106	76	24	14

Table 5.1: Number of multi-unit sites and single-units for each ferret in auditory cortex (AC) and hippocampus (HPC)

5.2.4 Neural analysis

To identify the location of sites within the brain, sites were firstly assessed on whether they were 'auditory evoked'. Responsiveness was statistically analysed via the use of the ZETA test for time series data, *zetatstest* (Montijn et al., 2021). This test compared the evoked activity of the averaged LFP from the first 300ms of sound onset of a site across all trials within a session, to a null hypothesis distribution by running multiple bootstraps on jittered stimulus-onset times. A ZETA p-value of < 0.05 indicated significant auditory evoked onset activity for that recording session and site. Frequency response areas were measured as described in 4.2.2 to identify whether the shanks were in high or low frequency auditory cortex. To identify the theta power I performed a Welch's power spectral density estimate (PSD), *pwelch* (MATLAB), on the LFP on the first 2 minutes of the recording with a window length of approximately 1.6s (4096 samples). I then normalised and averaged the power between the range of 3-7Hz, known to be the range of theta within the ferret (Dunn et al., 2022). To calculate the correlation matrix, I took the first second of recording and calculated the correlation coefficient, *corrcoef* (MATLAB), between each of the channels.

To calculate the difference in overall spike count during regularity compared to the random sequence I calculated a modulation index. For each trial, the number of spikes was summed from the transition to the end of the stimulus (2s). Trials that were a correction trial, contained a manual training reward at centre, contained a false alarm before the transition or were the first four trials of a recording session were excluded

from analysis. To calculate the change in spike count between random and regular sequence modulation index, for each unit and condition the difference between the mean spike count (SC) of random and regular trials were taken and divided by the sum.

$$Spike\ count\ (SC)\ modulation\ index = (mean\ \ SC_{\ REG} - mean\ SC_{RAN})/(mean\ SC_{REG} + mean\ SC_{RAN})$$

(10)

To examine the location of different layers in auditory cortex I calculated the current source density (CSD) profile of the LFP along the probe, of sites within putative AC, using the Delta-Source iCSD method with spatial smoothing (Pettersen et al., 2006) and spacing of 91μm. This was calculated on the mean LFP across trials in response to pure tones 100ms in length and at various frequencies (120Hz to 19.3kHz with 1/3 octave spacing) and sound levels (20 to 70dBSPL in 10dBSPL spacing).

To assess the oscillatory power within the LFP at specific frequencies of interest (FOIs) as in chapter 3, a power spectral density estimate was performed and the power at these frequencies calculated for each individual site. Two second epochs of trials, starting from the onset of the transition, across sessions from the same site were concatenated. Sites and conditions that contained < 10 epochs in the concatenation were excluded from analysis. A Welch's power spectral density estimate (PSD), *pwelch* (MATLAB), was then performed on these concatenated trials with a window length of approximately 12s (17,824 samples) to achieve high frequency resolution at the lower frequencies needed to assess the pattern repetition rate. The RMS of the PSD at the FOI (± two frequency bins either side of the signal frequency bin) was then calculated and then divided by the RMS at neighbouring frequencies (± 5 frequency bins either side of the signal frequency bins) giving the signal-to-noise ratio (SNR) at the FOI (see **Figure 3.3**).

A modulation index was calculated for the SNR to identify differences between the random and regular conditions such that:

$$SNR\ Modulation\ index = (SNR_{REG} - SNR_{RAN})/(SNR_{REG} + SNR_{RAN})$$

(11)

Statistical analysis of effects of pattern length, random alphabet and shank used a general linear mixed model fitted using fitglme in MATLAB (version 2022a). Only two-way interactions or less were modelled. The details of each model are outlined alongside the relevant results. For each model, I report the magnitude of coefficients (estimate) of fixed and random effects, the t-statistic for a hypothesis test that the coefficient is equal to 0 (T) and its respective p-value (p) in full in the tables in the Appendix. The 95% confidence intervals are also reported for each fixed-effect coefficient and the adjusted R^2 value of the model to assess model fit. Post-hoc analysis was performed in Python with the *scipy.stats* and *scikit_posthocs* modules with the appropriate pairwise comparisons stated in text.

5.2.5 Histology

To confirm electrode location and position, at the end of the experiment only F2101 was transcardially perfused, as F2003 is still undergoing experimentation, with 0.9% saline and 4% paraformaldehyde (PFA) under anaesthesia. The brain was then removed for storage in PFA, before cryoprotecting in 30% sucrose for 4-5 days prior to cryosectioning. Coronal sections (50μm) were taken through the full extent of the ectosylvian gyrus. Slices were then mounted on slides in 0.5% gelatine and dried for at least 14 days. Slices were Nissl stained to identify electrode tracts and major structures within the brain to localise the position of these tracts. Sections were then stained with cresyl violet and washed with chloroform and acetic acid. The sections then went through a series of increasing concentrations of ethanol solutions to dehydrate the slides. Sections were then cleared with Histoclear, and cover slipped with a mounting agent (Omnimount). Slices were imaged using the Zeiss AxioScan Z1 at 10x magnification.

5.3 RESULTS

5.3.1 Localisation of auditory cortex and hippocampus on Neuropixels probes

In this chapter, I used Neuropixels 2.0 probes to simultaneously record neural activity from AC and HPC in the ferret. With 5120 densely spaced possible recording sites covering a 1 x 10 mm plane, with 384 being recorded from at any one time, the probes offer a powerful means to sample neural activity across multiple depths, including regions beneath AC such as HPC. However, accurately determining the location of each recording site relative to specific brain regions can be challenging due to the large sampling area, anatomical variations and histological limitations (such as shrinkage). To address this, I employed three key metrics: correlation between channels to identify connected regions, theta power in the LFP to pinpoint the location of HPC, and the ZETA test to identify auditory cortex and its cortical surface by assessing whether sites were 'auditory evoked'. The combination of these metrics allowed for approximate identification of recording sites in relation to these brain regions.

In order to capture neural responses from primary and secondary areas of AC whilst also passing through CA1 of the hippocampus, I placed the probe in a coronal orientation, targeting the boundary between MEG and PEG in F2003 (see **Figure 5.2A**). The acute angle, in relation to cortical surface, allowed the electrodes to pass through CA1 of hippocampus (see **Figure 5.2B**) whilst keeping the probe in a position that minimised ear occlusion after implantation. In **Figure 5.2C** I present a schematic of the approximate probe placement within the brain, based on a coronal section from a ferret atlas (Radtke-Schuller, 2018), with the theta power (3-7Hz) of the local field potential in red aligned to the probe in purple. Sites that were classed as 'auditory evoked' based on the LFP are indicated with black squares aligned to their position on the probe.

I identified the hippocampal region from which the theta power began to increase and at where the power stopped decreasing after reaching its peak along the depth of the probe. AC was identified between the maximum and minimum depth of sites that were 'auditory evoked'. In the case of F2003, putative AC sat across approximately 2mm of the probe. FRAs highlight that the ventral shank (shank 1) has a wider tuning curve, and is therefore more secondary-like, compared to the dorsal shank (shank 4) which has a narrower tuning curve with both shanks showing that the

probe is in low to mid frequency AC. Correlation matrices of the LFP between channels (see **Figure 5.2D**) further confirm sites that are outside of the brain due to reduced correlation in activity to putative AC.

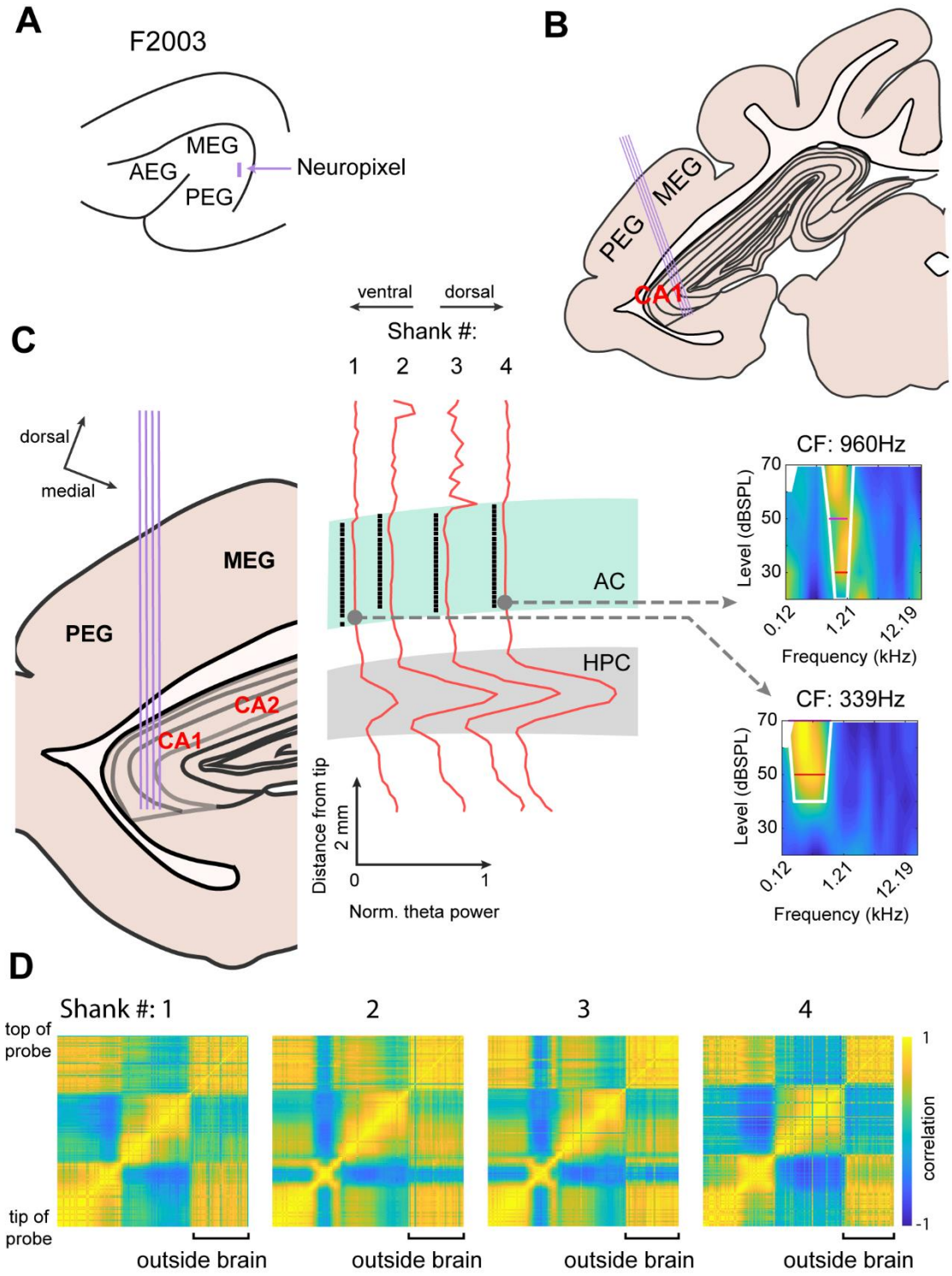

Figure 5.2: Neuropixels probe location in F2003. A) Schematic of the approximate probe position (purple) on the surface of auditory cortex, positioned between MEG and PEG. B) Schematic of the approximate probe position through a coronal slice of auditory cortex, showing the four shanks of the probe passing through MEG/PEG and CA1 (red) of

hippocampus. C) Zoomed in and rotated (left) to vertically align the probe with the theta power (red) for each shank along its depth, and whether the site at that depth was auditory evoked (black squares indicate $p < 0.05$). Putative AC and HPC are highlighted in blue and grey respectively. Example FRAs are shown from sites marked with the grey circles. The FRA is a normalized heat map with yellow areas showing higher neural responses for the frequency-level combination and lower in blue. Tuning curves are shown (white line) and the Q10 and Q30 (red lines). The characteristic frequency (CF) is shown above each heat map. D) Correlation matrices for the correlation between the LFP at each site, bottom left indicating sites at the tip of the probe, and top right indicating sites towards the base of the probe. Sites that are likely to be outside of the brain tissue are highlighted.

To target A1, the probe was implanted in a transverse orientation and centrally within MEG for F2101 (see **Figure 5.3A**). The probe was positioned perpendicular to the surface of AC and passed through CA3 of the hippocampus and the lateral geniculate nucleus (LGN) of the midbrain (see **Figure 5.3B**). **Figure 5.3C** illustrates the approximate placement of an example shank (purple) aligned with the theta power (red) of the LFP and 'auditory evoked' sites. In F2101, shank 4, the most anterior shank, appears to pass through the edge of hippocampus as theta power starts to increase in this region as you move posteriorly across the probe. Due to the more perpendicular angle of implantation, the region of AC in F2101 was smaller than that in F2003. FRAs reveal that the probe was situated in the high frequency region of A1, and correlation matrices show two large, correlated regions and less correlated sites to AC that indicate they are outside of the brain (see **Figure 5.3D**). With these two animals, I show that I can target various regions of HPC, specifically CA1 and CA3, and auditory cortex simultaneously in the ferret and I can mark these regions putatively based on numerical metrics. **Table 5.2** summarizes the sites in each region by their depth from the tip of the probe.

	Probe depths in AC				Probe depths in HPC			
Subject no.	Shank 1	Shank 2	Shank 3	Shank 4	Shank 1	Shank 2	Shank 3	Shank 4
F2003	4005 to 6015	4365 to 6195	4290 to 6210	4380 to 6390	1590 to 3068	1545 to 3201	1545 to 3332	1485 to 3368
F2101	5240 to 6450	4960 to 6490	4810 to 6370	4920 to 6310	2850 to 4635	2910 to 4485	2910 to 4375	2955 to 4320

Table 5.2: Location of electrode sites, marked by depth from probe tip (μm) in auditory cortex and hippocampus for each ferret.

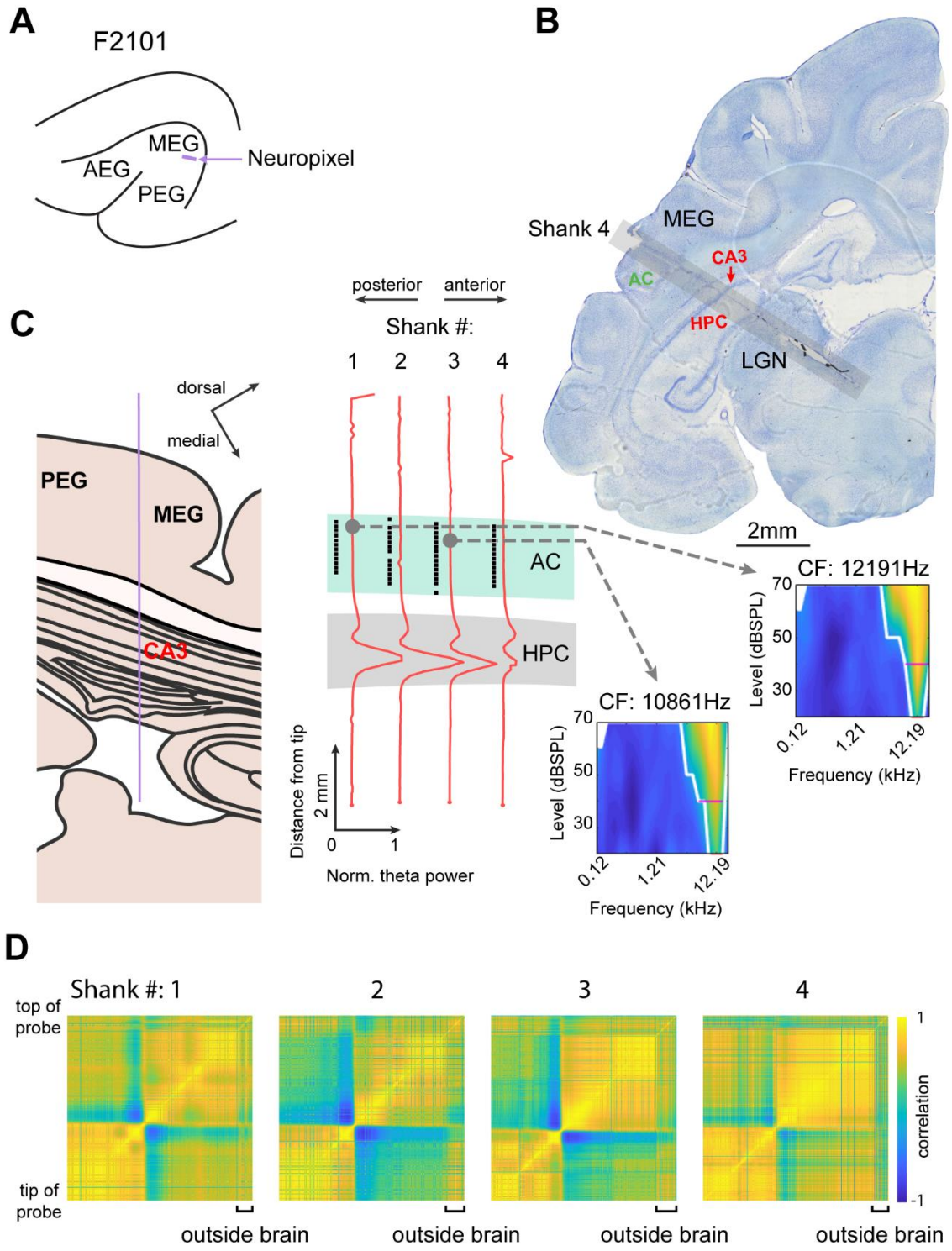

Figure 5.3: Neuropixels probe location in F2101. A) Schematic of the approximate probe position (purple) on the surface of auditory cortex, positioned at MEG. B) Nissl stained coronal slice through auditory cortex showing the position of shank four of the Neuropixels probe which passes through MEG and CA3 (red) of hippocampus. C) Schematic of the probe position through the tissue aligned with the theta power (red) for each shank along its depth, and whether the site at that depth was auditory evoked (black squares indicate $p < 0.05$). Putative AC and HPC are highlighted in blue and grey respectively. Example FRAs are shown from sites marked with the grey circles. The FRA is a normalized heat map with yellow areas showing higher neural responses for the frequency-level combination and lower in blue. Tuning curves are shown (white line) and the Q10 and Q30 (red lines). The characteristic

frequency (CF) is shown above each heat map. D) Correlation matrices for the correlation between the LFP at each site, bottom left indicating sites at the tip of the probe, and top right indicating sites towards the base of the probe. Sites that are likely to be outside of the brain tissue are highlighted.

Figure 5.4 and **Figure 5.5** display the responses of four example units in F2003 during behaviour, two in AC and two in HPC, respectively, in a manner similar to that presented in section 4.3.1 across trials in which there was a hit, miss or correct reject (no false alarms were included). In **Figure 5.4A,** I show a MU in AC that exhibits a strong period of firing in the random sequence and towards the end of the regular sequence, while **Figure 5.4B** shows a MU with robust tone-locked firing to the low frequency tone of the sequence. The units I observed in AC using the Neuropixels probe had similar profiles to that observed in chapter 4, some tone locked responses and some responses that were modulated by the regularity of the sequence. In HPC I did not observe tone locked responses but instead I observed some responses that seemed to be modulated by specific periods of the sequence. **Figure 5.5A** shows a MU in HPC with a gradual increase in firing towards the end of the regular sequence, whilst **Figure 5.5B** appears to ramp firing on before and during the stimulus onset and a marked suppression of activity from 3 to 4s after stimulus onset. Overall, the Neuropixels probe allow for the recording of spiking activity of neurons within AC and HPC, revealing a variety of responses. To understand the differences or similarities in how these two regions encode regularity detection through firing rate and/or spike timing, I pursue similar analysis to that used in chapters three and four.

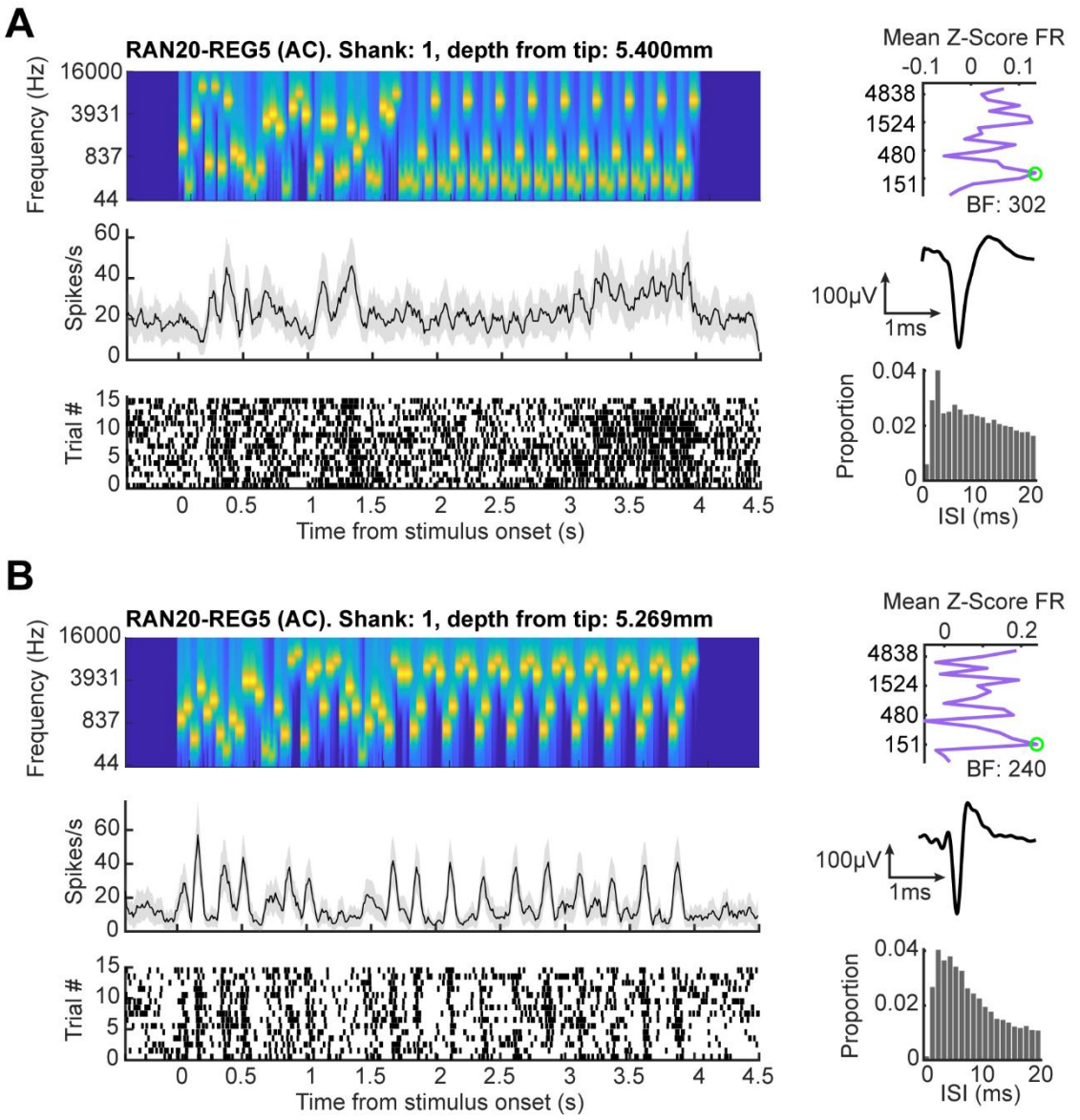

Figure 5.4: Example units in auditory cortex in F2003. A-B) Two example units from auditory cortex recorded by the Neuropixels probe in F2003. Top – spectrogram of the auditory stimulus presented and (right) the mean Z-scored firing rate to each frequency during all tone presented in the recording session before transition. The frequency which elicited the maximum firing (circled in green) was identified as the neurons best frequency (BF). Middle – Spike rate, binned at 25ms, of the unit in response to the above spectrogram with the standard error shaded in grey and (right) the broadband waveform of the unit. Bottom – Raster plot of the spikes of the unit to the above spectrogram and (right) inter-spike-interval histogram (ISI) of the unit. Spike count modulation indices: A = 0.0275, B = -0.00836.

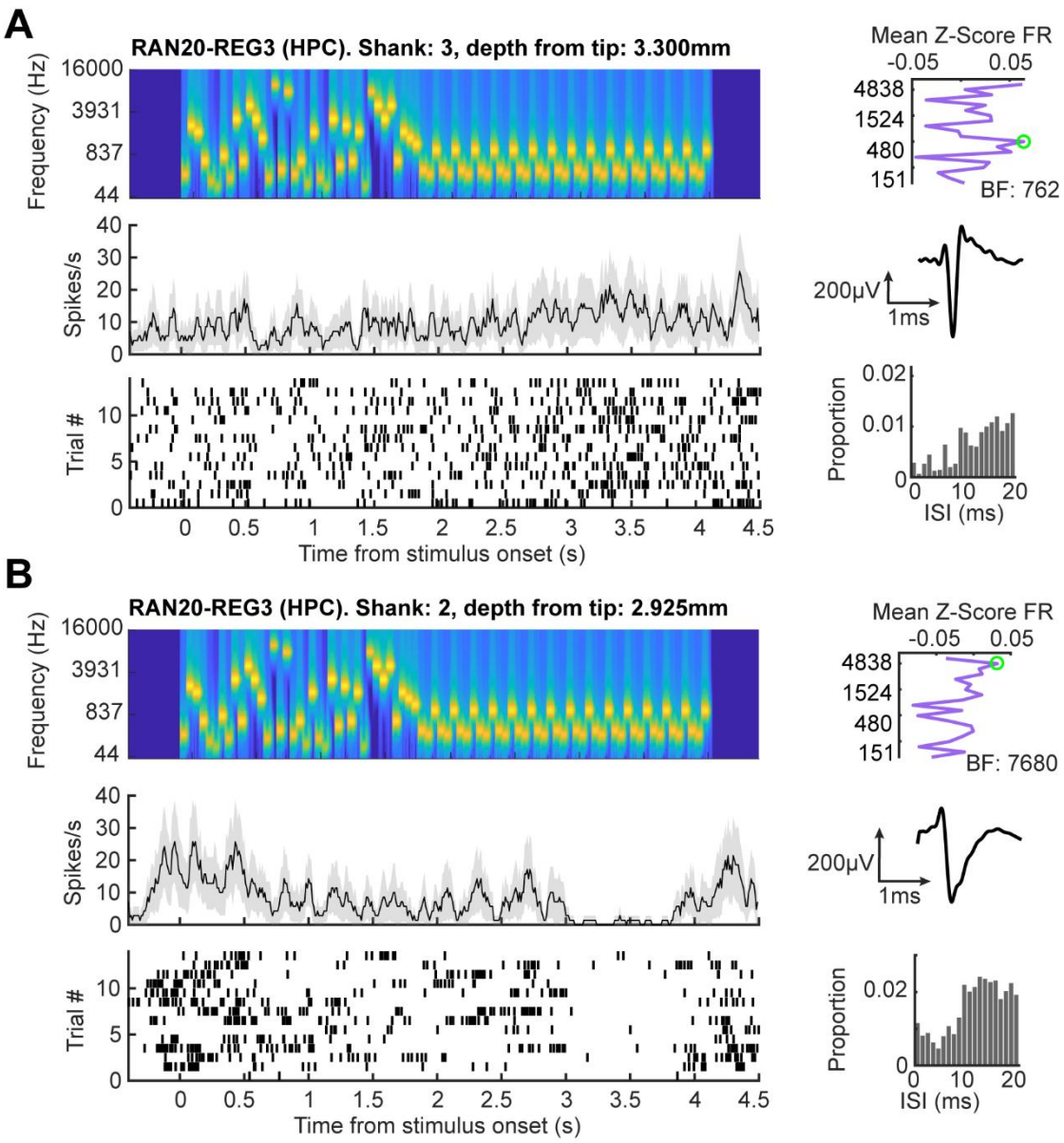

Figure 5.5: Example units in hippocampus in F2003. A-B) Two example units from hippocampus recorded by the Neuropixels probe in F2003. Top – spectrogram of the auditory stimulus presented and (right) the mean Z-scored firing rate to each frequency during all tone presented in the recording session before transition. The frequency which elicited the maximum firing (circled in green) was identified as the neurons best frequency (BF). Middle – Spike rate, binned at 25ms, of the unit in response to the above spectrogram with the standard error shaded in grey and (right) the broadband waveform of the unit. Bottom – Raster plot of the spikes of the unit to the above spectrogram and (right) inter-spike-interval histogram (ISI) of the unit. Spike count modulation indices: A = 0.119, B = -0.0124.

5.3.2 Spike count decreases during regularity with increasing pattern lengths for auditory cortex and hippocampus

Developing the technique to record from AC and HPC simultaneously in a behaving ferret now allows me to expand on my data from my previous WARP recordings in chapters 3 and 4. In chapter 4, I observed that the spike count of neurons in auditory cortex of the ferrets were modulated during the presentation of regular sequences compared to random and that these changes were affected by the pattern length: increased spiking for shorter pattern lengths during regularity. I can test whether this effect is maintained in the Neuropixels recording, but more importantly, previous research has implicated hippocampus in the detection of regularity, as evidenced by increased hippocampal activity in MagEG recordings (Barascud et al., 2016). Therefore I aim to investigate whether firing changes in response to random and regular sequences in AC and HPC. In this section, spike counts of neurons in auditory cortex and hippocampus were recorded in two animals (F2003, behaving; and F2101, passive) and the activity of the neuronal population in both regions were assessed during the presentation of random and regular sequences.

For this analysis, I took the MU activity for each trial/condition for each site (n = 106 MU sites in AC and n = 76 MU sites in HPC) and SU activity (n = 24 SUs in AC and n = 14 in HPC) for trials in which the pattern was generated anew each trial. This approach differs slightly from chapter 4, in which I took trials in which the pattern was repeated across trials, as it enables the presentation of multiple conditions to the same units, despite a reduced number of analysed recordings with the Neuropixels probes. Next, I determine the average spike count per condition for each site during the 2s epoch following the transition from random to regular, with an equivalent time point in the random sequence. To account for differences in overall spiking between SUs and MUs, I calculated a modulation index for each SU and MU, where an index greater than 0 indicating higher firing during the regular sequence.

Analysis was split between MU and SU activity and region (AC or HPC). First, in AC I observed a significant difference in activity between regular or random sequences in MU activity (mean = 0.0298; $p < 0.001$, W = 1668. *Wilcoxon*) but no significant difference in SU activity (mean = -0.00439; $p = 0.406$, W = 120. *Wilcoxon*) in AC. When describing spiking activity in the form of a modulation index (indices greater than 0 indicating a higher spike count for regular sequences over random

sequences), I observe across the population of MUs a positive index for all RAN20 conditions (see **Figure 5.6A**). Across the SUs, I observe a positive index for RAN20-REG3 which then decreases for increasing pattern lengths, ending negatively for RAN20-REG7 (see **Figure 5.6B**). Within HPC I observed no significant difference in activity between regular or random sequences in the MU activity (mean = -0.00775; p = 0.154, W = 1188. *Wilcoxon*) and the SU activity (mean = 0.0402; p = 0.0676, W = 23. *Wilcoxon*). The modulation index of MU activity remained close to 0 for all conditions apart from RAN20-REG7 (see **Figure 5.6C**) but is positive for SUs for RAN20-REG3 and RAN20-REG5 and RAN5-REG5 (see **Figure 5.6D**).

A mixed effects general linear model for SU and MU activity individually in both AC and HPC (see **Table 5.3**) revealed a main effect of pattern length on the modulation index for both SU and MU in both regions, with the modulation index (spiking during the regular sequence compared to the random sequence) decreasing with increasing pattern length. Pairwise comparisons revealed only a significant increase in the modulation index for MUs in HPC for the RAN20-REG5 over the RAN20-REG7 condition (p = 0.00534, Dunn test, Bonferroni). These data (which are likely underpowered to detect population-wide differences) suggest that neurons within HPC are in fact modulated by the number of tones within a pattern, decreasing their firing during the regular sequence when compared to the random sequence for increasing pattern lengths.

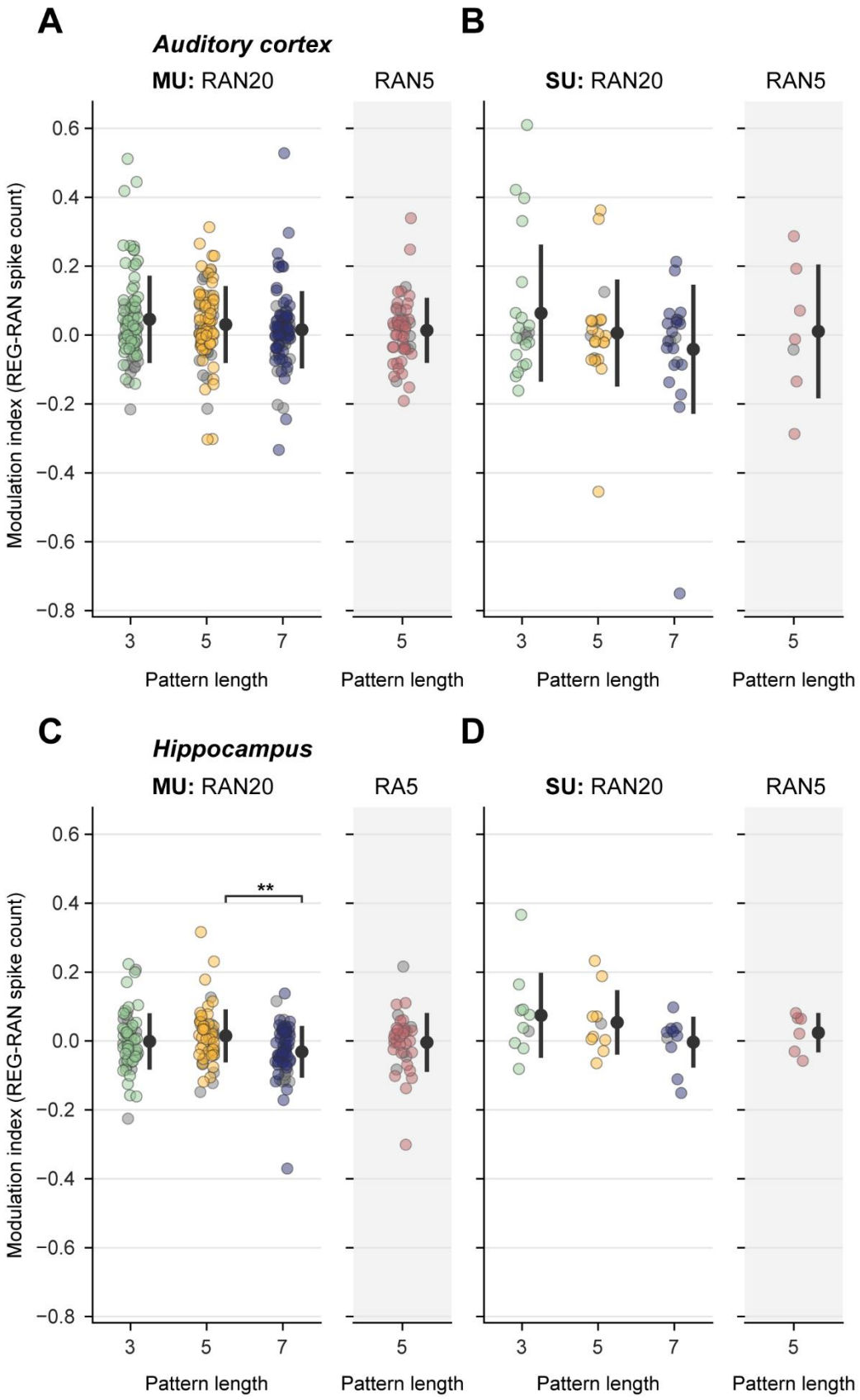

Figure 5.6: Changes in multi and single-unit firing during the presence of regular sequences compared to random sequences in auditory cortex and hippocampus. A-B) Modulation index for each MU (A) and SU (B) for each condition (F2003 (behaving): colour

filled circles; F2101 (passive): grey filled circles) for auditory cortex. C-D) Modulation index for each MU (C) and SU (D) for each condition (coloured circles) for hippocampus. The grey error bars indicate the mean and standard deviation across units for that condition. Significance bars between conditions from a pairwise Dunn test are indicated. * = $p < 0.05$, ** = $p < 0.01$, *** = $p < 0.001$.

					CI 95%	
Fixed effects	Estimate	Standard error	T	p value	Lower	Upper
AC (MU)						
Intercept	0.052	0.025	2.114	**0.035**	0.004	0.1
Random alphabet	0.001	0.001	0.929	0.354	-0.001	0.003
Pattern length	-0.008	0.003	-2.239	**0.026**	-0.014	-0.001
AC (SU)						
Intercept	0.102	0.099	1.029	0.307	-0.096	0.299
Random alphabet	0.001	0.004	0.333	0.74	-0.007	0.01
Pattern length	-0.025	0.012	-2.067	**0.042**	-0.048	-0.001
HPC (MU)						
Intercept	0.032	0.022	1.439	0.151	-0.012	0.076
Random alphabet	0.000	0.001	-0.197	0.844	-0.002	0.002
Pattern length	-0.007	0.003	-2.134	**0.034**	-0.013	-0.001
HPC (SU)						
Intercept	0.126	0.065	1.946	0.060	-0.006	0.258
Random alphabet	0.001	0.003	0.25	0.804	-0.005	0.006
Pattern length	-0.019	0.009	-2.202	**0.035**	-0.037	-0.001

Table 5.3: Mixed effect linear regression on the spike count modulation index (spike count during regular sequences – spike count during random sequences) for multi and single unit activity in auditory cortex (AC) and hippocampus (HPC). AC (MU): $R^2 = 0.223$; Df = 319; random effect std. = 0.0589. AC (SU): $R^2 = 0.105$; Df = 72; random effect std. = 0.0696. HPC (MU): $R^2 = 0.0219$; Df = 236; random effect std. = 0.0190. HPC (SU): $R^2 = 0.187$; Df = 33; random effect std. = 0.0399.

5.3.3 Spike count as a function of depth down auditory cortex

In chapter 4, to analyse the impact of cortical depth on regularity encoding, I grouped sites into lower, middle and upper bins (0.3 to 0.75, 0.75 to 1.5 and 1.5 to 2.25mm from putative cortical surface respectively). I observed upper layers exhibiting higher spiking for regular sequences compared to random sequences, in contrast to middle and lower layers. Yet, as the electrodes moved in 0.1 to 0.2mm jumps, the depth resolution I obtained was coarse and I could not obtain simultaneous recordings down the depth of a cortical column. Moreover our estimate of the cortical surface is based on measuring an impedance drop which may not equate precisely with cortical surface. Using Neuropixels probe I can leverage the recording sites that target down the entire depth of auditory cortex and approximate the location of each of the cortical layers and how spiking is modulated in response to random and regular sequences.

The auditory cortex of the ferret is comprised of several distinct layers: layer I, layer II/III, layer IV, layer V, and layer VI (Bajo et al., 2007), and each of these layers receives a unique profile of inputs with varying projections. In the ferret, layer I, the most superficial layer, is located within 100μm from the surface of the cortex (Bajo et al., 2007). The subsequent layers, II/III and IV, are situated between 100μm and 650μm from the cortical surface, while layer V is found at approximately 650μm to 875μm. The deepest layer, layer VI, is located between 975μm and 1200μm beneath the cortical surface. Though anatomy varies with individual ferrets I can combine this with this with current source density (CSD) analysis on the tone evoked LFP across the sites on each shank of the probe of F2003. Laminar CSD profiles that have been evoked by pure tones (100ms; see 5.2.4 for methods) can provide insight into the laminar organisation by its structure of sources and sinks, where the earliest source is indicative of afferent thalamocortical projections that terminate in layers III and IV (Happel et al., 2010).

In F2003, I analysed the CSD profile in response to pure tones (0 to 100ms) between the four shanks of the probe (see **Figure 5.7**). Notably, I observed a clear onset response across all shanks, characterized by a large sink shortly after tone onset that spans approximately 1mm of the probe at stimulus onset. In shank 1, there is a clear source which is earliest at approximately 500μM which is likely to be layers III and IV. Though the laminar structure is not well defined given the CSD profiles for

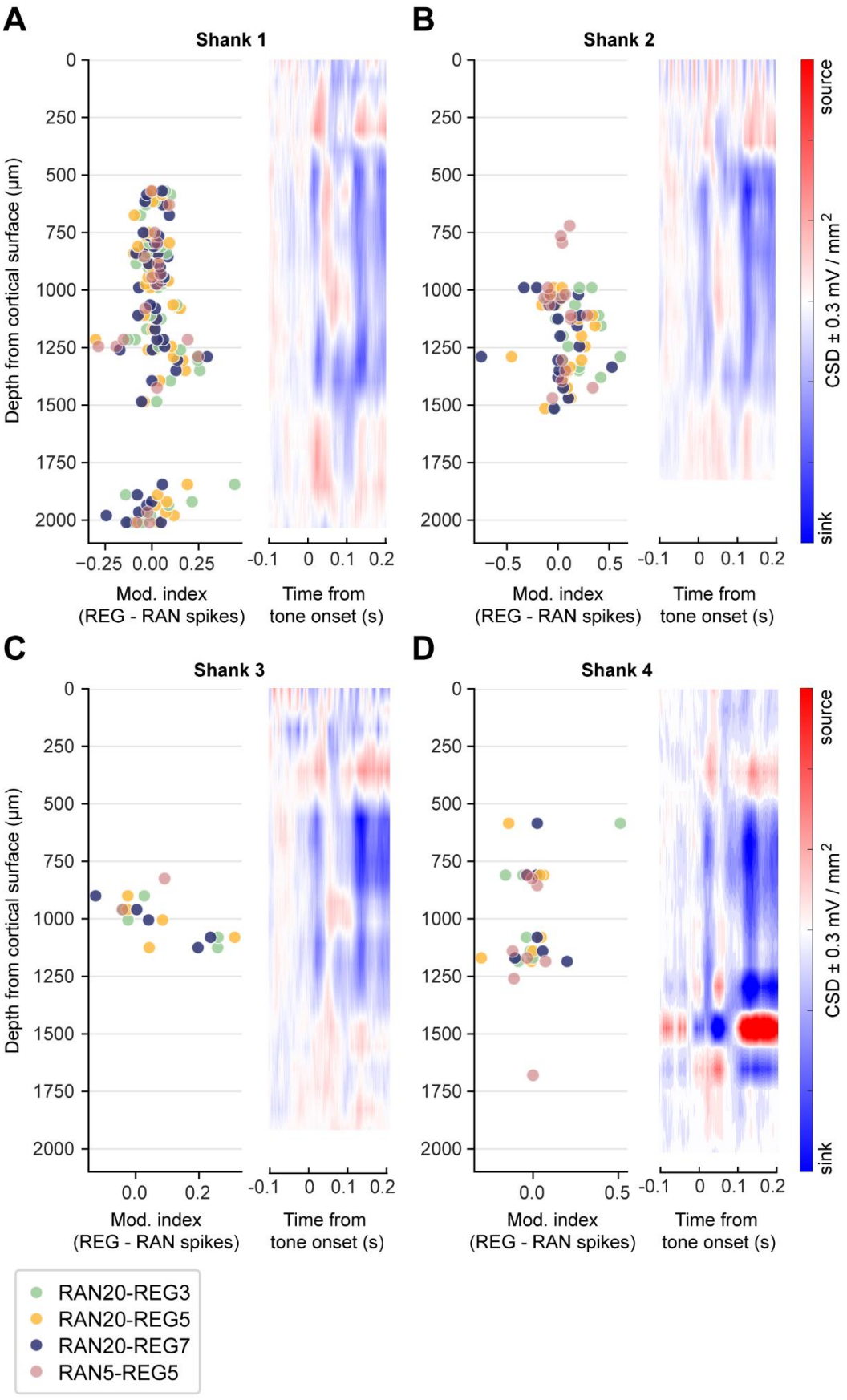

Figure 5.7: Modulation of spike count as a function of depth and shank with corresponding current source density plots. A-D) Shanks 1-4 respectively of the

Neuropixels probe of F2003. Left – Scatter plot of the modulation index for spike count during the regular sequence compared to random (REG-RAN) for each condition and MU/SU (coloured circles). Right – CSD profile of the mean LFP across trials in response to pure tones 100ms in length and at various frequencies (120Hz to 19.3kHz with 1/3 octave spacing) and sound levels (20 to 70dBSPL in 10dBSPL spacing).

each shank, and that the probe is not perpendicular to cortical surface, given previous ferret anatomy I can make some approximations on how spike count is modulated with depth. There appears to be an increase in modulation index in putative layer V and VI (approximately 1250μM from surface and below; see **Figure 5.7A**). Shanks 2 and 3 also present larger modulation indices at approximately 1250μM (see **Figure 5.7B-C**), whereas it is less clear with shank 4. Overall, qualitatively there does seem to be difference in the number of spikes dependent on whether the sequence is random or regular, with deeper layers more likely containing units that increase their firing to regular sequences compared to that of random. However this analysis is preliminary and currently limited by the lack of sampling of units across the whole probe.

5.3.4 Entrainment of neurons within hippocampus to the tone presentation rate and pattern rate

In chapter four, I presented evidence that neurons in auditory cortex exhibit stronger entrainment to the pattern rate during regular vs. random sequences, but no difference in entrainment to the tone presentation rate in random vs. regular contexts. Neural entrainment to auditory stimuli is not limited to just AC, but has been shown in other brain regions such as the HPC, where 40Hz click trains entrained neurons in CA1 (Martorell et al., 2019). However it remains unclear how neurons in ferret hippocampus respond to stimuli that unfold over slower rates such as the tone presentation rate of 20Hz, or even the pattern repetition rates of 6.67Hz, 4.0Hz, and 2.86Hz (for pattern lengths of 3, 5, and 7, respectively). Therefore I computed the vector strength at these frequencies of interest (FOIs) in the 2s window after the transition from random to regular, and the corresponding time period in the random sequence, for each MU and SU. The vector strength value ranges between 0 and 1, with 1 indicating exact phase locking of spike times to the FOI and 0 indicating no phase locking.

When assessing the entrainment of neurons in hippocampus to the tone presentation rate (see **Figure 5.8**), I found significant increases in entrainment to regular sequences over random for all conditions (RAN20-REG3: $W = 490$, $p < 0.001$;

RAN20-REG5: W = 989, p = 0.0152; RAN20-REG7: W = 1210, p = 0.0273; RAN5-REG5: W = 265, p = 0.0291. *Wilcoxon*, *Bonferroni*), suggesting that regularity enhances tone-locking in the HPC. A Kruskal Wallis test revealed significant differences between these conditions (W = 12.959, p = 0.00473) with pairwise comparison revealing RAN20-REG3 showing significantly increased entrainment at the tone presentation rate when compared to RAN20-REG7 (p = 0.00407, *Dunn test, Bonferroni*). Entrainment at the pattern rate was also observed (see **Figure 5.9**), with significant increases in vector strength at each conditions pattern rate during regularity across all conditions apart from RAN20-REG7 (RAN20-REG3: W = 652, p < 0.001, RAN20-REG5: W = 673, p < 0.001; RAN20-REG7: W = 1268, p = 0.0536 ; RAN5-REG5: W = 204, p < 0.001. *Wilcoxon, Bonferroni*). A Kruskal Wallis test revealed no significant differences between conditions (W = 7.170, p = 0.0667), suggesting that the change in vector strength, increasing for the tone presentation rate during the presence of regularity, remains consistent across conditions. These data suggests that neurons within hippocampus are entraining their firing to the tone presentation rate and pattern rate when the sequence is regular, when compared to presentation of a random sequence.

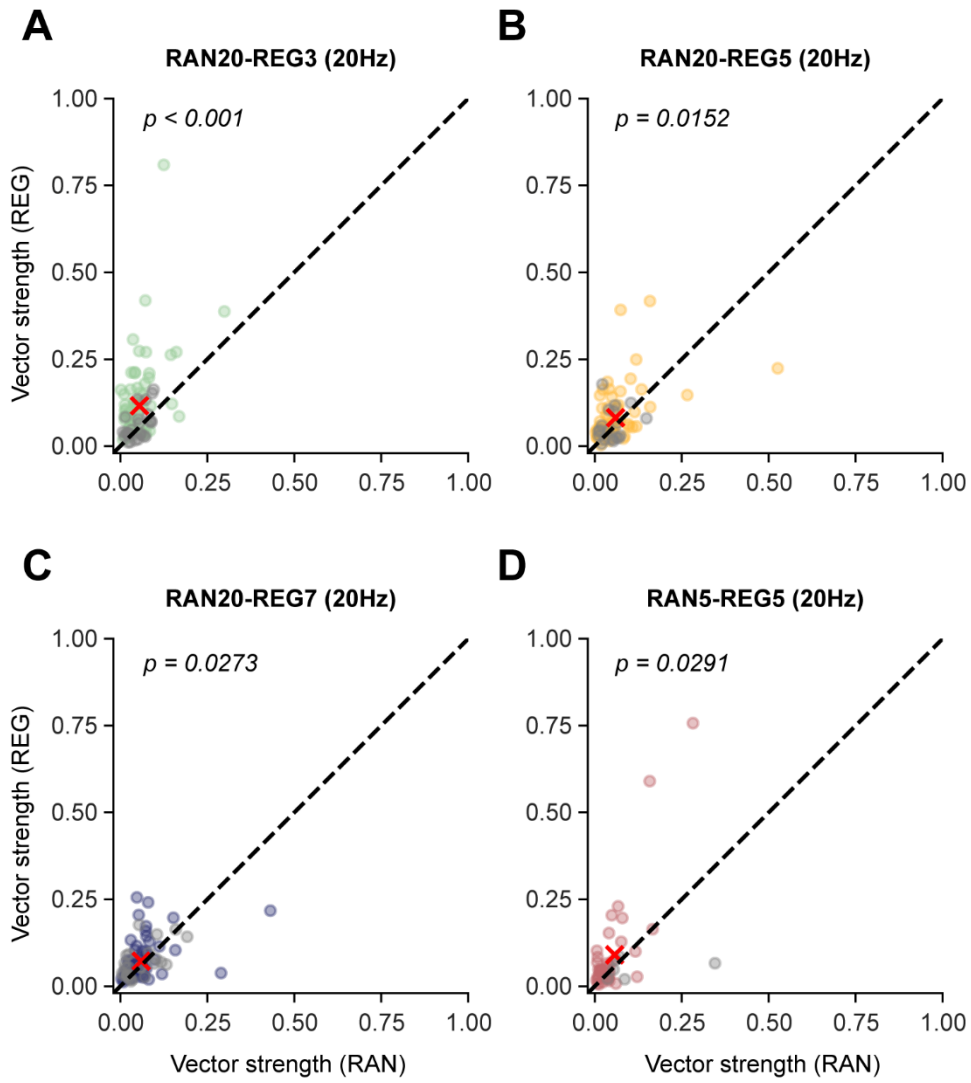

Figure 5.8: Vector strength of MU and SU firing in hippocampus to the tone presentation rate (20Hz) for each condition. Vector strength at 20Hz for each SU in the REG and RAN condition (coloured circle = F2003, grey circle = F2101) for each condition (A = RAN20-REG3; B = RAN20-REG5; C = RAN20-REG7; D = RAN5-REG). A red cross denotes the centroid of the cluster. Equality line (dashed line).

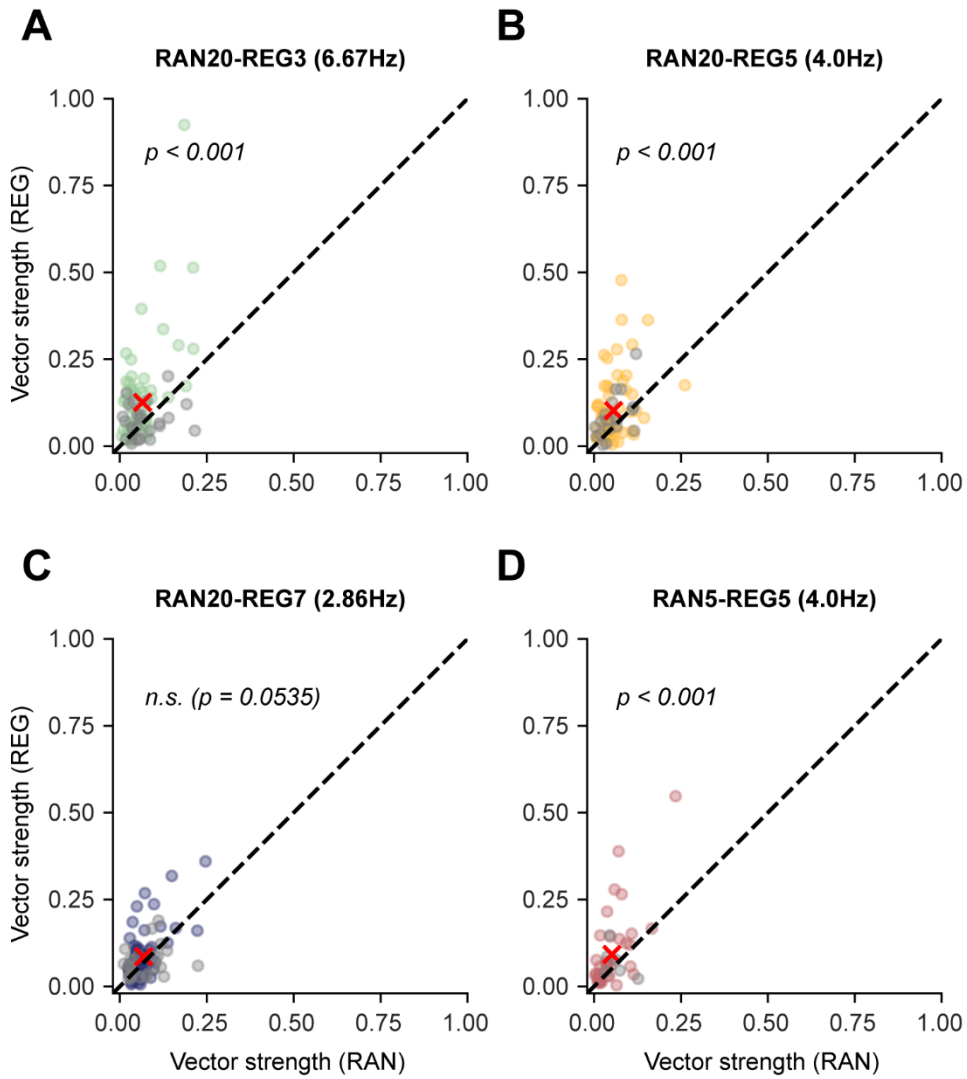

Figure 5.9: Vector strength of MU and SU firing in hippocampus to the pattern repetition rate for each condition. Vector strength at 20Hz for each SU in the REG and RAN condition (coloured circle = F2003, grey circle = F2101) for each condition. A = RAN20-REG3 (6.67Hz); B = RAN20-REG5 (4.0Hz); C = RAN20-REG7 (2.86Hz); D = RAN5-REG (4.0Hz)). A red cross denotes the centroid of the cluster. Equality line (dashed line).

5.3.5 Power at the tone presentation rate and pattern rate are modulated by regularity in hippocampus

In chapter 3, I demonstrated that the local field potential in auditory cortex, contained oscillations at the tone presentation rate (20Hz) and the pattern repetition rate (6.67Hz, 4.0Hz and 2.86Hz for pattern lengths 3, 5 and 7 respectively). The data showed that regular sequences evoked smaller oscillations in the tone repetition rate compared to that of random, but larger oscillations at the pattern rate. In HPC, theta (3-7Hz; Dunn et al., 2022) and gamma (30-100Hz; Bragin et al., 1995) are the most prevalent oscillations. Theta oscillations have been linked to spatial navigation but also memory and higher-cognitive tasks (see for a review: Nuñez and Buño, 2021), however it is unknown whether oscillations at different rates could be induced and modulated through the presentation of random and regular acoustic sequences. Given that I demonstrated that neurons in HPC entrain both to the tone presentation rate and pattern rates during regularity, I would predict increases in oscillatory power for both rates during regular sequences as well.

To test this, I performed some preliminary analysis of the LFP. Spectra of single sessions (akin to **Figure 3.3** for AC; see **Figure 5.10**) did not reveal the same clear peaks that were evident in AC, possible due to the dominance of theta oscillations. To explore this further, I performed similar analysis to that in chapter 3, in which I firstly took trials that did not contain a false alarm or hit (therefore only including misses and correct rejects where the animal was stationary at the central spout) to avoid any movement confounds as theta frequency in HPC is strongly modulated by movement (Dunn et al., 2022). Therefore I only included conditions: RAN20-REG5, RAN20-REG7 and RAN5-REG5 as they included enough miss trials for analysis, unlike RAN20-REG3. Next I performed a Welch's power spectral density estimate (PSD) on concatenated 2s epochs of the trial post-transition at each recording site in HPC. The signal-to-noise ratio (SNR) was calculated at each FOI where an SNR of > 1 indicates increased power at the FOI compared to the side frequency bands.

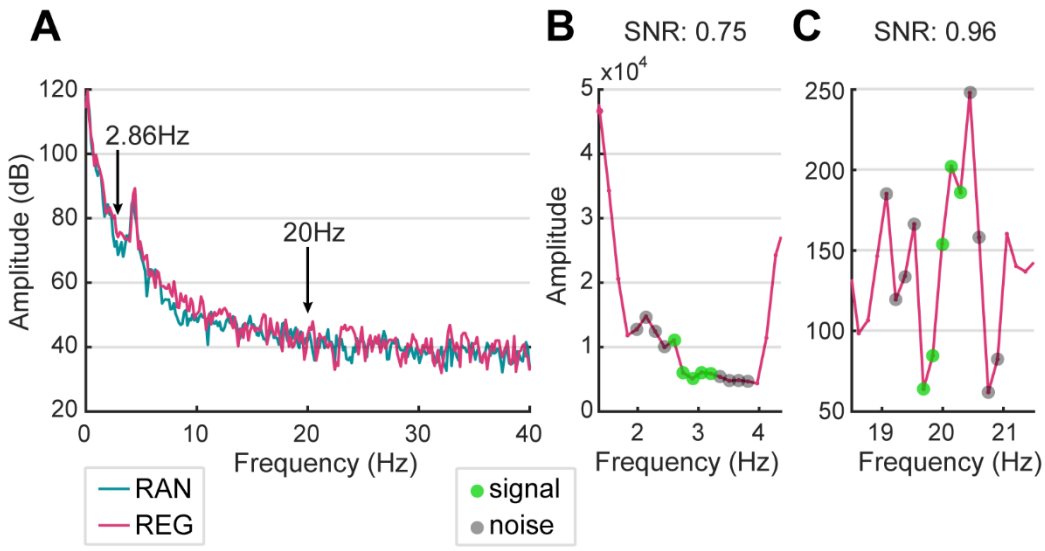

Figure 5.10: Power spectral density estimates of concatenated local field potential epochs post transition. A) Power spectral density estimate calculated for an example recording site in hippocampus when presented random (blue) or regular (pink) sequence with a pattern length of seven (RAN20-REG7). Unlike AC, where peaks were evident at the tone presentation rate and pattern rate, the spectrum shows a predominantly 1/f shape with theta being the only clear peak, with possibly an increase in low frequency power during regularity and a weak peak at 20Hz. B-C) The SNR at frequencies of interest (FOIs) are calculated by taking the RMS of five points around the FOI (green) and dividing it by the surrounding noise points (grey) to give a signal to noise ratio (SNR) at various FOIs such as the pattern rate (2.86Hz; B) and the tone rate (20Hz; C).

Analysis of the oscillatory power at the tone presentation rate of recording sites in hippocampus revealed that the mean SNR across all sites and conditions showed weak tone locked responses with an SNR of 0.994 for the random and 0.969 for the regular condition (n = 304 sites). A Mann-Whitney U test revealed a significant difference between the conditions ($U = 55399$, $p < 0.001$*; Mann-Whitney U, Bonferroni;* see **Figure 5.11A**). Analysis by pattern length and random alphabet, showed that the tone locked response was significantly lower in the regular sequence for RAN20-REG5 ($U = 42492$, $p < 0.001$) and RAN5-REG5 ($U = 59805$, $p < 0.001$) but higher for RAN20-REG7 ($U = 31979$, $p < 0.001$*;* see **Figure 5.11B**). This reveals that power during the presentation of regular sequences modulate the power at the tone presentation rate. However, the direction of this modulation, increasing or decreasing is not consistent across pattern lengths, and the size of the effect is very small, with most SNRs being < 1, providing little evidence of any true tone-evoked oscillation.

A mixed effects linear regression (with recording site as a random intercept) on the modulation index (REG-RAN/REG+RAN; positive index indicates a stronger response at the tone presentation rate for the regular sequence), revealed main effects of pattern length, random alphabet, shank, and significant interactions between shank and random alphabet (see **Table 5.4**). Pairwise comparisons revealed that the modulation indices for pattern length 7 were significantly larger than that of RAN20-REG5 ($p < 0.001$; *Dunn test, Bonferroni*) or RAN5-REG ($p < 0.001$; see **Figure 5.11C**). Running the model separately by condition reveals significant effects of shank in all conditions, with RAN20-REG5 and RAN5-REG5 showing a decrease in the modulation index as shank number increases and therefore as the position of the shank moves dorsally through HPC, whereas in RAN20-REG7 the opposite is true.

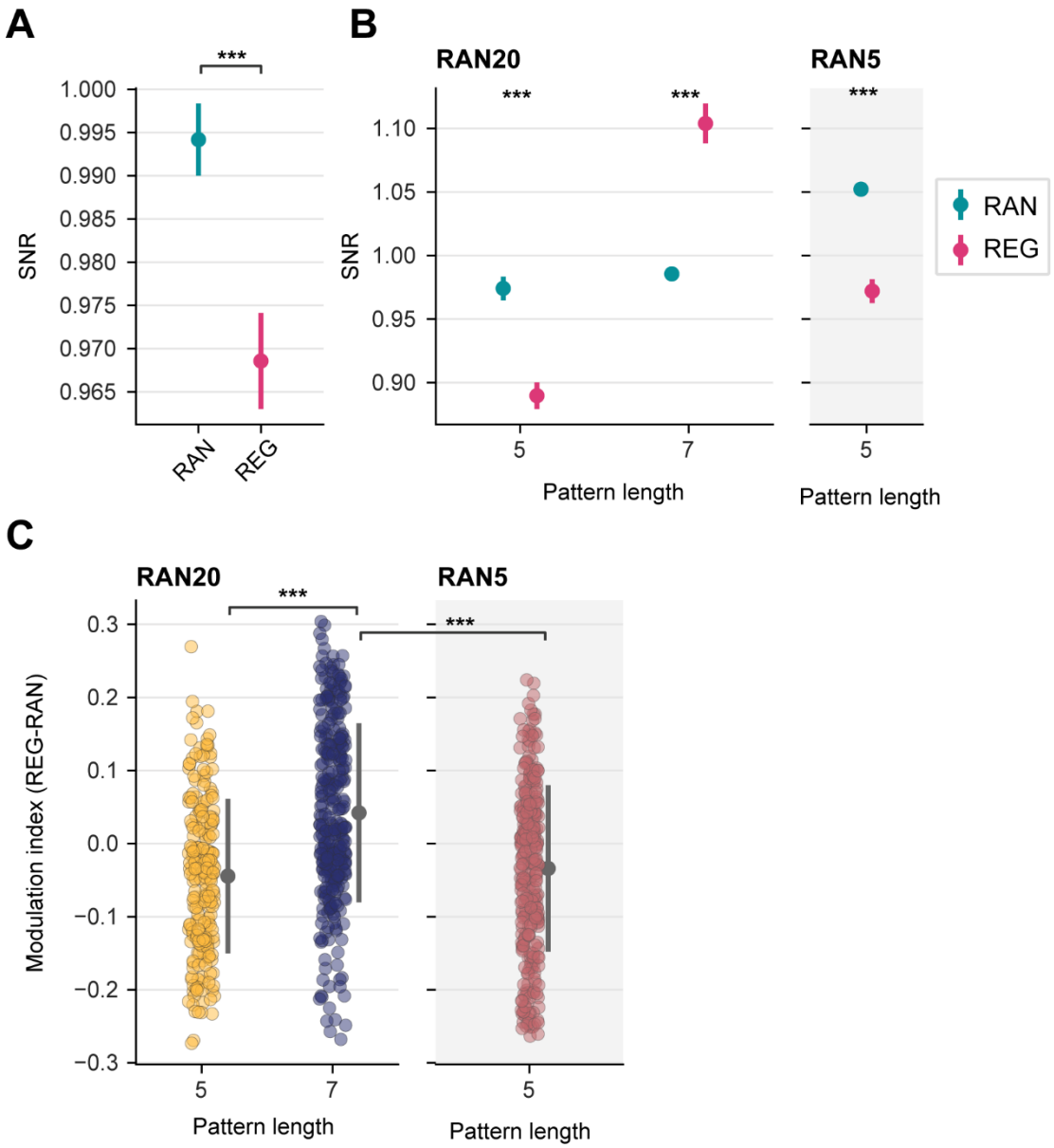

Figure 5.11: Differences in power in HPC at the tone presentation rate between random and regular sequences. A) The signal to noise ratio at 20Hz across sites for random and regular conditions. B) The SNR split by conditions RAN20-REG5, RAN20-REG7 and RAN5-REG5. C) Modulation index split by condition (each circle is a recording site) with the average and standard error shown across sites in grey. Error = standard error for A-B, error = standard deviation for C. * = $p < 0.05$, ** = $p < 0.01$, *** = $p < 0.001$

Fixed effects	Estimate	Standard error	T	p value	CI 95% Lower	CI 95% Upper
Intercept	0.651	0.053	12.192	**< 0.001**	0.546	0.756
Pattern length (PL)	-0.106	0.011	-9.677	**< 0.001**	-0.127	-0.084
Random alphabet (RA)	-0.004	0.001	-2.861	**0.004**	-0.007	-0.001
Shank	-0.364	0.022	-16.885	**< 0.001**	-0.406	-0.322
PL × Shank	0.062	0.005	13.545	**< 0.001**	0.053	0.07
RA × Shank	0.001	0.001	1.276	0.202	0.000	0.002
RAN20-REG5						
Intercept	0.04	0.018	2.15	**0.033**	0.003	0.076
Shank	-0.041	0.008	-4.906	**< 0.001**	-0.057	-0.024
RAN20-REG7						
Intercept	-0.172	0.012	-14.376	**< 0.001**	-0.195	-0.148
Shank	0.082	0.004	19.463	**< 0.001**	0.074	0.091
RAN5-REG5						
Intercept	0.102	0.014	7.144	**< 0.001**	0.074	0.13
Shank	-0.052	0.005	-10.353	**< 0.001**	-0.062	-0.042

Table 5.4: Model output for mixed effects linear regression on the modulation index for tone presentation rate. R^2 = 0.412; Df = 822; random effect std. = $3.42x10^{-6}$. RAN20-REG5: R^2 = 0.589; Df = 218; random effect std. = 0.0709. RAN20-REG7: R^2 = 0.856; Df = 302; random effect std. = 0.0578. RAN5-REG5: R^2 = 0.706; Df = 302; random effect std. = 0.0691.

When assessing the oscillations in the LFP at the pattern rate, the mean SNR across all sites and conditions showed even weaker power at the pattern rate, than the tone rate, with an SNR of 0.776 for the random and 0.878 for the regular condition (n = 304 sites). A Mann-Whitney U test revealed a significant difference between the SNR during presentation of the random and regular sequences (U = 18962, p < 0.001*,* see **Figure 5.12A**). Analysis by pattern length (including only REG5 and REG7) and random alphabet, showed that the power at the pattern rate was significantly higher in the regular sequence for only RAN20-REG5 (U = 18637, p < 0.001*; Mann-Whitney U, Bonferroni*) and RAN5-REG5 (U = 24784, p < 0.001*; Mann-Whitney U, Bonferroni;* see **Figure 5.12B**). This shows that out of pattern lengths 5 and 7, only 5 seems to elicit higher pattern rate power during regularity, and this was the only condition in which the SNR exceeded 1, providing some evidence that there is oscillatory power at the pattern rate. However the pattern rate of pattern length 5 is 4.0Hz which sits squarely in the middle of the theta power oscillation generated by hippocampus in the ferret (Dunn et al., 2022).

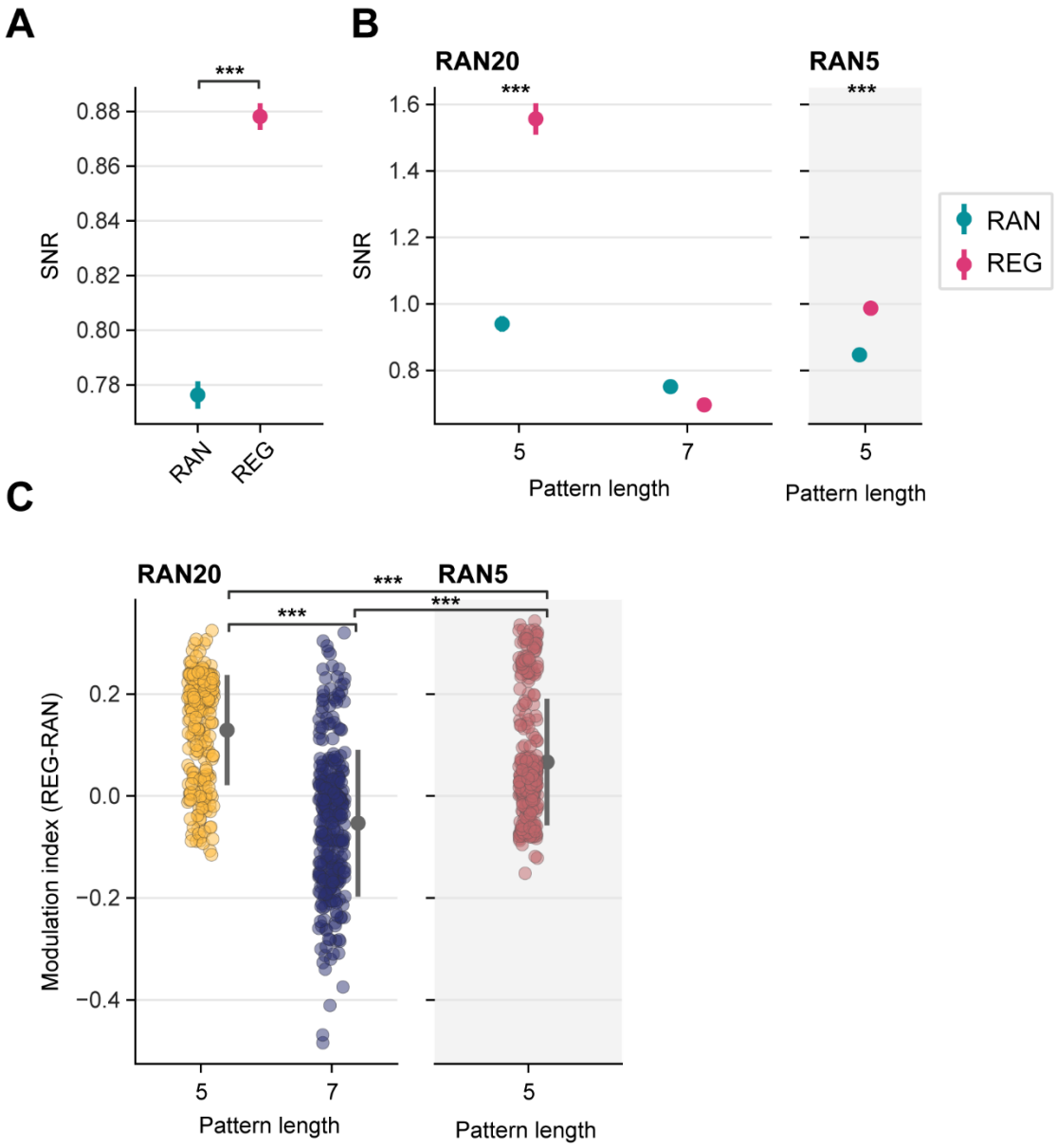

Figure 5.12: Differences in power at the pattern rate between random and regular sequences. A) The signal to noise ratio at 4.0Hz and 2.86Hz for pattern lengths 5 and 7 respectively, across sites and conditions for random and regular sequences. B) The SNR split by conditions RAN20-REG5, RAN20-REG7 and RAN5-REG5. C) Modulation index split by condition (each circle is a recording site) with the average and standard error shown across sites in grey. Error = standard error for A-B, error = standard deviation for C. * = $p < 0.05$, ** = $p < 0.01$, *** = $p < 0.001$

A mixed effects linear regression (recording site as a random intercept) on the pattern rate modulation index, revealed main effects of pattern length, random alphabet, shank, and significant interactions between shank and random alphabet, and shank and pattern length (see **Table 5.5**). Pairwise comparisons (*Dunn test, Bonferroni*) revealed that the modulation index for all conditions were significantly different from one another with RAN20-REG5 showing the highest modulation index,

followed by RAN5-REG5, and then RAN20-REG7 which shows a negative modulation index (see **Figure 5.12C**). Running the model separately by condition reveals significant effects of shank in the condition of RAN20-REG5 and RAN20-REG7, where RAN20-REG5 exhibits a larger negative coefficient such that as the recording sites become more ventral, and the oscillatory power at the pattern rate increase. Overall, these data show that oscillations at 4.0Hz (the pattern rate of pattern length 5) are enhanced during the presentation of regular sequences, and this increases the more ventral the recording site.

					CI 95%	
Fixed effects	Estimate	Standard error	T	p value	Lower	Upper
Intercept	0.642	0.068	9.426	**< 0.001**	0.508	0.776
Pattern length (PL)	-0.129	0.014	-9.282	**< 0.001**	-0.157	-0.102
Random alphabet (RA)	0.016	0.002	8.631	**< 0.001**	0.012	0.02
Shank	-0.094	0.027	-3.435	**0.001**	-0.148	-0.04
PL × Shank	0.024	0.006	4.137	**< 0.001**	0.013	0.035
RA × Shank	-0.006	0.001	-7.518	**< 0.001**	-0.007	-0.004
RAN20-REG5						
Intercept	0.316	0.014	21.83	**< 0.001**	0.288	0.345
Shank	-0.091	0.007	-13.88	**< 0.001**	-0.104	-0.078
RAN20-REG7						
Intercept	0.058	0.02	2.922	**0.004**	0.019	0.097
Shank	-0.043	0.007	-6.092	**< 0.001**	-0.057	-0.029
RAN5-REG5						
Intercept	0.076	0.018	4.205	**< 0.001**	0.04	0.112
Shank	-0.004	0.006	-0.565	0.572	-0.016	0.009

Table 5.5: Model output for mixed effects linear regression on the modulation index for pattern rate. R^2 = 0.355; Df = 822; random effect std. = 9.47×10^{-6}. RAN20-REG5: R^2 = 0.817; Df = 218; random effect std. = 0.0557. RAN20-REG7: R^2 = 0.597; Df = 302; random effect std. = 0.0959. RAN5-REG5: R^2 = 0.499; Df = 302; random effect std. = 0.0875.

5.4 DISCUSSION

The motivation behind this chapter was to begin to understand how non-auditory regions such as HPC, typically implicated in regularity detection in humans, respond during regularity detection. MagEG recordings in humans have shown increased activity during regular sequences when compared to random (Barascud et al., 2016), and another study has shown HPC neurons responding selectively to deviant sounds showing sensitivity to predictable structure within an auditory stimulus (Tzovara et al., 2022). Nonetheless, it is unknown how neurons in HPC respond to pure tone sequences that transition from random to regular during behaviour. In this chapter I show preliminary analysis, limited in scope due to time constraints, on how SU and MU activity changes in response to regular vs. random sequences in AC and HPC, and how power in the LFP at the tone presentation and pattern rate are modulated by regularity.

In this chapter I firstly present a technique that successfully records simultaneously HPC and AC of the ferret using high-density linear probes (Neuropixels 2.0). Whilst chronic recordings of Neuropixels are now commonplace in rodent research (Durand et al., 2023; Juavinett et al., 2019; Luo et al., 2020), I provide the first demonstration of their efficacy to target multiple brain regions for chronic recordings in the ferret. Due to significant anatomical variations between individual ferrets, accurately targeting structures beneath the cortex is challenging, and their larger size and strength requires that implants are extremely robust to prevent damage to the probe or ribbon cable after chronic implantation, particularly as animals are always housed in groups within enriched cages. Here I developed specialized tools and procedures to implant the probes and perform these recordings, with probes lasting over a year thus establishing a method for future research on the interactions between hippocampus and auditory cortex in the ferret model. The metrics I used such as whether sites are auditory evoked or the theta power in the LFP, give best estimates of the location of regions however do still contain limitations. For example, auditory evoked sites are based on the LFP which may overestimate the location of auditory cortex due to volume conduction outside the brain. Furthermore, though theta power does give a strong indication of hippocampus, some sublayers of hippocampus such as the stratum oriens, and stratum pyramidale don’t evoke strong theta oscillations in the ferret (Dunn et al., 2022).

Using this technique, I analysed the SU and MU activity of neurons in AC and HPC. Across the population of SU and MU activity in AC, I observed significant increases in the overall spike count between random and regular sequences, with shorter patterns inducing larger responses, supporting my findings in chapter 4. Performing the same analysis on units within HPC, I also observed changes in spike count corresponding to pattern, again shorter patterns eliciting larger spike counts, however the lack of a significant intercept in the GLMM suggests that there isn't an overall enhancement of firing to regularity within HPC. This is in contrast to studies that have shown an increase in power in MagEG recordings in hippocampus during the presentation of regular sequence (Barascud et al., 2016), but is supported by findings by Tzovara et al. (2022), which found HPC neurons responding selectivity to deviant rather than predictable sounds. Future work could target parahippocampal/entorhinal neurons, shown to be responsive to standard/predictable tones (Tzovara et al., 2022) to identify whether stronger responses would be present there.

In this chapter, the neurons in hippocampus were poorly separated from the neural signal, only a total of 14 single-units across two ferrets. This is likely due to chronic implantation of the Neuropixel implant damaging the brain and/or gliosis setting in by the time the animal is recorded from post-surgery. Additionally, it is unclear how much of the probe is in contact with the cell layer of hippocampus and whether the channel mapping of the probe was fine enough to capture the neurons in the cell layer. Unlike the rat or mouse that has more extensive literature, hippocampal markers and metrics for what constitutes a high yield of hippocampal neurons during chronic recordings in the ferret is unknown. Therefore there is much more work to be done on understanding and optimising chronic hippocampal recordings in the ferret using these high-channel count linear probes.

The predictive coding framework suggests the neurons encoding prediction are likely to reside within deeper layers of cortex such as layer V (Heilbron and Chait, 2018; Keller and Mrsic-Flogel, 2018). In line with this theory, by using tone-evoked LFPs to create CSD profiles of the linear probes, preliminary analysis suggests that there may be stronger modulation of spike count to regular sequences in deeper layers, potentially layers V and VI. However, these results are not yet conclusive and

require a more accurate estimate of the laminar structure of the auditory cortex (AC) along the probe, and a larger sampling of units across the depth of auditory cortex.

My findings demonstrated increased entrainment of unit activity to both the tone presentation rate and pattern rate in hippocampus during the presentation of the regular sequence compared to the random sequence. This is an interesting result as this is despite not showing strong oscillations at these rates in the LFP (typically SNRs of < 1). Whether this entrainment could be induced from other brain regions, such as PFC, is unknown but possible as neurons in PFC and HPC have been shown often to coactivate enhancing memory performance (Euston et al., 2007; Hyman et al., 2010). Moreover, given that I limited oscillatory analysis on trials in which the animal remained at the central spout (i.e. correct reject and miss trials), this may underestimate any oscillatory effects of regularity, as the animal did not behave in response to the regularity and likely did not perceive it. Therefore these results may change when incorporating trials in which the animal detected the regularity.

There is still much more opportunity for future work with the data gathered in this chapter, though beyond the scope of this thesis. Firstly, further analysis of the passive recordings in comparison to recordings gathered from the behaving ferret, will allows to unpick the influence of the attentional state, task relevance and movement on these neural correlates observed in HPC, particularly for shorter pattern lengths such as RAN20-REG3 which almost always elicits movement in the behaving ferret. I might expect these correlates to disappear if the regularity is no longer behaviourally relevant. Secondly, only a subset of the recordings were analysed, so with added recordings and SUs, I can perform waveform analysis to identify sub-populations of cells that facilitate or adapt their firing to regularity. Using the Poisson GLM implemented in chapter 4 can aid in the investigation of sensory and non-sensory effects on neural firing, which is important to understand the effects of regularity on HPC, a region strongly modulated by non-sensory effects such as movement. Lastly, the time course of these correlates and how they emerge jointly between AC and HPC could elucidate what region induced these correlates in the other.

To summarise, it is likely that neurons in hippocampus are responsive to regularity within the sequence, changing the amount of firing dependent on pattern length, but more importantly showing entrainment to both the tone presentation rate

and pattern rate. Preliminary analysis also suggests that units encoding the regularity of the sequence may be located in lower layers. Nevertheless, these are far from conclusive and more work is needed to understand the role of hippocampus in detection of these deterministic acoustic patterns.

6 CHAPTER SIX: OPTOGENETIC CORTICAL INACTIVATION IN THE FERRET

6.1 STATEMENT OF CONTRIBUTION

This chapter has been adapted from a published paper: Town, S.M., Poole, K.C., Wood, K.C., Bizley, J.K., 2023. Reversible inactivation of ferret auditory cortex impairs spatial and non-spatial hearing. J Neuroscience https://doi.org/10.1523/JNEUROSCI.1426-22.2022. I designed the optogenetic validation experiment. ST, JB and I acquired the data from the validation experiment. I analysed the data from the validation experiment. ST, JB and I interpreted the result. ST and JB designed the vowel discrimination task. ST, JB and I collected the data for the discrimination task. For the purposes of this thesis, I expanded the results and focused the chapter on the validation of the optogenetic method in the ferret.

6.2 INTRODUCTION

In this thesis I've shown the first evidence that ferrets can detect changes from random to regular tone sequences and neural correlates of acoustic regularity in AC and HPC. However, ultimately, to fully understand how the brain detects acoustic patterns, it is important to pinpoint the causal role of AC in regularity detection. Loss of function experiments allow us to probe the role of specific regions on a behavioural task or neural response. Reversible inactivation of cortex can provide temporally and spatially controlled deficits that aren't obscured by the potential recovery from recruitment of other neural structures during permanent inactivation (i.e. through lesioning of the target brain region). Temporal precision is specifically necessary in this paradigm to tease apart the causation of neural regions on the rapidly emerging repeating patterns of the sequences used in this thesis. Because of this optogenetics is an optimal candidate for inactivating AC in the ferret during regularity detection.

Optogenetics is well documented in rodent animal species with a large variety of tools and procedures. In contrast, in the ferret model, optogenetic methods are limited with only a few studies using it within the ferret (Murphy et al., 2021; Roy et al., 2016; Zhang and Frohlich, 2022) and even less showing behavioural impairment and neural impairment through inactivation (Bajo et al., 2019). Bajo et al. (2019) used an ArchT opsin to inactivate excitatory neurons and observed that inactivating the high-frequency region of A1 in the ferret perturbed behavioural adaptation to sound

localisation after an ear plug, but not sound localisation in and of itself. This is likely due to the inability to silence a large enough area of AC as methods such as cooling have shown behavioural impairment, in the ferret, in auditory localisation tasks when silencing auditory cortex (Lomber and Malhotra, 2008; Wood et al., 2017).

Recently a viral vector with high interneuron specificity in the non-mouse model has given us the tools to inhibit circuit activity through excitation of inhibitory interneurons. This method employs the natural inhibitory circuit of the brain and silences the output of excitatory cells (Wiegert et al., 2017) and has been shown to produce more effective photoinhibition than direct photoinhibition (Li et al., 2019).This viral vector uses the mDlx promoter to target GABAergic neurons, previously shown in ferrets to express in 98.2% of cells containing GAD67 (Dimidschstein et al., 2016). Combined with Channelrhodopsin-2, it will allow the activation of this opsin in the membrane of these neurons with blue light, which in turn cause an influx of sodium ions into the cell increasing the likelihood of firing. In contrast, I will also assess another viral construct that targets excitatory neurons through a CamKII promoter, using the JAWS opsin that inhibits excitatory neurons through the influx of chloride ions when activated with red light (Chuong et al., 2014).

In this chapter, I develop an optogenetic method in the ferret that will allow us to inactivate areas of auditory cortex by using the inhibitory network of the cortex. Firstly, I compare the expression of two different viral constructs, AAV5-CamkII-JAWS-GFP and AAV2-mDlx-ChR2-mCherry. After assessing the expression patterns between the two, I then assess the efficacy of the AAV2-mDlx-ChR2-mCherry viral construct in inactivating auditory cortical neurons by measuring changes in firing rate, and the depth of these changes by leveraging the high-density linear Neuropixels probes whilst presenting broadband noise bursts. This is then followed with assessment of behaviour during inactivation of auditory cortex in a vowel discrimination in noise task, in which we observed impairments. With these results I conclude that AAV2-mDlx-ChR2-mCherry can be used to inactivate regions of auditory cortex and perturb both neural activity and behaviour in the ferret. Using optogenetics as a tool to inactivate auditory cortex will allow future work to use the temporal and spatial precision garnered by this technique to understand what regions of auditory cortex may be involved in detecting acoustic patterns, and what features of the pattern are important for regularity detection.

6.3 METHODS

6.3.1 Surgical procedure

Viral constructs (AAV5-CamkII-JAWS-GFP and/or AAV2-mDLX-ChR2-mCherry) were surgically injected in A1 of four ferrets (F1814, F1706, F1801 and F1807) at varying depths below the pia surface under sterile conditions whilst the ferret was under anaesthesia (see **Table 6.1** and **Figure 6.1** for injection sites and configurations). Viral constructs and vector packaging were performed by UPenn Vector Core, Philadelphia, PA (JAWS and mDLX plasmid and maps available at Addgene 65015 and 83900 respectively; Chuong et al., 2014; Dimidschstein et al., 2016). Local injections of a total of Marcaine was injected subcutaneously around the temporal muscle. The temporal muscle was then exposed through an incision and removed. The underlying skull was cleaned with citric acid (1%), and for animals implanted with an optic fibre, covered with dental adhesive (Supra-Bond C&B, Sun Medical). Two screws were embedded in the skull in each hemisphere approximately 5mm from the midline and either side of the craniotomy placement. To expose auditory cortex, I used the coordinates: 12mm from the midline and 11mm from the rear fissure, to target the top corner of auditory cortex in the ferret. The craniotomy was targeted to reveal the suprasylvian sulcus next to A1 of MEG and low frequency A1. The pia was then removed from the target injection sites and the glass pipette containing the virus was advanced into the brain at the furthest depth (typically 800µm) and 1µL of virus was injected at 0.1µL/min. The pipette was pulled up to the next depth location (typically 500µm) and another 1µL of virus was injected at the second depth. The virus was injected in two injection sites in auditory cortex per hemisphere.

For F1706, we implanted an optic fibre to deliver light to the injection sites chronically. The fibre was positioned close to the injection site with the surface of the fibre touching the cortical surface. The implant was then embedded within inert silicone elastomer in the craniotomy (Kwik-Sil, World Precision Instruments). The implant was then affixed to the skull via dental cement (Palacos R+G, Heraeus) and the screws attached to the skull. Implant wells were then secured around the implant to protect it from physical damage and to act as fixation points for the optic fibre that is connected to deliver the photostimulation via a laser. Excess skin was then removed to secure the rest of the skin smoothly around the edges of the implant. Animals were then allowed to recover for at least two weeks before undergoing water restriction and

testing. Pre-operative, peri-operative and post-operative analgesia and anti-inflammatory drugs were provided to animals under veterinary advice. Due to COVID-19, behavioural testing of F1706 occurred 20 months after viral injection and neural recordings of F1801 and F1807 occurred approximately 21 and 18 months after injection respectively.

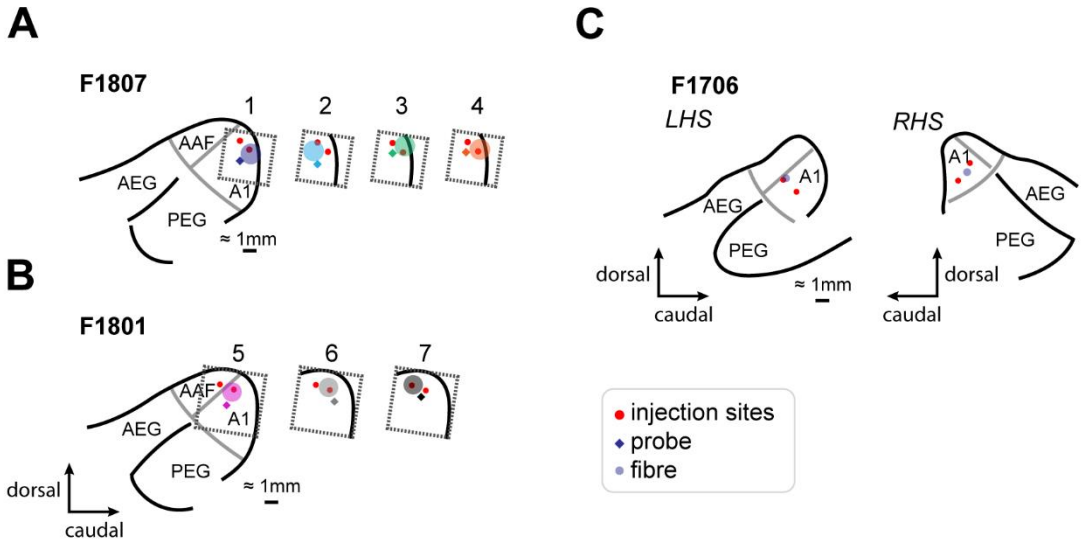

Figure 6.1: Locations of injection sites, fibres and electrode probes. A-B) Multiple probe and fibre configurations for F1807 (A) and F1801 (B) during recordings were used. C) Injection sites and fibre location for the left (LHS) and right (RHS) auditory cortices.

6.3.2 Histology

To confirm electrode location and position, at the end of the experiment the animals, apart from F1706 due to implant failure, were transcardially perfused with 0.9% saline and 4% paraformaldehyde (PFA) under anaesthesia. The brain was then removed for storage in PFA, before cryoprotecting in 30% sucrose for 4-5 days prior to cryosectioning. Because of the unavailability of a functioning cryostat (delayed by COVID-19), brains of F1801 and F1807 were stored in PFA for 6 months, limiting the quality of fluorescent signals. F1814 was sectioned 12 weeks from viral injection. Coronal sections (50µm) were taken through the full extent of the ectosylvian gyrus for F1801 and F1807, and sagittal sections (50µm) for F1814. However, the histology for F1801 is not shown as the terminal recordings severely compromised brain quality. Slices were then mounted on slides using mounting medium that stained the cell bodies with DAPI (Vectashield HardSet Antifade Mounting Medium with DAPI). Slices

were imaged to measure either mCherry or GFP and cell body (DAPI) labelling using a Zeiss Axio Imager 2.0 and Zeiss Confocal and processed on Zen Blue.

Subject no.	Left hemisphere		Right hemisphere	
	Virus	Fibre	Virus	Fibre
F1814	**Site 1:** AAV2-mDLX-ChR2- mCherry (2 depths @ 1uL) *Depth 1: 1000uM* *Depth 2: 400uM* **Site 2:** AAV5-CamkII-JAWS-GFP (2 depths @ 1uL) *Depth 1: 800uM* *Depth 2: 500uM*	-	**Site 1:** AAV2-mDLX-ChR2-mCherry (2 depths @ 0.5uL) *Depth 1: 800uM* *Depth 2: 400uM* **Site 2:** AAV5-CamkII-JAWS-GFP (2 depths @ 0.5uL) *Depth 1: 800uM* *Depth 2: 400uM*	-
F1706	**Site 1:** AAV2-mDLX-ChR2- mCherry (2 depths @ 1uL) Depth 1: 800uM Depth 2: 500uM	NeuroNexus optrode	**Site 1:** AAV2-mDLX-ChR2- mCherry (2 depths @ 1uL) Depth 1: 800uM Depth 2: 500uM	NeuroNexus optrode
F1801	**Site 1:** AAV2-mDLX-ChR2-mCherry (2 depths @ 1uL) *Depth 1: 800uM* *Depth 2: 500uM* **Site 2:** AAV2-mDLX-ChR2-mCherry (2 depths @ 1uL) *Depth 1: 800uM* *Depth 2: 500uM*	Custom fibre	**Site 1:** AAV2-mDLX-ChR2- mCherry (2 depths @ 1uL) *Depth 1: 900uM* *Depth 2: 500uM* **Site 2:** AAV2-mDLX-ChR2- mCherry (2 depths @ 1uL) *Depth 1: 900uM* *Depth 2: 500uM*	Custom fibre
F1807	**Site 1:** AAV2-mDLX-ChR2-mCherry (2 depths @ 1uL) *Depth 1: 800uM* *Depth 2: 500uM* **Site 2:** AAV2-mDLX-ChR2-mCherry (2 depths @ 1uL) *Depth 1: 800uM* *Depth 2: 500uM*	Custom fibre	**Site 1:** AAV2-mDLX-ChR2- mCherry (2 depths @ 1uL) *Depth 1: 800uM* *Depth 2: 500uM* **Site 2:** AAV2-mDLX-ChR2- mCherry (2 depths @ 1uL) *Depth 1: 800uM* *Depth 2: 500uM*	Custom fibre

Table 6.1: Table of configuration of viral injections, constructs and optic fibres used for each ferret.

6.3.3 Neural recordings

To determine whether stimulation of ChR2 in GABAergic neurons is sufficient to suppress sound-driven responses in auditory cortex, we recorded the activity of auditory cortical neurons while presenting stimuli with and without laser stimulation to two ferrets (F1801 and F1807) under anaesthesia. Anaesthesia was induced by a single dose of ketamine (Ketaset; 5 mg/kg/h; Fort Dodge Animal Health) and medetomidine (Domitor; 0.022 mg/kg/h; Pfizer). The left radial vein was cannulated and anaesthesia was maintained throughout the experiment by continuous infusion (ketamine: 5 mg/kg/h; medetomidine: 0.022 mg/kg/h; atropine sulfate: 0.06 mg/kg/h and dexamethasone: 0.5 mg/kg/h in Hartmann's solution with 5% glucose). The ferret was intubated, placed on a ventilator (Harvard model 683 small animal ventilator; Harvard Apparatus), and supplemented with oxygen. Body temperature (38°C), ECG, and end tidal CO_2 were monitored throughout the experiment (approximately 48h). Animals were then placed in a stereotaxic frame, and the site of viral injection over both left and right auditory cortex was exposed. A metal bar was attached to the midline of the skull, holding the head without further need of a stereotaxic frame. The animal was then transferred to a small table in a soundproof chamber (Industrial Acoustics) for stimulus presentation and neural recording. During recordings, the craniotomy was covered with 3% agar, replaced at regular intervals.

During neural recordings to test the inactivation of neurons during photostimulation, I presented broadband noise bursts of varying levels (40-70dB SPL) and durations (50, 100, and 250ms), either alone or with the laser on. Stimuli were repeated 20 times, with a pseudo-random interval (0.5-0.7s) between trials. Laser stimulation was provided with a 463nm DPSS laser attached to a custom-made optic fibre (1.5mm diameter, Thorlabs FP1500URT) that was designed to maximize the area over which light was delivered and could provide up to 300mW at the fibre tip. I presented pulsed light with a target power of 50mW and frequency of 1 or 10Hz. Pulses had a square-wave design with 50% duty cycle, beginning 100ms before sound onset and ending 100ms after sound offset. In addition to laser testing with sound presentation, I also tested the effect of the laser on spontaneous activity without sound. The effects of laser light delivery were measured at several sites over auditory

cortex by placing the optic fibre and Neuropixels probe in various configurations over MEG and close to the viral injection sites of auditory cortex in each animal (see **Figure 6.1A-B** for recording configurations during recordings).

To record the neural activity, I used Neuropixels Probes (IMEC, version 1.0) inserted orthogonal to the cortical surface. The probes were connected via headstages to an IMEC PXIe data acquisition module within PCI eXtensions for Instrumentation (PXI) hardware (PXIe-1071 chassis and PXI-6132 I/O module, National Instruments) that sampled neural signals at 30kHz. Neural activity was recorded in SpikeGLX (version 3.0., billkarsh. github.io/SpikeGLX) and putative action potentials were then extracted and sorted in Kilosort (version 3.0., www.github.com/MouseLand/Kilosort), and manually curated to identify single (n=174) or multiunit (n=291) activity. Spike clusters were merged based on assessment of waveform similarity and classed as a SU using waveform size, consistency, and inter-spike interval distribution (all single units had 2% of spikes within 2ms). Neural spikes had biphasic waveforms that were notably different from positive-going monophasic waveforms containing sharp peaks that were interpreted as laser artefacts and discarded from the analysis.

6.3.4 Neural analysis

To contrast the effects of laser light delivery on sound-driven activity, I first calculated the mean firing rate of each unit during auditory evoked activity, taking a window from sound onset to sound offset (50, 100, or 250ms in length). For each unit, I compared the mean firing rate during this window calculated over all conditions in which the laser was present with the mean firing rate when the laser was absent (change in firing rate = laser OFF– laser ON). To contrast the effects of laser light delivery on spontaneous activity of each unit, I performed the same calculation on mean firing rates during the 100ms window before sound onset, on trials with and without the laser.

Inspection of neural activity with, and without, laser suggested that light delivery had distinct effects on subgroups of neurons. To test whether units could be distinguished by their modulation to laser delivery and to determine the number of separable groups of units using an unsupervised approach, I applied K-means clustering to the firing rates of each unit with and without laser. Clustering was based on the cosine distance between units (rather than Euclidean distance) to isolate the change in spike rate with laser stimulation across units with widely varying baseline

firing rates. I identified the appropriate number of clusters within the data by comparing the sum of point-to-centroid distances for K=1 to 10 and finding the knee-point using vector bisection (Dmitry Kaplan 2022, Knee Point, MATLAB Central File Exchange).

To map the extent of sound-evoked activity across the length of the probe, I compared the mean spike rates during sound presentation and a time window preceding sound onset of matched duration (*Wilcoxon*). This analysis was performed on each unit to each sound duration by sound level condition, with Bonferroni correction for multiple comparisons. Units that showed a significant response in any of the conditions were classed as an auditory evoked unit (n = 72, out of a total of 464 recorded units). I then contrasted the effects of laser light delivery on the firing rates of units recorded at different cortical depths during sound presentation, where depth refers to the distance on the probe from the most superficial channel on which spiking activity was observed.

I also investigated the temporal dynamics of the optogenetic stimulation to control for heating effects from laser delivery (Owen et al., 2019). To identify the latency at which light delivery induced a significant change in firing, I performed nonparametric cluster statistical analysis, which controls for multiple comparisons that would occur from calculating a test statistic over each time point, by calculating a test statistic from clusters of adjacent time samples of the PSTH in which firing rate with laser was greater than without laser (or vice versa; Maris and Oostenveld, 2007). This statistic was calculated during the 100ms after laser onset for each condition and the minimum time bin labelled as significant by the cluster statistic was averaged across conditions to calculate the latency for each unit.

6.3.5 Vowel discrimination task

6.3.5.1 Stimuli

Vowels were synthesized in MATLAB (The MathWorks) using an algorithm adapted from Malcolm Slaney's Auditory Toolbox (https://engineering.purdue.edu/;malcolm/interval/1998- 010/) that simulates vowels by passing a click train through a biquad filter with appropriate numerators such that formants are introduced in parallel. In the current study, four formants (F1-F4) were modelled: /u/ (F1-F4: 460, 1105, 2857, 4205 Hz), /Ɛ/ (730, 2058, 2857, 4205 Hz). F1706 was trained to discriminate between the pair of vowels: /Ɛ/ and /u/. All vowels

were generated with a 200Hz fundamental frequency. Vowels were presented in clean conditions as two repeated tokens, each of 250ms duration and of the same identity, separated with a silent interval of 250ms (see **Figure 6.2**). Here, two vowel tokens were used for consistency with previous work (Bizley et al., 2013; Town et al., 2015).

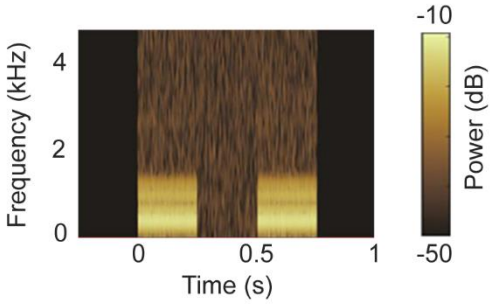

Figure 6.2: Spectrogram of vowels in discrimination task. Spectrogram shows vowels (e.g., two 250ms tokens of /u/, separated by 250ms interval) with additive broadband noise. Vowel identity was always the same for both tokens, and the animal was required to respond left or right based on that identity (i.e., there was no requirement to compare the two tokens).

Sounds were presented through loudspeakers (Visaton FRS 8) positioned on the left and right sides of the head at equal distance and approximate head height. These speakers produced a smooth response (62 dB) from 200 to 20,000 Hz, with a 20 dB drop-off from 200 to 20 Hz when measured in an anechoic environment using a microphone positioned at a height and distance equivalent to that of the ferrets in the testing chamber. All vowel sounds were passed through an inverse filter generated from calibration of speakers to Golay codes (Zhou et al., 1992). Vowels were presented with additive broadband noise fixed at 70 dB SPL generated afresh on each trial. The noise was timed to ramp on at the onset of the first vowel token and ramp off at the end of the second vowel token, and thus had a total duration of 750ms (i.e., that was equal to the two vowel tokens, plus the intervening silent interval). Onsets of both vowels and noise were ramped using a 5ms cosine function.

6.3.5.2 Task

F1706 was trained to discriminate between synthetic vowel sounds by reporting at a left response port if one type of vowel (e.g., /u/) was presented, or reporting at a right response port if a second type of vowel (e.g., /Ɛ/) was presented. The chamber contained three response ports housing infrared sensors that detected the ferret's presence. On each trial, the ferret was required to approach the centre spout and hold

their head position for a variable period (between 0 and 500ms) before stimulus presentation. Animals were required to maintain contact with the centre port until 250ms after the presentation of the first token, at which point they could respond at left or right response ports. Correct responses were rewarded with water, while incorrect responses led to a brief timeout (between 3 and 8 s) indicated by presentation of a 100ms broadband noise burst and in which the centre port was disabled so that animals could not initiate a new trial. During testing, light was delivered in the optic fibres implanted in F1706 from a 463 nm DPSS laser (Shanghai Laser & Optics Century) with a steady-state power of 40mW, measured at fibre termination before the optrode using an S140C integrating sphere photodiode sensor (ThorLabs).

6.3.5.3 Behavioural analysis

All analyses excluded responses on correction trials, or trials where ferrets failed to respond within the required time (60s). A minimum number of trials (n = 10) and sessions (n = 3) in both laser and control conditions to include a sound level or signal-to-noise ratio (SNR) value in the analysis. Statistical analysis of effects of the effect of photostimulation and vowel level on performance used a generalized linear model fitted using fitglm in MATLAB (version 2022a). The model used a binomial distribution and logit link function with condition (laser on = 1, laser off = 0) and vowel level as fixed effects. I reported the magnitude of coefficients (estimate) of fixed effects of interest, the t-statistic for a hypothesis test that the coefficient is equal to 0 (T) and its respective p-value (p). The 95% confidence intervals are also reported for each fixed-effect coefficient and the adjusted R^2 value of the model to assess model fit. All behavioural analysis was performed offline using Python packages and MATLAB.

6.4 RESULTS

6.4.1 AAV2-mDLX-ChR2-mCherry & AAV5-CamkII-JAWS-GFP expression within ferret auditory cortex

Optogenetic silencing can be performed either through driving inhibitory interneurons via Channelrhodopsin-2 with an inhibitory targeting promoter (i.e. mDLX (Dimidschstein et al., 2016) or suppressing spiking of excitatory neurons via a halorhodopsin such as JAWS (Chuong et al., 2014). During development of the technique, I wanted to test the expression of two viral constructs working in each of these ways, AAV5-CamkII-JAWS-GFP and AAV2-mDLX-ChR2-mCherry. To assess the expression, both constructs were injected into auditory cortex of F1814, and then sagittal sections were imaged on a confocal to identify the location of the fluorescently labelled opsins (see **Figure 6.3**). Both viral constructs showed adequate spread throughout the tissue, expressing in a region of approximately 1mm in diameter (see **Figure 6.3A and C**). However, AAV5-CamkII-JAWS-GFP showed expression mostly localised to the neuropil (see **Figure 6.3B**) whereas AAV2-mDLX-ChR2-mCherry was localised within the cell body membrane, as shown by its proximity to the DAPI stained nucleus.

With the more localised expression around the cell body with the AAV2-mDLX-ChR2-mCherry viral construct, and the increased effectiveness of leveraging the inhibitory network to inactivate cortex (Li et al., 2019), I focused my efforts on using the AAV2-mDLX-ChR2-mCherry viral construct to silence auditory cortex. To check the depth of expression I sectioned slices coronally in F1807 and assessed the localisation of the opsins to the cell body. Widefield imaging demonstrated viral expression in MEG, with labelled cells observed between 1 and 2 mm from injection sites (see **Figure 6.4A**). Confocal imaging again revealed some colocalization of mCherry with cell bodies (labelled by DAPI), however as the brain of F1807 was fixed after terminal recordings, and stored in PFA for 6 months, this limited the quality and contrast of fluorescent signals (see **Figure 6.4B**). Overall, I can conclude that AAV2-mDLX-ChR2-mCherry does successfully express within the cell body of neurons in auditory cortex with a spread of approximately 1 to 2mm per injection site.

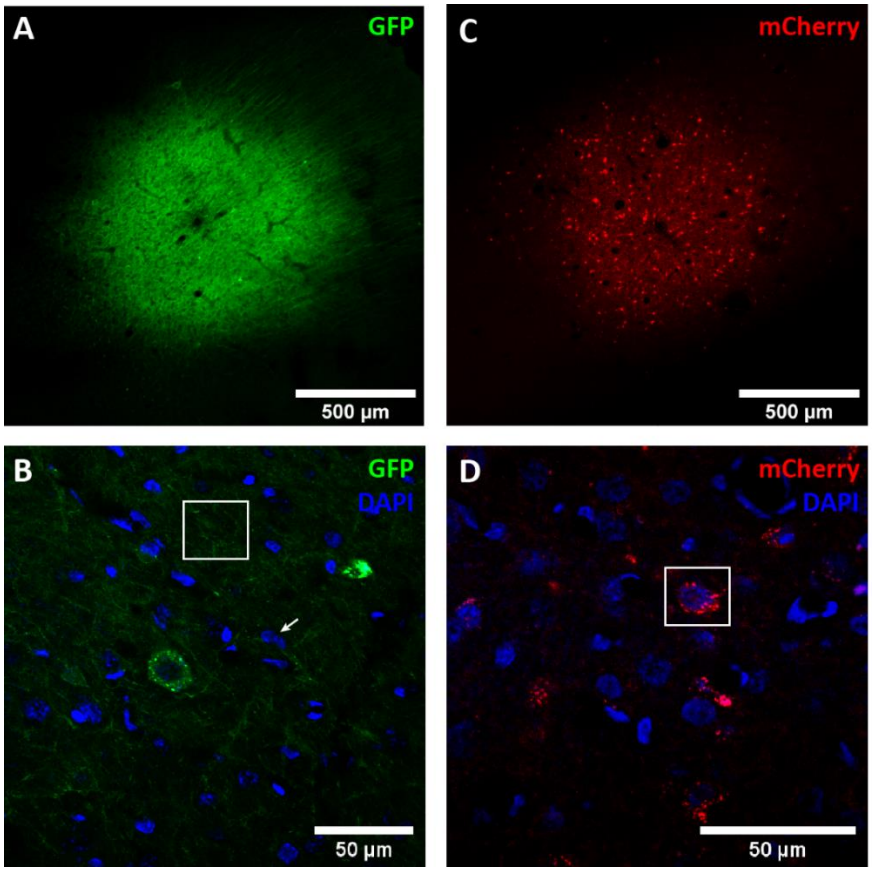

Figure 6.3: Fluorescent imaging of optogenetic viral injection sites in auditory cortex of F1814. A) Injection site in auditory cortex of the AAV5-CamkII-JAWS-GFP. Spread of injection site reaches approximately 1mm. B) Increased magnification and staining of cell nuclei with DAPI (white arrow) shows expression of construct within the neuropil (white box). C) Injection site in auditory cortex of the AAV2-mDLX-ChR2-mCherry. Spread of injection site reaches approximately 1mm and shows expression within the cell body. D) Expression of the construct is within the cell body membrane of multiple cell bodies around intact nuclei, stained by DAPI (white box).

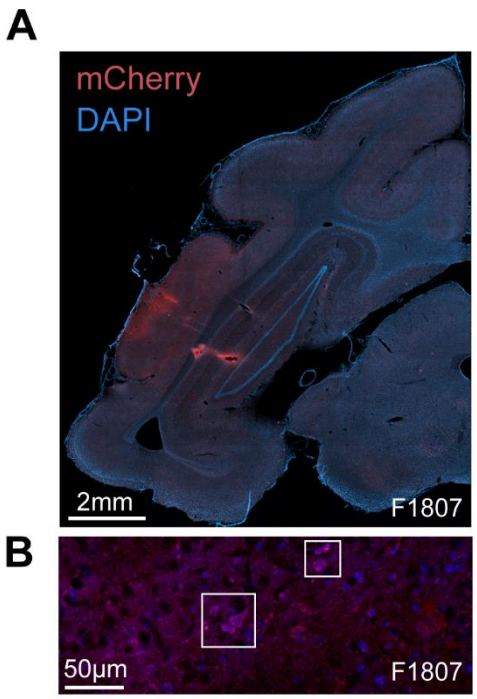

Figure 6.4: Fluorescent imaging of an example of a AAV2-mDLX-ChR2-mCherry injection site within auditory cortex of F1807. A) Widefield imaging of coronal sections through the ectosylvian gyrus with the cell bodies labeled with DAPI (blue) and ChR2 labeled with mCherry (red). B) Confocal imaging of the injection site showing colocalization of cell bodies and mCherry expression (outlined).

6.4.2 Cortical inactivation via activation of GABAergic interneurons

With the confirmed viral expression of AAV2-mDLX-ChR2-mCherry within ferret auditory cortex, I examined the electrophysiological efficacy of cortical inactivation through optogenetics. To do this I performed terminal recordings to record neural responses around the viral injection sites of F1801 and F1807. Using Neuropixel probes (NP1.0) I recorded the activity of 465 units in auditory cortex under ketamine-medetomidine anaesthesia. Multiple optic fibre and recording sites were tested over auditory cortex (see **Figure 6.1A-B**), and at each site, I presented broadband noise with half of the trials presenting a laser simultaneously (100ms before and after sound onset/offset; see **Figure 6.5**). Light delivery affected neural responses in a variety of ways, including suppressing neural responses to sound (see **Figure 6.5A & D**), suppressing baseline spontaneous firing (see **Figure 6.5B**) and, in some cases, driving firing (see **Figure 6.5C**).

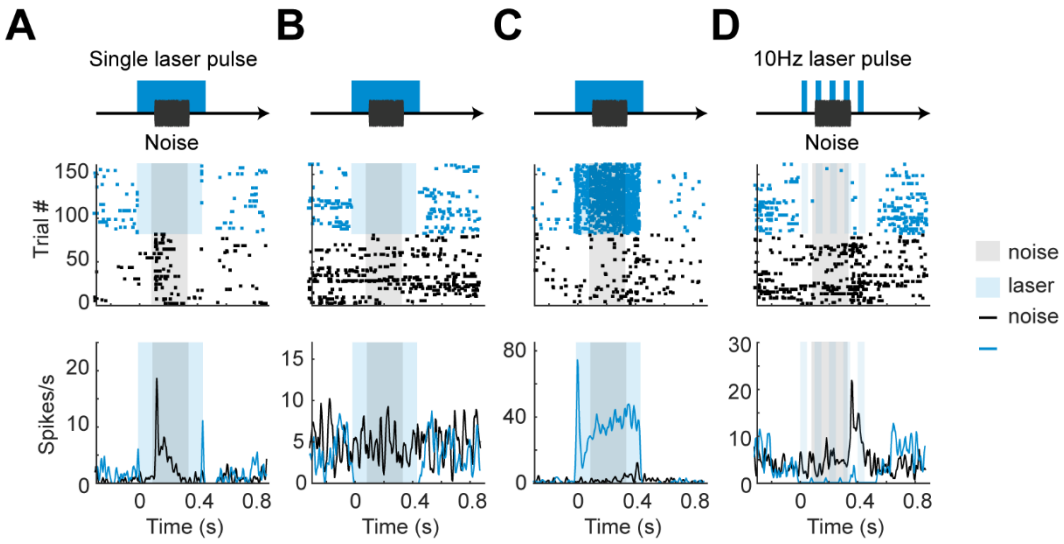

Figure 6.5: Neural responses during photostimulation of ChR2. Peristimulus time histogram and raster plots showing responses of four example units recorded from auditory cortex with and without light delivery in a single laser pulse (A-C) and a 10Hz laser pulse (D).

Across the population, I observed that photostimulation most commonly suppressed sound evoked and spontaneous activity in the majority of units (see **Figure 6.6**). While these patterns were most evident when examining firing in the time window around sound presentation (see **Figure 6.6A & C**), the same pattern was also evident in spontaneous activity (see **Figure 6.6B & D**). To capture distinct effects of light delivery on the neural population, I used K-means clustering to classify units into separate groups. I performed K-means clustering in a polar coordinate system to compare the mean firing rates of each unit, as it allowed me to capture the experimental effect of light delivery via the angle units, while standardising comparisons across units with widely varying firing rate. The angular distribution showed peaks that distinguished units showing strong suppression (angles tending to 0 radians), units that were unaffected by light (values near π/4 radians), and a smaller number of units showing laser driven activity (angles tending to π/2; see **Figure 6.6E**).

Cross-validation on the sum of point-to-centroid distances for K=1 to 10 indicated that two clusters captured the majority of variance between units (see **Figure 6.6F**), with the two groups being distinguished by their sensitivity to photostimulation (see **Figure 6.6**). Cluster 1 showed a significant decrease in sound evoked firing, median change of -1.296 spikes/s during photostimulation (*Wilcoxon signed rank test, Bonferroni*, $p < 0.001$, $Z = -14.3$), whilst cluster 2 showed a small but significant increase, with a median change of 0.0667 spikes/s ($p < 0.001$, $Z = 5.09$). Light delivery

was also successful in suppressing baseline spontaneous activity. Cluster 1 showed a significant decrease in spontaneous firing, median change of -0.4167 spikes/s during photostimulation (*Wilcoxon signed rank test, Bonferroni*, $p < 0.001$, $Z = -8.18$), whilst cluster 2 again showed a small but significant increase, with a median change of 0.0667 spikes/s ($p < 0.001$, $Z = 4.22$)). The lower firing rates of units without laser illumination gave less scope to observe modulation and thus the effects of inactivation were weaker.

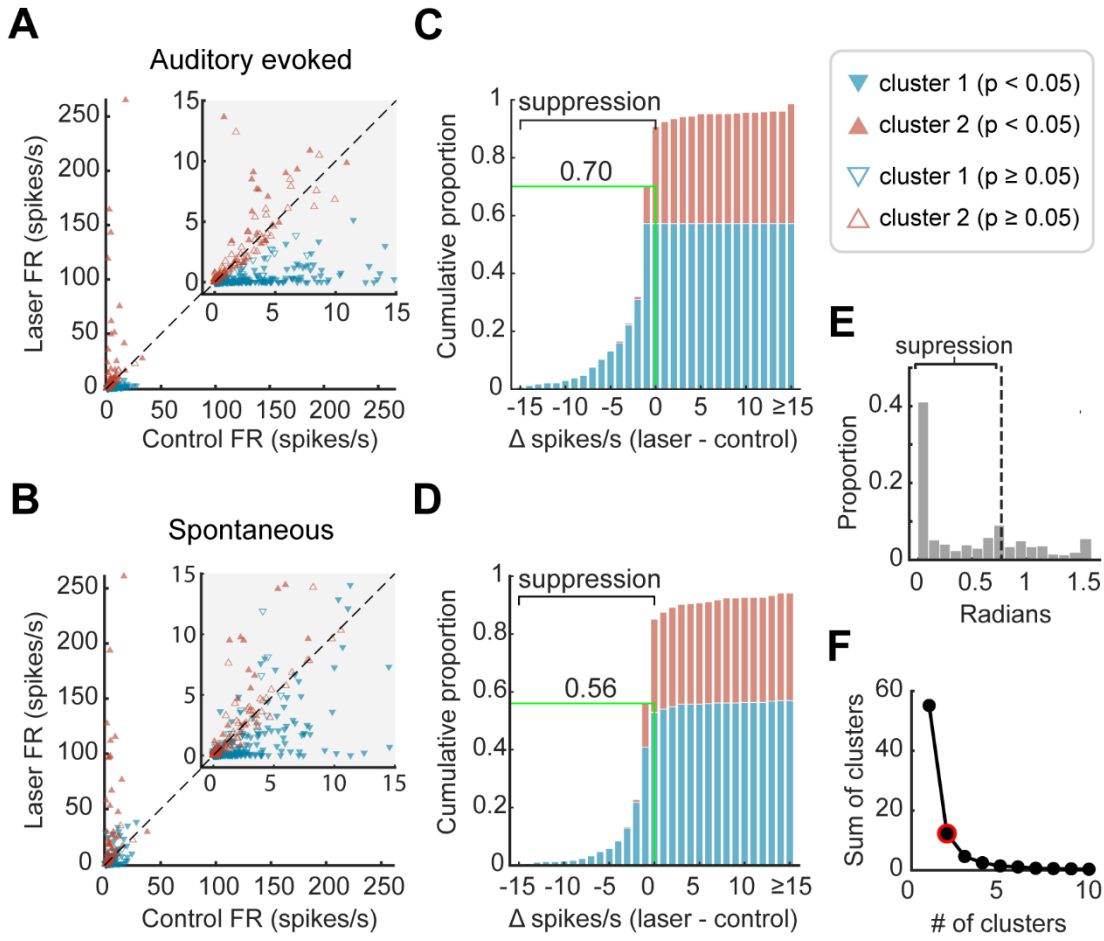

Figure 6.6: Optogenetic inactivation of auditory cortical activity. A-B) Scatterplots of firing rate with and without laser. C-D) Cumulative histograms of change in firing rate with laser light delivery. Plots show firing rate measured during (A, C) or before (B, D) sound presentation for each unit, coloured by cluster and filled if the change in firing rate between laser conditions was significant (Wilcoxon signed-rank, $p < 0.05$). Green lines/labels on cumulative histograms mark the proportion of units (across all clusters) in which laser presentation suppressed spiking activity (Δ spikes/s < 0). E) Histogram of the polar angle of units between the laser FR and control FR in radians for auditory evoked responses. F) Sum of point-to-centroid distances for K=1 to 10, with the knee point outlined in red.

For each unit within a cluster, I also asked if the mean sound-evoked firing rate (windowed between 50 to 150ms from laser onset, which included 50ms of baseline

activity and the first 50ms of sound evoked activity) differed between laser presentation and absence (two-tailed sided Wilcoxon signed rank test, $p < 0.05$). The majority of units in cluster 1 (60.3 %) showed significant changes in activity with light delivery, while only a minority of units (25.9%) in cluster 2 were affected by photostimulation. The pattern of results was similar, regardless of whether activity was recorded from SUs or MUs (see **Table 6.2**).

Cluster #	Single-units	Multi-units	Total
Cluster 1	58/103 (56.3%)	106/169 (62.7%)	164/272 (60.3%)
Cluster 2	16/71 (22.5%)	34/122 (27.9%)	50/193 (25.9%)
Total	74/174 (42.5%)	140/291 (48.1%)	214/465 (46.0%)

Table 6.2: Proportion of single and multi-units in each cluster that showed a significant change in firing rate with laser light delivery in 50-150ms window after laser onset (Wilcoxon, $p < 0.05$)

6.4.3 Spatial and temporal profile of optogenetic inactivation using AAV2-mDLx-ChR2-mCherry

The extent and speed of inactivation are major considerations when manipulating neural activity during behaviour. To understand how far and how fast it was possible to suppress neurons using ChR2 expressed via the mDlx promoter, I mapped the effects of laser light with cortical depth and time (see **Figure 6.7**). In our analysis of depth, I defined the limits of auditory cortex on the basis of sound-evoked responses, of which 95% were observed within 2.62 mm of the top of the probe (see **Figure 6.7A-B**). Such functional estimates are comparable with the thickness of ferret auditory cortex observed histologically (with correction for tissue shrinkage during fixation; see **Figure 6.4**).

Across the depth profile of AC, laser-driven suppression of neural activity was stronger in more superficial units and diminished with distance from the cortical surface (see **Figure 6.7C**). The effect of depth was evident in the median position of units in clusters 1 and 2 (identified through K-means clustering in the previous section), with light-suppressed units grouped in cluster 1 occurring significantly closer to the cortical surface (*rank-sum test*, $p < 0.001$). Modelling the laser-related change in single trial spike counts of individual units as a function of distance from the cortical surface confirmed a significant interaction between depth and light delivery (Poisson mixed-model regression with distance and light as fixed effects, ferret, unit, and sound duration as random effects, $p < 0.001$). However, the fall-off in suppression captured

by the model took place across several millimetres, with 90% of all significantly inactivated units (see **Table 6.2**) being located within 1.598 mm of the cortical surface. This prolonged fall-off over several millimetres contrasts with the rapid attenuation of blue light in tissue over hundreds of micrometres (Li et al., 2019), making it unlikely that light-based artefacts account for the spatial extent of inactivation observed.

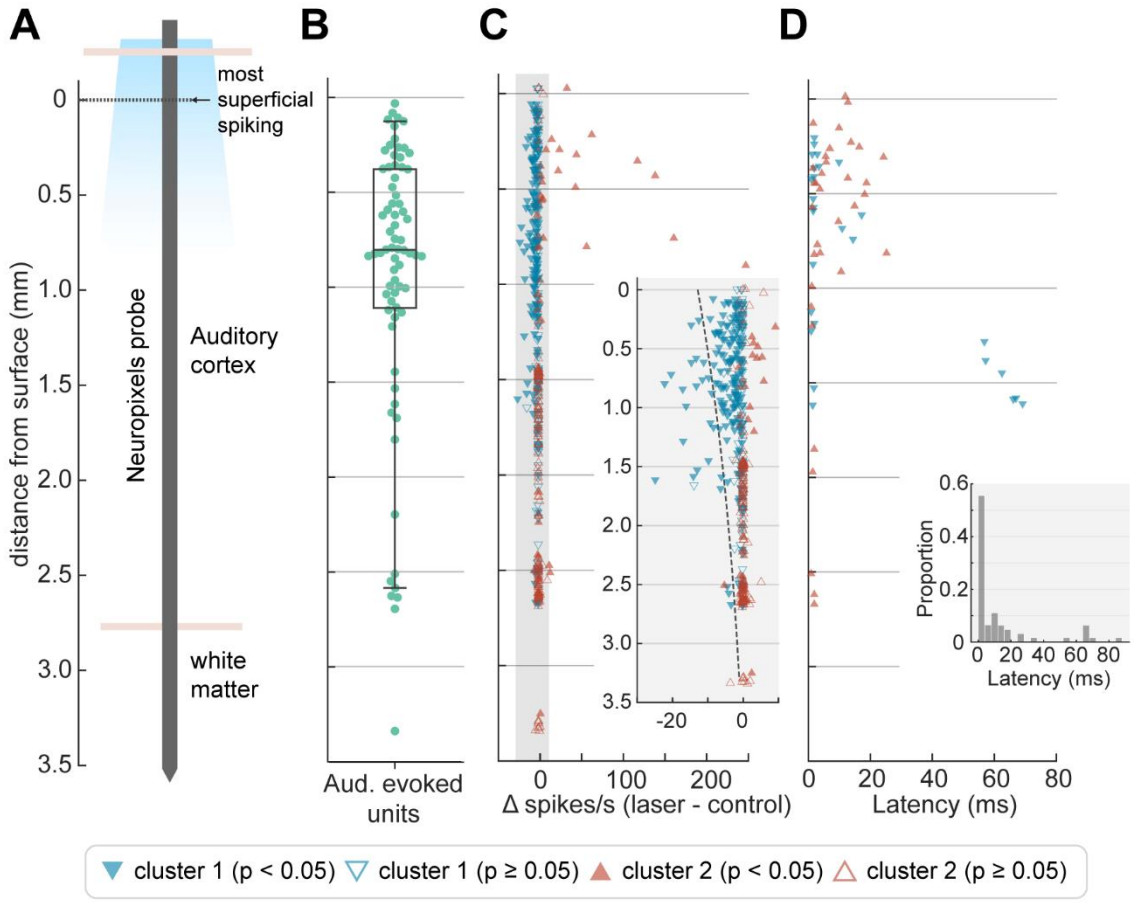

Figure 6.7: Optogenetic inactivation by depth and latency. A) Schematic of probe displaying approximate anatomic locations in reference to surface, defined as the most superficial depth at which spiking was observed. B) The location of auditory evoked units (n = 72) as a function of cortical depth from surface with boxplot showing quartiles with whiskers showing the 95th percentiles. C) Change in firing rate with light delivery as a function of cortical depth from surface. Inset, Magnified grey region with dotted line indicating predictions from fitted Poisson mixed-model. D) Latency of significant change in firing rate with light delivery as a function of depth. Marker colour and shape in panels C and D indicate cluster grouping identified via K-means clustering, as in Figure 6.6.

The temporal profile of inactivation also indicated that the effects we observed were not a trivial result of cortical heating, as light delivery suppressed cortical activity rapidly (see **Figure 6.7D**). Nonparametric cluster statistics revealed a median latency for significant change in firing at 2.5ms. Such rapid changes in firing rate show that the mDlx-induced expression of ChR2 in auditory cortex provided a fast method for cortical

inactivation, and are unlikely to be driven by changes in temperature of tissue that have been reported over longer time-scales, on the order of hundreds of milliseconds or seconds (Owen et al., 2019)

6.4.4 Optogenetic inactivation primarily affects broad-spiking neurons

Analysis of light-driven suppression of sound driven responses indicated that optogenetic inactivation affected a specific subgroup of neurons; that is, units in cluster 1 but not cluster 2, identified through K-means clustering. It is possible that cells within each cluster may be drawn from distinct populations of neurons suppressed by light-driven local network inhibition (cluster 1), and GABAergic interneurons driven by light (cluster 2). Pyramidal neurons and interneurons are often distinguished by their spike waveform as broad and narrow spiking cells, respectively (Moore and Wehr, 2013; Niell and Stryker, 2008); and so, I asked whether the clusters identified from firing rate data might have distinct spike shapes that correspond to these cell types.

To compare spike shapes, I measured the trough-to-peak latencies of average spike waveforms from well-isolated single units in cluster 1 (n = 80) and cluster 2 (n = 20) recorded within 1.598 mm from the cortical surface (i.e., the depth range within which 90% of significantly inactivated units were identified). I found that the trough-to-peak latencies of SUs in cluster 1 (i.e., those that were suppressed by the laser) were indeed longer (mean = 0.402ms) than those in cluster 2 (mean = 0.338ms), indicating a broader waveform (see **Figure 6.8A**). To determine whether differences in trough-to-peak latency observed between clusters might arise spuriously, I compared the difference I observed in the data with results when randomly shuffling cluster labels (see **Figure 6.8B**). Permutation testing confirmed that the difference in spike widths between clusters was significant (p = 0.01, n = 1000 iterations). Thus, my results are consistent with the suggestion that neurons suppressed by the laser were primarily broad-spiking excitatory/pyramidal neurons, while the remaining cells were more likely to be narrow spiking inhibitory interneurons. However, because the mDlx promotor is specific only to GABAergic neurons, light is likely to drive multiple subclasses of inhibitory interneurons including, but not restricted to, fast spiking PV neurons.

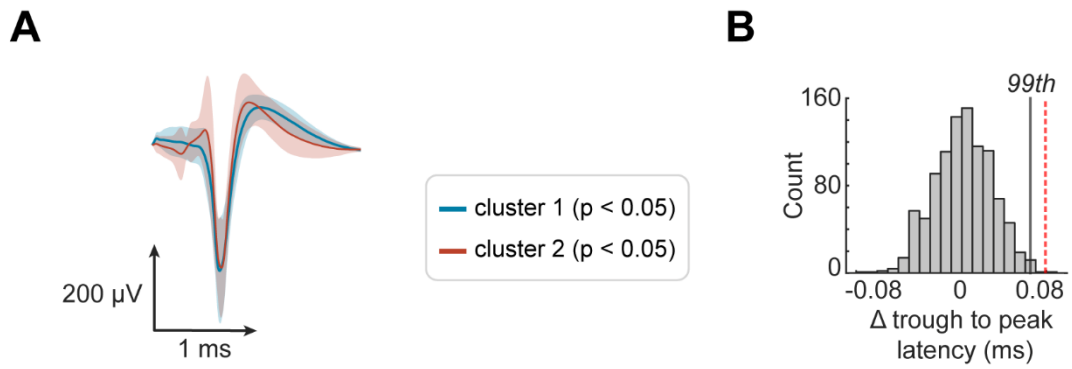

Figure 6.8: Optogenetic inactivation of broad spiking units. A) Spike shapes of well-isolated single units of cluster 1 (blue, n = 80 SUs) and cluster 2 (red, n = 20 SUs) recorded within 1.598 mm of the surface. Data are shown as mean 6 SD. B) Difference in trough-to-peak latency of each mean waveform (cluster 1 – cluster 2) for observed data (red dashed line, difference = 0.0648ms) or when randomly shuffling clusters labels (histogram, n = 1000 iterations) during permutation testing (97.5th percentile, black line).

6.4.5 Optogenetic silencing of auditory cortex impairs vowel discrimination in noise

To assess whether inactivation of auditory cortex through optogenetic means could impair behaviour, I used a behavioural vowel discrimination task, already previously demonstrated to show impaired performance during inactivation of auditory cortex through cortical cooling (Town et al., 2023). We trained one ferret (F1706) in a vowel discrimination task (/u/ or /Ɛ/) of varying sound level with vowels in additive broadband noise in control conditions and with laser light delivery. Performance increased with increasing vowel levels across conditions, but decreased when auditory cortex was photostimulated (see **Figure 6.9**). A logistic regression with condition (laser on or off), and vowel level as factors, revealed main effects of both. For every increase in vowel level by 1dBSPL, proportion of correct responses increased by 0.0557 ($p = 0.00272$) and photostimulation decreased performance by -0.590 ($p = 0.0160$). Overall, this shows that auditory cortical inactivation, through the activation of ChR2 in GABAergic neurons, impaired vowel discrimination in noise in the ferret.

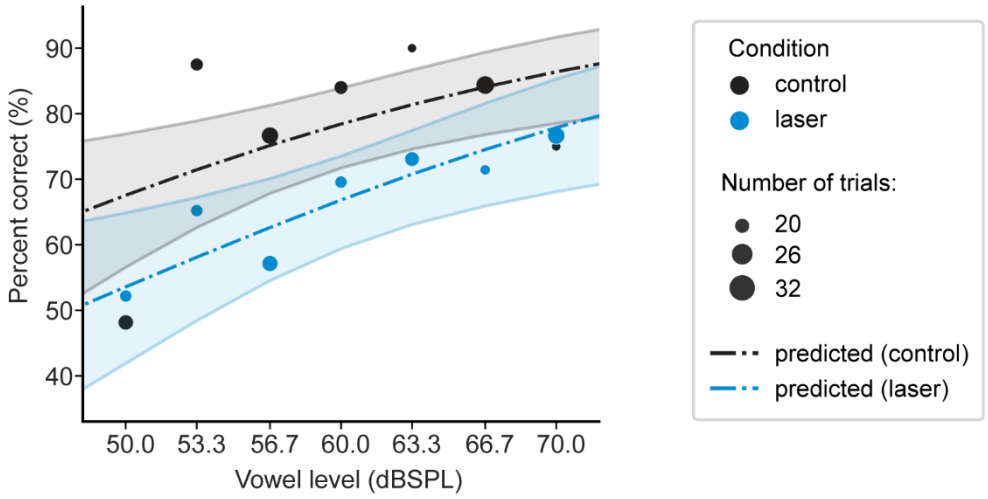

Figure 6.9: Performance of F1706 in the vowel discrimination task at various vowel levels. Performance is calculated by computing the percent correct for each vowel level in both the control condition (black circles) and condition with photostimulation (blue circles). The size of the circles represents the number of trials performed by the ferret at each vowel level and condition. The binomial linear regression prediction is plotted in the dotted-dashed line with the 95% confidence intervals for both the control (black dashed line) and laser condition (blue dashed line).

					CI 95%	
Fixed effects	Estimate	Standard error	T	p value	Lower	Upper
Intercept	-2.053	1.101	-1.865	0.0623	-4.475	0.370
Condition (0 = laser off; 1 = laser on)	-0.590	0.245	-2.410	**0.0160**	-1.130	-0.0512
Vowel level	0.0557	0.0186	2.998	**0.00272**	0.0148	0.0966

Table 6.3: Estimates of each fixed effect in the binomial linear regression on performance. R^2 = 0.716; Df = 11

6.5 DISCUSSION

The data in this chapter showed the successful development of a technique to inactivate AC in the ferret model using a recently developed viral construct: AAV2-mDlx-ChR2-mCherry. I showed strong evidence on the suppression of neural responses due to the activation of the inhibitory network and that this inactivation can impair behaviour in a vowel discrimination in noise task.

Outside of rodent research there has been a widespread lack of data and studies that shows the effectiveness of optogenetics at behavioural, physiological and histological levels, specifically in the ferret model. The most common techniques for temporary inactivation are through the use of cooling loops or Elvax implants that release muscimol which have much longer acting effects compared to that of optogenetics (see for a review: Slonina et al., 2022). Therefore the tools to have precise spatial and temporal precision in loss of function studies in ferret are limited. Studies have used ArchT in ferret auditory cortex to target excitatory neurons and reduce their likelihood of firing (Bajo et al., 2019), however the efficacy of this method to silence enough of auditory cortex is not as effective as leveraging the inhibitory network to silence cortex (Li et al., 2019). With the recent development of the mDlx promoter as a method of targeting the ChR2 opsin to GABAergic neurons in the ferret (Dimidschstein et al., 2016), it has created a new avenue for cortical silencing studies outside of the rodent model, thereby allowing the causal study of more complex auditory processing and behavioural tasks.

I injected auditory cortex in the ferret with AAV2-mDLx-ChR2-mCherry and recorded neural responses through the laminar structure of AC with Neuropixels probes whilst presenting photostimulation with a laser emitting 463nm. I showed that the majority of neurons showed suppression in both their auditory evoked firing and spontaneous firing when the opsin was activated. I also observed two clusters of neural responses, ones that showed strong inactivation and others that showed no change or in the rare case a strong activation. The cluster of neurons that were supressed were likely broad-spiking excitatory neurons, inhibited by the activation of their connected inhibitory interneurons. Whereas the other cluster were likely narrow-spiking interneurons, activated by the opsin, or neurons that were too deep in the cortical layers to be affected by the inhibitory network.

By using Neuropixel probes I was able to record single and multi-unit responses all along the laminar structure of AC and assess the efficacy of the optogenetic method as a function of depth. I showed that despite light typically dissipating within hundreds of micrometres in brain tissue (Li et al., 2019), that inactivation occurred over a depth of approximately 1.6mm. This amount of inactivation across depth would not be possible with methods that use opsins such as ArchT or JAWS to reduce the firing of excitatory neurons, as it is wholly reliant on light to provide the inactivation. In the case of targeting GABAergic neurons, due to the recurrent inhibitory connectivity in cortical circuits the suppression on excitatory neurons are amplified and therefore suppression in a small region near photostimulation withdraws input to the surrounding regions, reducing activity in the surrounding regions (Li et al., 2019). This property of photoinhibition is key for animal models with much larger brains than rodents, as much larger regions need to be inactivated to produce a deficit in behaviour or neural correlate due to the brain ability to recruit alternative neural circuits (Slonina et al., 2022).

Light delivery during photostimulation can cause cortical heating and this heating can perturb neural responses and thereby can alter behaviour (Owen et al., 2019; Peixoto et al., 2020). However this is typically on the time scale of hundreds of milliseconds or seconds (Owen et al., 2019), and I observed the median latency for significant suppression in neural firing to occur at 2.5ms. Therefore it is likely that the changes in firing are driven by optogenetic inactivation rather than changes in temperature in the tissue. However, future work in which the presentation of laser light at a different wavelength to that of the excitation wavelength of the opsin in control trials, would provide similar heating but no optogenetic inactivation as a control.

Through fluorescent imaging, I confirmed the successful expression of the AAV2-mDlx-ChR2-mCherry construct in neurons within auditory cortex, and that the spread of the virus reached approximately 1mm in diameter. Future work with immunofluorescence whilst staining for CamKII and GAD67 would allow me to confirm whether this viral construct is targeting excitatory neurons or inhibitory GABAergic interneurons respectively, and PV+ and SOM stains would identify the ratio of expression between inhibitory interneuron subtypes. This would aid in understanding the role of these interneurons in the vowel discrimination task, but more relevantly the role of these in a regularity detection task. This method was developed in order to

identify a causal link between auditory cortex and regularity detection in the behavioural paradigm I developed. Due to COVID-19 and other unforeseen circumstances this became beyond the scope of this project. However, now given the ability to precisely inactivate regions of auditory cortex with millisecond precision, it provides opportunities for understanding how the brain processes auditory patterns. Inactivation during later parts of the pattern could elucidate what number of repeats is important for detection in the ferret. Furthermore, inactivating secondary or primary regions of auditory cortex bilaterally across a trial could provide evidence for whether these regions are needed for the animal to successfully perform the task.

In conclusion, in this chapter I show the first evidence demonstrating the effectiveness of the mDlx promoter in the ferret in either enabling silencing sensory responses (in any sensory modality) or altering behaviour. This creates a foothold to expand on which future work can perturb neural responses with temporal precision in a ferret model.

7 CHAPTER SEVEN: DISCUSSION

In this thesis I aimed to understand how the brain detects and maintains a representation of deterministic acoustic patterns. I presented rapid sequences of tone-pips that transition from a random selection of frequencies to a regularly repeating pattern to a behaving animal model – the ferret. I varied the length of the pattern and the frequency pool used in the random sequence and measured behavioural performance, and neural correlates within both the local field potential and firing of single and multi-units within auditory cortex and hippocampus. My findings provided evidence that a non-primate model can detect these changes from random to regular tone sequences, and that auditory cortex and hippocampus showed neural correlates in neuronal firing and the LFP.

7.1 FERRETS AS A MODEL FOR INVESTIGATING REGULARITY DETECTION

In chapter 2 I introduced the ferret as a model species for the study of how the brain detects deterministic acoustic patterns. I tested whether ferrets could detect the transition from random sequences to regular patterns, and their perceptual capabilities in detecting increasingly complex patterns. I further investigated the cognitive strategies of the ferret during the task to test if they are performing true regularity detection. The stimulus I used to assess this auditory process was a rapid sequence of tone-pips that transitioned from a random sequence to a repeating regular sequence, with varying lengths of the pattern that had previously been used in human studies. My main findings were that ferrets could in fact perform regularity detection, but as the pattern length increased (from 3 to 5 to 7 tones in length), reaction time increased and performance decreased. Previous work has demonstrated that ferrets can detected repeated single frequency pure tones (Ma et al., 2010) and noise bursts (Saderi et al., 2019), and primates have shown changes in pupil diameter consistent with the emergence of regularity within the tone sequences (Barczak et al., 2018), yet my work is the first to demonstrate an animal model performing the regularity detection task developed by Barascud et al. (2016).

In comparison, human subjects displayed excellent performance in detecting these transitions, with near-perfect detection rates for pattern lengths of 10 and 20 tones (Barascud et al., 2016). Reaction times were also rapid for pattern length 10, with an average of 5.5 tones needed after the transition to detect the regularity, which

is comparable to an ideal observer based on the PPM model (which requires just 3 to 4 tones). However, for pattern length 20, despite achieving ceiling performance, human listeners required significantly longer, taking an average of 13.6 tones after the transition to detect the regularity, which is much more delayed than the predicted 3 to 4 tones needed by the model. To perform this task, it has been proposed that listeners must retain a subset of the previous tone frequencies in their short-term memory, which they can then compare with their stored internal model and transition probabilities between tones of the predicted stimulus (Barascud et al., 2016). This memory process has been shown to impose constraints on performance in the PPM model (Harrison et al., 2020), where the authors replicated the changes in latency across pattern lengths by manipulating short- and long-term auditory memory capacity. These findings suggest that there is an increased detection latency in humans for increasing pattern lengths due to limitations of auditory memory. A similar explanation may hold for the ferret data I present in this study, and suggest that more stringent memory constraints in the ferret limit performance to shorter pattern lengths, with the increasing latency as pattern length increases, providing similarities in the behaviour between the two species.

Conversely, this PPM model may not fully explain how the brain detects regularity, as it relies on the system encoding each individual tone on a discrete scale, and cannot generalise to continuous acoustic features (Skerritt-Davis and Elhilali, 2018). Moreover, there is likely the input of other extracted acoustic features, such as the regularity of a change in amplitude modulation of a salient frequency band that could inform whether this transition from random to regular has occurred. In fact, I showed that ferrets more easily detected patterns when they contained fewer unique frequencies, which you would not expect if all tones in the pattern were encoded by the auditory system equally. Ferrets were also able to make use of the cue of the reduction in unique frequencies in the random sequence, from an alphabet of 20, down to a restricted set of frequencies used in the pattern. When comparing performance for RAN20-REG5 and RAN5-REG5, ferrets were much better able to detect the RAN20-REG5, leveraging the added cue of the change in stimulus statistics. Yet when just tested on this reduction in unique frequency but no pattern (RAN20-RANX), the ferrets did not reliably detect this as a change, demonstrating that the repetition in

the pattern guides behaviour, whereas the change in stimulus statistics may enhance saliency.

My demonstration that ferrets can detect these transitions from random to regular sequences and exhibit similar patterns of behaviour to humans makes the ferret a prime model for understanding how the brain detects regularity, and what and why differences may occur in detection between animals and humans. Some of the main differences between animals and humans could occur because humans constantly use statistical learning for rules in speech (Santolin and Saffran, 2018; Wilson et al., 2017), and in music and rhythm (Large and Palmer, 2002; Tillmann et al., 2001) which all play a large role in human auditory perception. This up weighting of complex statistical rules within the incoming acoustic environment may cause differences in how the auditory system deals with regularity.

7.2 ARE NEURONAL OSCILLATIONS RESPONSIBLE FOR REGULARITY DETECTION?

Using the behavioural paradigm developed in chapter 2, I investigated the neural mechanisms underlying regularity detection in the local field potential of auditory cortex. Previous studies in humans have indicated that the detection of regular sequences is correlated with increased power in neural signals, larger signals for more predictable stimuli (e.g. shorter pattern lengths). Furthermore, EEG recordings have revealed oscillations at both tone presentation (20Hz) and pattern rates, and source localisation of EEG and MagEG recordings has suggested the involvement of AC, HPC and IFG (Barascud et al., 2016; Southwell, 2019; Southwell et al., 2017). Based on this prior research, I tested the hypothesis that regular sequences would elicit larger evoked LFP responses and increased oscillations in AC compared to random sequences, and whether the pattern length modulated the evoked or oscillatory power. My results showed no difference in the evoked power in the LFP between random and regular sequences, however, I did observe reduced oscillations at the tone presentation rate, and increased oscillations at the pattern rate during regularity. Furthermore, both of these oscillations were modulated by the pattern length in a manner that mirrored behaviour, with pattern lengths of 3 showing the most reduced tone presentation rates and the most enhanced pattern rates.

Given these findings, it is still unclear what the underlying neural mechanism driving the sustained response observed in humans in MagEG and EEG, and/or whether these changes in oscillatory power at various rates could contribute. Oscillations in the brain are ubiquitous, and low frequency oscillations (1-10Hz) propagate throughout the brain tissue easily and readily (Gourévitch et al., 2020), providing a manner in which to couple various brain regions (Bahmer and Gupta, 2018), increasing their coherence by coordinating rhythmic activity through entrainment (Lakatos et al., 2019). Oscillations provide a role in auditory processing, entraining neural responses to the structure in the auditory signal, and in particular the 1-10Hz rate has been shown to facilitate perception (Ding et al., 2017), memory (Calderone et al., 2014) and auditory scene analysis (Riecke et al., 2015). The patterns I employ in this thesis repeat at sub 10Hz rates (2.86Hz, 4.0Hz and 6.67Hz) and likely propagate to multiple brain regions, given I observe these oscillations in primary and secondary fields of auditory cortex, and hippocampus. It is likely that these oscillations are entraining activity and increasing the efficiency of stimulus encoding by aligning the relevant processes to the predictable events in the incoming sound. However the source of these oscillations are still unknown, but perhaps is more likely to be induced from higher-order areas, given that Barczak et al. (2018) observed pattern rate oscillations occurring earliest in the pulvinar which would likely be getting input from higher-order areas such as parietal cortex and PFC (Cappe et al., 2009; Romanski et al., 1997), and then outputting its signal to AC.

Whether these oscillations are functionally relevant in order to detect the transition from random to regular tone sequences is a question that has yet to be answered. These increased oscillations at the pattern rate during regularity have been observed in EEG in humans (Southwell, 2019), in LFP recordings in the macaque (Barczak et al., 2018), and now in my data in the ferret. My data showed that pattern rate oscillations decreased with increasing pattern length and the power at these oscillations mirrored behavioural performance, such that ferrets were best able to detect, and showed the largest pattern rate oscillations during regularity firstly for: RAN20-REG3 then RAN20-REG5, RAN20-REG7 followed by RAN5-REG5. However, my results also identified larger oscillations at the pattern rate during miss trials in the ferret over hit trials (for RAN20-REG3 and RAN20-REG7), which either suggests that

increased power does not enhance perception or perhaps that these oscillations may be supressed during detection or attenuated by movement.

In the hippocampus, I demonstrated changes in oscillatory power in the LFP in response to the regular sequences. Interestingly I observed a similar pattern of decreased power at the tone presentation rate during regularity, as I did in auditory cortex. However, I only observed differences in the pattern rate for RAN20-REG5 and RAN5-REG5 which have a pattern rate of 4.0Hz. Given the hippocampal role in memory, statistical learning and integrating acoustic patterns (see for a review: Billig et al., 2022) but also the strong persistent theta oscillation that coordinates neuronal activity throughout (Nuñez and Buño, 2021), it could be likely that theta may be modulated by the predictability of the incoming acoustic stimulus, or its behavioural relevance. The increases in oscillatory power I observed at 4.0Hz could be entrainment to the pattern – i.e. a correlate of regularity detection, or it could be an shift in the theta frequency (whether it is due to the pattern itself or some other response to behaviour), perhaps some anticipatory signal of reward (Benchenane et al., 2010) or a correlate of memory due to the task engaged behaviour (Buzsáki and Moser, 2013; Kragel et al., 2020). A comparison between passive and task engaged subjects would begin to unpick the role of hippocampus during behaviour, but given how strongly modulated hippocampus is by the behavioural relevance of the stimulus, removing behavioural relevance may remove any correlates of regularity.

7.3 How do neurons encode regularity?

With the identification of neuronal oscillations in the LFP of auditory cortex and hippocampus, it is likely that these oscillations modulate neuronal firing. Likewise, the sustained response seen in MagEG and EEG studies (Barascud et al., 2016; Southwell, 2019) could originate from changes in neural firing rather than an evoked LFP. I leveraged the micro-electrode recordings in the ferret to extract single and multi-unit activity and I investigated how firing changes in term of rate and spike timing in response to regular and random tone sequences, and how these correlates are modulated by pattern length and are influenced by sensory and non-sensory effects. My findings showed neurons elicited larger responses for shorter pattern lengths across the population of units, that these units entrained to the pattern rate during regularity, increased their temporal precision of firing to their BF during regular context

and that across the population of single-units, neurons increased their firing with increasing repetitions of the pattern.

Given the enhanced oscillatory power in the LFP, it is likely that spiking activity will entrain to these oscillations. Using vector strength as a measure of entrainment, I observed neurons in both auditory cortex and hippocampus during the presence of regularity, entrain to the pattern rate. Using the analysis developed by Asokan et al. (2021), I also demonstrated that neurons more precisely fire to their BF in a regular context compared to random. This evidence supports the idea that oscillations and entrainment are modulated by regularity, whether this modulation enhances regularity detection or is just the auditory system responding to low-level features in the incoming stimulus is unknown. Inherently, neurons in auditory cortex are not as tone locked as neurons in subcortical regions such as MGB or IC. Given a framework of hierarchical processing, this can be advantageous as auditory cortex can be more sensitive to slower contextual changes. Entrainment or the increased temporal precision of firing in auditory cortex can cause it to become more primary-like, reducing temporal smearing that may otherwise mask responses to deviant sounds. However if the entrainment was the sole method of modulating spike timing, then we would also expect enhanced temporal precision in the random context as the regular inter-tone interval does induce a higher oscillation in the LFP at the tone presentation rate. Therefore another mechanism that could increase firing precision, and may be more likely, are local or long-range inhibitory networks, through the decrease in latency of output to excitatory neurons, sharpen the neural firing of neurons in AC (Lee et al., 2020), and given the involvement of higher-order areas, this signal could originate from regions such as PFC and/or HPC that encode the predictability of a stimulus (Keller and Mrsic-Flogel, 2018).

Spiking activity to a repeating stimulus has been well characterised as SSA, where neurons adapt to the repeating stimulus and yield stronger responses to stimuli that deviate from the repeated stimulus (Nelken, 2014). Therefore it seems likely that neuronal adaptation whether it is SSA or some other form of habituation would play a role in how regularity is represented in neuronal firing. We may expect for shorter pattern lengths to generate the greatest adaptation, however I observed across the population of neurons, shorter pattern lengths eliciting more spikes. Nevertheless, these shorter patterns are also the easiest to detect so there may be confounds due

to detection or movement in the behavioural task that could modulate spiking activity. When using the Poisson GLMM to pull out these non-sensory effects, I found that the presence of regularity significantly decreased firing. I also observed this decrease in regular over random contexts when analysing the response of neurons to their BF. This suggests that regularity does supress neural firing, however for all conditions apart from RAN20-REG7, across the population, SUs significantly increased their firing with increasing repetitions of the pattern. This might suggest a dual effect of regularity detection, an initial adaptation to the repeating stimulus perhaps in part induced by SSA, but facilitation as the pattern emerges which could be either generated in auditory cortex or perhaps induced by higher-order areas that respond to much slower contextual changes in the stimulus.

Given that I showed these neurons don't respond to the repetition or regularity in isolation, it may suggest that the effects of adaptation and facilitation may occur within the same neurons. Additionally, while on average neurons adapted to regularity and facilitated over increasing repetitions, the population showed considerable heterogeneity. Therefore, ongoing work is seeking to establish if these effects are evident in the same neurons, or in distinct sub populations clustered by specific stimulus response properties, or whether adaptation or facilitation to either of these effects could be influenced by a neuronal subtype (i.e. excitatory or inhibitory neurons). Inhibitory interneurons seem to be a strong candidate given that they've already been shown to modulate the late responses to standards and deviants in an oddball paradigm (Yarden et al., 2022), and show preferences for periodic stimuli (Mehra et al., 2022). Further work, using techniques such as calcium imaging to opto-tag specific neuronal sub-types could be useful in identifying whether a demographic of neurons have a particular response profile to presentation of regular sequences.

7.4 THE DETECTION OF REGULARITY: FROM MESO-SCALE TO MACRO-SCALE

In chapter 1, I discussed how various studies and experiments have explored the brain's processing of predictive stimuli, ranging from single neuron analysis to cognitive brain-wide imaging. Whilst the mechanism underlying regularity detection in the auditory system has been a topic of debate, research has consistently shown that the auditory system operates on a processing hierarchy, with increasing complexity of feature encoding as you ascend the auditory pathway (Asokan et al., 2021; Norman-

Haignere et al., 2022; Parras et al., 2017; Phillips et al., 2016; Tzovara et al., 2022; Wacongne et al., 2011). This poses a complex question of how regularity is detected, as it can range from local low-level patterns to higher-order statistical regularities that unfold over longer timescales. This has been partially addressed by experiments using regularities that vary on local and global time scales (Asko et al., 2023; Bekinschtein et al., 2009; Costa-Faidella et al., 2011; El Karoui et al., 2015; Nourski et al., 2018; Yaron et al., 2012), yet has not been addressed in a random to regular tone sequence paradigm in which patterns contain multiple frequencies that repeat with various pattern lengths.

In this discussion, I will attempt to provide a general overview of the processes that could be involved in the regularity of deterministic acoustic patterns. As sound waves from the incoming pure tone sequence enters the ear, it is processed by the cochlea and the frequency information is transmitted up the lemniscal auditory pathway. Initially, as the incoming tone sequence is random, neurons respond strongly to each tone. Neurons in auditory cortex will then, across the population of frequency tuned neurons, begin to induce oscillations in the local field potential which in turn entrains other neurons in auditory cortex. Initially this occurs at the tone presentation rate of 20Hz due to the regular inter-tone interval present in the pure tone sequence. However, when the random sequence transitions to a regular pattern, a reduction in oscillations at the tone presentation rate is caused due to the smaller number of neurons firing due to the reduced variety of frequencies and/or repetition suppression from the increased predictability of the stimulus. On the other hand, neurons that are tuned to frequency elements in the pattern will continue firing but now begin to induce oscillations at the pattern rate. These oscillations may be propagated to higher-order areas such as hippocampus and perhaps PFC.

These oscillatory correlates might then update the predictive model and send back ‘prediction signals’ to AC through inhibitory networks to reduce the temporal smearing and increase precision of firing of the neurons in AC, encoding the incoming regular sequence with more precision and efficiency. With time, the expectation of precision is optimized, leading to an increase in firing as neurons become more primary-like. This could then induce and increase in firing as more repeats of the pattern are presented, up-weighting the representation of regularity and aiding behavioural detection. There are still major gaps in our knowledge on this process, but ferrets sit

at an advantageous mid-point, to perform single-unit recordings, and perform these complex perceptual tasks, to further probe how the brain detects acoustic patterns.

7.5 FUTURE WORK

7.5.1 Ongoing work

There are several avenues of work that are still on-going that will provide further insights in the work presented in this thesis. One such avenue is the comparison of neural correlates between passively listening and behaving animals. In addition to the behavioural recordings I captured with the WARP arrays and Neuropixels, I also collected a number of recordings in passively listening animals (a handful of cells were presented in section 5.3.2), in which the same random to regular tone sequences were presented. This data can shed light on how the neural correlates such as entrainment within the LFP or firing of single-units changes in AC and HPC by the animal's attentional state. By comparing these passive recordings with the behavioural recordings, it is possible to determine how much of the neural correlates identified exist as fundamental brain mechanisms within AC. For example, do neural responses become more adaptive as the pattern emerges or for shorter pattern lengths if the animal is not attended to the stimulus, or do we observe the same effects in AC and HPC despite attentional state. These passive recordings may also provide a better comparison to previous human studies in which EEG and MagEG recordings were obtained during passive listening of the sequences. By comparing the neural responses observed in the ferrets during passive listening to the results from previous human studies and probing of automatic detection of regularity, it is possible to draw further parallels between human and animal cognition.

Moreover, the selection of Neuropixels recordings included in this work was only a small subset of the data collected due to time constraints. However, with the analysis and spike sorting of more recordings, I can obtain more single-units and with that added power to perform waveform analysis, as in chapter 6, to determine if units that facilitate or adapt their firing to regularity, or any other correlate, are represented by a certain sub-population of cells such as excitatory broad-spiking or inhibitory narrow-spiking neurons. Additionally, by analysing more recordings, I can run the Poisson GLMM to investigate sensory and non-sensory effects on neural firing, as was done in chapter 4 in HPC. This is important to unpick as HPC is strongly modulated

by non-sensory effects such as movement, and the current approach of ignoring trials in which regularity is detected may underestimate the effects of regularity. Additionally, I would like to further look at how the time course of these correlates emerge jointly between AC and HPC; whether they emerge first in one region and if any coherence appears between regions during regularity.

7.5.2 Avenues for future investigations

A promising direction for future research is to further investigate PFC in the ferret, a brain region that has consistently been found to play a crucial role in regularity detection. Studies have shown that the PFC exhibits increased activity during regularity detection (Barascud et al., 2016; Heilbron and Chait, 2018; Southwell, 2019) with the right inferior frontal gyrus (IFG), a region of PFC, being a major source of the mismatch negativity (MMN) response (Alho, 1995). Therefore, it is possible that neural correlates of regularity detection could be identified within the PFC of ferrets, if this brain region is recruited similarly to humans, though the analogue of IFG in ferret frontal cortex is still unknown. Furthermore, recent advances in functional ultrasound technology in ferrets, as demonstrated by Bimbard et al. (2018), provide a promising tool for mapping the regions involved in regularity detection in this animal model. This technology could serve as a valuable bridge between imaging in humans and animal models, and help shed light on whether the PFC and HPC show increased activity via brain-wide imaging in the ferret brain as they do in humans, or if other brain regions may be implicated instead in the ferret.

Furthermore, it would be highly beneficial to expand our understanding of the neural mechanisms underlying the detection of complex pure tone sequences by recording subcortically and within higher-order thalamic areas, such as the pulvinar that been shown to entrain to the pattern rate more robustly than A1 (Barczak et al., 2018). As demonstrated by Asokan et al. (2021), investigating the transformation of neural encoding in random and regular contexts but instead with the regularity induced by repeating frequencies rather than inter-tone intervals, could provide another perspective on how information regarding the pure tone sequence is transformed as you ascend the auditory pathway. While the Neuropixels probe used in this thesis targeted auditory cortex and hippocampus, it could also be utilized to record from the medial geniculate body (MGB) and inferior colliculus (IC). If done with acute recordings, this may provide better signal-to-noise and may better allow us to

investigate how the laminar structure of auditory cortex influences the neural correlates.

On a behavioural level, another study could push the perceptual boundaries on what the ferrets can detect as regularity. At what pattern length do the ferrets fail to detect the repetition? It would also be a good opportunity to run this paradigm in the form of a 2AFC, now that we have the knowledge of how rapidly ferrets can detect regularity, which would remove the confounds of movement in neural recordings during the presentation of the regular sequence.

Finally, chapter 6 opened opportunities into identifying causal contributions of brain regions in regularity detection, via cortical inactivation by optogenetics. This technique is a powerful tool due to its high spatial and temporal resolution (see for a review: Slonina et al., 2022) and has now been successfully established in the ferret. One key question is whether silencing primary and/or secondary fields of auditory cortex impairs regularity detection, or if it differentially affects detection based on the complexity of the pattern (i.e. cortical silencing may only impair detection of pattern lengths 5 and longer). Further investigations could also target the subfields of auditory cortex individually to causally determine their role in regularity detection. Furthermore, the precise millisecond temporal control provided by optogenetics (as highlighted in Town et al., 2023), offers a unique opportunity to perturb neural firing to unpick the neural mechanisms underlying regularity detection. For example, does perturbation of entrainment through activation of oscillations at rates other than the pattern rate impair behaviour or increase/decrease firing to regularity, or can regularity detection be delayed by inactivating just one cycle of the pattern. These are all questions that still need to be answered, and the ferret provides a valuable model system, a mid-point between human and rodent studies, to manipulate complex perceptual processes and identify causal contributions to regularity detection.

8 REFERENCES

Adams, R.P., MacKay, D.J.C., 2007. Bayesian Online Changepoint Detection. ArXiv07103742 Stat.

Ahmed, M.S., Priestley, J.B., Castro, A., Stefanini, F., Solis Canales, A.S., Balough, E.M., Lavoie, E., Mazzucato, L., Fusi, S., Losonczy, A., 2020. Hippocampal Network Reorganization Underlies the Formation of a Temporal Association Memory. Neuron 107, 283-291.e6. https://doi.org/10.1016/j.neuron.2020.04.013

Alain, C., Woods, D.L., Knight, R.T., 1998. A distributed cortical network for auditory sensory memory in humans. Brain Res. 812, 23–37. https://doi.org/10.1016/S0006-8993(98)00851-8

Alho, K., 1995. Cerebral Generators of Mismatch Negativity (MMN) and Its Magnetic Counterpart (MMNm) Elicited by Sound Changes. Ear Hear. 16, 38.

Alves-Pinto, A., Sollini, J., Wells, T., Sumner, C.J., 2016a. Behavioural estimates of auditory filter widths in ferrets using notched-noise maskers. J. Acoust. Soc. Am. 139, EL19–EL24. https://doi.org/10.1121/1.4941772

Alves-Pinto, A., Sollini, J., Wells, T., Sumner, C.J., 2016b. Behavioural estimates of auditory filter widths in ferrets using notched-noise maskers. J. Acoust. Soc. Am. 139, EL19–EL24. https://doi.org/10.1121/1.4941772

Aman, L., Picken, S., Andreou, L.-V., Chait, M., 2021. Sensitivity to temporal structure facilitates perceptual analysis of complex auditory scenes. Hear. Res. 400, 108111. https://doi.org/10.1016/j.heares.2020.108111

Amaral, D.G., Insausti, R., Cowan, W.M., 1983. Evidence for a direct projection from the superior temporal gyrus to the entorhinal cortex in the monkey. Brain Res. 275, 263–277. https://doi.org/10.1016/0006-8993(83)90987-3

Anderson, L.A., Christianson, G.B., Linden, J.F., 2009. Stimulus-Specific Adaptation Occurs in the Auditory Thalamus. J. Neurosci. 29, 7359–7363. https://doi.org/10.1523/JNEUROSCI.0793-09.2009

Anderson, L.A., Malmierca, M.S., 2013. The effect of auditory cortex deactivation on stimulus-specific adaptation in the inferior colliculus of the rat. Eur. J. Neurosci. 37, 52–62. https://doi.org/10.1111/ejn.12018

Andreou, L.-V., Kashino, M., Chait, M., 2011. The role of temporal regularity in auditory segregation. Hear. Res. 280, 228–235. https://doi.org/10.1016/j.heares.2011.06.001

Antunes, F.M., Malmierca, M.S., 2011. Effect of Auditory Cortex Deactivation on Stimulus-Specific Adaptation in the Medial Geniculate Body. J. Neurosci. 31, 17306–17316. https://doi.org/10.1523/JNEUROSCI.1915-11.2011

Antunes, F.M., Nelken, I., Covey, E., Malmierca, M.S., 2010. Stimulus-Specific Adaptation in the Auditory Thalamus of the Anesthetized Rat. PLOS ONE 5, e14071. https://doi.org/10.1371/journal.pone.0014071

Aronov, D., Nevers, R., Tank, D.W., 2017. Mapping of a non-spatial dimension by the hippocampal–entorhinal circuit. Nature 543, 719–722. https://doi.org/10.1038/nature21692

Asko, O., Blenkmann, A.O., Leske, S.L., Foldal, M.D., Llorens, A., Funderud, I., Meling, T.R., Knight, R.T., Endestad, T., Solbakk, A.-K., 2023. Altered hierarchical auditory predictive processing after lesions to the orbitofrontal cortex. https://doi.org/10.1101/2023.01.04.521570

Asokan, M.M., Williamson, R.S., Hancock, K.E., Polley, D.B., 2021. Inverted central auditory hierarchies for encoding local intervals and global temporal patterns. Curr. Biol. 0. https://doi.org/10.1016/j.cub.2021.01.076
Ayala, Y.A., Malmierca, M.S., 2013. Stimulus-specific adaptation and deviance detection in the inferior colliculus. Front. Neural Circuits 6. https://doi.org/10.3389/fncir.2012.00089
Bahmer, A., Gupta, D.S., 2018. Role of Oscillations in Auditory Temporal Processing: A General Model for Temporal Processing of Sensory Information in the Brain? Front. Neurosci. 12.
Bajo, V.M., Nodal, F.R., Bizley, J.K., Moore, D.R., King, A.J., 2007. The Ferret Auditory Cortex: Descending Projections to the Inferior Colliculus. Cereb. Cortex 17, 475–491. https://doi.org/10.1093/cercor/bhj164
Bajo, V.M., Nodal, F.R., Korn, C., Constantinescu, A.O., Mann, E.O., Boyden, E.S., King, A.J., 2019. Silencing cortical activity during sound-localization training impairs auditory perceptual learning. Nat. Commun. 10, 1–12. https://doi.org/10.1038/s41467-019-10770-4
Bao, X., Gjorgieva, E., Shanahan, L.K., Howard, J.D., Kahnt, T., Gottfried, J.A., 2019. Grid-like Neural Representations Support Olfactory Navigation of a Two-Dimensional Odor Space. Neuron 102, 1066-1075.e5. https://doi.org/10.1016/j.neuron.2019.03.034
Barascud, N., Pearce, M.T., Griffiths, T.D., Friston, K.J., Chait, M., 2016. Brain responses in humans reveal ideal observer-like sensitivity to complex acoustic patterns. Proc. Natl. Acad. Sci. 113, E616–E625. https://doi.org/10.1073/pnas.1508523113
Barczak, A., O'Connell, M.N., McGinnis, T., Ross, D., Mowery, T., Falchier, A., Lakatos, P., 2018. Top-down, contextual entrainment of neuronal oscillations in the auditory thalamocortical circuit. Proc. Natl. Acad. Sci. 115, E7605–E7614. https://doi.org/10.1073/pnas.1714684115
Başar-Eroglu, C., Başar, E., 1991. A Compound P300-40Hz Response of the Cat Hippocampus. Int. J. Neurosci. 60, 227–237. https://doi.org/10.3109/00207459109167035
Bastos, A.M., Lundqvist, M., Waite, A.S., Kopell, N., Miller, E.K., 2020. Layer and rhythm specificity for predictive routing. Proc. Natl. Acad. Sci. 117, 31459–31469. https://doi.org/10.1073/pnas.2014868117
Behrens, W. von der, Bäuerle, P., Kössl, M., Gaese, B.H., 2009. Correlating Stimulus-Specific Adaptation of Cortical Neurons and Local Field Potentials in the Awake Rat. J. Neurosci. 29, 13837–13849. https://doi.org/10.1523/JNEUROSCI.3475-09.2009
Bekinschtein, T.A., Dehaene, S., Rohaut, B., Tadel, F., Cohen, L., Naccache, L., 2009. Neural signature of the conscious processing of auditory regularities. Proc. Natl. Acad. Sci. 106, 1672–1677. https://doi.org/10.1073/pnas.0809667106
Benchenane, K., Peyrache, A., Khamassi, M., Tierney, P.L., Gioanni, Y., Battaglia, F.P., Wiener, S.I., 2010. Coherent Theta Oscillations and Reorganization of Spike Timing in the Hippocampal- Prefrontal Network upon Learning. Neuron 66, 921–936. https://doi.org/10.1016/j.neuron.2010.05.013
Bendixen, A., Denham, S.L., Gyimesi, K., Winkler, I., 2010. Regular patterns stabilize auditory streams. J. Acoust. Soc. Am. 128, 3658–3666. https://doi.org/10.1121/1.3500695

Berger, T.W., Alger, B., Thompson, R.F., 1976. Neuronal substrate of classical conditioning in the hippocampus. Science 192, 483–485. https://doi.org/10.1126/science.1257783
Bigelow, J., Morrill, R.J., Dekloe, J., Hasenstaub, A.R., 2019. Movement and VIP Interneuron Activation Differentially Modulate Encoding in Mouse Auditory Cortex. eNeuro 6, ENEURO.0164-19.2019. https://doi.org/10.1523/ENEURO.0164-19.2019
Billig, A.J., Lad, M., Sedley, W., Griffiths, T.D., 2022. The hearing hippocampus. Prog. Neurobiol. 218, 102326. https://doi.org/10.1016/j.pneurobio.2022.102326
Bimbard, C., Demene, C., Girard, C., Radtke-Schuller, S., Shamma, S., Tanter, M., Boubenec, Y., 2018. Multi-scale mapping along the auditory hierarchy using high-resolution functional UltraSound in the awake ferret. eLife 7, e35028. https://doi.org/10.7554/eLife.35028
Bizley, J.K., Cohen, Y.E., 2013. The what, where and how of auditory-object perception. Nat. Rev. Neurosci. 14, 693–707. https://doi.org/10.1038/nrn3565
Bizley, J.K., Nodal, F.R., Nelken, I., King, A.J., 2005. Functional Organization of Ferret Auditory Cortex. Cereb. Cortex 15, 1637–1653. https://doi.org/10.1093/cercor/bhi042
Bizley, J.K., Walker, K.M., King, A.J., Schnupp, J.W., 2013. Spectral timbre perception in ferrets; discrimination of artificial vowels under different listening conditions. J. Acoust. Soc. Am. 133, 365–376. https://doi.org/10.1121/1.4768798
Bordi, F., LeDoux, J.E., 1994. Response properties of single units in areas of rat auditory thalamus that project to the amygdala. Exp. Brain Res. 98, 275–286. https://doi.org/10.1007/BF00228415
Bragin, A., Jando, G., Nadasdy, Z., Hetke, J., Wise, K., Buzsaki, G., 1995. Gamma (40-100 Hz) oscillation in the hippocampus of the behaving rat. J. Neurosci. 15, 47–60. https://doi.org/10.1523/JNEUROSCI.15-01-00047.1995
Bregman, A.S., 1994. Auditory scene analysis: The perceptual organization of sound. MIT press.
Burwell, R.D., Amaral, D.G., 1998. Cortical afferents of the perirhinal, postrhinal, and entorhinal cortices of the rat. J. Comp. Neurol. 398, 179–205. https://doi.org/10.1002/(SICI)1096-9861(19980824)398:2<179::AID-CNE3>3.0.CO;2-Y
Buzsáki, G., Anastassiou, C.A., Koch, C., 2012. The origin of extracellular fields and currents — EEG, ECoG, LFP and spikes. Nat. Rev. Neurosci. 13, 407–420. https://doi.org/10.1038/nrn3241
Buzsáki, G., Moser, E.I., 2013. Memory, navigation and theta rhythm in the hippocampal-entorhinal system. Nat. Neurosci. 16, 130–138. https://doi.org/10.1038/nn.3304
Calderone, D.J., Lakatos, P., Butler, P.D., Castellanos, F.X., 2014. Entrainment of neural oscillations as a modifiable substrate of attention. Trends Cogn. Sci. 18, 300–309. https://doi.org/10.1016/j.tics.2014.02.005
Camalier, C.R., Scarim, K., Mishkin, M., Averbeck, B.B., 2019. A Comparison of Auditory Oddball Responses in Dorsolateral Prefrontal Cortex, Basolateral Amygdala, and Auditory Cortex of Macaque. J. Cogn. Neurosci. 31, 1054–1064. https://doi.org/10.1162/jocn_a_01387
Cappe, C., Morel, A., Barone, P., Rouiller, E.M., 2009. The Thalamocortical Projection Systems in Primate: An Anatomical Support for Multisensory and

Sensorimotor Interplay. Cereb. Cortex N. Y. NY 19, 2025–2037. https://doi.org/10.1093/cercor/bhn228
Carandini, M., 2000. Visual cortex: Fatigue and adaptation. Curr. Biol. 10, R605–R607. https://doi.org/10.1016/S0960-9822(00)00637-0
Carandini, M., Ferster, D., 1997. A Tonic Hyperpolarization Underlying Contrast Adaptation in Cat Visual Cortex. Science 276, 949–952. https://doi.org/10.1126/science.276.5314.949
Carbajal, G.V., Malmierca, M.S., 2018. The Neuronal Basis of Predictive Coding Along the Auditory Pathway: From the Subcortical Roots to Cortical Deviance Detection. Trends Hear. 22. https://doi.org/10.1177/2331216518784822
Chen, J., ten Cate, C., 2017. Bridging the gap: Learning of acoustic nonadjacent dependencies by a songbird. J. Exp. Psychol. Anim. Learn. Cogn. 43, 295–302. https://doi.org/10.1037/xan0000145
Cherry, E.C., 1953. Some Experiments on the Recognition of Speech, with One and with Two Ears. J. Acoust. Soc. Am. https://doi.org/10.1121/1.1907229
Cheung, V.K.M., Harrison, P.M.C., Meyer, L., Pearce, M.T., Haynes, J.-D., Koelsch, S., 2019. Uncertainty and Surprise Jointly Predict Musical Pleasure and Amygdala, Hippocampus, and Auditory Cortex Activity. Curr. Biol. 29, 4084-4092.e4. https://doi.org/10.1016/j.cub.2019.09.067
Chuong, A.S., Miri, M.L., Busskamp, V., Matthews, G.A.C., Acker, L.C., Sørensen, A.T., Young, A., Klapoetke, N.C., Henninger, M.A., Kodandaramaiah, S.B., Ogawa, M., Ramanlal, S.B., Bandler, R.C., Allen, B.D., Forest, C.R., Chow, B.Y., Han, X., Lin, Y., Tye, K.M., Roska, B., Cardin, J.A., Boyden, E.S., 2014. Noninvasive optical inhibition with a red-shifted microbial rhodopsin. Nat. Neurosci. 17, 1123–1129. https://doi.org/10.1038/nn.3752
Cleary, J.G., Witten, I.H., 1984. Data compression using adaptive coding and partial string matching. IEEE Trans. Commun. 32, 396–402. https://doi.org/10.1109/TCOM.1984.1096090
Constantinescu, A.O., O'Reilly, J.X., Behrens, T.E.J., 2016. Organizing conceptual knowledge in humans with a gridlike code. Science 352, 1464–1468. https://doi.org/10.1126/science.aaf0941
Costa-Faidella, J., Baldeweg, T., Grimm, S., Escera, C., 2011. Interactions between "What" and "When" in the Auditory System: Temporal Predictability Enhances Repetition Suppression. J. Neurosci. 31, 18590–18597. https://doi.org/10.1523/JNEUROSCI.2599-11.2011
Covington, N.V., Brown-Schmidt, S., Duff, M.C., 2018. The Necessity of the Hippocampus for Statistical Learning. J. Cogn. Neurosci. 30, 680–697. https://doi.org/10.1162/jocn_a_01228
Cowan, N., 1984. On short and long auditory stores. Psychol. Bull. 96, 341–370.
Daikhin, L., Ahissar, M., 2012. Responses to deviants are modulated by subthreshold variability of the standard. Psychophysiology 49, 31–42. https://doi.org/10.1111/j.1469-8986.2011.01274.x
Denham, S.L., Winkler, I., 2006. The role of predictive models in the formation of auditory streams. J. Physiol.-Paris, Theoretical and Computational Neuroscience: Understanding Brain Functions 100, 154–170. https://doi.org/10.1016/j.jphysparis.2006.09.012
Deutsch, D., Lapidis, R., Henthorn, T., 2008. The speech-to-song illusion. J. Acoust. Soc. Am. 124, 2471–2471. https://doi.org/10.1121/1.4808987

Devergie, A., Grimault, N., Tillmann, B., Berthommier, F., 2010. Effect of rhythmic attention on the segregation of interleaved melodies. J. Acoust. Soc. Am. 128, EL1–EL7. https://doi.org/10.1121/1.3436498

Dietz, M.J., Friston, K.J., Mattingley, J.B., Roepstorff, A., Garrido, M.I., 2014. Effective Connectivity Reveals Right-Hemisphere Dominance in Audiospatial Perception: Implications for Models of Spatial Neglect. J. Neurosci. 34, 5003–5011. https://doi.org/10.1523/JNEUROSCI.3765-13.2014

Dimidschstein, J., Chen, Q., Tremblay, R., Rogers, S., Saldi, G., Guo, L., Xu, C., Liu, R., Lu, C., Chu, J., Avery, M., Rashid, S., Baek, M., Jacob, A., Smith, G., Wilson, D., Kosche, G., Kruglikov, I., Rusielewicz, T., Kotak, V., Mowery, T., Anderson, S., Callaway, E., Dasen, J., Fitzpatrick, D., Fossati, V., Long, M., Noggle, S., Reynolds, J., Sanes, D., Rudy, B., Feng, G., Fishell, G., 2016. A viral strategy for targeting and manipulating interneurons across vertebrate species. Nat. Neurosci. 19, 1743–1749. https://doi.org/10.1038/nn.4430

Ding, N., Melloni, L., Yang, A., Wang, Y., Zhang, W., Poeppel, D., 2017. Characterizing Neural Entrainment to Hierarchical Linguistic Units using Electroencephalography (EEG). Front. Hum. Neurosci. 11.

Drake, C., Jones, M.R., Baruch, C., 2000. The development of rhythmic attending in auditory sequences: attunement, referent period, focal attending. Cognition 77, 251–288. https://doi.org/10.1016/S0010-0277(00)00106-2

Dudai, Y., 2002. Molecular bases of long-term memories: a question of persistence. Curr. Opin. Neurobiol. 12, 211–216. https://doi.org/10.1016/S0959-4388(02)00305-7

Dunn, S.L.S., Town, S.M., Bizley, J.K., Bendor, D., 2022. Behaviourally modulated hippocampal theta oscillations in the ferret persist during both locomotion and immobility. Nat. Commun. 13, 5905. https://doi.org/10.1038/s41467-022-33507-2

Durand, S., Heller, G.R., Ramirez, T.K., Luviano, J.A., Williford, A., Sullivan, D.T., Cahoon, A.J., Farrell, C., Groblewski, P.A., Bennett, C., Siegle, J.H., Olsen, S.R., 2023. Acute head-fixed recordings in awake mice with multiple Neuropixels probes. Nat. Protoc. 18, 424–457. https://doi.org/10.1038/s41596-022-00768-6

Dürschmid, S., Edwards, E., Reichert, C., Dewar, C., Hinrichs, H., Heinze, H.-J., Kirsch, H.E., Dalal, S.S., Deouell, L.Y., Knight, R.T., 2016. Hierarchy of prediction errors for auditory events in human temporal and frontal cortex. Proc. Natl. Acad. Sci. 113, 6755–6760. https://doi.org/10.1073/pnas.1525030113

Eidelberg, E., White, J.C., Brazier, M.A.B., 1959. The hippocampal arousal pattern in rabbits. Exp. Neurol. 1, 483–490. https://doi.org/10.1016/0014-4886(59)90045-7

El Karoui, I., King, J.-R., Sitt, J., Meyniel, F., Van Gaal, S., Hasboun, D., Adam, C., Navarro, V., Baulac, M., Dehaene, S., Cohen, L., Naccache, L., 2015. Event-Related Potential, Time-frequency, and Functional Connectivity Facets of Local and Global Auditory Novelty Processing: An Intracranial Study in Humans. Cereb. Cortex 25, 4203–4212. https://doi.org/10.1093/cercor/bhu143

Euston, D.R., Tatsuno, M., McNaughton, B.L., 2007. Fast-Forward Playback of Recent Memory Sequences in Prefrontal Cortex During Sleep. Science 318, 1147–1150. https://doi.org/10.1126/science.1148979

Fishman, Y.I., Steinschneider, M., 2012. Searching for the Mismatch Negativity in Primary Auditory Cortex of the Awake Monkey: Deviance Detection or Stimulus Specific Adaptation? J. Neurosci. 32, 15747–15758. https://doi.org/10.1523/JNEUROSCI.2835-12.2012
Garrido, M.I., Friston, K.J., Kiebel, S.J., Stephan, K.E., Baldeweg, T., Kilner, J.M., 2008. The functional anatomy of the MMN: a DCM study of the roving paradigm. NeuroImage 42, 936–944. https://doi.org/10.1016/j.neuroimage.2008.05.018
Garrido, M.I., Kilner, J.M., Kiebel, S.J., Friston, K.J., 2007. Evoked brain responses are generated by feedback loops. Proc. Natl. Acad. Sci. 104, 20961–20966. https://doi.org/10.1073/pnas.0706274105
Garrido, M.I., Kilner, J.M., Stephan, K.E., Friston, K.J., 2009. The mismatch negativity: A review of underlying mechanisms. Clin. Neurophysiol. 120, 453–463. https://doi.org/10.1016/j.clinph.2008.11.029
Garrido, M.I., Sahani, M., Dolan, R.J., 2013. Outlier Responses Reflect Sensitivity to Statistical Structure in the Human Brain. PLOS Comput. Biol. 9, e1002999. https://doi.org/10.1371/journal.pcbi.1002999
Garrido, M.I., Teng, C.L.J., Taylor, J.A., Rowe, E.G., Mattingley, J.B., 2016. Surprise responses in the human brain demonstrate statistical learning under high concurrent cognitive demand. Npj Sci. Learn. 1, 1–7. https://doi.org/10.1038/npjscilearn.2016.6
Gaucher, Q., Panniello, M., Ivanov, A.Z., Dahmen, J.C., King, A.J., Walker, K.M., 2020. Complexity of frequency receptive fields predicts tonotopic variability across species. eLife 9, e53462. https://doi.org/10.7554/eLife.53462
Geiser, E., Walker, K.M.M., Bendor, D., 2014. Global timing: a conceptual framework to investigate the neural basis of rhythm perception in humans and non-human species. Front. Psychol. 5. https://doi.org/10.3389/fpsyg.2014.00159
Gourévitch, B., Martin, C., Postal, O., Eggermont, J.J., 2020. Oscillations in the auditory system and their possible role. Neurosci. Biobehav. Rev. 113, 507–528. https://doi.org/10.1016/j.neubiorev.2020.03.030
Green, J.D., Arduini, A.A., 1954. Hippocampal electrical activity in arousal. J. Neurophysiol. 17, 533–557. https://doi.org/10.1152/jn.1954.17.6.533
Griffiths, T.D., Warren, J.D., 2004. What is an auditory object? Nat. Rev. Neurosci. 5, 887. https://doi.org/10.1038/nrn1538
Grill-Spector, K., Henson, R., Martin, A., 2006. Repetition and the brain: neural models of stimulus-specific effects. Trends Cogn. Sci. 10, 14–23. https://doi.org/10.1016/j.tics.2005.11.006
Hafting, T., Fyhn, M., Molden, S., Moser, M.-B., Moser, E.I., 2005. Microstructure of a spatial map in the entorhinal cortex. Nature 436, 801–806. https://doi.org/10.1038/nature03721
Halgren, E., Squires, N.K., Wilson, C.L., Rohrbaugh, J.W., Babb, T.L., Crandall, P.H., 1980. Endogenous potentials generated in the human hippocampal formation and amygdala by infrequent events. Science 210, 803–805. https://doi.org/10.1126/science.7434000
Hämäläinen, M., Hari, R., Ilmoniemi, R.J., Knuutila, J., Lounasmaa, O.V., 1993. Magnetoencephalography---theory, instrumentation, and applications to noninvasive studies of the working human brain. Rev. Mod. Phys. 65, 413–497. https://doi.org/10.1103/RevModPhys.65.413
Happel, M.F.K., Jeschke, M., Ohl, F.W., 2010. Spectral Integration in Primary Auditory Cortex Attributable to Temporally Precise Convergence of

Thalamocortical and Intracortical Input. J. Neurosci. 30, 11114–11127. https://doi.org/10.1523/JNEUROSCI.0689-10.2010
Harrison, L.M., Duggins, A., Friston, K.J., 2006. Encoding uncertainty in the hippocampus. Neural Netw. 19, 535–546. https://doi.org/10.1016/j.neunet.2005.11.002
Harrison, P.M.C., Bianco, R., Chait, M., Pearce, M.T., 2020. PPM-Decay: A computational model of auditory prediction with memory decay. PLOS Comput. Biol. 16, e1008304. https://doi.org/10.1371/journal.pcbi.1008304
Heffner, H.E., Heffner, R.S., 2007. Hearing ranges of laboratory animals. J. Am. Assoc. Lab. Anim. Sci. JAALAS 46, 20–22.
Heilbron, M., Chait, M., 2018. Great Expectations: Is there Evidence for Predictive Coding in Auditory Cortex? Neuroscience, Sensory Sequence Processing in the Brain 389, 54–73. https://doi.org/10.1016/j.neuroscience.2017.07.061
Henin, S., Turk-Browne, N.B., Friedman, D., Liu, A., Dugan, P., Flinker, A., Doyle, W., Devinsky, O., Melloni, L., 2020. Learning hierarchical sequence representations across human cortex and hippocampus. bioRxiv 583856. https://doi.org/10.1101/583856
Hofmann-Shen, C., Vogel, B.O., Kaffes, M., Rudolph, A., Brown, E.C., Tas, C., Brüne, M., Neuhaus, A.H., 2020. Mapping adaptation, deviance detection, and prediction error in auditory processing. NeuroImage 207, 116432. https://doi.org/10.1016/j.neuroimage.2019.116432
Hyman, J., Zilli, E., Paley, A., Hasselmo, M., 2010. Working memory performance correlates with prefrontal-hippocampal theta interactions but not with prefrontal neuron firing rates. Front. Integr. Neurosci. 4.
Jablonowski, J., Taesler, P., Fu, Q., Rose, M., 2018. Implicit acoustic sequence learning recruits the hippocampus. PLOS ONE 13, e0209590. https://doi.org/10.1371/journal.pone.0209590
Jones, M.R., Boltz, M., Kidd, G., 1982. Controlled attending as a function of melodic and temporal context. Percept. Psychophys. 32, 211–218. https://doi.org/10.3758/BF03206225
Jones, M.R., Johnston, H.M., Puente, J., 2006. Effects of auditory pattern structure on anticipatory and reactive attending. Cognit. Psychol. 53, 59–96. https://doi.org/10.1016/j.cogpsych.2006.01.003
Jones, M.R., Moynihan, H., MacKenzie, N., Puente, J., 2002. Temporal Aspects of Stimulus-Driven Attending in Dynamic Arrays. Psychol. Sci. 13, 313–319. https://doi.org/10.1111/1467-9280.00458
Juavinett, A.L., Bekheet, G., Churchland, A.K., 2019. Chronically implanted Neuropixels probes enable high-yield recordings in freely moving mice. eLife 8, e47188. https://doi.org/10.7554/eLife.47188
Kajikawa, Y., Schroeder, C.E., 2011. How local is the local field potential? Neuron 72, 847–858. https://doi.org/10.1016/j.neuron.2011.09.029
Kalm, K., Davis, M.H., Norris, D., 2013. Individual Sequence Representations in the Medial Temporal Lobe. J. Cogn. Neurosci. 25, 1111–1121. https://doi.org/10.1162/jocn_a_00378
Kavanagh, G.L., Kelly, J.B., 1988. Hearing in the ferret (Mustela putorius): effects of primary auditory cortical lesions on thresholds for pure tone detection. J. Neurophysiol. 60, 879–888.
Keating, P., Nodal, F.R., Gananandan, K., Schulz, A.L., King, A.J., 2013. Behavioral Sensitivity to Broadband Binaural Localization Cues in the Ferret. J. Assoc. Res. Otolaryngol. 14, 561–572. https://doi.org/10.1007/s10162-013-0390-3

Keller, G.B., Mrsic-Flogel, T.D., 2018. Predictive Processing: A Canonical Cortical Computation. Neuron 100, 424–435. https://doi.org/10.1016/j.neuron.2018.10.003
Kiebel, S.J., Garrido, M.I., Friston, K.J., 2007. Dynamic causal modelling of evoked responses: The role of intrinsic connections. NeuroImage 36, 332–345. https://doi.org/10.1016/j.neuroimage.2007.02.046
Kok, P., Rahnev, D., Jehee, J.F.M., Lau, H.C., de Lange, F.P., 2012. Attention reverses the effect of prediction in silencing sensory signals. Cereb. Cortex N. Y. N 1991 22, 2197–2206. https://doi.org/10.1093/cercor/bhr310
Kok, P., Rait, L.I., Turk-Browne, N.B., 2019. Content-based Dissociation of Hippocampal Involvement in Prediction. J. Cogn. Neurosci. 32, 527–545. https://doi.org/10.1162/jocn_a_01509
Kok, P., Turk-Browne, N.B., 2018. Associative Prediction of Visual Shape in the Hippocampus. J. Neurosci. 38, 6888–6899. https://doi.org/10.1523/JNEUROSCI.0163-18.2018
Kragel, J.E., VanHaerents, S., Templer, J.W., Schuele, S., Rosenow, J.M., Nilakantan, A.S., Bridge, D.J., 2020. Hippocampal theta coordinates memory processing during visual exploration. eLife 9, e52108. https://doi.org/10.7554/eLife.52108
Kropotov, J.D., Alho, K., Näätänen, R., Ponomarev, V.A., Kropotova, O.V., Anichkov, A.D., Nechaev, V.B., 2000. Human auditory-cortex mechanisms of preattentive sound discrimination. Neurosci. Lett. 280, 87–90. https://doi.org/10.1016/S0304-3940(00)00765-5
Kumar, S., Gander, P.E., Berger, J.I., Billig, A.J., Nourski, K.V., Oya, H., Kawasaki, H., Howard, M.A., Griffiths, T.D., 2021. Oscillatory correlates of auditory working memory examined with human electrocorticography. Neuropsychologia 150, 107691. https://doi.org/10.1016/j.neuropsychologia.2020.107691
Kumar, S., Joseph, S., Gander, P.E., Barascud, N., Halpern, A.R., Griffiths, T.D., 2016. A Brain System for Auditory Working Memory. J. Neurosci. 36, 4492–4505. https://doi.org/10.1523/JNEUROSCI.4341-14.2016
Kumaran, D., Maguire, E.A., 2007. Match–Mismatch Processes Underlie Human Hippocampal Responses to Associative Novelty. J. Neurosci. 27, 8517–8524. https://doi.org/10.1523/JNEUROSCI.1677-07.2007
Lakatos, P., Gross, J., Thut, G., 2019. A New Unifying Account of the Roles of Neuronal Entrainment. Curr. Biol. 29, R890–R905. https://doi.org/10.1016/j.cub.2019.07.075
Lakatos, P., O'Connell, M.N., Barczak, A., McGinnis, T., Neymotin, S., Schroeder, C.E., Smiley, J.F., Javitt, D.C., 2020. The Thalamocortical Circuit of Auditory Mismatch Negativity. Biol. Psychiatry, Brain Circuits and the Emergence of Schizophrenia 87, 770–780. https://doi.org/10.1016/j.biopsych.2019.10.029
Large, E.W., Jones, M.R., 1999. The dynamics of attending: How people track time-varying events. Psychol. Rev. 106, 119–159. https://doi.org/10.1037/0033-295X.106.1.119
Large, E.W., Palmer, C., 2002. Perceiving temporal regularity in music. Cogn. Sci. 26, 1–37. https://doi.org/10.1016/S0364-0213(01)00057-X
LeDoux, J.E., Ruggiero, D.A., Reis, Donald.J., 1985. Projections to the subcortical forebrain from anatomically defined regions of the medial geniculate body in the rat. J. Comp. Neurol. 242, 182–213. https://doi.org/10.1002/cne.902420204

Lee, J.H., Wang, X., Bendor, D., 2020. The role of adaptation in generating monotonic rate codes in auditory cortex. PLoS Comput. Biol. 16, e1007627. https://doi.org/10.1371/journal.pcbi.1007627
Li, N., Chen, S., Guo, Z.V., Chen, H., Huo, Y., Inagaki, H.K., Chen, G., Davis, C., Hansel, D., Guo, C., Svoboda, K., 2019. Spatiotemporal constraints on optogenetic inactivation in cortical circuits. eLife 8, e48622. https://doi.org/10.7554/eLife.48622
Linden, J.F., Schreiner, C.E., 2003. Columnar Transformations in Auditory Cortex? A Comparison to Visual and Somatosensory Cortices. Cereb. Cortex 13, 83–89. https://doi.org/10.1093/cercor/13.1.83
Loebel, A., Nelken, I., Tsodyks, M., 2007. Processing of sounds by population spikes in a model of primary auditory cortex. Front. Neurosci. 1.
Logan, C.G., Grafton, S.T., 1995. Functional anatomy of human eyeblink conditioning determined with regional cerebral glucose metabolism and positron-emission tomography. Proc. Natl. Acad. Sci. 92, 7500–7504. https://doi.org/10.1073/pnas.92.16.7500
Lomber, S.G., Malhotra, S., 2008. Double dissociation of “what” and “where” processing in auditory cortex. Nat. Neurosci. 11, 609–616. https://doi.org/10.1038/nn.2108
Lopes da Silva, F., 2013. EEG and MEG: Relevance to Neuroscience. Neuron 80, 1112–1128. https://doi.org/10.1016/j.neuron.2013.10.017
Lu, K., Liu, W., Zan, P., David, S.V., Fritz, J.B., Shamma, S.A., 2018. Implicit Memory for Complex Sounds in Higher Auditory Cortex of the Ferret. J. Neurosci. Off. J. Soc. Neurosci. 38, 9955–9966. https://doi.org/10.1523/JNEUROSCI.2118-18.2018
Lumaca, M., Dietz, M.J., Hansen, N.C., Quiroga-Martinez, D.R., Vuust, P., n.d. Perceptual learning of tone patterns changes the effective connectivity between Heschl’s gyrus and planum temporale. Hum. Brain Mapp. n/a. https://doi.org/10.1002/hbm.25269
Luo, T.Z., Bondy, A.G., Gupta, D., Elliott, V.A., Kopec, C.D., Brody, C.D., 2020. An approach for long-term, multi-probe Neuropixels recordings in unrestrained rats. eLife 9, e59716. https://doi.org/10.7554/eLife.59716
Ma, L., Micheyl, C., Yin, P., Oxenham, A.J., Shamma, S.A., 2010. Behavioral measures of auditory streaming in ferrets (Mustela putorius). J. Comp. Psychol. 124, 317–330. https://doi.org/10.1037/a0018273
MacDonald, C.J., Lepage, K.Q., Eden, U.T., Eichenbaum, H., 2011. Hippocampal “Time Cells” Bridge the Gap in Memory for Discontiguous Events. Neuron 71, 737–749. https://doi.org/10.1016/j.neuron.2011.07.012
Malmierca, M.S., Anderson, L.A., Antunes, F.M., 2015. The cortical modulation of stimulus-specific adaptation in the auditory midbrain and thalamus: a potential neuronal correlate for predictive coding. Front. Syst. Neurosci. 9. https://doi.org/10.3389/fnsys.2015.00019
Malmierca, M.S., Cristaudo, S., Pérez-González, D., Covey, E., 2009. Stimulus-Specific Adaptation in the Inferior Colliculus of the Anesthetized Rat. J. Neurosci. 29, 5483–5493. https://doi.org/10.1523/JNEUROSCI.4153-08.2009
Maris, E., Oostenveld, R., 2007. Nonparametric statistical testing of EEG- and MEG-data. J. Neurosci. Methods 164, 177–190. https://doi.org/10.1016/j.jneumeth.2007.03.024
Martorell, A.J., Paulson, A.L., Suk, H.-J., Abdurrob, F., Drummond, G.T., Guan, W., Young, J.Z., Kim, D.N.-W., Kritskiy, O., Barker, S.J., Mangena, V., Prince,

S.M., Brown, E.N., Chung, K., Boyden, E.S., Singer, A.C., Tsai, L.-H., 2019. Multi-sensory Gamma Stimulation Ameliorates Alzheimer's-Associated Pathology and Improves Cognition. Cell 177, 256-271.e22. https://doi.org/10.1016/j.cell.2019.02.014
Mehra, M., Mukesh, A., Bandyopadhyay, S., 2022. Separate Functional Subnetworks of Excitatory Neurons Show Preference to Periodic and Random Sound Structures. J. Neurosci. 42, 3165–3183. https://doi.org/10.1523/JNEUROSCI.0333-21.2022
Micheyl, C., Oxenham, A.J., 2010a. Objective and subjective psychophysical measures of auditory stream integration and segregation. J. Assoc. Res. Otolaryngol. JARO 11, 709–724. https://doi.org/10.1007/s10162-010-0227-2
Micheyl, C., Oxenham, A.J., 2010b. Pitch, harmonicity and concurrent sound segregation: Psychoacoustical and neurophysiological findings. Hear. Res., Special Issue: Annual Reviews 2010 266, 36–51. https://doi.org/10.1016/j.heares.2009.09.012
Milne, A.E., Bianco, R., Poole, K.C., Zhao, S., Oxenham, A.J., Billig, A.J., Chait, M., 2020. An online headphone screening test based on dichotic pitch. Behav. Res. Methods. https://doi.org/10.3758/s13428-020-01514-0
Molholm, S., Martinez, A., Ritter, W., Javitt, D.C., Foxe, J.J., 2005. The Neural Circuitry of Pre-attentive Auditory Change-detection: An fMRI Study of Pitch and Duration Mismatch Negativity generators. Cereb. Cortex 15, 545–551. https://doi.org/10.1093/cercor/bhh155
Montijn, J.S., Seignette, K., Howlett, M.H., Cazemier, J.L., Kamermans, M., Levelt, C.N., Heimel, J.A., 2021. A parameter-free statistical test for neuronal responsiveness. eLife 10, e71969. https://doi.org/10.7554/eLife.71969
Moore, A.K., Wehr, M., 2013. Parvalbumin-Expressing Inhibitory Interneurons in Auditory Cortex Are Well-Tuned for Frequency. J. Neurosci. 33, 13713–13723. https://doi.org/10.1523/JNEUROSCI.0663-13.2013
Morillon, B., Schroeder, C.E., Wyart, V., Arnal, L.H., 2016. Temporal prediction in lieu of periodic stimulation. J. Neurosci. 36, 2342–2347. https://doi.org/10.1523/JNEUROSCI.0836-15.2016
Munoz-Lopez, M.M., Mohedano-Moriano, A., Insausti, R., 2010. Anatomical pathways for auditory memory in primates. Front. Neuroanat. 4, 129. https://doi.org/10.3389/fnana.2010.00129
Murphy, A.J., Shaw, L., Hasse, J.M., Goris, R.L.T., Briggs, F., 2021. Optogenetic activation of corticogeniculate feedback stabilizes response gain and increases information coding in LGN neurons. J. Comput. Neurosci. 49, 259–271. https://doi.org/10.1007/s10827-020-00754-5
Musial, P.G., Baker, S.N., Gerstein, G.L., King, E.A., Keating, J.G., 2002. Signal-to-noise ratio improvement in multiple electrode recording. J. Neurosci. Methods 115, 29–43. https://doi.org/10.1016/S0165-0270(01)00516-7
Näätänen, R., Paavilainen, P., Rinne, T., Alho, K., 2007. The mismatch negativity (MMN) in basic research of central auditory processing: A review. Clin. Neurophysiol. 118, 2544–2590. https://doi.org/10.1016/j.clinph.2007.04.026
Näätänen, R., Tervaniemi, M., Sussman, E., Paavilainen, P., Winkler, I., 2001. 'Primitive intelligence' in the auditory cortex. Trends Neurosci. 24, 283–288. https://doi.org/10.1016/S0166-2236(00)01790-2
Natan, R.G., Briguglio, J.J., Mwilambwe-Tshilobo, L., Jones, S.I., Aizenberg, M., Goldberg, E.M., Geffen, M.N., 2015. Complementary control of sensory

adaptation by two types of cortical interneurons. eLife 4. https://doi.org/10.7554/eLife.09868
Nelken, I., 2014. Stimulus-specific adaptation and deviance detection in the auditory system: experiments and models. Biol. Cybern. 108, 655–663. https://doi.org/10.1007/s00422-014-0585-7
Nelken, I., Bizley, J., Shamma, S.A., Wang, X., 2014. Auditory Cortical Processing in Real-World Listening: The Auditory System Going Real. J. Neurosci. 34, 15135–15138. https://doi.org/10.1523/JNEUROSCI.2989-14.2014
Nelken, I., Yaron, A., Polterovich, A., Hershenhoren, I., 2013. Stimulus-Specific Adaptation Beyond Pure Tones, in: Moore, B.C.J., Patterson, R.D., Winter, I.M., Carlyon, R.P., Gockel, H.E. (Eds.), Basic Aspects of Hearing, Advances in Experimental Medicine and Biology. Springer, New York, NY, pp. 411–418. https://doi.org/10.1007/978-1-4614-1590-9_45
Niell, C.M., Stryker, M.P., 2008. Highly selective receptive fields in mouse visual cortex. J. Neurosci. Off. J. Soc. Neurosci. 28, 7520–7536. https://doi.org/10.1523/JNEUROSCI.0623-08.2008
Nodal, F.R., Bajo, V.M., Parsons, C.H., Schnupp, J.W., King, A.J., 2008. Sound localization behavior in ferrets: comparison of acoustic orientation and approach-to-target responses. Neuroscience 154, 397–408. https://doi.org/10.1016/j.neuroscience.2007.12.022
Noorden, van, L.P.A.S., 1975. Temporal coherence in the perception of tone sequences (Phd Thesis 1 (Research TU/e / Graduation TU/e)). Technische Hogeschool Eindhoven, Eindhoven.
Norman-Haignere, S.V., Long, L.K., Devinsky, O., Doyle, W., Irobunda, I., Merricks, E.M., Feldstein, N.A., McKhann, G.M., Schevon, C.A., Flinker, A., Mesgarani, N., 2022. Multiscale temporal integration organizes hierarchical computation in human auditory cortex. Nat. Hum. Behav. 6, 455–469. https://doi.org/10.1038/s41562-021-01261-y
Nourski, K.V., Steinschneider, M., Rhone, A.E., Kawasaki, H., Howard, M.A., Banks, M.I., 2018. Processing of auditory novelty across the cortical hierarchy: An intracranial electrophysiology study. NeuroImage 183, 412–424. https://doi.org/10.1016/j.neuroimage.2018.08.027
Nuñez, A., Buño, W., 2021. The Theta Rhythm of the Hippocampus: From Neuronal and Circuit Mechanisms to Behavior. Front. Cell. Neurosci. 15.
Nunez, P.L., Silberstein, R.B., 2000. On the Relationship of Synaptic Activity to Macroscopic Measurements: Does Co-Registration of EEG with fMRI Make Sense? Brain Topogr. 13, 79–96. https://doi.org/10.1023/A:1026683200895
O'Keefe, J., Dostrovsky, J., 1971. The hippocampus as a spatial map. Preliminary evidence from unit activity in the freely-moving rat. Brain Res. 34, 171–175. https://doi.org/10.1016/0006-8993(71)90358-1
O'Keefe, J., Recce, M.L., 1993. Phase relationship between hippocampal place units and the EEG theta rhythm. Hippocampus 3, 317–330. https://doi.org/10.1002/hipo.450030307
Olds, J., Hirano, T., 1969. Conditioned responses of hippocampal and other neurons. Electroencephalogr. Clin. Neurophysiol. 26, 159–166. https://doi.org/10.1016/0013-4694(69)90206-5
Opitz, B., Rinne, T., Mecklinger, A., von Cramon, D.Y., Schröger, E., 2002. Differential Contribution of Frontal and Temporal Cortices to Auditory Change Detection: fMRI and ERP Results. NeuroImage 15, 167–174. https://doi.org/10.1006/nimg.2001.0970

Owen, S.F., Liu, M.H., Kreitzer, A.C., 2019. Thermal constraints on in vivo optogenetic manipulations. Nat. Neurosci. 22, 1061–1065. https://doi.org/10.1038/s41593-019-0422-3
Park, Y., Geffen, M.N., 2020. A circuit model of auditory cortex. PLOS Comput. Biol. 16, e1008016. https://doi.org/10.1371/journal.pcbi.1008016
Parras, G.G., Nieto-Diego, J., Carbajal, G.V., Valdés-Baizabal, C., Escera, C., Malmierca, M.S., 2017. Neurons along the auditory pathway exhibit a hierarchical organization of prediction error. Nat. Commun. 8, 1–17. https://doi.org/10.1038/s41467-017-02038-6
Paulk, A.C., Kfir, Y., Khanna, A.R., Mustroph, M.L., Trautmann, E.M., Soper, D.J., Stavisky, S.D., Welkenhuysen, M., Dutta, B., Shenoy, K.V., Hochberg, L.R., Richardson, R.M., Williams, Z.M., Cash, S.S., 2022. Large-scale neural recordings with single neuron resolution using Neuropixels probes in human cortex. Nat. Neurosci. 25, 252–263. https://doi.org/10.1038/s41593-021-00997-0
Pearce, M.T., 2018. Statistical learning and probabilistic prediction in music cognition: Mechanisms of stylistic enculturation. Ann. N. Y. Acad. Sci. 1423, 378–395. https://doi.org/10.1111/nyas.13654
Pearce, M.T., 2005. The Construction and Evaluation of Statistical Models of Melodic Structure in Music Perception and Composition. Dissertation 267.
Peixoto, H.M., Cruz, R.M.S., Moulin, T.C., Leão, R.N., 2020. Modeling the Effect of Temperature on Membrane Response of Light Stimulation in Optogenetically-Targeted Neurons. Front. Comput. Neurosci. 14.
Pérez-González, D., Malmierca, M.S., Covey, E., 2005. Novelty detector neurons in the mammalian auditory midbrain. Eur. J. Neurosci. 22, 2879–2885. https://doi.org/10.1111/j.1460-9568.2005.04472.x
Pérez-González, D., Parras, G.G., Morado-Díaz, C.J., Aedo-Sánchez, C., Carbajal, G.V., Malmierca, M.S., 2020. Deviance detection in physiologically identified cell types in the rat auditory cortex. Hear. Res. 107997. https://doi.org/10.1016/j.heares.2020.107997
Perrodin, C., Verzat, C., Bendor, D., 2020. Courtship behaviour reveals temporal regularity is a critical social cue in mouse communication. bioRxiv 2020.01.28.922773. https://doi.org/10.1101/2020.01.28.922773
Petkov, C.I., Cate, C. ten, 2020. Structured Sequence Learning: Animal Abilities, Cognitive Operations, and Language Evolution. Top. Cogn. Sci. 12, 828–842. https://doi.org/10.1111/tops.12444
Pettersen, K.H., Devor, A., Ulbert, I., Dale, A.M., Einevoll, G.T., 2006. Current-source density estimation based on inversion of electrostatic forward solution: effects of finite extent of neuronal activity and conductivity discontinuities. J. Neurosci. Methods 154, 116–133. https://doi.org/10.1016/j.jneumeth.2005.12.005
Phillips, H.N., Blenkmann, A., Hughes, L.E., Bekinschtein, T.A., Rowe, J.B., 2015. Hierarchical Organization of Frontotemporal Networks for the Prediction of Stimuli across Multiple Dimensions. J. Neurosci. 35, 9255–9264. https://doi.org/10.1523/JNEUROSCI.5095-14.2015
Phillips, H.N., Blenkmann, A., Hughes, L.E., Kochen, S., Bekinschtein, T.A., Cam-CAN, Rowe, J.B., 2016. Convergent evidence for hierarchical prediction networks from human electrocorticography and magnetoencephalography. Cortex 82, 192–205. https://doi.org/10.1016/j.cortex.2016.05.001

Polterovich, A., Jankowski, M.M., Nelken, I., 2018. Deviance sensitivity in the auditory cortex of freely moving rats. PLOS ONE 13, e0197678. https://doi.org/10.1371/journal.pone.0197678
Qasim, S.E., Fried, I., Jacobs, J., 2020. Phase precession in the human hippocampus and entorhinal cortex. bioRxiv 2020.09.06.285320. https://doi.org/10.1101/2020.09.06.285320
Quiroga-Martinez, D.R., Hansen, N.C., Højlund, A., Pearce, M., Brattico, E., Vuust, P., 2020. Musical prediction error responses similarly reduced by predictive uncertainty in musicians and non-musicians. Eur. J. Neurosci. 51, 2250–2269. https://doi.org/10.1111/ejn.14667
Radtke-Schuller, S., 2018. Cyto- and Myeloarchitectural Brain Atlas of the Ferret (Mustela putorius) in MRI Aided Stereotaxic Coordinates. Springer International Publishing. https://doi.org/10.1007/978-3-319-76626-3
Recasens, M., Gross, J., Uhlhaas, P.J., 2018. Low-Frequency Oscillatory Correlates of Auditory Predictive Processing in Cortical-Subcortical Networks: A MEG-Study. Sci. Rep. 8, 14007. https://doi.org/10.1038/s41598-018-32385-3
Riecke, L., Sack, A.T., Schroeder, C.E., 2015. Endogenous Delta/Theta Sound-Brain Phase Entrainment Accelerates the Buildup of Auditory Streaming. Curr. Biol. 25, 3196–3201. https://doi.org/10.1016/j.cub.2015.10.045
Rimmele, J., Schröger, E., Bendixen, A., 2012. Age-related changes in the use of regular patterns for auditory scene analysis. Hear. Res. 289, 98–107. https://doi.org/10.1016/j.heares.2012.04.006
Rimmele, J.M., Morillon, B., Poeppel, D., Arnal, L.H., 2018. Proactive Sensing of Periodic and Aperiodic Auditory Patterns. Trends Cogn. Sci., Special Issue: Time in the Brain 22, 870–882. https://doi.org/10.1016/j.tics.2018.08.003
Roberts, B., Glasberg, B.R., Moore, B.C.J., 2008. Effects of the build-up and resetting of auditory stream segregation on temporal discrimination. J. Exp. Psychol. Hum. Percept. Perform. 34, 992–1006. https://doi.org/10.1037/0096-1523.34.4.992
Rocchi, F., Oya, H., Balezeau, F., Billig, A.J., Kocsis, Z., Jenison, R.L., Nourski, K.V., Kovach, C.K., Steinschneider, M., Kikuchi, Y., Rhone, A.E., Dlouhy, B.J., Kawasaki, H., Adolphs, R., Greenlee, J.D.W., Griffiths, T.D., Howard, M.A., Petkov, C.I., 2021. Common fronto-temporal effective connectivity in humans and monkeys. Neuron 109, 852-868.e8. https://doi.org/10.1016/j.neuron.2020.12.026
Romanski, L.M., Giguere, M., Bates, J.F., Goldman-Rakic, P.S., 1997. Topographic organization of medial pulvinar connections with the prefrontal cortex in the rhesus monkey. J. Comp. Neurol. 379, 313–332.
Roy, A., Osik, J.J., Ritter, N.J., Wang, S., Shaw, J.T., Fiser, J., Van Hooser, S.D., 2016. Optogenetic spatial and temporal control of cortical circuits on a columnar scale. J. Neurophysiol. 115, 1043–1062. https://doi.org/10.1152/jn.00960.2015
Rummell, B.P., Klee, J.L., Sigurdsson, T., 2016. Attenuation of Responses to Self-Generated Sounds in Auditory Cortical Neurons. J. Neurosci. 36, 12010–12026. https://doi.org/10.1523/JNEUROSCI.1564-16.2016
Saderi, D., Buran, B.N., David, S.V., 2019. Streaming of repeated noise in primary and secondary fields of auditory cortex (preprint). Neuroscience. https://doi.org/10.1101/738583
Sanchez-Vives, M.V., Nowak, L.G., McCormick, D.A., 2000a. Membrane Mechanisms Underlying Contrast Adaptation in Cat Area 17In Vivo. J.

Neurosci. 20, 4267–4285. https://doi.org/10.1523/JNEUROSCI.20-11-04267.2000
Sanchez-Vives, M.V., Nowak, L.G., McCormick, D.A., 2000b. Cellular Mechanisms of Long-Lasting Adaptation in Visual Cortical Neurons In Vitro. J. Neurosci. 20, 4286–4299. https://doi.org/10.1523/JNEUROSCI.20-11-04286.2000
Santolin, C., Saffran, J.R., 2018. Constraints on Statistical Learning Across Species. Trends Cogn. Sci. 22, 52–63. https://doi.org/10.1016/j.tics.2017.10.003
Schapiro, A.C., Gregory, E., Landau, B., McCloskey, M., Turk-Browne, N.B., 2014. The Necessity of the Medial Temporal Lobe for Statistical Learning. J. Cogn. Neurosci. 26, 1736–1747. https://doi.org/10.1162/jocn_a_00578
Schneggenburger, R., Sakaba, T., Neher, E., 2002. Vesicle pools and short-term synaptic depression: lessons from a large synapse. Trends Neurosci. 25, 206–212. https://doi.org/10.1016/S0166-2236(02)02139-2
Schneider, D.M., Nelson, A., Mooney, R., 2014. A synaptic and circuit basis for corollary discharge in the auditory cortex. Nature 513, 189–194. https://doi.org/10.1038/nature13724
Schneider, F., Balezeau, F., Distler, C., Kikuchi, Y., van Kempen, J., Gieselmann, A., Petkov, C.I., Thiele, A., Griffiths, T.D., 2021. Neuronal figure-ground responses in primate primary auditory cortex. Cell Rep. 35, 109242. https://doi.org/10.1016/j.celrep.2021.109242
Schneider, F., Dheerendra, P., Balezeau, F., Ortiz-Rios, M., Kikuchi, Y., Petkov, C.I., Thiele, A., Griffiths, T.D., 2018. Auditory figure-ground analysis in rostral belt and parabelt of the macaque monkey. Sci. Rep. 8, 1–8. https://doi.org/10.1038/s41598-018-36903-1
Schönwiesner, M., Krumbholz, K., Rübsamen, R., Fink, G.R., von Cramon, D.Y., 2007. Hemispheric Asymmetry for Auditory Processing in the Human Auditory Brain Stem, Thalamus, and Cortex. Cereb. Cortex 17, 492–499. https://doi.org/10.1093/cercor/bhj165
Schwindt, P.C., Spain, W.J., Crill, W.E., 1989. Long-lasting reduction of excitability by a sodium-dependent potassium current in cat neocortical neurons. J. Neurophysiol. 61, 233–244. https://doi.org/10.1152/jn.1989.61.2.233
Shipp, S., 2016. Neural Elements for Predictive Coding. Front. Psychol. 7.
Skerritt-Davis, B., Elhilali, M., 2018. Detecting change in stochastic sound sequences. PLOS Comput. Biol. 14, e1006162. https://doi.org/10.1371/journal.pcbi.1006162
Slonina, Z.A., Poole, K.C., Bizley, J.K., 2022. What can we learn from inactivation studies? Lessons from auditory cortex. Trends Neurosci. 45, 64–77. https://doi.org/10.1016/j.tins.2021.10.005
Sohoglu, E., Chait, M., 2016. Detecting and representing predictable structure during auditory scene analysis [WWW Document]. eLife. https://doi.org/10.7554/eLife.19113
Sohoglu, E., Kumar, S., Chait, M., Griffiths, T.D., 2020. Multivoxel codes for representing and integrating acoustic features in human cortex. NeuroImage 217, 116661. https://doi.org/10.1016/j.neuroimage.2020.116661
Solomon, E.A., Lega, B.C., Sperling, M.R., Kahana, M.J., 2019. Hippocampal theta codes for distances in semantic and temporal spaces. Proc. Natl. Acad. Sci. 116, 24343–24352. https://doi.org/10.1073/pnas.1906729116
Southwell, R., 2019. Brain Responses Track Patterns in Sound. University College London, UK.

Southwell, R., Baumann, A., Gal, C., Barascud, N., Friston, K., Chait, M., 2017. Is predictability salient? A study of attentional capture by auditory patterns. Philos. Trans. R. Soc. B Biol. Sci. 372. https://doi.org/10.1098/rstb.2016.0105
Southwell, R., Chait, M., 2018. Enhanced deviant responses in patterned relative to random sound sequences. Cortex J. Devoted Study Nerv. Syst. Behav. 109, 92–103. https://doi.org/10.1016/j.cortex.2018.08.032
Srinivasan, R., 2006. Anatomical constraints on source models for high-resolution EEG and MEG derived from MRI. Technol. Cancer Res. Treat. 5, 389–399.
Stanislaw, H., Todorov, N., 1999. Calculation of signal detection theory measures. Behav. Res. Methods Instrum. Comput. 31, 137–149. https://doi.org/10.3758/BF03207704
Steinmetz, N.A., Aydin, C., Lebedeva, A., Okun, M., Pachitariu, M., Bauza, M., Beau, M., Bhagat, J., Böhm, C., Broux, M., Chen, S., Colonell, J., Gardner, R.J., Karsh, B., Kloosterman, F., Kostadinov, D., Mora-Lopez, C., O'Callaghan, J., Park, J., Putzeys, J., Sauerbrei, B., van Daal, R.J.J., Vollan, A.Z., Wang, S., Welkenhuysen, M., Ye, Z., Dudman, J.T., Dutta, B., Hantman, A.W., Harris, K.D., Lee, A.K., Moser, E.I., O'Keefe, J., Renart, A., Svoboda, K., Häusser, M., Haesler, S., Carandini, M., Harris, T.D., 2021. Neuropixels 2.0: A miniaturized high-density probe for stable, long-term brain recordings. Science 372, eabf4588. https://doi.org/10.1126/science.abf4588
Strange, B.A., Duggins, A., Penny, W., Dolan, R.J., Friston, K.J., 2005. Information theory, novelty and hippocampal responses: unpredicted or unpredictable? Neural Netw. 18, 225–230. https://doi.org/10.1016/j.neunet.2004.12.004
Sumner, C.J., Palmer, A.R., 2012. Auditory nerve fibre responses in the ferret. Eur. J. Neurosci. 36, 2428–2439. https://doi.org/10.1111/j.1460-9568.2012.08151.x
Sumner, C.J., Wells, T.T., Bergevin, C., Sollini, J., Kreft, H.A., Palmer, A.R., Oxenham, A.J., Shera, C.A., 2018. Mammalian behavior and physiology converge to confirm sharper cochlear tuning in humans. Proc. Natl. Acad. Sci. U. S. A. 115, 11322–11326. https://doi.org/10.1073/pnas.1810766115
Sutter, M.L., Schreiner, C.E., 1991. Physiology and topography of neurons with multipeaked tuning curves in cat primary auditory cortex. J. Neurophysiol. 65, 1207–1226. https://doi.org/10.1152/jn.1991.65.5.1207
Suzuki, M., Larkum, M.E., 2017. Dendritic calcium spikes are clearly detectable at the cortical surface. Nat. Commun. 8, 276. https://doi.org/10.1038/s41467-017-00282-4
Suzuki, W.L., Amaral, D.G., 1994. Perirhinal and parahippocampal cortices of the macaque monkey: Cortical afferents. J. Comp. Neurol. 350, 497–533. https://doi.org/10.1002/cne.903500402
Szymanski, F.D., Garcia-Lazaro, J.A., Schnupp, J.W.H., 2009. Current Source Density Profiles of Stimulus-Specific Adaptation in Rat Auditory Cortex. J. Neurophysiol. 102, 1483–1490. https://doi.org/10.1152/jn.00240.2009
Taaseh, N., Yaron, A., Nelken, I., 2011. Stimulus-Specific Adaptation and Deviance Detection in the Rat Auditory Cortex. PLOS ONE 6, e23369. https://doi.org/10.1371/journal.pone.0023369
Teki, S., Barascud, N., Picard, S., Payne, C., Griffiths, T.D., Chait, M., 2016. Neural Correlates of Auditory Figure-Ground Segregation Based on Temporal Coherence. Cereb. Cortex N. Y. NY 26, 3669–3680. https://doi.org/10.1093/cercor/bhw173

Teki, S., Chait, M., Kumar, S., Kriegstein, K. von, Griffiths, T.D., 2011. Brain Bases for Auditory Stimulus-Driven Figure–Ground Segregation. J. Neurosci. 31, 164–171. https://doi.org/10.1523/JNEUROSCI.3788-10.2011
Temperley, D., 2014. Information Flow and Repetition in Music. J. Music Theory 58, 155–178. https://doi.org/10.1215/00222909-2781759
Tillmann, B., Bharucha, J.J., Bigand, E., 2001. Implicit Learning of Regularities in Western Tonal Music by Self-Organization, in: French, R.M., Sougné, J.P. (Eds.), Connectionist Models of Learning, Development and Evolution, Perspectives in Neural Computing. Springer, London, pp. 175–184. https://doi.org/10.1007/978-1-4471-0281-6_18
Town, S.M., Atilgan, H., Wood, K.C., Bizley, J.K., 2015. The role of spectral cues in timbre discrimination by ferrets and humans. J. Acoust. Soc. Am. 137, 2870–2883. https://doi.org/10.1121/1.4916690
Town, S.M., Brimijoin, W.O., Bizley, J.K., 2017. Egocentric and allocentric representations in auditory cortex. PLOS Biol. 15, e2001878. https://doi.org/10.1371/journal.pbio.2001878
Town, S.M., Poole, K.C., Wood, K.C., Bizley, J.K., 2023. Reversible Inactivation of Ferret Auditory Cortex Impairs Spatial and Nonspatial Hearing. J. Neurosci. 43, 749–763. https://doi.org/10.1523/JNEUROSCI.1426-22.2022
Tzovara, A., Fedele, T., Sarnthein, J., Ledergerber, D., Lin, J.J., Knight, R.T., 2022. Auditory prediction hierarchy in the human hippocampus and amygdala. https://doi.org/10.1101/2022.11.16.516768
Ulanovsky, N., Las, L., Farkas, D., Nelken, I., 2004. Multiple Time Scales of Adaptation in Auditory Cortex Neurons. J. Neurosci. 24, 10440–10453. https://doi.org/10.1523/JNEUROSCI.1905-04.2004
Ulanovsky, N., Las, L., Nelken, I., 2003. Processing of low-probability sounds by cortical neurons. Nat. Neurosci. 6, 391–398. https://doi.org/10.1038/nn1032
Umbach, G., Kantak, P., Jacobs, J., Kahana, M., Pfeiffer, B.E., Sperling, M., Lega, B., 2020. Time cells in the human hippocampus and entorhinal cortex support episodic memory. Proc. Natl. Acad. Sci. 117, 28463–28474. https://doi.org/10.1073/pnas.2013250117
Valdés-Baizabal, C., Casado-Román, L., Bartlett, E.L., Malmierca, M.S., 2021. In vivo whole-cell recordings of stimulus-specific adaptation in the inferior colliculus. Hear. Res., Stimulus-specific adaptation, MMN and predicting coding 399, 107978. https://doi.org/10.1016/j.heares.2020.107978
Vinogradova, O.S., 1975. Functional Organization of the Limbic System in the Process of Registration of Information: Facts and Hypotheses, in: Isaacson, R.L., Pribram, K.H. (Eds.), The Hippocampus: Volume 2: Neurophysiology and Behavior. Springer US, Boston, MA, pp. 3–69. https://doi.org/10.1007/978-1-4684-2979-4_1
Wacongne, C., Labyt, E., Wassenhove, V. van, Bekinschtein, T., Naccache, L., Dehaene, S., 2011. Evidence for a hierarchy of predictions and prediction errors in human cortex. Proc. Natl. Acad. Sci. 108, 20754–20759. https://doi.org/10.1073/pnas.1117807108
Wahlstrom, K.L., Huff, M.L., Emmons, E.B., Freeman, J.H., Narayanan, N.S., McIntyre, C.K., LaLumiere, R.T., 2018. Basolateral Amygdala Inputs to the Medial Entorhinal Cortex Selectively Modulate the Consolidation of Spatial and Contextual Learning. J. Neurosci. 38, 2698–2712. https://doi.org/10.1523/JNEUROSCI.2848-17.2018

Walker, K.M.M., Schnupp, J.W.H., Hart-Schnupp, S.M.B., King, A.J., Bizley, J.K., 2009. Pitch discrimination by ferrets for simple and complex sounds. J. Acoust. Soc. Am. 126, 1321–1335. https://doi.org/10.1121/1.3179676
Wiegert, J.S., Mahn, M., Prigge, M., Printz, Y., Yizhar, O., 2017. Silencing Neurons: Tools, Applications, and Experimental Constraints. Neuron 95, 504–529. https://doi.org/10.1016/j.neuron.2017.06.050
Wilson, B., Marslen-Wilson, W.D., Petkov, C.I., 2017. Conserved Sequence Processing in Primate Frontal Cortex. Trends Neurosci. 40, 72–82. https://doi.org/10.1016/j.tins.2016.11.004
Wilson, C.J., Higgs, M.H., Simmons, D.V., Morales, J.C., 2018. Oscillations and Spike Entrainment. F1000Research 7, F1000 Faculty Rev-1960. https://doi.org/10.12688/f1000research.16451.1
Winer, J.A., 1992. The Functional Architecture of the Medial Geniculate Body and the Primary Auditory Cortex, in: Webster, D.B., Popper, A.N., Fay, R.R. (Eds.), The Mammalian Auditory Pathway: Neuroanatomy, Springer Handbook of Auditory Research. Springer, New York, NY, pp. 222–409. https://doi.org/10.1007/978-1-4612-4416-5_6
Winkler, I., Denham, S., Mill, R., Bőhm, T.M., Bendixen, A., 2012. Multistability in auditory stream segregation: a predictive coding view. Philos. Trans. R. Soc. B Biol. Sci. 367, 1001–1012. https://doi.org/10.1098/rstb.2011.0359
Winkler, I., Denham, S.L., Nelken, I., 2009. Modeling the auditory scene: predictive regularity representations and perceptual objects. Trends Cogn. Sci. 13, 532–540. https://doi.org/10.1016/j.tics.2009.09.003
Wood, K.C., Town, S.M., Atilgan, H., Jones, G.P., Bizley, J.K., 2017. Acute Inactivation of Primary Auditory Cortex Causes a Sound Localisation Deficit in Ferrets. PLOS ONE 12, e0170264. https://doi.org/10.1371/journal.pone.0170264
Xiao, C., Liu, Y., Xu, J., Gan, X., Xiao, Z., 2018. Septal and Hippocampal Neurons Contribute to Auditory Relay and Fear Conditioning. Front. Cell. Neurosci. 12. https://doi.org/10.3389/fncel.2018.00102
Yarden, T.S., Mizrahi, A., Nelken, I., 2022. Context-Dependent Inhibitory Control of Stimulus-Specific Adaptation. J. Neurosci. Off. J. Soc. Neurosci. 42, 4629–4651. https://doi.org/10.1523/JNEUROSCI.0988-21.2022
Yarden, T.S., Nelken, I., 2017. Stimulus-specific adaptation in a recurrent network model of primary auditory cortex. PLOS Comput. Biol. 13, e1005437. https://doi.org/10.1371/journal.pcbi.1005437
Yaron, A., Hershenhoren, I., Nelken, I., 2012. Sensitivity to Complex Statistical Regularities in Rat Auditory Cortex. Neuron 76, 603–615. https://doi.org/10.1016/j.neuron.2012.08.025
Yi, G.-L., Zhu, M.-Z., Cui, H.-C., Yuan, X.-R., Liu, P., Tang, J., Li, Y.-Q., Zhu, X.-H., 2022. A hippocampus dependent neural circuit loop underlying the generation of auditory mismatch negativity. Neuropharmacology 206, 108947. https://doi.org/10.1016/j.neuropharm.2022.108947
Yin, P., Fritz, J.B., Shamma, S.A., 2010. Do ferrets perceive relative pitch? J. Acoust. Soc. Am. 127, 1673–1680. https://doi.org/10.1121/1.3290988
Zhang, M., Frohlich, F., 2022. Cell type-specific excitability probed by optogenetic stimulation depends on the phase of the alpha oscillation. Brain Stimulat. 15, 472–482. https://doi.org/10.1016/j.brs.2022.02.014

Zhao, L., Liu, Y., Shen, L., Feng, L., Hong, B., 2011. Stimulus-specific adaptation and its dynamics in the inferior colliculus of rat. Neuroscience 181, 163–174. https://doi.org/10.1016/j.neuroscience.2011.01.060

Zhou, M., Liang, F., Xiong, X.R., Li, L., Li, H., Xiao, Z., Tao, H.W., Zhang, L.I., 2014. Laminar-specific Scaling Down of Balanced Excitation and Inhibition in Auditory Cortex by Active Behavioral States. Nat. Neurosci. 17, 841–850. https://doi.org/10.1038/nn.3701

9 APPENDICES

9.1 ONLINE PSYCHOPHYSICS

9.1.1 Consent form

Removed due to personal data

9.1.2 Example information sheet *(H1)*

Removed due to personal data

9.2 METHODS

9.2.1 Permutation testing

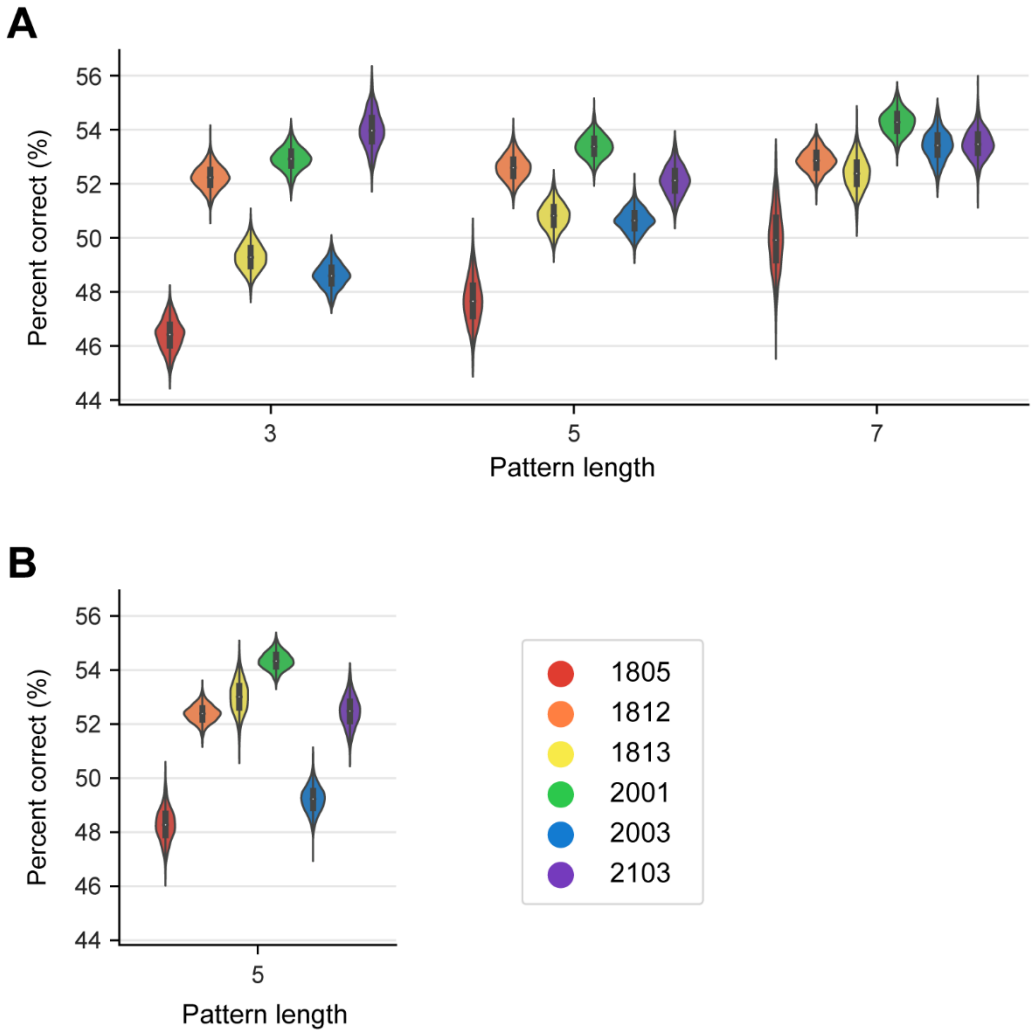

Figure 9.1: Permutation testing for each ferret. Violin plots of the chance distribution created through permuting each ferrets reaction times for each condition (each ferret coloured according to the legend) for RAN20 (A) and RAN5 (B).

9.3 GLMM TABLES

9.3.1 Chapter Three tables

Fixed effects	Estimate	Standard error	T	p value	CI 95% Lower	CI 95% Upper
Intercept	0.117	0.028	4.228	**< 0.001**	0.063	0.172
Pattern length	-0.012	0.004	-2.842	**0.005**	-0.02	-0.004
Random alphabet	-0.004	0.001	-4.126	**< 0.001**	-0.006	-0.002
AEG (ref MEG)	-0.037	0.03	-1.216	0.224	-0.097	0.023
PEG (ref MEG)	-0.024	0.029	-0.839	0.401	-0.081	0.033
Lower (ref Upper)	-0.083	0.028	-2.991	**0.003**	-0.137	-0.028
Middle (ref Upper)	-0.143	0.032	-4.402	**< 0.001**	-0.206	-0.079
Novelty (Novel = 1)	-0.144	0.024	-6.13	**< 0.001**	-0.19	-0.098
PL × AEG	0.005	0.004	1.176	0.24	-0.004	0.014
PL × PEG	0.01	0.004	2.301	**0.021**	0.001	0.018
RA × AEG	0	0.001	0.314	0.753	-0.002	0.002
RA × PEG	-0.002	0.001	-1.685	0.092	-0.003	0
PL × Lower	0.01	0.004	2.563	**0.01**	0.002	0.018
PL × Middle	0.022	0.005	4.542	**< 0.001**	0.012	0.031
RA × Lower	-0.002	0.001	-2.24	**0.025**	-0.004	0
RA × Middle	-0.003	0.001	-2.7	**0.007**	-0.005	-0.001
PL × Novelty	0.019	0.003	5.57	**< 0.001**	0.012	0.025
RA × Novelty	0.003	0.001	3.56	**< 0.001**	0.001	0.004
AEG × Novelty	0.023	0.013	1.75	0.08	-0.003	0.048
PEG × Novelty	-0.005	0.012	-0.367	0.713	-0.029	0.02
Lower × Novelty	0.006	0.012	0.539	0.59	-0.017	0.029
Middle × Novelty	0.028	0.014	2.052	**0.04**	0.001	0.055

Table 9.1. Mixed effect linear regression on the modulation index (SNR during regular sequences – SNR during random sequences) at the tone presentation rate in the local field potential. R^2 = 0.303; Df = 1953; random effects std. = 0.0563

Fixed effects	Estimate	Standard error	T	p value	CI 95% Lower	CI 95% Upper
Intercept	0.178	0.033	5.389	**< 0.001**	0.113	0.243
Pattern length	-0.026	0.005	-4.842	**< 0.001**	-0.036	-0.015
Random alphabet	0.004	0.001	3.812	**< 0.001**	0.002	0.006
AEG (ref MEG)	-0.028	0.034	-0.816	0.415	-0.095	0.039
PEG (ref MEG)	0.024	0.033	0.732	0.464	-0.04	0.088
Lower (ref Upper)	-0.061	0.032	-1.887	0.059	-0.125	0.002
Middle (ref Upper)	-0.036	0.037	-0.971	0.332	-0.109	0.037
Novelty (Novel = 1)	-0.058	0.027	-2.148	**0.032**	-0.111	-0.005
PL × AEG	0.009	0.005	1.709	0.088	-0.001	0.02
PL × PEG	-0.002	0.005	-0.374	0.709	-0.012	0.008
RA × AEG	-0.001	0.001	-0.769	0.442	-0.003	0.001
RA × PEG	-0.002	0.001	-1.771	0.077	-0.004	0
PL × Lower	0.011	0.005	2.181	**0.029**	0.001	0.021
PL × Middle	0.005	0.006	0.884	0.377	-0.006	0.017
RA × Lower	0	0.001	-0.162	0.871	-0.002	0.002
RA × Middle	-0.002	0.001	-1.753	0.08	-0.004	0
PL × Novelty	0.017	0.004	4.181	**< 0.001**	0.009	0.025
RA × Novelty	-0.003	0.001	-3.079	**0.002**	-0.004	-0.001
AEG × Novelty	-0.005	0.015	-0.323	0.747	-0.033	0.024
PEG × Novelty	0.007	0.014	0.521	0.603	-0.02	0.034
Lower × Novelty	-0.024	0.013	-1.782	0.075	-0.05	0.002
Middle × Novelty	0.003	0.015	0.181	0.856	-0.027	0.033

Table 9.2: Mixed effect linear regression on the modulation index (SNR during regular sequences – SNR during random sequences) at the pattern rate in the local field potential. R^2 = 0.185; Df = 1772; random effects std. = 0.0565

Fixed effects	Estimate	Standard error	T	p value	CI 95% Lower	CI 95% Upper
RAN20-REG3						
Intercept	-0.024	0.027	-0.897	0.370	-0.077	0.029
AEG	-0.025	0.025	-0.973	0.331	-0.074	0.025
PEG	-0.005	0.025	-0.179	0.858	-0.054	0.045
Lower	-0.030	0.028	-1.05	0.294	-0.086	0.026
Middle	-0.078	0.031	-2.493	**0.013**	-0.139	-0.016
Novelty	-0.027	0.035	-0.755	0.451	-0.096	0.043
AEG × Novelty	0.071	0.038	1.859	0.064	-0.004	0.146
PEG × Novelty	-0.010	0.034	-0.300	0.764	-0.076	0.056
Lower × Novelty	0.070	0.037	1.889	0.060	-0.003	0.143
Middle × Novelty	0.043	0.041	1.068	0.286	-0.036	0.123
RAN20-REG5						
Intercept	0.092	0.017	5.434	**< 0.001**	0.059	0.125
AEG	-0.002	0.022	-0.102	0.919	-0.045	0.04
PEG	0.047	0.020	2.311	**0.021**	0.007	0.087
Lower	-0.05	0.019	-2.653	**0.008**	-0.087	-0.013
Middle	-0.025	0.023	-1.090	0.276	-0.069	0.020
Novelty	-0.028	0.024	-1.187	0.236	-0.074	0.018
AEG × Novelty	-0.028	0.030	-0.945	0.345	-0.087	0.031
PEG × Novelty	-0.023	0.028	-0.802	0.423	-0.079	0.033
Lower × Novelty	0.083	0.026	3.128	**0.002**	0.031	0.134
Middle × Novelty	0.042	0.031	1.333	0.183	-0.020	0.103
RAN20-REG7						
Intercept	0.013	0.019	0.676	0.500	-0.024	0.050
AEG	-0.031	0.023	-1.334	0.183	-0.076	0.014
PEG	0.007	0.019	0.37	0.712	-0.031	0.045
Lower	-0.07	0.020	-3.461	**0.001**	-0.109	-0.03
Middle	-0.044	0.023	-1.93	0.054	-0.089	0.001
Novelty	-0.056	0.024	-2.325	**0.021**	-0.103	-0.009
AEG × Novelty	0.003	0.030	0.114	0.910	-0.055	0.062
PEG × Novelty	-0.014	0.026	-0.512	0.609	-0.066	0.038
Lower × Novelty	0.067	0.026	2.550	**0.011**	0.015	0.119
Middle × Novelty	0.016	0.030	0.541	0.589	-0.043	0.076
RAN5-REG5						
Intercept	0.126	0.017	7.418	**< 0.001**	0.093	0.159
AEG	-0.035	0.020	-1.714	0.087	-0.074	0.005
PEG	0.025	0.018	1.385	0.167	-0.011	0.061
Lower	-0.055	0.018	-3.014	**0.003**	-0.091	-0.019
Middle	-0.044	0.021	-2.103	**0.036**	-0.086	-0.003

Novelty	-0.022	0.022	-1.014	0.311	-0.065	0.021
AEG × Novelty	0.000	0.027	0.016	0.987	-0.052	0.053
PEG × Novelty	-0.021	0.025	-0.860	0.390	-0.069	0.027
Lower × Novelty	0.040	0.024	1.691	0.091	-0.007	0.087
Middle × Novelty	0.017	0.028	0.614	0.539	-0.037	0.071

Table 9.3: Mixed effect linear regression on the behavioural modulation index (SNR during regular hit trials – SNR during regular miss sequences) at the pattern rate in the local field potential for each condition separately. RAN20-REG3: R^2 = 0.153; Df = 341; random effect std. = 0.0622. RAN20-REG5: R^2 = 0.0281; Df = 479; random effect std. = 0.0199. RAN20-REG7: R^2 = 0.0318; Df = 436; random effect std. = 0.0124. RAN5-REG5: R^2 = 0.0443; Df = 437; random effect std. = 0.0279.

9.3.2 Chapter Four tables

Fixed effects	Estimate	Standard error	T	p value	CI 95% Lower	CI 95% Upper
Multi-unit						
Intercept	0.098	0.014	7.22	**< 0.001**	0.071	0.125
AEG	-0.062	0.022	-2.873	**0.004**	-0.104	-0.02-
PEG	-0.106	0.02	-5.432	**< 0.001**	-0.144	-0.068
Random alphabet	-0.001	0.00	-1.519	0.129	-0.001	0.000
Pattern length	-0.018	0.002	-10.368	**< 0.001**	-0.022	-0.015
Middle	-0.063	0.018	-3.449	**0.001**	-0.098	-0.027
Lower	-0.05	0.029	-1.736	0.083	-0.107	0.007
AEG × RA	0.003	0.001	4.231	**< 0.001**	0.001	0.004
PEG × RA	0.001	0.001	2.491	**0.013**	0.000	0.002
AEG × PL	0.005	0.003	1.376	0.169	-0.002	0.011
PEG × PL	0.012	0.003	4.448	**< 0.001**	0.007	0.017
Middle × RA	0.000	0.001	0.600	0.549	-0.001	0.001
Lower × RA	0.000	0.001	0.050	0.96	-0.002	0.002
Middle × PL	0.013	0.003	4.926	**< 0.001**	0.008	0.018
Lower × PL	0.015	0.004	3.759	**< 0.001**	0.007	0.023
Single-unit						
Intercept	0.115	0.016	7.421	**< 0.001**	0.085	0.146
AEG	-0.056	0.036	-1.552	0.121	-0.127	0.015
PEG	-0.086	0.025	-3.478	**0.001**	-0.134	-0.037
Random alphabet	-0.001	0.000	-2.84	**0.005**	-0.002	0.000
Pattern length	-0.021	0.002	-10.863	**< 0.001**	-0.025	-0.017
Middle	-0.115	0.031	-3.751	**< 0.001**	-0.174	-0.055
Lower	-0.129	0.043	-2.986	**0.003**	-0.214	-0.044
AEG × RA	0.001	0.001	1.168	0.243	-0.001	0.004
PEG × RA	0.003	0.001	4.365	**< 0.001**	0.002	0.004
AEG × PL	0.003	0.006	0.532	0.595	-0.009	0.016
PEG × PL	0.006	0.003	1.815	0.070	0.000	0.013
Middle × RA	0.000	0.001	-0.014	0.988	-0.002	0.002
Lower × RA	0.001	0.001	0.907	0.365	-0.002	0.004
Middle × PL	0.024	0.005	5.005	**< 0.001**	0.015	0.034
Lower × PL	0.033	0.005	6.037	**< 0.001**	0.022	0.043

Table 9.4: Mixed effects linear regression on the spike count modulation index (spike count during regular sequences – spike count during random sequences) for multi and single unit activity. MU: R^2 = 0.469; Df = 1526; random effect std. = 0.0622. SU: R^2 = 0.448; Df = 1482; random effect std. = 0.0705.

Fixed effects	Estimate	Standard error	T	p value	CI 95% Lower	CI 95% Upper
RAN20-REG3						
Intercept	-1.280	0.0762	-16.8	**< 0.001**	-1.43	-1.13
Regularity	-0.0223	0.00441	-5.07	**< 0.001**	-0.031	-0.0137
Reward	-0.0114	0.0133	-0.855	0.393	-0.0375	0.0147
Movement	0.0342	0.00414	8.25	**< 0.001**	0.026	0.0423
Pattern repetitions	0.00466	0.000621	7.5	**< 0.001**	0.00344	0.00587
Frequency dist.	-0.0322	0.0004	-80.3	**< 0.001**	-0.033	-0.0314
RAN20-REG5						
Intercept	-1.160	0.0808	-14.3	**< 0.001**	-1.32	-0.999
Regularity	-0.0258	0.00624	-4.13	**< 0.001**	-0.038	-0.0136
Reward	-0.0231	0.0229	-1.01	0.311	-0.0679	0.0217
Movement	0.00434	0.00564	0.769	0.442	-0.00671	0.0154
Pattern repetitions	0.0116	0.0014	8.33	**< 0.001**	0.00891	0.0144
Frequency dist.	-0.030	0.000543	-55.4	**< 0.001**	-0.0311	-0.029
RAN20-REG7						
Intercept	-1.120	0.0922	-12.1	**< 0.001**	-1.30	-0.935
Regularity	-0.0122	0.00856	-1.43	0.153	-0.029	0.00454
Reward	0.0683	0.0355	1.93	0.0542	-0.00123	0.138
Movement	0.0316	0.0081	3.89	**< 0.001**	0.0157	0.0474
Pattern repetitions	$7.14x10^5$	0.0025	0.0285	0.977	-0.00484	0.00498
Frequency dist.	-0.0329	0.000755	-43.6	**< 0.001**	-0.0344	-0.0314
RAN5-REG5						
Intercept	-1.15	0.0748	-15.4	**< 0.001**	-1.3	-1.01
Regularity	-0.0467	0.00604	-7.74	**< 0.001**	-0.0586	-0.0349
Reward	-0.0878	0.0266	-3.3	**< 0.001**	-0.14	-0.0356
Movement	0.0356	0.00547	6.51	**< 0.001**	0.0249	0.0463
Pattern repetitions	8.57E-03	0.00136	6.29	**< 0.001**	0.0059	0.0112
Frequency dist.	-0.0272	0.000537	-50.7	**< 0.001**	-0.0283	-0.0262

Table 9.5 Mixed effects Poisson regression on the spike count across single units for each condition. RAN20-REG3: $R^2 = 0.111$; Df = 964000; random effect std. = 0.789. RAN20-REG5: $R^2 = 0.103$; Df = 461000; random effect std. = 0.715. RAN20-REG7: $R^2 = 0.0860$; Df = 269000; random effect std. = 0.717. RAN5-REG5: $R^2 = 0.0990$; Df = 459000; random effect std. = 0.629

9.4 SUPPLEMENTARY FIGURES

9.4.1 Categorisation of factors influencing single unit activity

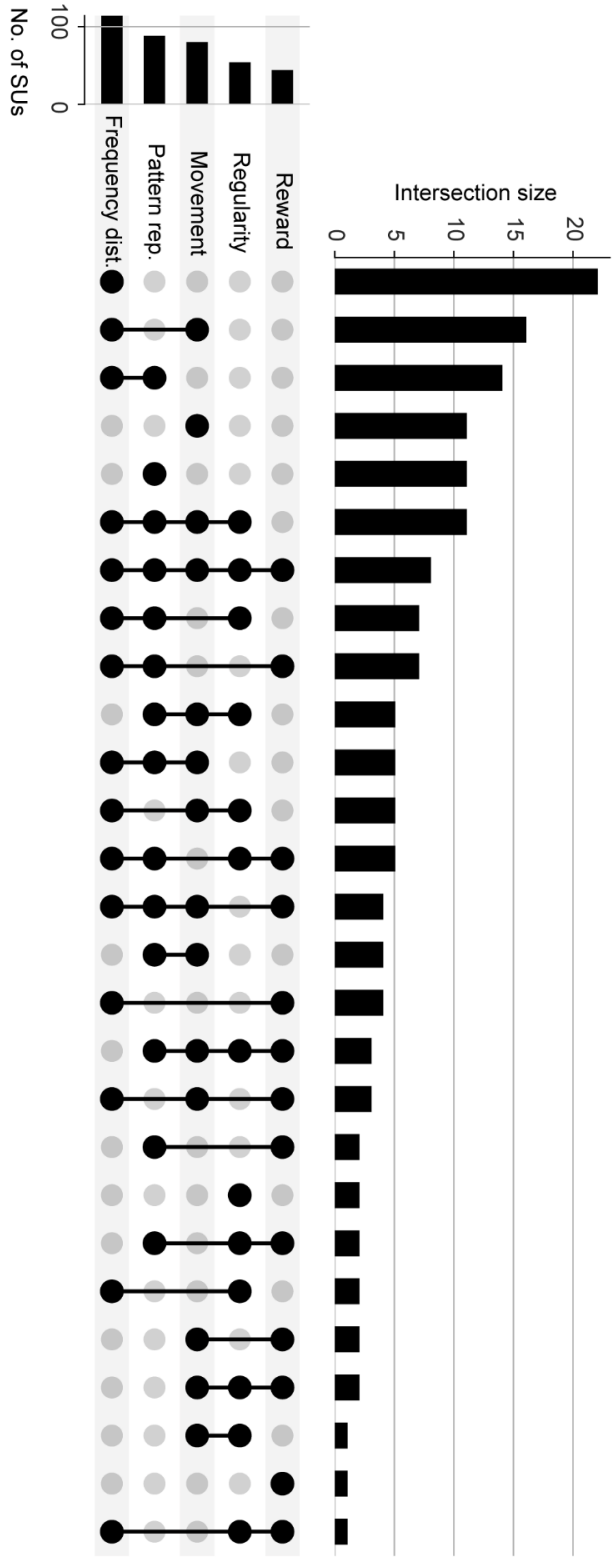

Figure 9.2: Categorisation plot of significant effects identified by a GLMM (Poisson) on each single unit and the number of times each combination of effects occurs across the population of single units.

9.4.2 Custom syringe pump for passive recordings

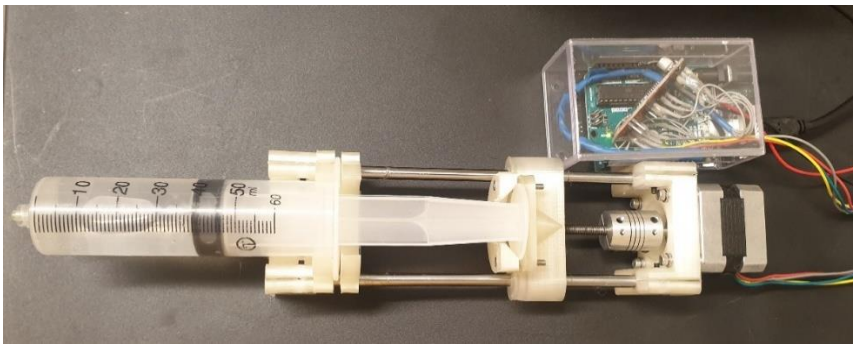

Figure 9.3: Custom syringe pump. A custom syringe pump was modified from the Open-source lab (Wijnen et al. 2014) to provide a continual water reward for passive electrophysiological recordings from awake ferrets. The custom syringe pump was powered by a battery to avoid electrical noise that may interfere with the recordings. All hardware was 3D printed on an Ultimaker 2+ with a stepper motor to drive the carriage to push/pull the syringe pump. The custom syringe pump was controlled via an Arduino and a Stepper Motor Driver (EasyDriver) with custom code written in the Arduino IDE which was uploaded to the microcontroller. Functionality was added to allow custom code within MATLAB to control the syringe pump remotely.